ORNL/TM-10122
~~Applied~~

ornl

OAK RIDGE
NATIONAL
LABORATORY

MARTIN MARIETTA

Dynamic Subcriticality Measurements Using the ^{252}CF-Source-Driven Noise Analysis Method

J. T. Mihalczo
E. D. Blakeman
G. E. Ragan
E. B. Johnson

OPERATED BY
MARTIN MARIETTA ENERGY SYSTEMS, INC.
FOR THE UNITED STATES
DEPARTMENT OF ENERGY

Printed in the United States of America. Available from
the U.S. Department of Energy
Technical Information Center
P.O. Box 62, Oak Ridge, Tennessee 37830

ORNL/TM-10122
Dist. Category S-526
~~Applied~~

Consolidated Fuel Reprocessing Program

DYNAMIC SUBCRITICALITY MEASUREMENTS USING THE ^{252}CF-SOURCE-DRIVEN NOISE ANALYSIS METHOD

J. T. Mihalczo
E. D. Blakeman
G. E. Ragan
E. B. Johnson

Instrumentation and Controls Division

Date Published - August 1988

Research jointly sponsored under the provisions of a Memorandum of Agreement between the United States Department of Energy and the Power Reactor and Nuclear Fuel Development Corporation of Japan for Criticality Data Development, dated August 12, 1983.

Prepared by
OAK RIDGE NATIONAL LABORATORY
Oak Ridge, Tennessee 37831
operated by
MARTIN MARIETTA ENERGY SYSTEMS, INC.
for the
U.S. DEPARTMENT OF ENERGY
under Contract No. DE-AC05-840R21400

TABLE OF CONTENTS

	Page
LIST OF FIGURES	v
LIST OF TABLES	xi
ACKNOWLEDGMENTS	xv
ABSTRACT	xvii
1. INTRODUCTION	1
2. DESCRIPTION OF THE EXPERIMENTAL SYSTEM AND THE AQUEOUS URANYL NITRATE	2
3. DESCRIPTION AND LOCATION OF THE ^{252}Cf SOURCE AND THE DETECTORS	6
4. DESCRIPTION OF THE DATA-ACQUISITION SYSTEM	11
5. EXPERIMENTAL APPROACH	12
6. STATIC MEASUREMENTS OF THE RATIOS OF SPECTRAL DENSITIES AND NEUTRON MULTIPLICATION FACTORS	13
6.1 VARYING SOLUTION HEIGHT WITH CENTRAL SOURCE	13
6.2 VERTICAL VARIATION OF THE SOURCE HEIGHT WITH FIXED SOLUTION HEIGHT	14
6.3 VARYING SOLUTION HEIGHT WITH THE SOURCE AT THE BOTTOM OF THE SOLUTION	23
7. DYNAMIC MEASUREMENTS OF THE RATIOS OF SPECTRAL DENSITIES AND NEUTRON MULTIPLICATION FACTORS	27
7.1 FILLING THE EXPERIMENTAL VESSEL	28
7.2 DRAINING THE EXPERIMENTAL VESSEL	32
7.2.1 Draining at a Rate of 3 cm/min	32
7.2.2 Draining at a Rate of 5 cm/min	36
7.2.3 Draining at a Rate of 23 cm/min	36
7.3 SOLUTION PERTURBED BY BUBBLES	42
8. BREAK-FREQUENCY NOISE ANALYSIS METHOD	45
9. CONCLUSIONS AND RECOMMENDATIONS	49
REFERENCES	50
APPENDIX A. THEORY OF THE MEASUREMENT METHOD	53
APPENDIX B. ADDITIONAL DATA FROM STATIC MEASUREMENTS	61

TABLE OF CONTENTS (continued)

		Page
APPENDIX C.	PARAMETERS FOR INTERPRETATION OF THE RATIO OF SPECTRAL DENSITIES TO OBTAIN THE NEUTRON MULTIPLICATION FACTOR	81
APPENDIX D.	CALCULATED NEUTRON MULTIPLICATION FACTORS	89
APPENDIX E.	REACTIVITY EFFECT OF THE DETECTORS	93
APPENDIX F.	ADDITIONAL DYNAMIC EXPERIMENTS	99
APPENDIX G.	ADDITIONAL DATA FROM DYNAMIC MEASUREMENTS WITH THE EXPERIMENTAL VESSEL FILLING AT A RATE OF 1 CM/MIN	121
APPENDIX H.	ADDITIONAL DATA FROM DYNAMIC MEASUREMENTS WITH THE EXPERIMENTAL VESSEL DRAINING AT A RATE OF 3 CM/MIN	145
APPENDIX I.	ADDITIONAL DATA FROM DYNAMIC MEASUREMENTS WITH THE EXPERIMENTAL VESSEL DRAINING AT A RATE OF 5 CM/MIN	153
APPENDIX J.	ADDITIONAL DATA FROM DYNAMIC MEASUREMENTS WITH THE EXPERIMENTAL VESSEL DRAINING AT A RATE OF 23 CM/MIN	161
APPENDIX K.	ADDITIONAL DATA FROM DYNAMIC MEASUREMENTS WITH SOLUTION PERTURBED BY BUBBLES	169
APPENDIX L.	TYPICAL LEAST-SQUARES FITTING OF APSDs AND CPSDs . .	177
APPENDIX M.	OTHER NOISE EQUIVALENT SOURCE FORMULATIONS	187

LIST OF FIGURES

Figure

Page

1. Photograph of the experimental vessel 3

2. Sketch of the system for filling and draining the experimental vessel 4

3. Sketch of the ^{252}Cf ion chamber attached to the Lexan tubing 7

4. Location of the ^{3}He detectors adjacent to the experimental vessel for a solution height of 29.2 cm . . . 8

5. Photograph of a scintillation detector, photomultiplier tube, and tube base configuration 9

6. Location of the ^{6}Li-glass-plastic scintillators for the dynamic measurements 2.5 cm from the experimental vessel 10

7. Ratio of spectral densities at low frequency versus solution height from static measurements with ^{3}He detectors and a central source 16

8. Neutron multiplication factor versus solution height from static measurements with ^{3}He detectors and a central source 18

9. Ratios of spectral densities at low frequency as a function of source height for solution heights of 15.2, 20.3, and 25.4 cm 22

10. K_{eff} values as a function of solution height from measurements with the Cf source on the bottom of the tank 26

11. Ratios of spectral densities at low frequency as a function of solution height for dynamic measurements . . . 30

12. Neutron multiplication factor versus solution height from measurements while the solution height was increasing at a rate of 1 cm/min with the Cf source at the bottom of the solution 31

13. Coherence squared, γ^2_{12} and γ^2_{23}, at low frequency as a function of solution height for experiments with scintillation detectors and the Cf source at the bottom of the solution 33

LIST OF FIGURES (continued)

Figure		Page
14.	Neutron multiplication factor versus solution height for dynamic measurements with the Cf source at the bottom of the tank	37
15.	Comparison of neutron multiplication factors from BFNA with those from ratios of spectral densities	48
B.1.	Ratios of spectral densities as a function of frequency for various solution heights with the source in the center of the solution	64
B.2.	APSDs and CPSDs as a function of frequency for a solution height of 10.2 cm with the source in the center of the solution	66
B.3.	APSDs and CPSDs as a function of frequency for a solution height of 20.4 cm with the source in the center of the solution	67
B.4.	APSDs and CPSDs as a function of frequency for a solution height of 30.5 cm with the source in the center of the solution	68
B.5.	Ratios of spectral densities as a function of frequency for a solution height of 15.2 cm and various source heights	69
B.6.	APSDs and CPSDs as a function of frequency for a solution height of 15.2 cm and a source height of 0.0 cm	72
B.7.	APSDs and CPSDs as a function of frequency for a solution height of 15.2 cm and a source height of 1.27 cm	73
B.8.	APSDs and CPSDs as a function of frequency for a solution height of 15.2 cm and a source height of 2.54 cm	74
B.9.	APSDs and CPSDs as a function of frequency for a solution height of 15.2 cm and a source height of 5.08 cm	75
B.10.	APSDs and CPSDs as a function of frequency for a solution height of 15.2 cm and a source height of 7.62 cm	76
B.11.	APSDs and CPSDs as a function of frequency for a solution height of 15.2 cm and a source height of 10.2 cm	77
B.12.	APSDs and CPSDs as a function of frequency for a solution height of 15.2 cm and a source height of 12.7 cm	78

LIST OF FIGURES (continued)

Figure		Page
B.13.	APSDs and CPSDs as a function of frequency for a solution height of 15.2 cm and a source height of 13.92 cm	79
B.14.	APSDs and CPSDs as a function of frequency for a solution height of 15.2 cm and a source height of 15.24 cm	80
C.1.	Ratio of neutron importance I_c/I as a function of height of uranyl nitrate solution in a 25.1-cm ID cylindrical tank with the source at the bottom of the tank	85
C.2.	Ratio of importance I_c/I as a function of axial location of the source for solution heights of 15.2, 20.3, and 25.4 cm	86
C.3.	Global spatial correction factor R as a function of height of uranyl nitrate solution in a 25.1-cm ID cylindrical tank	87
F.1.	Ratios of spectral densities as a function of frequency as the experimental vessel was draining at a rate of ~12 cm/min with the source 2.5 cm from the bottom of the tank	108
F.2.	Ratios of spectral densities as a function of frequency as the experimental vessel was draining at a rate of ~16 cm/min with the source 5.1 cm from the bottom of the tank	113
F.3.	Ratios of spectral densities as a function of frequency as the experimental vessel was draining at a rate of ~17 cm/min with the source 7.6 cm from the bottom of the tank	117
F.4.	Coherence squared at low frequency as a function of solution height with the source 2.5 and 5.1 cm from the bottom of the tank	120
G.1.	APSDs and CPSDs as a function of frequency for a dynamic measurement with a filling rate of 1 cm/min, average solution height of 6.46 cm, and a Cf source located on the bottom of the tank	124
G.2.	APSDs and CPSDs as a function of frequency for a dynamic measurement with a filling rate of 1 cm/min, average solution height of 6.61 cm, and a Cf source located on the bottom of the tank	125

LIST OF FIGURES (continued)

Figure		Page
G.3.	APSDs and CPSDs as a function of frequency for a dynamic measurement with a filling rate of 1 cm/min, average solution height of 7.36 cm, and a Cf source located on the bottom of the tank	126
G.4.	APSDs and CPSDs as a function of frequency for a dynamic measurement with a filling rate of 1 cm/min, average solution height of 8.50 cm, and a Cf source located on the bottom of the tank	127
G.5.	APSDs and CPSDs as a function of frequency for a dynamic measurement with a filling rate of 1 cm/min, average solution height of 9.88 cm, and a Cf source located on the bottom of the tank	128
G.6.	APSDs and CPSDs as a function of frequency for a dynamic measurement with a filling rate of 1 cm/min, average solution height of 11.44 cm, and a Cf source located on the bottom of the tank	129
G.7.	APSDs and CPSDs as a function of frequency for a dynamic measurement with a filling rate of 1 cm/min, average solution height of 13.08 cm, and a Cf source located on the bottom of the tank	130
G.8.	APSDs and CPSDs as a function of frequency for a dynamic measurement with a filling rate of 1 cm/min, average solution height of 14.75 cm, and a Cf source located on the bottom of the tank	131
G.9.	APSDs and CPSDs as a function of frequency for a dynamic measurement with a filling rate of 1 cm/min, average solution height of 16.54 cm, and a Cf source located on the bottom of the tank	132
G.10.	APSDs and CPSDs as a function of frequency for a dynamic measurement with a filling rate of 1 cm/min, average solution height of 18.36 cm, and a Cf source located on the bottom of the tank	133
G.11.	APSDs and CPSDs as a function of frequency for a dynamic measurement with a filling rate of 1 cm/min, average solution height of 20.17 cm, and a Cf source located on the bottom of the tank	134

LIST OF FIGURES (continued)

Figure		Page
G.12.	APSDs and CPSDs as a function of frequency for a dynamic measurement, with a filling rate of 1 cm/min, average solution height of 22.01 cm, and a Cf source located on the bottom of the tank	135
G.13.	APSDs and CPSDs as a function of frequency for a dynamic measurement, with a filling rate of 1 cm/min, average solution height of 23.84 cm, and a Cf source located on the bottom of the tank	136
G.14.	APSDs and CPSDs as a function of frequency for a dynamic measurement, with a filling rate of 1 cm/min, average solution height of 25.70 cm, and a Cf source located on the bottom of the tank	137
G.15.	APSDs and CPSDs as a function of frequency for a dynamic measurement, with a filling rate of 1 cm/min, average solution height of 27.59 cm, and a Cf source located on the bottom of the tank	138
G.16.	Ratios of spectral densities as a function of frequency as the experimental vessel was filling at a rate of 1 cm/min	139
H.1	Ratios of spectral densities as a function of frequency for a draining rate of 3 cm/min at various solution heights	148
I.1.	Ratios of spectral densities as a function of frequency for a draining rate of 5 cm/min at varied solution heights	156
J.1.	Ratios of spectral densities as a function of frequency for a draining rate of 23 cm/min at various solution height	164
K.1.	APSDs as a function of frequency for the solution unperturbed by bubbles (solution height = 29.5 cm)	172
K.2.	Real and imaginary parts of the CPSDs as a function of frequency for the solution unperturbed by bubbles (solution height = 29.5 cm)	173
K.3	APSDs as a function of frequency for the solution perturbed by bubbles (solution height = 29.5 cm)	174
K.4.	CPSDs as a function of frequency for the solution perturbed by bubbles (solution height = 29.5 cm)	175

LIST OF FIGURES (continued)

Figure		Page
K.5.	Ratios of spectral densities as a function of frequency for a solution height of 29.5 cm	176
L.1.	CPSDs, G_{12} and G_{13}, as a function of frequency for a solution height of 29.5 cm with the source on the bottom of the tank and the scintillators located as in Fig. 6. (Lines are fitted functions.)	180
L.2.	CPSD, G_{23}, and APSDs, G_{22} and G_{33}, as a function of frequency for a solution height of 29.5 cm with the source on the bottom of the tank and the scintillators located as in Fig. 6. (Lines are fitted functions.) . . .	181
L.3.	CPSDs, G_{12} and G_{13}, as a function of frequency for a solution height of 20.2 cm with the source on the bottom of the tank and the scintillators located as in Fig. 6. (Lines are fitted functions.)	182
L.4.	CPSD, G_{23}, and APSDs, G_{22} and G_{33}, as a function of frequency for a solution height of 20.2 cm with the source on the bottom of the tank and the scintillators located as in Fig. 6. (Lines are fitted functions.) . . .	183
L.5.	CPSDs, G_{12} and G_{13}, as a function of frequency for a solution height of 13.1 cm with the source on the bottom of the tank and the scintillators located as in Fig. 6. (Lines are fitted functions.)	184
L.6.	CPSD, G_{23}, and APSDs, G_{22} and G_{33}, as a function of frequency for a solution height of 13.1 cm with the source on the bottom of the tank and the scintillators located as in Fig. 6. (Lines are fitted functions.) . . .	185
M.1.	Comparison of neutron multiplication factors obtained from the ratios of spectral densities using various noise equivalent source terms for spontaneous fission with independent BFNA measurements and with calculated values .	190

LIST OF TABLES

Table

Page

1. Trace elements in the aqueous uranyl nitrate 5

2. Ratios of spectral densities, $G_{12}^{*}G_{13}/G_{11}G_{23}$, at low frequency for various solution heights from static measurements with central source and ^{3}He proportional counters adjacent to the outer surface of the experimental vessel 15

3. Neutron multiplication factors for various solution heights from measurements with ^{3}He proportional counters and a central source 17

4. Ratios of spectral densities, $G_{12}^{*}G_{13}/G_{11}G_{23}$, at low frequency as a function of source height for a solution height of 15.2 cm 19

5. Ratios of spectral densities, $G_{12}^{*}G_{13}/G_{11}G_{23}$, at low frequency as a function of source height from static measurements for a solution height of 20.3 cm 20

6. Ratios of spectral densities, $G_{12}^{*}G_{13}/G_{11}G_{23}$, at low frequency as a function of source height for a solution height of 25.4 cm 21

7. k_{eff} values from ratios of spectral densities at low frequency using point kinetic interpretation for solution heights of 15.2, 20.3, and 25.4 cm for a variety of axial heights of the source 23

8. Ratios of spectral densities at low frequency and neutron multiplication factors from static measurements with the source at the bottom of the solution 25

9. Ratios of spectral densities at low frequency and neutron multiplication factors for dynamic measurements while filling the experimental vessel 29

10. Ratios of spectral densities at low frequency and neutron multiplication factors for dynamic measurements while draining the experimental vessel at a rate of ~3 cm/min . . 34

11. Ratios of spectral densities at low frequency and neutron multiplication factors for dynamic measurements while draining the experimental vessel at a rate of 5 cm/min . . . 38

12. Ratios of spectral densities at low frequency and neutron multiplication factors for dynamic measurements while draining the experimental vessel at a rate of 23 cm/min . . 40

LIST OF TABLES (continued)

Table		Page
13.	Ratios of spectral densities at low frequency and neutron multiplication factors for dynamic measurements with solution perturbed by bubbles	44
14.	Break frequencies obtained from least-squares fitting of APSDs and CPSDs and neutron multiplication factors from the BFNA method as a function of solution height	46
C.1.	Parameters I_c/I and R used to interpret the ratio of spectral densities as a function of solution height	84
C.2.	I_c/I from Monte Carlo calculation as a function of axial source position for solution heights of 15.2, 20.3, and 25.4 cm	86
C.3.	Sensitivity of k_{eff} to parameters used in interpretation of experimental data for various k_{eff} values	87
D.1.	Neutron multiplication factors from Monte Carlo calculations with Hansen-Roach cross sections	91
E.1.	Summary of reactivity effects of the ^{6}Li-glass-plastic scintillators from several measurements	96
F.1.	Ratios of spectral densities at low frequency and neutron multiplication factors for dynamic measurements while filling the experimental vessel with the source 2.5 cm from the bottom of the vessel	102
F.2.	Ratios of spectral densities at low frequency and neutron multiplication factors for dynamic measurements while draining the experimental vessel at a rate of ~12 cm/min with the source 2.5 cm from the bottom of the vessel	103
F.3.	Ratios of spectral densities at low frequency and neutron multiplication factors for dynamic measurements while draining the experimental vessel at a rate of ~16 cm/min with the source 5.1 cm from bottom of the vessel	105
F.4.	Ratios of spectral densities at low frequency and neutron multiplication factors for dynamic measurements while draining the experimental vessel at a rate of 23 cm/min with the source 7.6 cm from the bottom of the vessel	107

LIST OF TABLES (continued)

Table		Page
G.1.	On-line ratios of spectral densities at low frequency and neutron multiplication factors for dynamic measurements while filling the experimental vessel at a rate of 1 cm/min	144
H.1.	On-line ratios of spectral densities at low frequency and neutron multiplication factors for dynamic measurements while draining the experimental vessel at a rate of ~3 cm/min	151
I.1.	On-line ratios of spectral densities at low frequency and neutron multiplication factors for dynamic measurements while draining the experimental vessel at a rate of 5 cm/min	159
J.1.	Ratios of spectral densities at low frequency and neutron multiplication factors for dynamic measurements while draining the experimental vessel at a rate of 23 cm/min . .	167

ACKNOWLEDGMENTS

The work of R. W. Hayes, R. C. Kryter, and C. W. Ricker of Oak Ridge National Laboratory, in the specification, procurement, assembly, testing, and modification of the measurement system was essential to the successful development of this system, without which this experiment would not have been possible. Also essential to this measurement was the work of R. A. Todd and M. S. Emery in the design and modification of the analog-to-digital conversion system; of M. M. Chiles and V. C. Miller for the design, testing, and development of the high efficiency scintillation detectors; of G. W. Allin in engineering support; and of C. E. Murphy for technical assistance. For the use of the ^{252}Cf, the authors are indebted to the Division of Chemical Sciences, Office of Basic Energy Sciences, U.S. Department of Energy, through the transplutonium element production facilities at Oak Ridge National Laboratory (ORNL). The authors acknowledge the support of the Power Reactor and Nuclear Fuel Development Corporation of Japan (PNC) and the Department of Energy through the Consolidated Fuel Reprocessing Program at ORNL. The work of Y. Hachiya and H. Yamana of PNC was essential in planning experiments during their assignment at ORNL. The thorough review of this report by H. Funabashi of PNC is gratefully acknowledged.

ABSTRACT

Dynamic measurements of the subcritical neutron multiplication factor, k_{eff}, using the ^{252}Cf-source-driven neutron noise analysis method, were performed for an unreflected 25.1-cm-ID cylindrical tank containing aqueous uranyl nitrate as the solution height was changed at rates of 1 cm/min to 23 cm/min, with corresponding rates of change of the neutron multiplication factor of 4×10^{-4}/s to 0.01/s.

These experiments, which were the first test of this method of measuring k_{eff} while it is changing, showed that (1) this method has the capability to measure subcriticality for a multiplying system to a k_{eff} as low as 0.30; (2) experimental k_{eff} values can be obtained from the ratio of spectral densities with as little as 6 s of data accumulation and a small fraction of a second analysis time while the solution tank is drained from 29.5 to 6.5 cm height in ~60 s with corresponding changes in k_{eff} from 0.95 to 0.30; (3) the measured k_{eff} values obtained do not depend on the speed at which the solution height is changed or whether it is filling or draining; (4) the results of the dynamic measurements agreed with the static measurements; (5) as in previous experiments, the ratios of spectral densities at low frequency were used successfully to obtain k_{eff} values using point kinetics interpretation of the data; (6) the neutron multiplication factors from independent measurements using the break frequency noise analysis method agree with the values of k_{eff} from the measured ratios of spectral densities down to k_{eff} values of 0.65; (7) this method's effectiveness for systems where conditions are changing as demonstrated probably exceeds the dynamic requirements of most nuclear fuel plant processing applications; (8) calculated k_{eff} values using KENO Monte Carlo code and Hansen-Roach cross sections compare well with the experimental values. Before the dynamic capability of the method can be considered fully explored, additional experiments are required for other geometries and fissile materials.

1. INTRODUCTION

This report describes static and dynamic measurements of the subcritical neutron multiplication factor using the ^{252}Cf source-driven noise analysis method[1,2] for an unreflected cylindrical tank containing uranyl nitrate solution. These experiments are part of a program at Oak Ridge National Laboratory, which is a collaboration between the U.S. Department of Energy (DOE) and the Power Reactor and Nuclear Fuel Development Corporation of Japan to study criticality safety related to the development of fast breeder technology.[3]

The ^{252}Cf-source-driven noise analysis method for obtaining the subcritical neutron multiplication factor of a configuration of fissile material from cross-power spectral densities (CPSDs) was developed to avoid difficulties inherent in other subcriticality measurement methods, such as dependence on detection efficiency and need for a reference measurement at some known reactivity state near delayed critical. This method requires measurement of the frequency-dependent CPSD, $G_{23}(\omega)$, between a pair of detectors (Nos. 2 and 3) located in or near the fissile material and CPSDs $G_{12}(\omega)$ and $G_{13}(\omega)$ between these same detectors and a source of neutrons emanating from an ionization chamber (No. 1) containing ^{252}Cf, also positioned in or near the fissile material. Also, the auto-power spectral density (APSD), $G_{11}(\omega)$, of the source is required. A particular ratio of spectral densities, $G_{12}^{*} G_{13}/G_{11} G_{23}$ (* denotes complex conjugation) is then formed, which is independent of detector efficiency and can be related to the subcritical neutron multiplication factor.

Some applications of this method for which experiments have been performed are (1) initial fuel loading of reactors,[4] (2) refueling of reactors,[5] (3) fuel preparation facilities,[6] (4) fuel processing facilities,[7] (5) fuel storage facilities,[8] (6) zero-power testing of reactors,[9] and (7) verification of calculational methods for assemblies with $k_{eff} < 1$.[10] These previous measurements, performed with a wide variety of systems, demonstrated the usefulness of the method. In these previous experiments, this method was used to obtain the subcritical neutron multiplication factor, k_{eff}, for a variety of static systems with k_{eff} values varying from ~0.5 to ~0.99.

If the capability of the method is demonstrated for situations in which the value of k_{eff} is changing as a result of changes in concentrations or volumes of fissile material, the possible applications of the method will be extended. The purpose of this experiment with a cylindrical tank of aqueous uranyl nitrate was to demonstrate the capability of this method to measure subcriticality where k_{eff} is changing continuously.

2. DESCRIPTION OF THE EXPERIMENTAL SYSTEM AND THE AQUEOUS URANYL NITRATE

The experimental vessel was a right circular, 25.1-cm-ID acrylic cylinder with a height of 53.3 cm and a wall thickness of 0.95 cm. The bottom of the vessel was 0.63-cm-thick type 304 stainless steel plate. The acrylic was sealed at the bottom against an O-ring recessed in the base plate and compressed through four 0.63-cm-diam threaded steel tie rods, equispaced around the circumference of the vessel, joining the base and a stainless steel upper flange. An 0.63-cm-thick acrylic plate on top of the upper flange provided access for the source and minimized evaporation of the solution.

The height of solution above the base plate was determined by an ultrasonic device whose transducer was mounted on the acrylic cover of the vessel over a circular opening. Every 0.125 s this device sampled and stored in the computer the solution height to within $\pm$ 0.2 mm. Figure 1 is a photograph of the experimental vessel showing the mounted transducer and the ^{252}Cf source ionization chamber at the top of the solution. The arrangement of the system with the lines connecting components and the pump for transferring solution are shown in Fig. 2.

The vessel was mounted on a 127-cm-square aluminum table 76 cm above a steel grating covered with stainless steel sheet. This grating was 3.6 m above the concrete floor of the experiment cell. The cell in which the equipment was assembled was about 9.1 x 12.2 x 9.1 m high with thick concrete walls and roof. The experiment vessel was located 4.4 m from the 9.1-m side of the cell, 3.0 m from the 12.2-m side, and 1.85 m from a 2.9-m-diam empty steel tank also present in the cell.

The aqueous uranyl nitrate contained 482 g of uranium per liter and a solution density of 1.643 g/cm^3, with a free acid content $<$0.1 wt % HNO_3. Uranium isotope content in wt % was ^{234}U = 1.02, ^{235}U = 93.2, ^{236}U = 0.41, and ^{238}U = 5.37. Trace elements in the solution are listed in Table 1.

ORNL-PHOTO 7128-86A

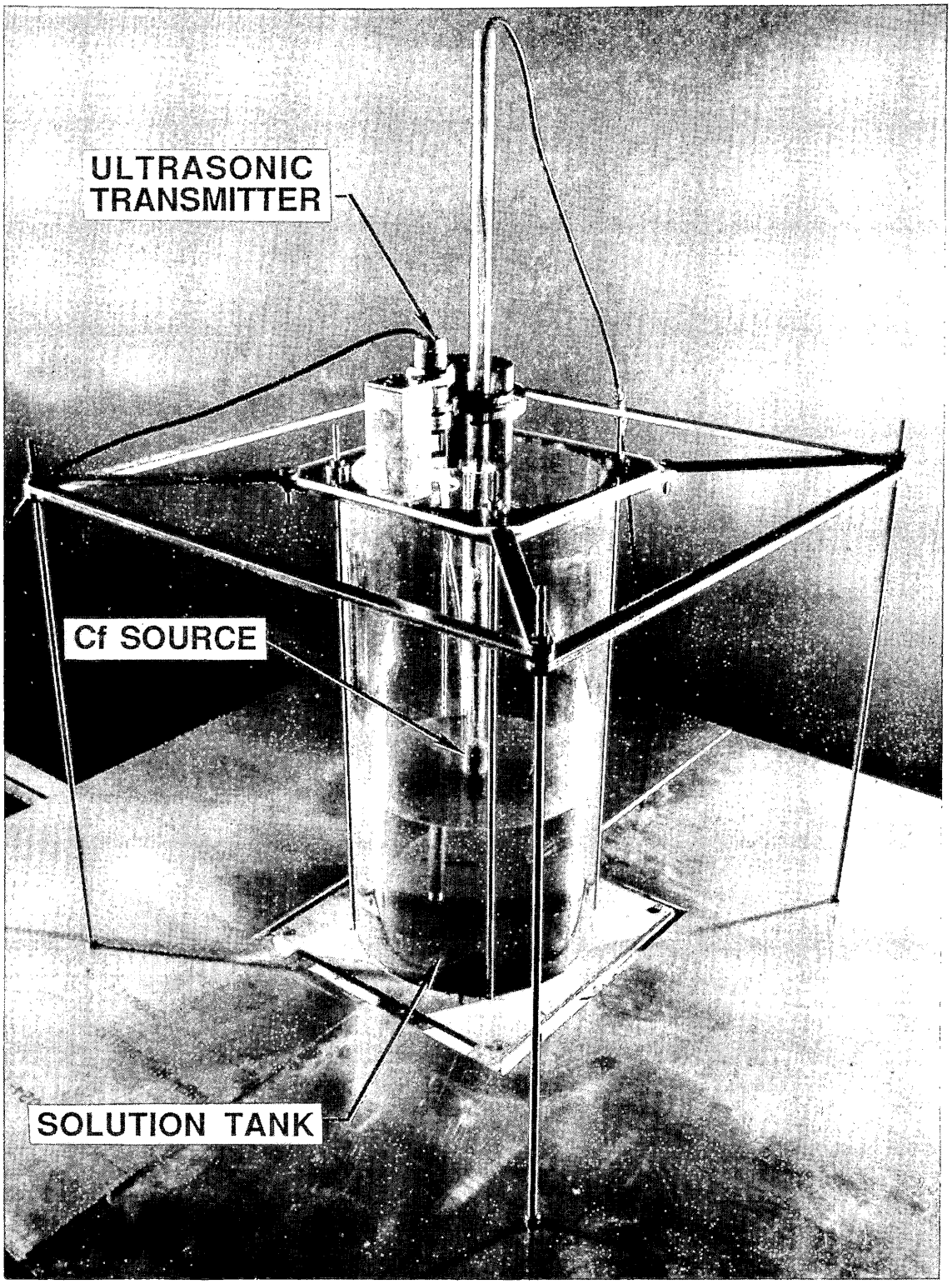

Fig. 1. Photograph of the experimental vessel.

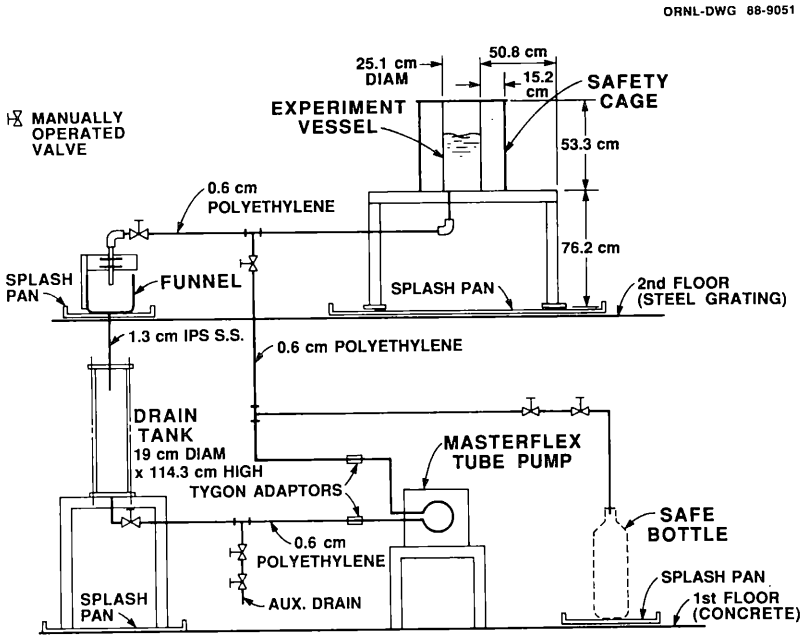

Fig. 2. Sketch of the system for filling and draining the experimental vessel. (Drain lines and lines connecting tanks are 0.6 cm OD polyethlene tubing.)

Table 1. Trace elements in the aqueous uranyl nitrate

Element[a]	Content[b] (ppm)
Al	2
As, Ca, Mo, Nb, Si, Sn, Zn	<10
Au, Bi, Co, Cu, Ga, Ge, Na, Po, V	<1
B, Be, Cd	<0.1
Ba, Mg, Sb	<2
Cr	9
Fe	55
Li	<0.2
Mn	1
Ni	4
P, W	<100
Pb	<5
Sr	<20
Ti	<4

[a]Each element listed has the content given in the right-hand column.

[b]Determined by spectrochemical analysis.

3. DESCRIPTION AND LOCATION OF THE ^{252}Cf SOURCE AND THE DETECTORS

The ^{252}Cf was electroplated on one plate of a parallel-plate ionization chamber, and the spontaneous fission rate was 60,000/s (~0.1 μg ^{252}Cf). The source ionization chamber was mounted at the end of a Lexan tube (1.90 cm OD, 1.27 cm ID) with the signal cable from the chamber inside the Lexan tube (Fig. 1). The source was sealed from the solution with shrink tubing and epoxy as shown in Fig. 3. The Lexan tubing and the signal cable protruded out the top of the solution through a central hole in the lid of the experimental vessel. The source could be located anywhere along the axis of the cylindrical experimental vessel. In most of the dynamic experiments, the source was located at the bottom of the experimental vessel. In practical applications involving cylindrical tanks, the bottom of the tank would be a convenient location for the source. For most static measurements at various solution heights, the source was located on the axis at the vertical midplane of the solution, but in some measurements its vertical location on the axis was varied.

Two types of detectors were used in these experiments: commercially available ^{3}He proportional counters for static measurements and specially assembled composite ^{6}Li-glass-plastic scintillators for dynamic measurements. The ^{3}He proportional counters (5.1-cm diam, 38-cm active length Reuter Stokes Model No. RS-P4-1641-101) were located with their axes parallel to the axis of the experimental vessel. The location of these detectors is shown in Fig. 4. In some experiments, a single ^{3}He detector on each side of the vessel was used for each detection channel. In other measurements the signals from two ^{3}He chambers on each side, adjacent to each other and the outer surface of the tank, were summed prior to being amplified by the preamplifiers for detection channel 2 of the noise analysis system. A similar pair of detectors was used for detection channel 3.

The scintillation detectors were composite ^{6}Li-glass-plastic scintillators sensitive to fast and thermal neutrons and gamma rays. Each scintillation detector consisted of a 15.2 x 15.2 x 0.5-cm-thick ^{6}Li glass scintillator optically coupled to a 15.2 x 15.2 x 10.2-cm-thick plastic scintillator sensitive to fast neutrons and gamma rays. The ^{6}Li glass scintillator was located toward the experimental vessel with the plastic scintillator behind it so that the plastic was almost neutronically decoupled from the solution by the absorption of slow neutrons in the ^{6}Li. Each detection channel consisted of two adjacent 15.2 x 15.2 x 10.7-cm-thick scintillators, each mounted in an aluminum box (Fig. 5) which then formed a detection channel with overall dimensions of 15.2 x 30.5 x 10.7 cm. The signals from each of the scintillators were summed to form the signal for detection channel 2. There were two detection channels of this type, one on each side of the experimental vessel for the dynamic measurements. The location of the scintillators 2.5 cm from the surface of the experimental vessel is shown in Fig. 6 for the dynamic experiments.

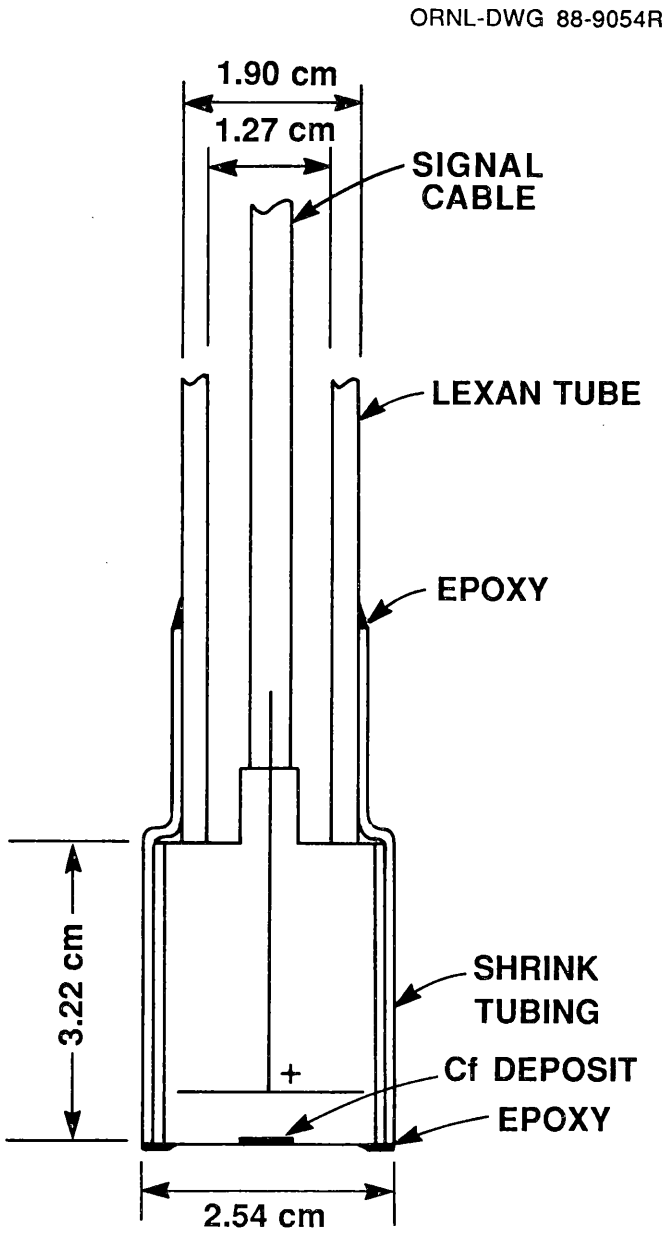

Fig. 3. Sketch of the ^{252}Cf ion chamber attached to the Lexan tubing.

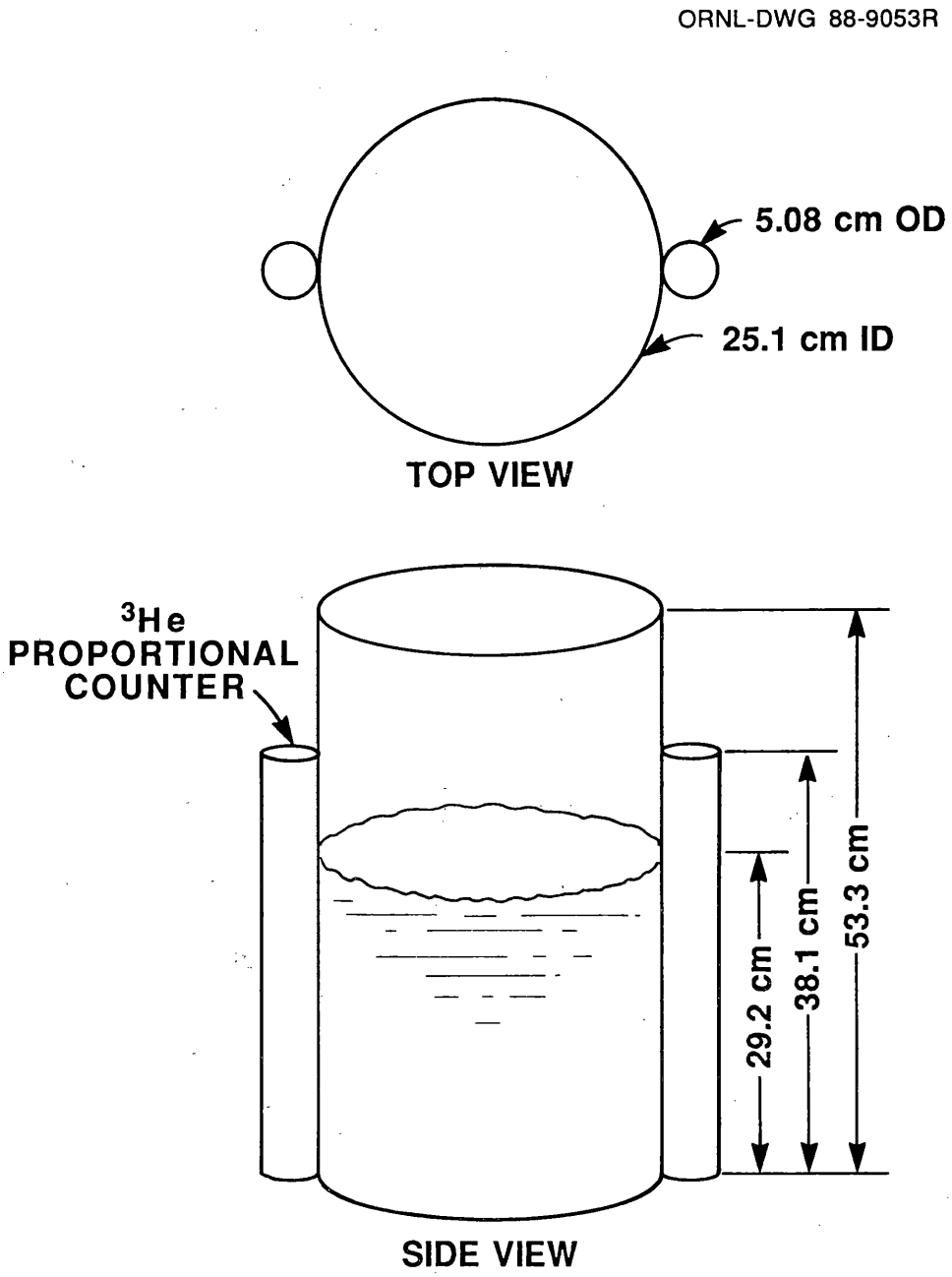

Fig. 4. Location of the ^{3}He detectors adjacent to the experimental vessel for a solution height of 29.2 cm.

ORNL-PHOTO 7126-86

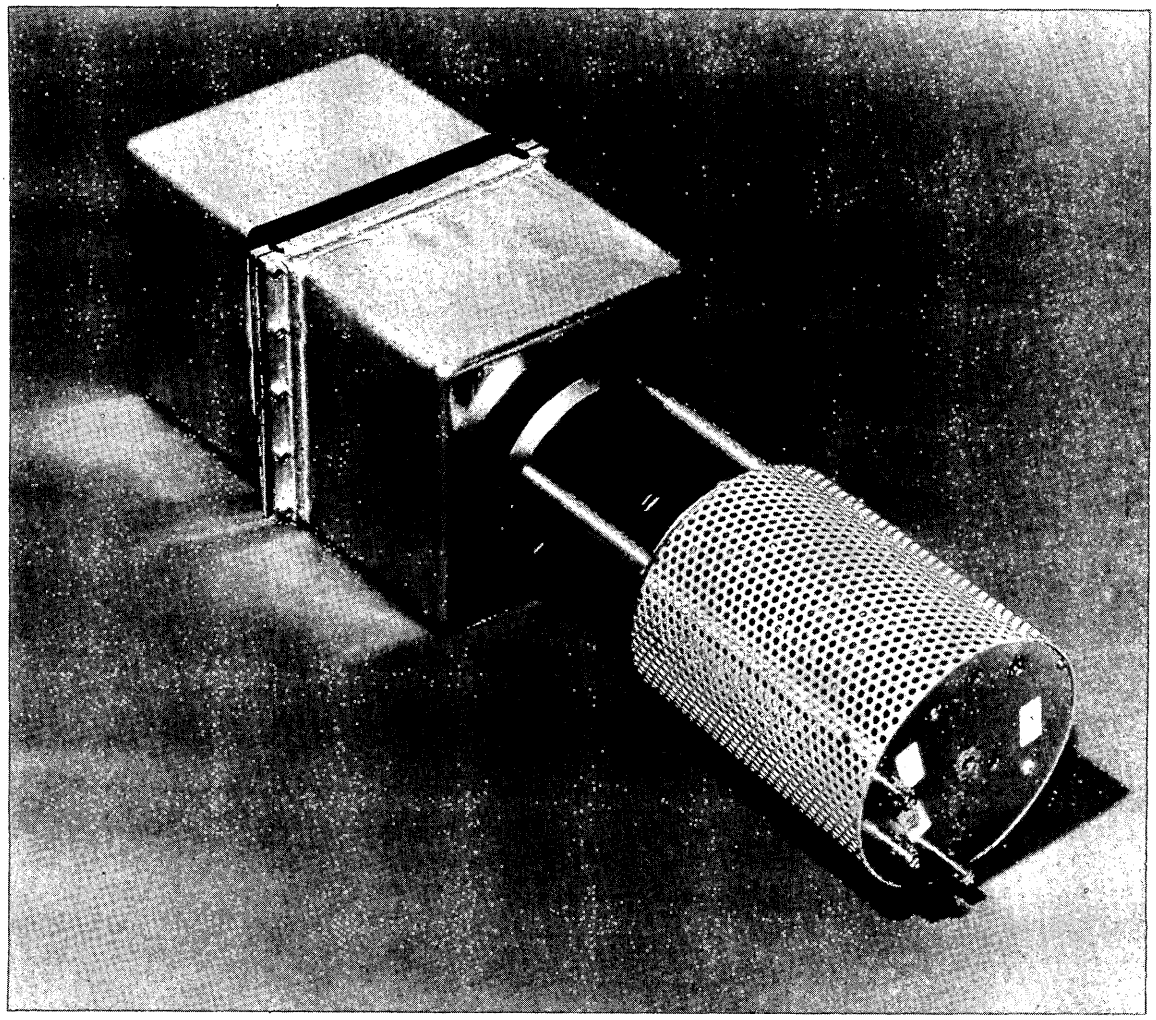

Fig. 5. Photograph of a scintillation detector, photomultiplier tube, and tube base configuration.

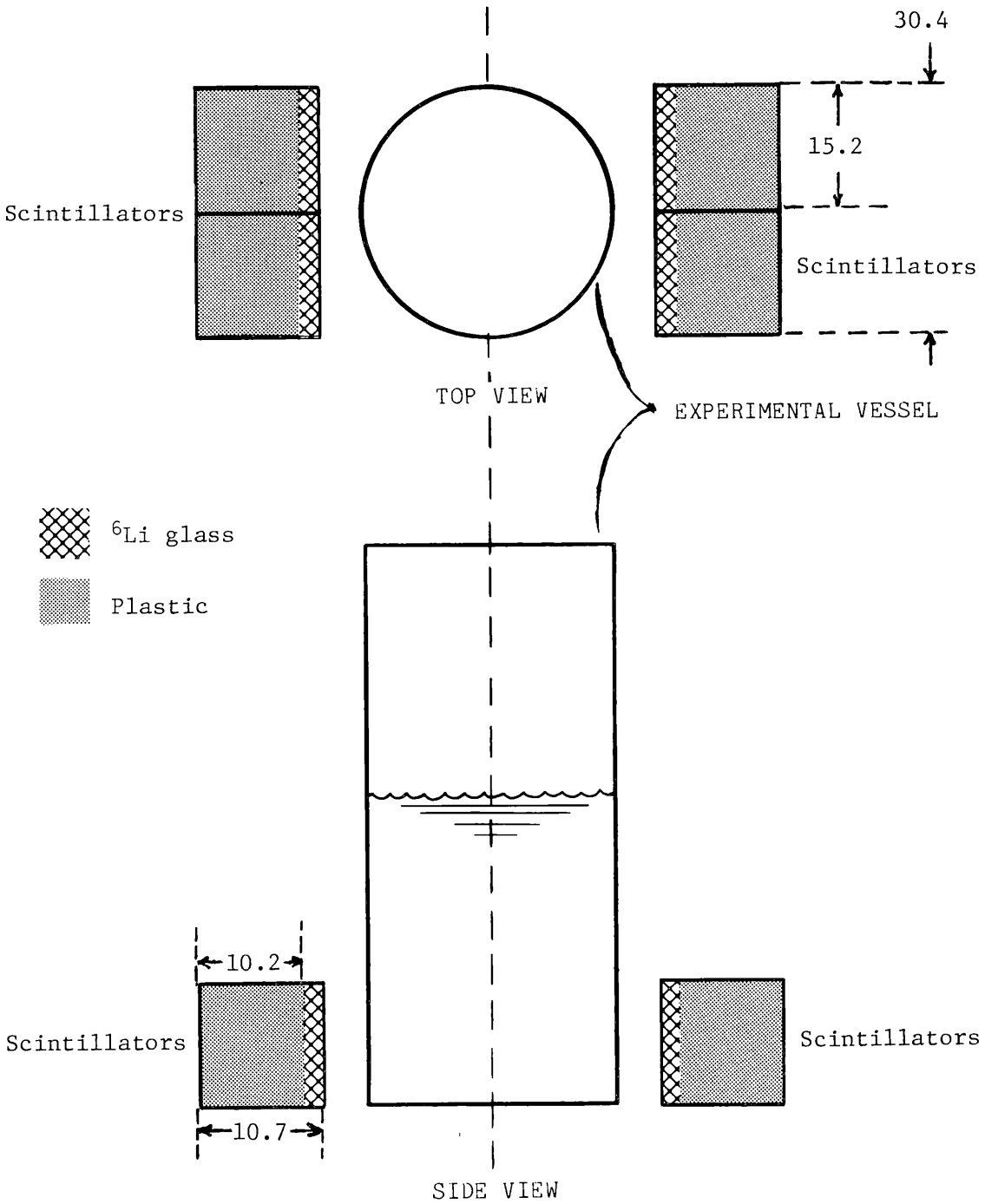

Fig. 6. Location of the ^{6}Li-glass-plastic scintillators for the dynamic measurements 2.5 cm from the experimental vessel (all dimensions in cm).

4. DESCRIPTION OF THE DATA-ACQUISITION SYSTEM

The data-acquisition system[11] consists of three main parts: (1) detection systems and processing electronics, (2) an analog-to-digital conversion (ADC) and Fourier analysis system, and (3) a control computer. Detection system electronics is conventional and has been described previously.[12] The analog-to-digital sampling system and the array processor (Signal Processing Systems, Inc., SPS-1000), used as a Fourier analyzer, are capable of real-time sampling and processing of three channels of 1024 data points per data block at sampling rates up to 200,000/s in each channel. For three-channel operation the maximum sampling rate of the ADC system is 300,000/s in each channel; the Fourier analyzer cannot process the data at this rate, so the ADC system goes into a gapped operation mode during which the signals are sampled whenever the array processor is capable of accepting the data. For five-channel operation of the system, sampling and processing rates are reduced. The array processor and ADC system are controlled by a computer (VAX-750) that takes the average APSDs, G_{ii}, and average CPSDs, G_{ik}, from the array processor intermittently and further averages them appropriately and stores them in data files. The ratio of spectral densities and coherences are calculated from these data files using the VAX-750.

5. EXPERIMENTAL APPROACH

In these experiments, as in those performed in the past,[2] detector-source configurations were varied to find detector locations for which the theory of the measurement (Appendix A) was applicable and where a point kinetics interpretation of the ratio of spectral densities yields meaningful results. The relevant equations for point kinetics interpretation of the measured ratio of spectral densities are given in Appendix A. From past experiments,[2] several criteria have been observed that, in most cases, result in measurements that are interpretable using point kinetics. Some of these criteria are consistent with experience from pulsed neutron and other kinetic measurements. These criteria are (1) central location of the source, (2) symmetric location of the detectors with respect to the source, (3) detector location far enough from the source to avoid events in the detector from particles directly from the source and to avoid higher spatial modal effects near the source, (4) detectors located far enough from each other so that the probability of detecting particles in each detector from the same fission (inherent or induced) is small, (5) use of detectors that span the full length of fissile material, and (6) use of the low-frequency ratio of spectral densities to obtain the neutron multiplication factor using point kinetics. However, even with these criteria, there is no guarantee that the results will be interpretable using point kinetics. If a point kinetics interpretation is not applicable, there are two approaches to interpret the experimental results: (1) use a model that treats spatial and energy modal effects, or (2) fit the data to sums of spatial modes and subtract the contribution of higher modes from the ratio of spectral densities. Previous experiments have been performed with a cylindrical solution tank in which all criteria except criterion 4 were satisfied. Those experiments were not interpretable using point kinetics, and a modal correction factor was developed and applied to satisfactorily obtain the subcriticality.[13]

In most of the experiments reported here, the source was located on the axis of the experimental vessel of the solution, and measurements were performed to meet the above criteria as far as practical. The solution concentration for these experiments was selected so that if spatial modal effects are important, the ability to fit data to sums of modes would be improved. Also, measurements that did not satisfy the above criteria were performed intentionally to emphasize modal effects so that if a model with modal effects is used to interpret the results, the model can be more fully tested and verified.

6. STATIC MEASUREMENTS OF THE RATIOS OF SPECTRAL DENSITIES AND NEUTRON MULTIPLICATION FACTORS

Static measurements were performed in order to have reference measurements to compare with the results of dynamic measurements. These measurements were performed as a function of solution height with the ^{252}Cf source located on the axis at the center of the solution; for fixed solution heights of 15.2, 20.3, and 25.4 cm where the axial location of the source was varied from the bottom to the top of the solution; and with the source located at the bottom of the solution tank and solution height varied. In all three types of static measurements, the detectors were ^{3}He proportional counters 180° apart, adjacent to the outer surface of the vessel with their axes parallel to the axis of the experimental vessel. In the third series of measurements the ^{6}Li-glass-plastic scintillators were also used and were located as shown in Fig. 6.

6.1 VARYING SOLUTION HEIGHT WITH CENTRAL SOURCE

In the measurements with the source on the axis at the center, the detectors were two ^{3}He proportional counters (located as in Fig. 4). The solution height was varied from 30.5 to 10.2 cm in steps, and the position of the source was adjusted as the solution height changed so that the source remained in the center of the solution on the axis of the tank. This location of source and detectors was chosen because in all but one[13] of the previous measurements spatial modal effects were minimized. The length of the ^{3}He detectors was more than the height of the solution. Typical data from these measurements (APSDs, CPSDs, and ratios of spectral densities) are shown in Appendix B (Fig. B.1) for experiments with solution height varying from 10.2 to 30.5 cm.

The ratios of spectral densities as a function of frequency were examined visually to determine the range of frequencies at low frequency over which the ratio of spectral densities was constant. This range of frequencies is generally greater for more subcritical systems because the frequency response of the experimental system $H_s(\omega)$ has significant amplitude at higher frequency. The range of frequencies over which the ratio was arithmetically averaged was then selected to eliminate high-frequency points for which the statistical error is large and would lead to high or low values of the ratio that would distort the average value of the ratio. Thus, both of these criteria, constant ratio and small statistical error, determined the upper frequency limit. The lowest frequency point for the measurements was well above that frequency for which delayed neutron effects are important. This procedure was used to obtain the low-frequency ratio of spectral densities. (This procedure could be automated for in-plant applications). The frequency range over which the measurements were performed was usually selected in order to measure G_{12} or G_{13}, which for fundamental mode behavior fall off at a rate of one decade in amplitude

for each full decade of frequency, while for fundamental mode behavior, G_{23} falls off at a rate of two decades in amplitude per decade in frequency. Thus, G_{23} approaches zero before G_{12} and G_{13} and at the high frequencies needed for the measurement of G_{12} or G_{13}, the ratio of spectral density loses statistical precision. Also, precision of the spectral densities G_{12}, G_{13}, and G_{23} generally decreases with increasing frequency. If the ratio of spectral densities was not constant with frequency at low frequency, the ratio at the lowest frequency of the measurement was used to obtain the subcriticality. Better estimates of the ratio may be obtained by fitting the data and taking ratios of fitted parameters at low frequency, especially where statistical precision is low or where there is a strong frequency dependence at low frequency.

The ratios of spectral densities at low frequency obtained from these measurements are given in Table 2 and Fig. 7. The upper limits of the frequency range for which the average ratio was determined are also given in Table 2. The average ratio of spectral densities at low frequency was used with the parameters given in Appendix C to obtain the subcritical neutron multiplication factor, k_{eff}, using point kinetics interpretation of the data. For the measurement with a solution height of 10.2 cm, the value of the ratio at the lowest frequency point was used. The neutron multiplication factors obtained in this way are compared with calculations in Table 3 and Fig. 8. The calculations were performed using KENO Monte Carlo calculations with Hansen-Roach cross sections (Appendix D, Table D.1 provides details of calculations).

6.2 VERTICAL VARIATION OF THE SOURCE HEIGHT WITH FIXED SOLUTION HEIGHT

To investigate the dependence of spatial modal effects on source location, the axial location of the ^{252}Cf source was varied from the bottom to the top of the solution for solution heights of 15.2, 20.3, and 25.4 cm. The ^{3}He proportional counters were located as shown in Fig. 4. The ratios of spectral densities at low frequency for these detector locations and these variations of source positions are given in Tables 4, 5, and 6. These data are plotted as a function of the source location shown in Fig. 9. The asymmetry with source height results from neutron streaming effects up the Lexan tube (Fig. 3) supporting the source. The ratios of spectral densities as a function of frequency are plotted in Appendix B. The interpretation of these ratios of spectral densities to obtain the subcritical neutron multiplication factors (Table 7) without correction for spatial effects will yield estimates of k_{eff} that vary with source position only as a result of the neglected spatial modal effects or neutron streaming in the source tube. The calculated k_{eff} values (Appendix D) for these three configurations are 0.721, 0.831, and 0.895 for solution heights of 15.2, 20.3, and 25.4, respectively. Measurements with the source in the center of the tank agree with the calculated k_{eff} values.

Table 2. Ratios of spectral densities, $G_{12}^{*}G_{13}/G_{11}G_{23}$, at low frequency for various solution heights from static measurements with central source and ^{3}He proportional counters adjacent to the outer surface of the experimental vessel

Solution height (cm)	Bandwidth of measurement (kHz)	Number of data samples (10^3)	Ratios of spectral densities[a] (10^{-3})	Upper limit of frequency range for ratio (kHz)
30.5	20	80	100 ± 1	3
30.5	40	80	96 ± 1	3
27.9	40	80	139 ± 1	3
25.4	50	240	190 ± 1	3
22.9	20	40	248 ± 3	5
20.3	100	160	304 ± 3	8
20.3	100	40	303 ± 5	7
15.2	100	80	502 ± 15	6
15.2	50	840	465 ± 3	5
10.2	100	9360	525[b]	0.4[b]

[a]Uncertainties are one standard deviation of the mean.

[b]For this measurement the ratio of spectral densities was not constant at low frequency (Fig. B.1), so the value measured at 400 Hz was used to obtain the neutron multiplication factor.

For a solution height of 25.4 cm, the variation of the k_{eff} values obtained using a point kinetics interpretation of the low-frequency ratio of spectral densities was only 0.02 as the source height from the bottom of the solution tank varied from 25.4 to 0. This indicated an absence of significant modal effects for any axial location of the source. However, for a solution height of 15.2 cm, this variation with height was significant ($\Delta k = 0.15$) and indicated a strong dependence on modal effects related to the location of the source. Because this effect depends also on whether the source was above or below the center of the solution, streaming effects in the Lexan tube were also significant.

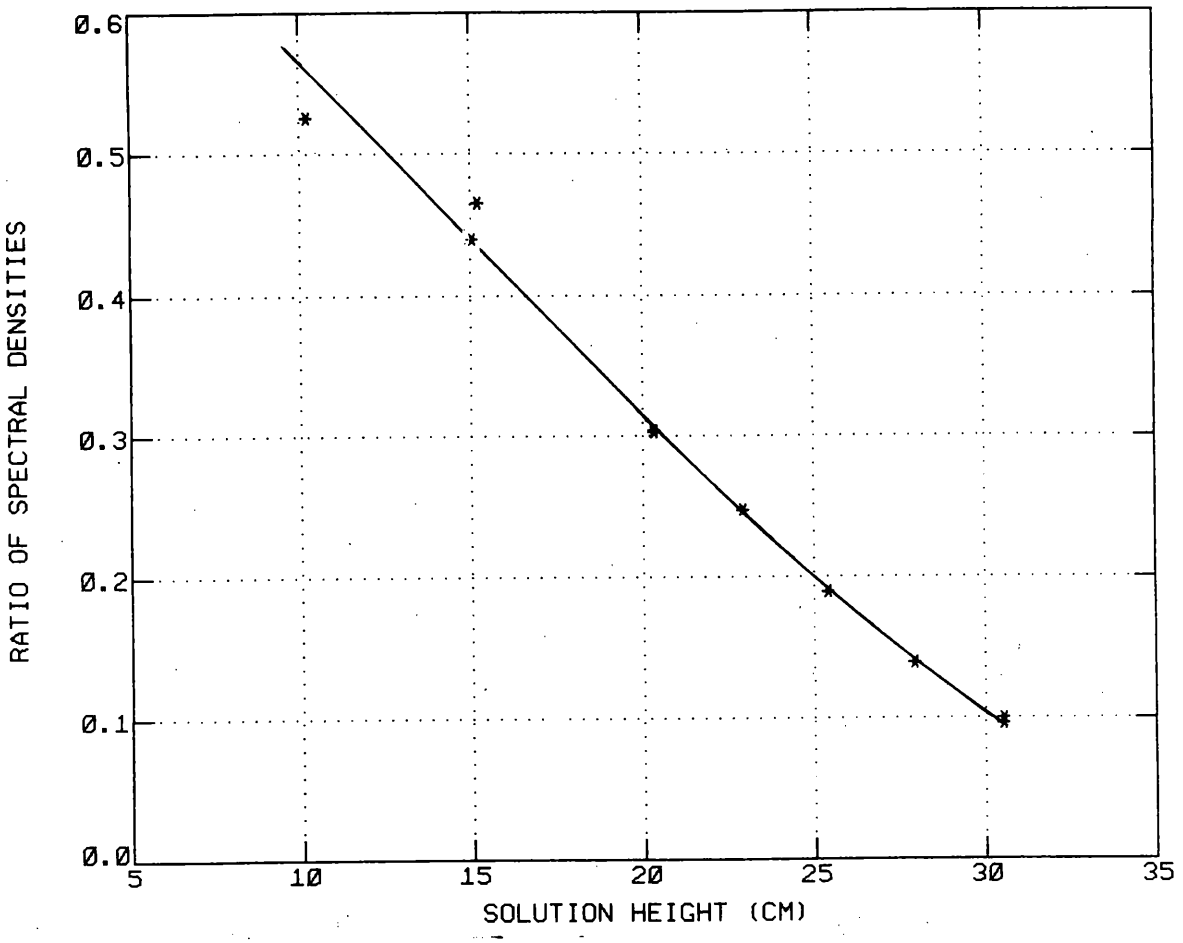

Fig. 7. Ratio of spectral densities at low frequency versus solution height from static measurements with ^{3}He detectors and a central source.

Table 3. Neutron multiplication factors for various solution heights from measurements with ^{3}He proportional counters and a central source

Solution height (cm)	Neutron multiplication factor, k_{eff}	
	measurement	calculation[a]
30.5	0.963,0.964	0.950
27.9	0.945	0.916
25.4	0.919	0.896
22.9	0.884	0.870
20.3	0.843,0.843	0.831
15.2	0.679,0.704[b]	0.721
10.2	0.570	0.547

[a]Monte Carlo using Hansen-Roach cross sections with the effects of the source materials included.

[b]The first entry in Table 2 for a solution height of 15.2 cm is not included here because much better statistics on the ratio of spectral densities are found for the second entry for this height in Table 2 and the value in Table 4.

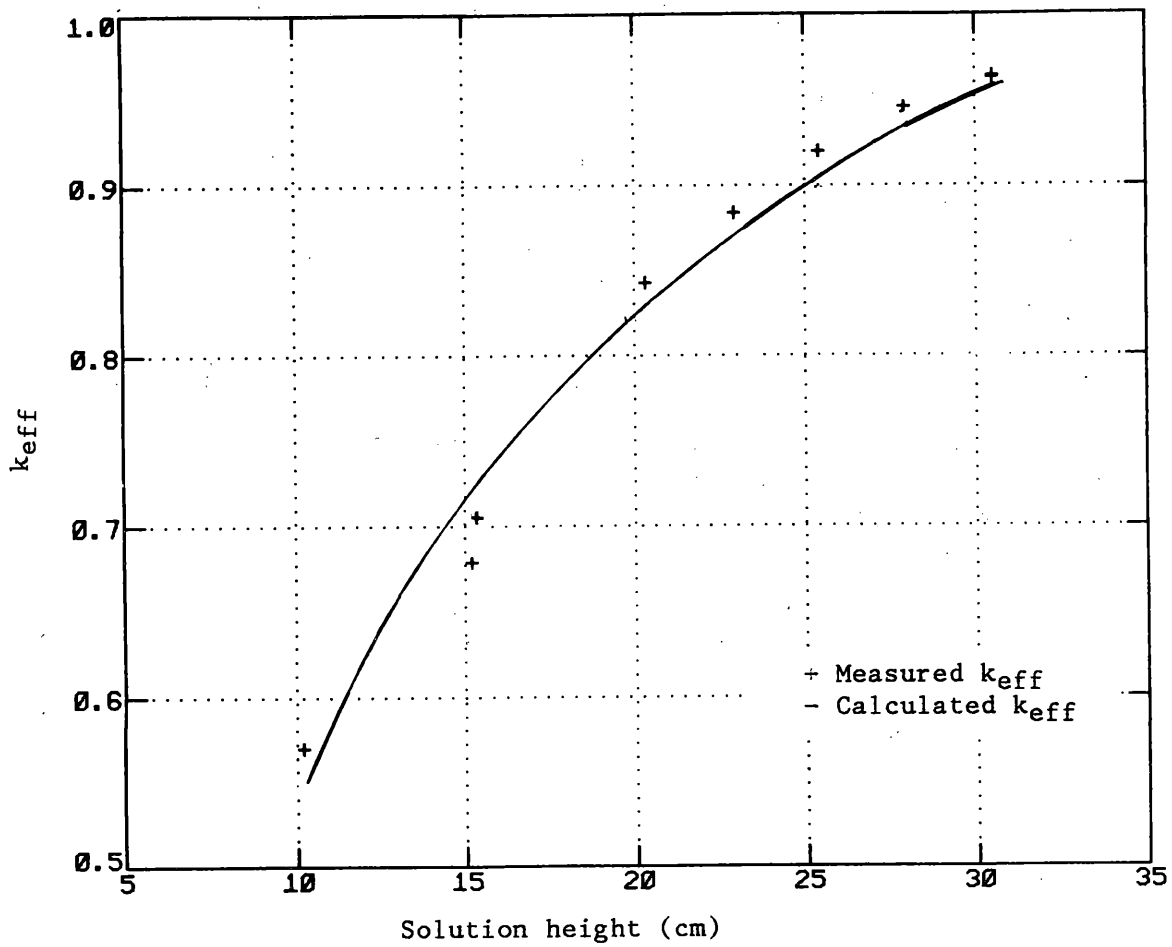

Fig. 8. Neutron multiplication factor versus solution height from static measurements with ^{3}He detectors and a central source.

Table 4. Ratios of spectral densities, $G^{*}_{12}G_{13}/G_{11}G_{23}$, at low frequency as a function of source height for a solution height of 15.2 cm

Source height (cm)	Ratio of spectral densities[a] (10^{-4})	Upper limit of frequency for ratio (kHz)	Number of data samples (10^3)
15.2	2980 ± 46	8	480
14.0	3590 ± 80	8	400
12.7	4090 ± 60	7	280
10.2	4364 ± 100	10	200
7.6	4442 ± 71	8	360
5.1	4128 ± 60	7	320
2.5	3680 ± 60	8	320
1.3	3180 ± 40	10	1160
0.0	2725 ± 20	10	5920

[a]The bandwidth of the measurements was 50 kHz. The precision given is one standard deviation of the mean. All measurements were performed with ^{3}He detectors.

Table 5. Ratios of spectral densities, $G_{12}^{*}G_{13}/G_{11}G_{23}$, at low frequency as a function of source height from static measurements for a solution height of 20.3 cm

Source height (cm)	Ratio of spectral densities[a] (10^{-4})	Upper limit of frequency for ratio (kHz)	Number of data samples (10^3)
20.3	1476 ± 22	3	160
19.1	2303 ± 22	3	160
17.8	2648 ± 24	8	160
16.5	2843 ± 30	8	200
16.5	2804 ± 28	4	120
15.2	2876 ± 18	2.5	200
12.7	3031 ± 19	4	200
10.2	3032 ± 27	4	160
7.6	2969 ± 23	4	200
5.1	2685 ± 18	4	200
3.8	2452 ± 22	3	160
2.5	2169 ± 19	2	200
1.3	1944 ± 17	4	160
0.0	1578 ± 19	3	160

[a]The bandwidth of the measurements is 5.0 kHz except for the measurements with a source height of 20.3, 19.1, 17.8, and 16.5 cm where it was 50 kHz. The precision given is one standard deviation of the mean. All measurements were with ^{3}He detectors.

Table 6. Ratios of spectral densities, $G_{12}^{*}G_{13}/G_{11}G_{23}$, at low frequency as a function of source height for a solution height of 25.4 cm

Source height (cm)	Ratio of spectral densities[a] (10^{-4})	Upper limit of frequency range for the ratio (kHz)	Number of data samples (10^3)
25.4	654 ± 1	2.5	1200
24.1	857 ± 4	3.5	200
24.1	854 ± 4	2	200
22.86	1078 ± 5	3	200
22.86	1073 ± 9	2	160
20.32	1395 ± 9	3	160
17.78	1662 ± 7	4	160
12.7	1842 ± 3	1	160
7.6	1751 ± 5	4	280
5.1	1536 ± 6	4	280
2.5	1229 ± 7	4	200

[a]The bandwidth of the measurement was 50 kHz. The precision given is one standard deviation of the mean. All measurements were made with ^{3}He detectors.

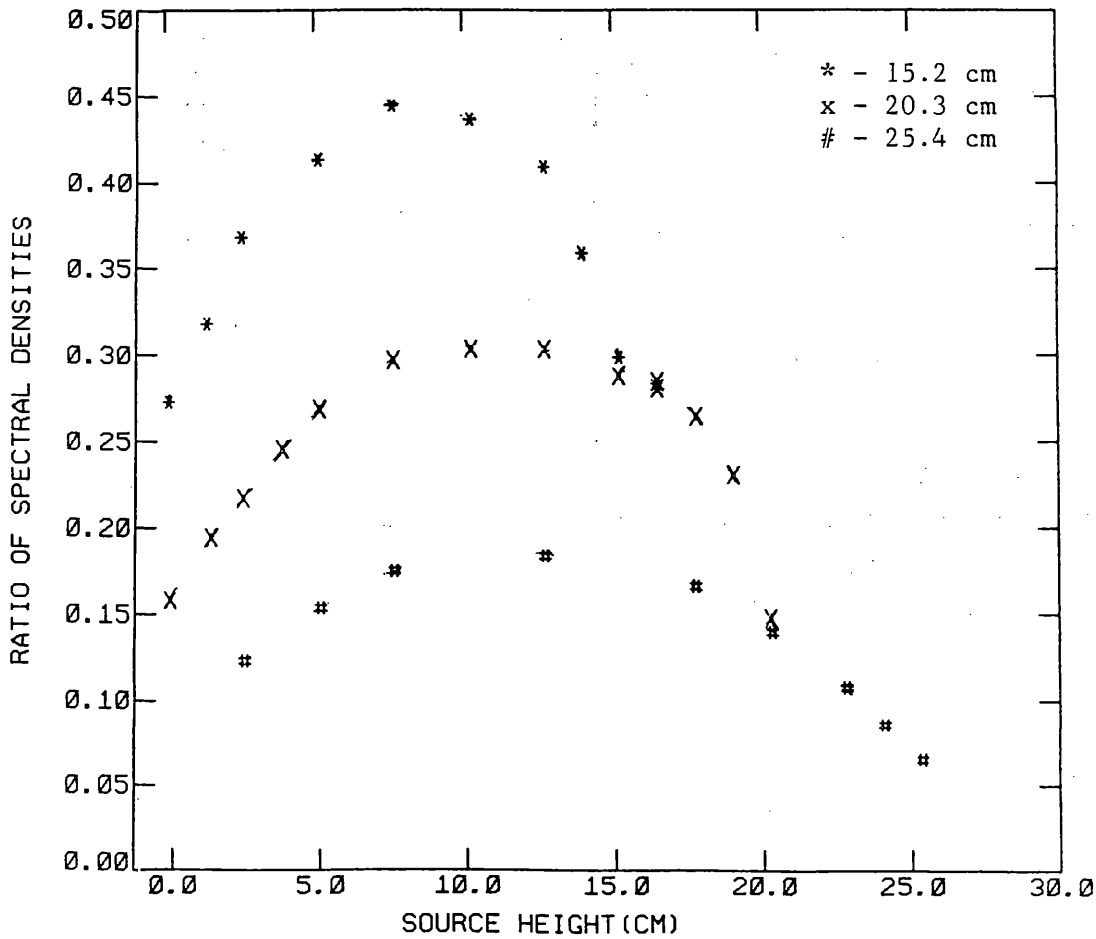

Fig. 9. Ratios of spectral densities at low frequency as a function of source height for solution heights of 15.2, 20.3, and 25.4 cm.

Table 7. k_{eff} values from ratios of spectral densities at low frequency using point kinetic interpretation for solution heights of 15.2, 20.3, and 25.4 cm for a variety of axial heights of the source

Source height[a] (cm)	k_{eff} from ratio of spectral densities for solution heights		
	25.4 cm	20.3 cm	15.2 cm
25.4	0.896	-	-
24.1	0.906, 0.906[b]	-	-
22.9	0.911, 0.912[b]	-	-
20.3	0.914	0.790	-
19.1	-	0.757	-
17.8	0.915	0.771	-
16.5	-	0.787, 0.791[b]	-
15.2	-	0.817	0.597
14.0	-	-	0.630
12.7	0.920[c]	0.832	0.636
10.2	-	0.843[c]	0.691
7.6	0.922	0.842	0.704[c]
5.1	0.918	0.847	0.738
3.8	-	0.856	
2.5	0.919	0.860	0.740
1.3	-	0.852	0.752
0.0	-	0.854	0.753
Calculated[d] keff	0.895	0.831	0.721

[a]Distance from the bottom of the solution. All measurements are with the detectors and are given in Tables 4-6.
[b]Repeated measurements.
[c]Source at the center of solution.
[d]See Appendix D for details.

6.3 VARYING SOLUTION HEIGHT WITH THE SOURCE AT THE BOTTOM OF THE SOLUTION

These static measurements were performed with both ^{6}Li-glass-plastic scintillators and ^{3}He detectors located as they were for the dynamic measurements as follows: The ^{6}Li-glass-plastic scintillation detectors were located as shown in Fig. 6; the ^{3}He detectors were located as shown in Fig. 4, except that two ^{3}He detectors were located on each side of the tank and the signals summed for each detection channel in the noise

analysis system. The scintillators were used in channels 2 and 3, while the summed ^{3}He detectors were used as channels 4 and 5 for noise analysis. The ratios of spectral densities at low frequency for both types of detectors are given in Table 8. For low solution heights (<10 cm), statistically meaningful measurements with the ^{3}He proportional counters were not practical because of the low detection efficiency of the ^{3}He proportional counters. Where measurements with ^{3}He detectors were practical, the k_{eff} values agreed with those from measurements with the scintillators. Values of k_{eff} from these static measurements of the ratios of spectral densities at low frequency were obtained using point kinetics interpretation of the data without correction for modal effects. Values are plotted as a function of solution height in Fig. 10, in which they are compared with the results of calculations using the KENO Monte Carlo code with Hansen-Roach cross sections (Appendix D). The calculations included the detectors as located in the experiments. The change in k_{eff} values from the reflection effect of the detectors was evaluated experimentally, and the results, given in Appendix E, show that the reflection effect of the scintillators is about 0.015 in k_{eff} value. There is agreement between the calculations and the experiment for all k_{eff} values, even as low as ~0.3. For this source-detector configuration, point kinetics interpretation of the low-frequency ratio of spectral densities is adequate although the source is at the bottom of the tank. The scintillation detectors, because they are also sensitive to gamma rays from fission, view a larger volume of the solution since the gamma ray attenuation properties of aqueous solution are not as good as the neutron attenuation. The location of the scintillators on the bottom of the tank is also a favorable location for solution heights comparable to or smaller than the scintillator height (15.2 cm). These two effects enhance the applicability of point kinetics for interpretation of the data.

Table 8. Ratios of spectral densities at low frequency and neutron multiplication factors from static measurements with the source at the bottom of the solution

Solution height (cm)	Ratio of spectral densities[a]		Neutron multiplication factors, k_{eff}[b]		Number of data blocks (10^3)
	^{3}He detectors (10^{-4})	Scintillators (10^{-4})	^{3}He detectors	Scintillators	
29.2	453 ± 12 (5)	436 ± 5 (2)	0.952 ± 0.002	0.954 ± 0.001	20
25.8	767 ± 40 (5)	774 ± 20 (2)	0.924 ± 0.005	0.923 ± 0.003	20
20.3	1590 ± 20 (5)	1616 ± 10 (6)	0.853 ± 0.005	0.850 ± 0.005	20
15.3	2896 ± 90 (5)	2843 ± 10 (10)	0.732 ± 0.015	0.738 ± 0.010	40
10.1	4508 ± 90 (5)	4477 ± 60 (10)	0.535 ± 0.030	0.540 ± 0.027	20
9.8	--	4723 ± 60 (10)	--	0.505 ± 0.030	7
9.0	--	4960 ± 60 (10)	--	0.472 ± 0.035	100
7.5	--	5293 ± 210 (10)	--	0.414 ± 0.055	40
6.5	--	5650 ± 60 (10)	--	0.346 ± 0.049	60
5.7	--	5943 ± 360 (10)	--	0.278 ± 0.097	55

[a]Values in parentheses are the upper limit of the frequency range in kHz over which the ratio was averaged. The precision given is one standard deviation of the mean.

[b]Uncertainties are statistical precision of the ratio of spectral densities and uncertainties in the parameters of Appendix C. The largest contribution to the uncertainty was from I_c/I (e.g., 80% of the uncertainty for a solution height of 6.5 cm). All tables in this report other than Tables 8 and 9 have uncertainties from the precision of the ratio of spectral densities only.

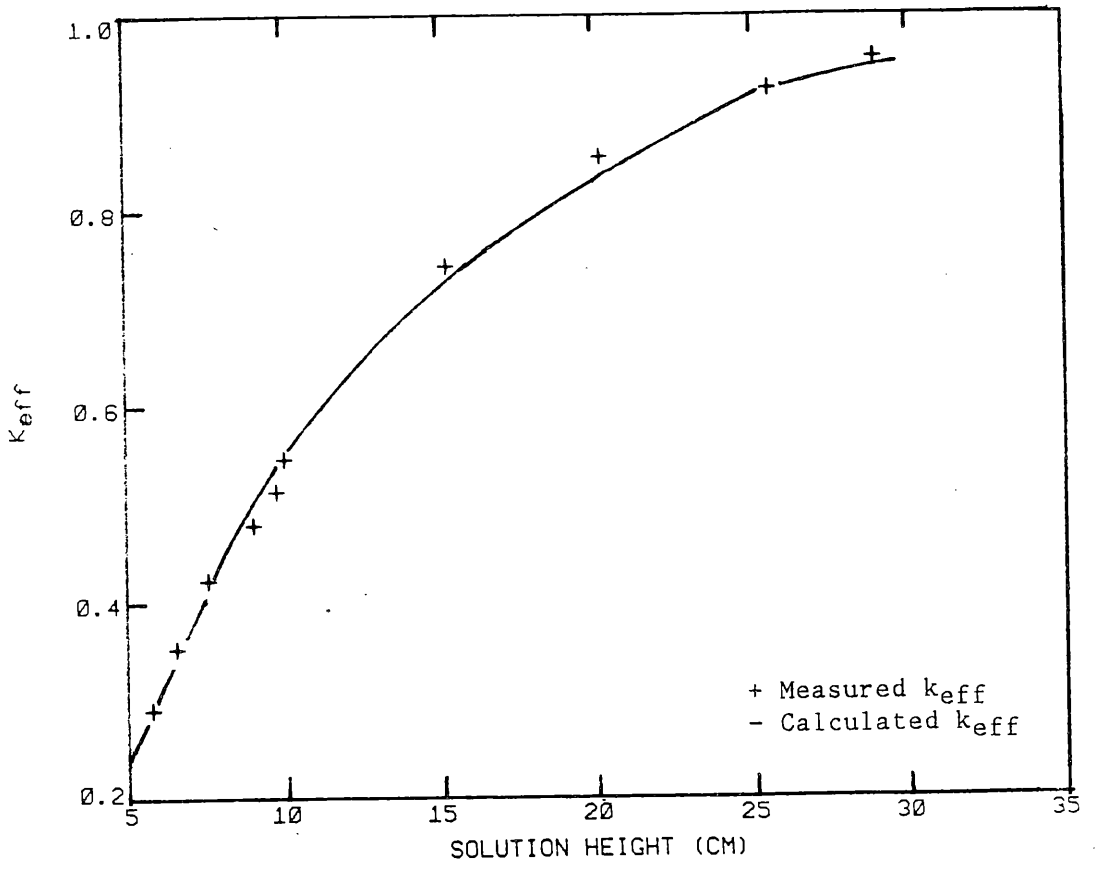

Fig. 10. K_{eff} values as a function of solution height from measurements with the Cf source on the bottom of the tank.

7. DYNAMIC MEASUREMENTS OF THE RATIOS OF SPECTRAL DENSITIES AND NEUTRON MULTIPLICATION FACTORS

Dynamic experiments were performed while the experimental vessel was drained at a variety of rates, while it was being filled, and also while air bubbles were passing through the solution. For many of these measurements, the ^{252}Cf neutron source was located on the axis of the experimental vessel at the bottom. This source location is typical of one which is practical for in-plant applications. The detectors were identical pairs of ^{6}Li-glass-plastic scintillators located on opposite sides of the vessel as shown in Fig. 6. The solution height was changed at rates varying from ~1 cm/min to ~23 cm/min with corresponding changes in the neutron multiplication factor, Δk_{eff}, varying from ~0.03/min to ~0.01/s. These experiments were performed with a variety of measurement times varying from 102 to 6.4 s. After each measuring interval, the average measured ratios of spectral densities at low frequency for the measuring interval were interpreted and the resulting neutron multiplication factor displayed on-line on the computer terminal (i.e., immediately after the data accumulation). Typical on-line data obtained and the results of interpretation obtained during the dynamic measurements are shown in the Appendix F. Listed are the times, solution heights, measured ratios of spectral densities averaged up to 5 kHz for all heights with the measured statistical uncertainty, and the neutron multiplication factors and their statistical uncertainty.

The detector and source locations were chosen so that measurements for all solution heights could be meaningfully interpreted using point kinetics. Initially, the scintillation detector pairs were located with one on top of the other rather than side by side as shown in Fig. 6. In this case the total height of the scintillation detector pair was ~31 cm, which was slightly greater than the solution height with the center of one detector of the pair at 8 cm above the bottom of the solution and the center of the top detector ~21 cm above the bottom of the experimental vessel. In the upright location for low solution heights (<15 cm) the top detectors of each pair had no solution between them, and most particles arriving at the detectors came from the top of the solution. When it was realized that the detection efficiency was such that measurements at very low solution heights were possible, the pairs of detectors were rotated 90° so that the centers of both detectors of each pair were about 8 cm above the bottom of the solution rather than one at 8 cm and the other at 21 cm. The planes defined by the front surfaces of the detector pairs were 2.5 cm from the outside of the acrylic tank. Some measurements for limited heights were also performed with ^{3}He detectors located as shown in Fig. 4, except that a pair of detectors was located on each side of the tank.

7.1 FILLING THE EXPERIMENTAL VESSEL

Measurements were performed with the ^{252}Cf source on the bottom of the solution while the vessel was filled. Because of safety limitations on the addition of solution to the experimental vessel, the solution addition rate was a maximum of ~1 cm of solution height per minute. For this experiment the vessel was filled from 6.5 cm to 27.6 cm, and the data accumulation rates were such that 102 s of data were accumulated by the Fourier analyzer before uploading the data file to the VAX computer. The data file consisted of APSDs and CPSDs from which the VAX computer formed the ratio of spectral densities and then interpreted this ratio using a point kinetics model with prestored values of I_c/I and R as functions of solution height and other parameters to obtain the neutron multiplication factors. The APSDs, CPSDs, and ratios of spectral densities from these measurements are given in Appendix G (Figs. G.1-G.16).

At data accumulation intervals of 102 s, the measured ratios of spectral densities and the corresponding neutron multiplication factors were displayed as on-line computer output. Visual examination of the data shows that the frequency range over which the ratios of spectral densities are constant varies with solution height. This was expected because modal effects vary with solution height, as does the frequency response of the system, $H(\omega)$. Visual examination of the data showed that for solution heights up to 20 cm, the ratio of spectral densities was constant up to a frequency of ~10 kHz. For solution heights between 20 and 25 cm, the ratio is approximately constant up to 6 kHz; for solution heights >25 cm, the ratio is approximately constant up to 2.5 kHz. The results of interpretation of the data, which was performed on-line during the measurement, are shown in Appendix G. The ratios of spectral densities in Table G.1 were averaged over frequencies up to 5 kHz independent of solution height.

The data from this experiment were re-evaluated using values of I_c/I, R, and other parameters of Appendix C along with averaging over a frequency range which varies with height. The results of these interpretations are given in Table 9. The results of the interpretation with the re-evaluated parameters were only slightly different (less than 0.01 for k_{eff} values >0.50) from the results obtained during the experiments (Table G.1.). The ratio of spectral densities at low frequency is plotted as a function of solution height in Fig. 11 and the k_{eff} value as a function of solution height in Fig. 12. Measured values during the filling of the vessel agree with those from the static measurements described above. The calculated values are compared to the measured values, also, in Fig. 12. The calculated values (Appendix D) agree with those measured. The statistical uncertainty in the measured ratio of spectral densities is sufficiently small that the statistical precision in the measured neutron multiplication factor varies from ~0.01 at the lowest k_{eff} (~0.31) to <0.001 at higher k_{eff} values (0.93).

Table 9. Ratios of spectral densities at low frequency and neutron multiplication factors for dynamic measurements while filling the experimental vessel

Time[a] (h:m:s)	Solution height[b] (cm)	Ratio of spectral densities[c]	k_{eff} from ratio of spectral densities[d]
14:47:04	6.45	0.566 ± 0.006	0.348 ± 0.049
14:48:46	6.46	0.571 ± 0.016	0.338 ± 0.059
14:50:29	6.46	0.559 ± 0.005	0.362 ± 0.047
14:52:12	6.61	0.562 ± 0.005	0.356 ± 0.047
14:53:53	7.36	0.551 ± 0.004	0.376 ± 0.048
14:55:34	8.50	0.513 ± 0.004	0.443 ± 0.038
14:57:16	9.88	0.462 ± 0.002	0.522 ± 0.027
14:58:58	11.44	0.414 ± 0.002	0.588 ± 0.021
15:00:39	13.08	0.354 ± 0.002	0.662 ± 0.015
15:02:20	14.75	0.298 ± 0.001	0.723 ± 0.011
15:04:02	16.54	0.249 ± 0.001	0.771 ± 0.008
15:05:44	18.36	0.204 ± 0.001	0.812 ± 0.006
15:07:25	20.17	0.167 ± 0.001	0.845 ± 0.005
15:09:06	22.01	0.135 ± 0.001	0.872 ± 0.004
15:10:47	23.84	0.107 ± 0.001	0.896 ± 0.003
15:12:29	25.70	0.079 ± 0.001	0.921 ± 0.002
15:14:11	27.59	0.058 ± 0.001	0.940 ± 0.002

[a]End of a measurement time interval of ~102 s over which the data were averaged and then the interpreted results displayed on the terminal. This time does not correspond to the average height during the measurement interval, but rather to the height at the end of the interval. The time that corresponds to the average height can be obtained by averaging the time listed with the time at the end of the previous interval.

[b]Average height of solution during the time interval of the measurement, which ends at the time given in Col. 1.

[c]Average value during the time interval of the measurement. The statistical uncertainty given here is one standard deviation of the mean. The ratio of spectral densities was averaged up to a frequency of 10 kHz for heights <20 cm, 6 kHz for heights of 20 to 25 cm, and 2 kHz for heights of >25 cm. The number of points per data block was 1024, and 20,000 data blocks were averaged in ~102 s with a sampling rate of ~200 kHz.

[d]The uncertainty in k_{eff} is from the statistical uncertainty in the ratio of spectral densities and uncertainties in the parameters of Appendix C. The largest contribution to the uncertainty was from I_c/I (80 and 55% of the uncertainty for solution heights of 6.45 and 27.6, respectively). All tables in this report other than Tables 8 and 9 have uncertainties in k_{eff} from the precision of the ratio of spectral densities only.

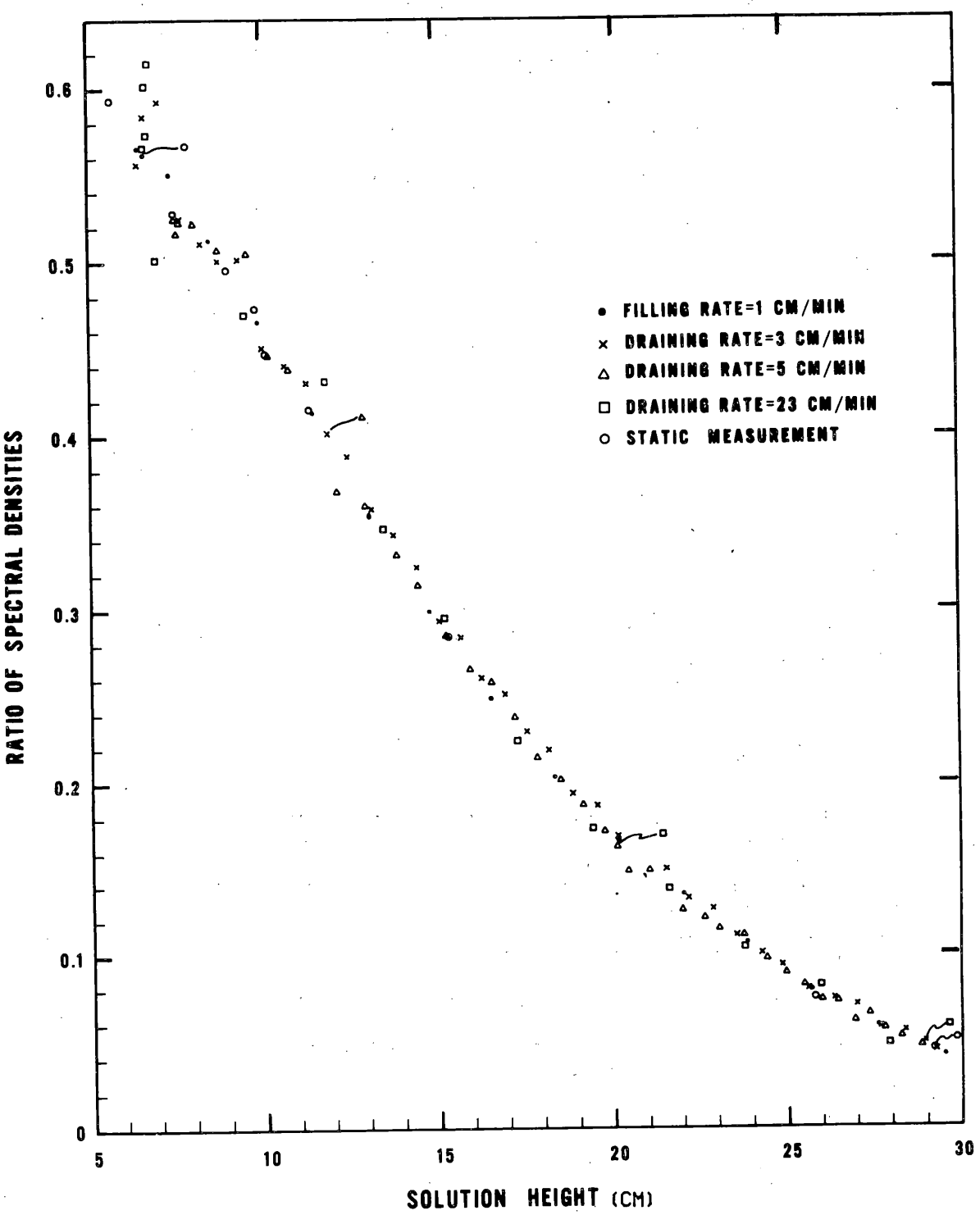

Fig. 11. Ratios of spectral densities at low frequency as a function of solution height for dynamic measurements.

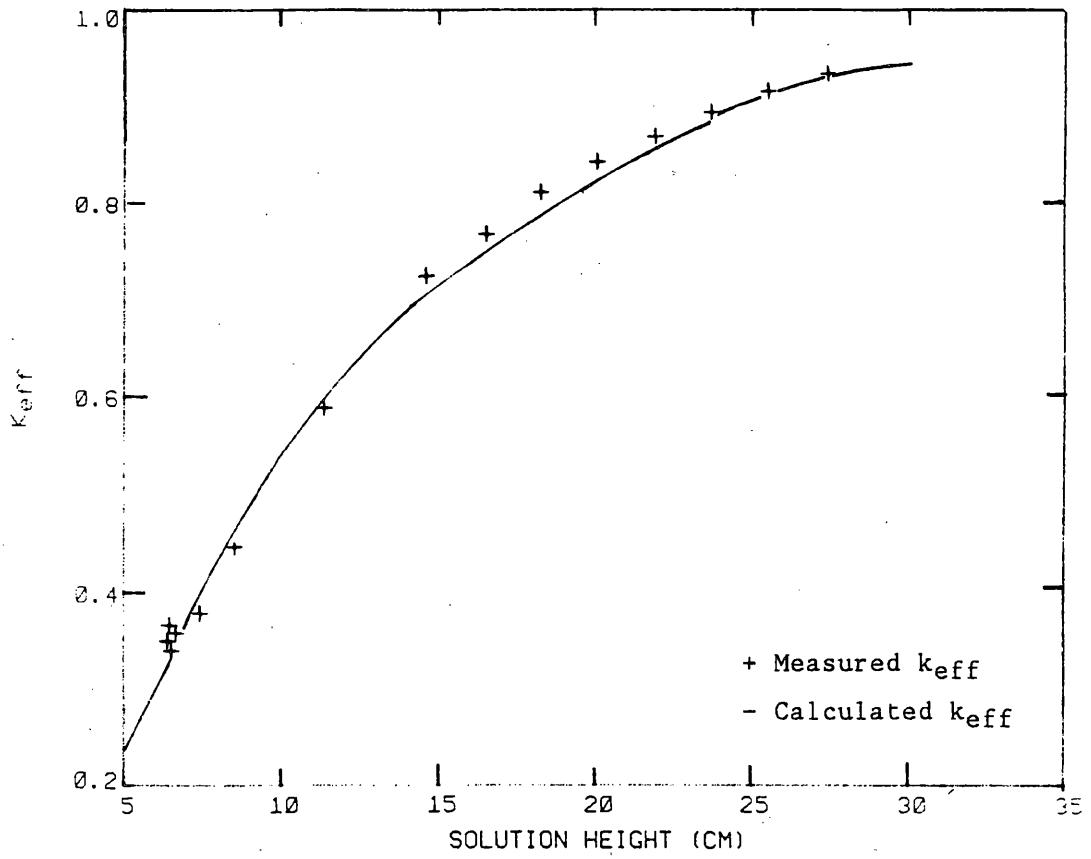

Fig. 12. Neutron multiplication factor versus solution height from measurements while the solution height was increasing at a rate of 1 cm/min with the Cf source at the bottom of the solution.

The first three entries of Table 9 are for the same solution height. Intercomparison of these three measurements (102 s of data accumulation time) shows that the ratios and the resulting neutron multiplication factors are reproducible even at k_{eff} values as low as ~0.35. Measurements with this precision are possible because of the high detection efficiency of the scintillators, which detect thermal neutrons, fast neutrons, and gamma rays from fission. This high detection efficiency results in large coherence values and short measurement times. The square of the coherences at low frequency between one scintillator channel and the Cf source, γ^2_{12}, and that between the two scintillator channels, γ^2_{23}, are plotted in Fig. 13 as a function of solution height. The squared coherence values at low frequency at the lowest solution height of 6.5 cm are $\gamma^2_{12} = 0.045$ and $\gamma^2_{23} = 0.01$, while those for a solution height of 27.6 cm are $\gamma^2_{12} = 0.045$ and $\gamma^2_{23} = 0.9$. As in previous measurements,[1] γ^2_{12} is not as strong a function of subcriticality as γ^2_{23}.

7.2 DRAINING THE EXPERIMENTAL VESSEL

The experimental vessel was drained at three different draining rates with the source on the bottom of the tank. The fastest rate was such that the height varied from 29.5 to 6.5 cm in ~60 s. This limit on the draining rate resulted from the 1.27-cm-diam opening in the bottom of the tank. Other draining rates were such that the height of solution changed 3 and 5 cm per min.

7.2.1 Draining at a Rate of 3 cm/min

For this experiment the Cf source was at the bottom of the solution and the draining rate resulted in a reduction in the solution height of ~3 cm/min, which corresponded to a change in k_{eff} of ~8×10^{-3}/min. The solution height varied continuously from 29.2 to 6.5 cm. For this draining rate, the data accumulation time before the Fourier processor uploaded the data to the VAX computer for interpretation was ~13 s. Thus, these data have a larger statistical error than data for filling the experimental vessel because the data accumulation time is a factor of 8 shorter. The results of data interpretation performed on-line during the measurement are given in Appendix H (Table H.1). Typical APSDs, CPSDs, and ratios of spectral densities as a function of frequency are plotted in Appendix H (Fig. H.1). These data were examined off-line to better select the upper limit of the frequency range for averaging the ratios of spectral densities. The choice of frequency range over which to determine the low-frequency ratio of spectral densities is the same as for filling the vessel. The results of the interpretation of the data using the parameters of Appendix C are given in Table 10. The results differ slightly (less than 0.01 for k_{eff} values >0.5) from those obtained during the measurements given in Table H.1. For this dynamic measurement, where only 12.8 s of data were accumulated while the solution height changed ~3 cm/min, the statistical

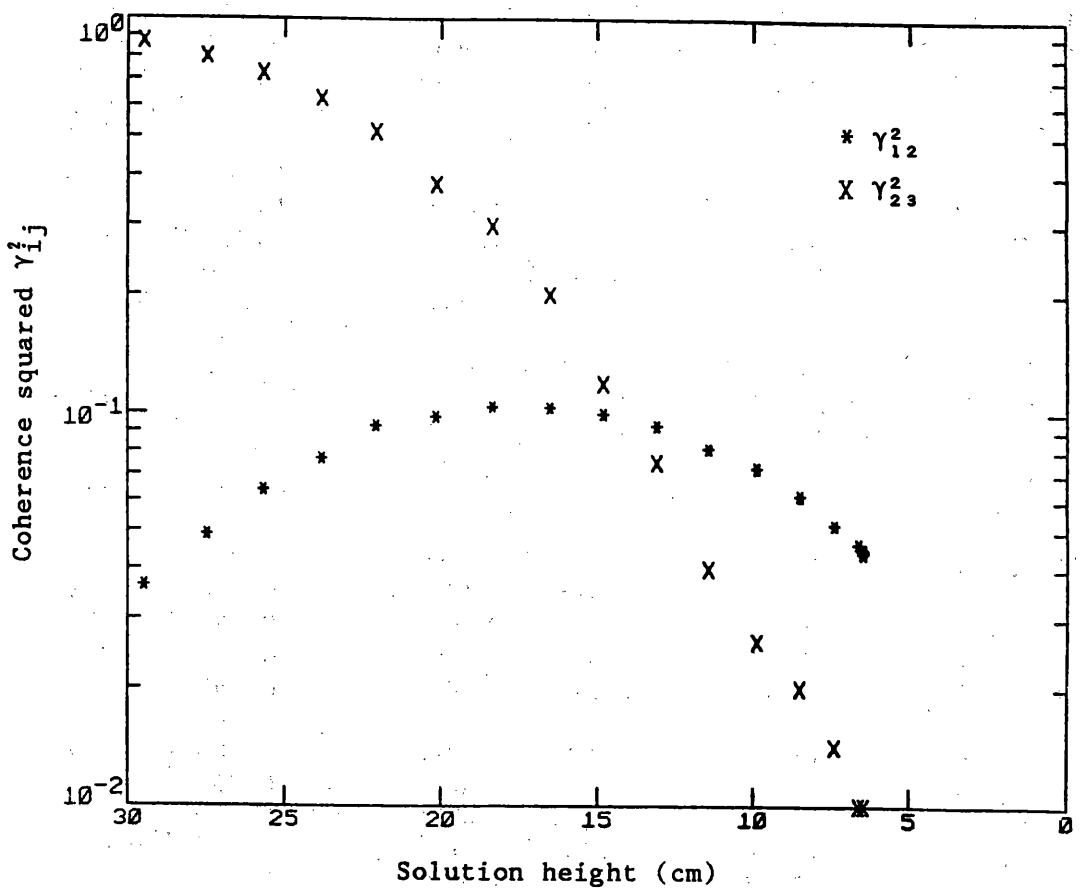

Fig. 13. Coherence squared, γ^2_{12} and γ^2_{23}, at low frequency as a function of solution height for experiments with scintillation detectors and the Cf source at the bottom of the solution.

Table 10. Ratios of spectral densities at low frequency and neutron multiplication factors for dynamic measurements while draining the experimental vessel at a rate of ~3 cm/min

Time[a] (h:m:s)	Solution height[b] (cm)	Ratio of spectral densities[c]	k_{eff} from ratio of spectral densities[d]
14:22:32	29.25	0.043 ± 0.001	0.954 ± 0.001
14:22:44	29.26	0.041 ± 0.002	0.957 ± 0.003
14:22:57	29.25	0.042 ± 0.001	0.955 ± 0.001
14:23:10	28.96	0.048 ± 0.002	0.949 ± 0.002
14:23:22	28.36	0.055 ± 0.003	0.943 ± 0.003
14:23:35	27.67	0.058 ± 0.001	0.941 ± 0.001
14:23:48	27.00	0.070 ± 0.009	0.929 ± 0.009
14:24:01	26.34	0.074 ± 0.001	0.926 ± 0.001
14:24:13	25.62	0.080 ± 0.004	0.920 ± 0.005
14:24:26	24.88	0.094 ± 0.003	0.908 ± 0.003
14:24:39	24.22	0.101 ± 0.001	0.902 ± 0.002
14:24:52	23.57	0.111 ± 0.003	0.893 ± 0.004
14:25:05	22.86	0.126 ± 0.005	0.879 ± 0.005
14:25:17	22.19	0.133 ± 0.002	0.874 ± 0.002
14:25:29	21.54	0.150 ± 0.002	0.859 ± 0.003
14:25:42	20.85	0.155 ± 0.005	0.855 ± 0.005
14:25:55	20.19	0.168 ± 0.002	0.844 ± 0.002
14:26:07	19.56	0.187 ± 0.003	0.826 ± 0.003
14:26:20	18.87	0.194 ± 0.002	0.822 ± 0.002
14:26:34	18.19	0.219 ± 0.004	0.798 ± 0.004
14:26:46	17.54	0.230 ± 0.003	0.789 ± 0.004
14:26:58	16.92	0.252 ± 0.003	0.767 ± 0.003
14:27:11	16.28	0.261 ± 0.003	0.760 ± 0.004
14:27:23	15.66	0.284 ± 0.004	0.737 ± 0.004
14:27:36	15.05	0.294 ± 0.004	0.728 ± 0.004
14:27:49	14.44	0.324 ± 0.004	0.694 ± 0.004
14:28:02	13.78	0.343 ± 0.005	0.674 ± 0.006
14:28:15	13.12	0.358 ± 0.007	0.658 ± 0.009
14:28:28	12.48	0.389 ± 0.007	0.620 ± 0.009
14:28:40	11.85	0.402 ± 0.003	0.605 ± 0.005

Table 10 (continued)

Time[a] (h:m:s)	Solution height[b] (cm)	Ratio of spectral densities[c]	k_{eff} from ratio of spectral densities[d]
14:28:52	11.26	0.432 ± 0.008	0.564 ± 0.012
14:29:06	10.63	0.441 ± 0.009	0.554 ± 0.014
14:29:18	9.99	0.451 ± 0.008	0.542 ± 0.013
14:29:30	9.32	0.502 ± 0.011	0.460 ± 0.019
14:29:43	8.75	0.501 ± 0.011	0.465 ± 0.019
14:29:55	8.25	0.511 ± 0.013	0.449 ± 0.015
14:30:08	7.63	0.525 ± 0.012	0.425 ± 0.023
14:30:21	7.05	0.593 ± 0.012	0.291 ± 0.027
14:30:34	6.63	0.584 ± 0.020	0.311 ± 0.046
14:30:47	6.46	0.557 ± 0.021	0.368 ± 0.045
14:30:59	6.45	0.538 ± 0.015	0.404 ± 0.029
14:31:11	6.45	0.562 ± 0.022	0.358 ± 0.047
14:31:24	6.45	0.587 ± 0.019	0.305 ± 0.042
14:31:37	6.46	0.594 ± 0.032	0.289 ± 0.077

[a]End of a measurement time interval of ~12.8 s over which the data were averaged and then the interpreted results displayed on a terminal as the solution was drained. This time does not correspond to the average height during the measurement interval, but rather to the height at the end of the interval. The time which corresponds to the average height can be obtained by averaging the time listed with the time at the end of the previous interval.

[b]Average height of solution during the time interval of the measurement, which ends at the time given in Col. 1.

[c]Average value during the time interval of the measurement. The statistical uncertainty given here is one standard deviation of the mean. The ratio of spectral densities was averaged up to a frequency of 10 kHz for heights <20 cm, 6 kHz for heights of 20 to 25 cm, and 2.5 kHz for heights >25 cm. The number of points per data block was 256, and 10,000 data blocks were averaged in 12.8 s with a sampling rate of ~200 kHz.

[d]The uncertainty in k_{eff} value is from the statistical uncertainty in the ratio of spectral densities only.

uncertainties in the ratios of spectral densities are quite low at high values of the neutron multiplication factor (<0.01 down to heights of ~11 cm and k_{eff} of ~0.5). The resulting uncertainties in k_{eff} values at values of 0.32 are about 0.05, and this leads to the scatter in the data for the last five measurements of this set, which correspond to a solution height fixed at ~6.45 cm.

The ratio of spectral densities at low frequency is plotted as a function of solution height in Fig. 11. The k_{eff} values obtained from these measurements are in agreement with those from filling the vessel (Fig. 14). The k_{eff} values obtained from KENO Monte Carlo calculations with Hansen-Roach cross sections agree with the measured values and are shown in Fig. 14.

7.2.2 Draining at a Rate of 5 cm/min

The solution height in this experiment was varied continuously from 28.8 to 7.5 cm at a draining rate which corresponded to a reduction in solution height of 5 cm/min and with the Cf source at the bottom of the solution. For this draining rate, data accumulation time was ~6.4 s before the Fourier processor uploaded the data to the VAX computer for interpretation. The results of the on-line interpretation of the data during the experiment are given in Appendix I (Table I.1). Typical APSDs, CPSDs, and ratios of spectral densities also are plotted as a function of frequency in Appendix I. The results of the interpretation of the data using the parameters of Appendix C are given in Table 11 and differ only slightly (<0.01 for k_{eff} values >0.50) from the data obtained during the experiment (Table I.1). The statistical uncertainty in the k_{eff} values at a solution height of 7.5 cm is about 0.04. The ratios of spectral densities and neutron multiplication factors are plotted as a function of solution height in Figs. 11 and 14 and agree with the values for draining at a rate of 3 cm/min and for filling the vessel.

7.2.3 Draining at a Rate of 23 cm/min

For a draining rate which corresponds to a change in solution height of 23 cm/min (Δk per s $\approx$ 0.01), data accumulation time was 6.4 s before the Fourier analyzer uploaded the data to the VAX computer for interpretation. In this experiment the solution was drained continuously from 28.9 to 5.7 cm, and the source was at the bottom of the tank. The draining rate was limited by the size of the hole (1.27 cm) provided in the bottom of the tank. The results of the on-line interpretation of the data during the experiment are given in Appendix J. The APSDs, CPSDs, and ratios of spectral densities are also plotted as a function of frequency in Fig. J.1. The results of the interpretation of the data using the parameters of Appendix C are given in Table 12 and are only slightly different (<0.01 for k_{eff} values >0.5)

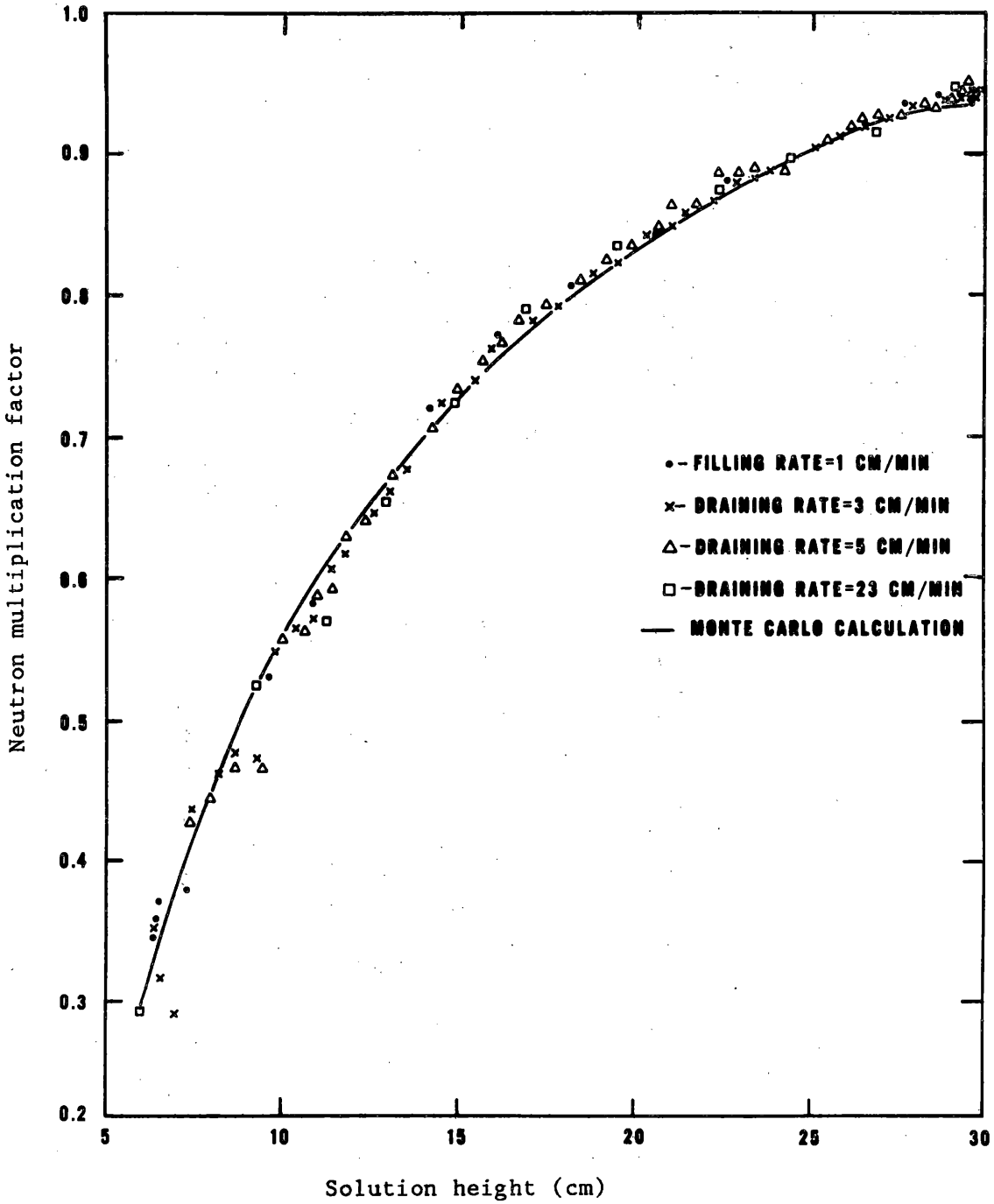

Fig. 14. Neutron multiplication factor versus solution height for dynamic measurements with the Cf source at the bottom of the tank.

Table 11. Ratios of spectral densities at low frequency and neutron multiplication factors for dynamic measurements while draining the experimental vessel at a rate of 5 cm/min

Time[a] (h:m:s)	Solution height[b] (cm)	Ratio of spectral densities[c]	k_{eff} from ratio of spectral densities[d]
16:10:36	28.88	0.046 ± 0.002	0.951 ± 0.002
16:10:42	28.88	0.051 ± 0.004	0.946 ± 0.004
16:10:49	28.88	0.046 ± 0.001	0.952 ± 0.001
16:10:55	28.88	0.044 ± 0.001	0.954 ± 0.001
16:11:01	28.87	0.052 ± 0.003	0.946 ± 0.003
16:11:08	28.65	0.045 ± 0.004	0.953 ± 0.004
16:11:14	28.23	0.052 ± 0.002	0.946 ± 0.002
16:11:20	27.80	0.056 ± 0.003	0.942 ± 0.003
16:11:27	27.36	0.065 ± 0.001	0.934 ± 0.001
16:11:33	26.91	0.061 ± 0.001	0.938 ± 0.002
16:11:39	26.45	0.072 ± 0.004	0.927 ± 0.004
16:11:46	25.96	0.073 ± 0.002	0.927 ± 0.003
16:11:52	25.46	0.082 ± 0.001	0.919 ± 0.001
16:11:58	24.94	0.089 ± 0.001	0.912 ± 0.001
16:12:05	24.40	0.097 ± 0.002	0.906 ± 0.002
16:12:11	23.72	0.111 ± 0.002	0.892 ± 0.002
16:12:17	23.11	0.115 ± 0.001	0.891 ± 0.001
16:12:23	22.62	0.122 ± 0.002	0.885 ± 0.002
16:12:29	21.95	0.126 ± 0.006	0.882 ± 0.006
16:12:36	21.08	0.149 ± 0.002	0.861 ± 0.003
16:12:42	20.41	0.149 ± 0.004	0.863 ± 0.004
16:12:49	20.12	0.163 ± 0.004	0.850 ± 0.004
16:12:55	19.72	0.172 ± 0.004	0.842 ± 0.005
16:13:02	19.14	0.187 ± 0.002	0.828 ± 0.002
16:13:08	18.50	0.202 ± 0.005	0.815 ± 0.005
16:13:14	17.84	0.215 ± 0.004	0.804 ± 0.005
16:13:21	17.20	0.238 ± 0.007	0.782 ± 0.008
16:13:27	16.55	0.258 ± 0.003	0.763 ± 0.004
16:13:33	15.91	0.266 ± 0.003	0.756 ± 0.004
16:13:40	15.25	0.285 ± 0.004	0.737 ± 0.004

Table 11 (continued)

Time[a] (h:m:s)	Solution height[b] (cm)	Ratio of spectral densities[c]	k_{eff} from ratio of spectral densities[d]
16:13:46	14.48	0.314 ± 0.008	0.707 ± 0.009
16:13:52	13.83	0.332 ± 0.006	0.688 ± 0.008
16:14:59	12.97	0.360 ± 0.005	0.657 ± 0.007
16:14:05	12.13	0.368 ± 0.009	0.639 ± 0.012
16:14:11	11.82	0.411 ± 0.008	0.592 ± 0.011
16:14:18	11.38	0.415 ± 0.009	0.589 ± 0.014
16:14:24	10.74	0.439 ± 0.009	0.557 ± 0.014
16:14:30	10.13	0.446 ± 0.007	0.548 ± 0.011
16:14:37	9.51	0.505 ± 0.010	0.455 ± 0.018
16:14:44	8.78	0.507 ± 0.023	0.454 ± 0.042
16:14:50	8.06	0.522 ± 0.017	0.429 ± 0.031
16:14:57	7.67	0.523 ± 0.013	0.428 ± 0.024
16:15:04	7.56	0.517 ± 0.016	0.442 ± 0.030
16:15:10	7.54	0.525 ± 0.021	0.427 ± 0.040
16:15:16	7.56	0.518 ± 0.017	0.440 ± 0.031
16:15:22	7.54	0.549 ± 0.016	0.381 ± 0.032
16:15:29	7.52	0.547 ± 0.021	0.385 ± 0.042
16:15:36	7.53	0.491 ± 0.011	0.486 ± 0.018
16:15:42	7.54	0.549 ± 0.020	0.381 ± 0.041

[a]End of a measurement time interval of ~6.4 s over which the data were averaged and then the interpreted results displayed on a terminal. This time does not correspond to the average height during the measurement interval, but rather to the height at the end of the interval. The time which corresponds to the average height can be obtained by averaging the time listed with the time at the end of the previous interval.

[b]Average height of solution during the time interval of the measurement, which ends at the time given in Col. 1.

[c]Average value during the time interval of the measurement. The statistical uncertainty given here is one standard deviation of the mean. The ratio of spectral densities was averaged up to a frequency of 10 kHz for heights <20 cm, 6 kHz for heights of 22 to 25 cm, and 2.5 kHz for heights of >25 cm. The number of points per data block was 256, and 5,000 data blocks were averaged in ~6.4 s with a sampling rate of ~200 kHz.

[d]The uncertainty in k_{eff} is from the statistical uncertainty in the ratio of spectral densities only.

Table 12. Ratios of spectral densities at low frequency and neutron multiplication factors for dynamic measurements while draining the experimental vessel at a rate of 23 cm/min

Time[a] (h:m:s)	Solution height[b] (cm)	Ratio of spectral densities[c]	k_{eff} from ratio of spectral densities[d]
16:50:60	28.91	0.049 ± 0.001	0.948 ± 0.001
16:51:07	28.91	0.047 ± 0.002	0.950 ± 0.002
16:51:14	28.91	0.041 ± 0.002	0.957 ± 0.002
16:51:20	28.88	0.046 ± 0.003	0.951 ± 0.003
16:51:26	27.96	0.047 ± 0.002	0.952 ± 0.002
16:51:33	25.97	0.082 ± 0.003	0.918 ± 0.003
16:51:39	23.77	0.104 ± 0.003	0.900 ± 0.003
16:51:45	21.59	0.138 ± 0.003	0.871 ± 0.002
16:51:51	19.42	0.173 ± 0.003	0.842 ± 0.003
16:51:58	17.30	0.224 ± 0.003	0.796 ± 0.003
16:52:04	15.22	0.295 ± 0.004	0.726 ± 0.005
16:52:10	13.49	0.347 ± 0.007	0.670 ± 0.008
16:52:16	11.81	0.432 ± 0.010	0.562 ± 0.015
16:52:23	9.49	0.470 ± 0.010	0.513 ± 0.017
16:52:30	6.93	0.502 ± 0.015	0.469 ± 0.026
16:52:36	5.69	0.602 ± 0.036	0.269 ± 0.086
16:52:42	5.68	0.566 ± 0.030	0.347 ± 0.066
16:52:48	5.71	0.574 ± 0.031	0.329 ± 0.068
16:52:55	5.73	0.615 ± 0.041	0.237 ± 0.104
16:53:01	5.72	0.613 ± 0.032	0.243 ± 0.080
16:53:07	5.72	0.620 ± 0.030	0.227 ± 0.075
16:53:14	5.72	0.553 ± 0.020	0.373 ± 0.042
16:53:20	5.72	0.639 ± 0.041	0.129 ± 0.112
16:53:26	5.72	0.571 ± 0.030	0.336 ± 0.065
16:53:33	5.72	0.618 ± 0.043	0.229 ± 0.111

Table 12 (continued)

Time[a] (h:m:s)	Solution height[b] (cm)	Ratio of spectral densities[c]	k_{eff} from ratio of spectral densities[d]
16:53:39	5.70	0.572 ± 0.022	0.332 ± 0.047
16:53:45	5.70	0.518 ± 0.022	0.440 ± 0.042
16:53:52	5.70	0.602 ± 0.033	0.269 ± 0.080
16:53:58	5.73	0.616 ± 0.025	0.236 ± 0.063

[a]End of a measurement time interval of ~6.4 s over which the data were averaged and then the interpreted results displayed on a computer terminal. This time does not correspond to the average height during the measurement interval, but rather to the height at the end of the interval. The time which corresponds to the average height can be obtained by averaging the time listed with the time at the end of the previous interval.

[b]Average height of solution during the time interval of the measurement, which ends at the time given in Col. 1.

[c]Average value during the time interval of the measurement. The statistical uncertainty given here is one standard deviation of the mean. The ratio of spectral densities was averaged up to a frequency of 10 kHz for heights <20 cm, 6 kHz for heights of 20 to 25 cm, and 2.5 kHz for heights of >25 cm. The number of points per data block was 256, and 5000 data blocks were averaged in ~6.4 s with a sampling rate of ~200 kHz.

[d]The uncertainty in k_{eff} is from the statistical uncertainty in the ratio of spectral densities only.

from Table J.1 obtained during the measurement. The precision of the measured ratio of spectral densities is such that the precision in the k_{eff} value is 0.01% down to k_{eff} values of ~0.60 (solution height of 12 cm) for the data collection time of 6.4 s and the draining rate of 23 cm/min. For the last four entries of Table 12, the solution height was fixed at 5.7 cm and the average k_{eff} value obtained is 0.30. The ratio of spectral densities and neutron multiplication factors are plotted as a function of solution height in Figs. 11 and 14, where they are compared with the other dynamic measurements. These values agree with other dynamic experiments.

The rate of change of the neutron multiplication factor in this experiment was 0.01 in k_{eff} per second (data collection was performed in 6.4 s with the source on the bottom of the tank). The neutron multiplication factor from all dynamic measurements (filling at a rate of 1 cm/min and draining at rates of 3, 5, and 23 cm/min) and the static measurements are in agreement. Thus, over the range of filling and draining rates investigated, the k_{eff} values measured do not depend on the rate of change of k_{eff} or whether the solution height is increased, decreased, or stationary. The dynamic capability of the method may be more than that required for most nuclear fuel processing or reprocessing plant applications.

7.3 SOLUTION PERTURBED BY BUBBLES

After the experimental vessel was filled to 29.5 cm, exploratory experiments were performed with air bubbles introduced into the bottom of the tank by leaving the pump running with no fuel solution in the drain tank. As a result, air was continuously added to the bottom of the tank through a 1.3-cm-diam hole at a radius of 7.6 cm. Air bubbles moved vertically through the solution, displacing fuel solution from the interior of the solution tank and also perturbing the upper surface of the solution. This displacement of fuel solution from the interior to the upper surface decreased the reactivity. For this measurement, the source was on the axis at the bottom of the tank.

These exploratory experiments were the first experiments in which a solution was perturbed during this type of measurement (a perturbed solution tank may be typical of some tanks in in-plant applications). Since these were exploratory measurements, no quantitative characterization of the bubbling was performed other than the estimate that the volume of air continuously introduced into the solution was ~500 cc/min. The data accumulation rates were such that 102 s of data were accumulated by the Fourier analyzer before uploading the data file to the VAX computer. The APSDs, CPSDs, and ratios of spectral densities as a function of frequency are plotted in Appendix K, both with bubbles passing through the solution and with the fuel solution stationary.

The ratios of spectral densities at low frequency with and without bubbles are given in Table 13 along with the k_{eff} values obtained using the same parameters with and without bubbles. This assumption that the same parameters can be used is probably valid since the air introduction was not a large perturbation and the air was added at a radius of 7.6 cm with the Cf source at a radius of 0. With bubbles passing through the solution, the average ratio of spectral densities was 0.0421 ± 0.0013 while that for the solution stationary was 0.0408 ± 0.0010. This indicates an increase in the ratio with the bubbles and a decrease in k_{eff}. The neutron multiplication factor for this solution height is ~0.95; therefore, this change in the ratio of spectral densities implies that the change in Δk associated with the bubbles is a small decrease ($\sim 1.6 \times 10^{-3}$).

Table 13. Ratios of spectral densities at low frequency and neutron multiplication factors for dynamic measurements with solution perturbed by bubbles

Time[a] (h:m:s)	Solution height[b] (cm)	Ratio of spectral densities[c,d]	k_{eff} from ratio of spectral densities[e]
	Solution perturbed by bubbles		
15:15:54	-	0.0437 ± 0.001	0.953 ± 0.001
15:17:38	-	0.0427 ± 0.001	0.955 ± 0.001
15:19:17	-	0.0419 ± 0.001	0.955 ± 0.001
15:20:59	-	0.0426 ± 0.001	0.955 ± 0.001
15:22:40	-	0.0394 ± 0.001	0.958 ± 0.001
15:24:22	-	0.0427 ± 0.001	0.955 ± 0.001
15:26:05	-	0.0414 ± 0.001	0.956 ± 0.001
	No bubbles in solution		
15:27:46	29.50	0.0401 ± 0.001	0.958 ± 0.001
15:29:27	29.51	0.0399 ± 0.001	0.957 ± 0.001
15:31:10	29.51	0.0418 ± 0.001	0.955 ± 0.001
15:32:52	29.51	0.0412 ± 0.001	0.956 ± 0.001

[a]End of a measurement time interval of 102 s over which the data were averaged and then the interpreted results displayed on a terminal. This time does not correspond to the average height during the measurement interval, but rather to the height at the end of the interval. The time which corresponds to the average height can be obtained by averaging the time listed with the time at the end of the previous interval.

[b]Average height of solution during the time interval of the measurement. Where no entry appears, bubbles introduced into the solution perturbed the upper surface of the solution.

[c]Average value during the time interval of the measurement. The statistical uncertainty given here is one standard deviation of the mean. The ratio of spectral densities was averaged up to a frequency of 2 kHz. The number of points per data block was 1024, and 20,000 data blocks were averaged in 102 s.

[d]The same parameters were used to interpret the ratio of spectral densities with and without bubbles in the solution.

[e]The uncertainty in k_{eff} is from the statistical uncertainty in the ratio of spectral densities only.

8. BREAK-FREQUENCY NOISE ANALYSIS METHOD

The various spectral densities as a function of frequency can be least-squares fitted to obtain the fundamental mode break frequency, f_b. The reactivity at a given subcritical state is related to the fundamental mode break frequency at that subcritical state, f_b (or to the prompt-neutron decay constant, $\alpha = 2\pi f_b$) and to the fundamental mode break frequency at delayed criticality, f_{bdc} (or prompt neutron decay constant, $\alpha_{dc} = \beta/\ell$) as follows:[14]

$$\frac{\alpha}{\alpha_{dc}} = \frac{f_b}{f_{bdc}} = \frac{1 - k}{k\beta} + 1 \quad . \tag{1}$$

Equation (1) must be corrected for the changes in the neutron lifetime and in the effective delayed-neutron fraction from the delayed critical state to the subcritical state of interest as follows:

$$\frac{1 - k}{k\beta} + 1 = \frac{f_b}{f_{bdc}} \frac{\ell}{\ell_{dc}} \frac{\beta_{dc}}{\beta} \quad . \tag{2}$$

For the reactivity changes in these experiments, corrections for neutron lifetime and effective delayed neutron fraction changes were made. The ratios of prompt neutron lifetimes and the ratios of effective delayed neutron fractions were obtained from calculations of these quantities as a function of solution height, which used fixed-source forward fluxes and k-eigenvalue adjoint fluxes from S_8 transport theory calculations.

The break frequency for each solution height was obtained by fitting the various CPSDs and APSDs as functions of frequency ω to functional forms with (1) a single pole in the transfer function $[H(\omega) = a_o/(\alpha_o + j\omega)]$, and (2) two poles in the transfer function $[H(\omega) = a_o/(\alpha_o + j\omega) + a_1/(\alpha_1 + j\omega)]$ to determine whether spatial modal effects are significant. The APSDs and CPSDs (real and imaginary parts), after correction for the frequency response of the instrumentation, were simultaneously least-squares fitted to obtain the values of f_b for both single-mode and two-mode fittings. The fundamental mode break frequencies used to obtain the subcriticality were the lowest break frequency from the two-mode fitting. The results of this fitting for the experiments are given in Table 14, and typical fitted functions are plotted with the data in Appendix L.

The break frequency at delayed criticality was obtained from the measured subcritical reactivity from the ratio of spectral densities for a solution height of 29.5 cm with the source at the bottom of the solution and the ^{6}Li-glass-plastic scintillators located as in Fig. 6. For this solution height the neutron multiplication factor obtained from the measurements in Table 13 is $0.956_3 \pm 0.000_2$, which for a β_{eff} value of 0.0075 corresponds to a subcritical reactivity of -6.13 dollars. The break frequency obtained for this solution height was 1340 ± 13 s^{-1}. The break frequency at delayed criticality, obtained from this known

Table 14. Break frequencies obtained from least-squares fitting of APSDs and CPSDs and neutron multiplication factors from the BFNA method as a function of solution height

Solution height (cm)	Fundamental mode break frequency (s^{-1})		Percentage change in $\frac{\ell\ \beta_{dc}}{\ell_{dc}\ \beta}$	Reactivity from BFNA (dollars)	k_{eff}[a]	
	One-mode	Two-mode			BFNA	Ratio of spectral densities
29.5	1369 ± 7[b]	1328 ± 12	0	6.13[c]	0.956[d] ± 0.003	0.956[c] ± 0.001
29.5	1385 ± 7	1357 ± 24	0	6.13[c]	0.956[d] ± 0.003	0.956[c] ± 0.001
29.5	1375 ± 7	1336 ± 16	0	6.13[c]	0.956[d] ± 0.003	0.956c ± 0.001
27.6	1819 ± 13	1776 ± 21	1.1	8.6	0.939 ± 0.004	0.940 ± 0.002
25.7	2320 ± 9	2265 ± 15	2.4	11.3	0.921 ± 0.004	0.921 ± 0.002
23.8	2889 ± 12	2850 ± 15	3.7	14.7	0.899 ± 0.005	0.896 ± 0.003
22.0	3563 ± 14	3503 ± 18	5.3	18.6	0.875 ± 0.006	0.872 ± 0.004
20.2	4327 ± 8	4308 ± 30	6.5	23.4	0.845 ± 0.007	0.845 ± 0.005
18.4	5175 ± 20	5117 ± 36	9.7	28.8	0.814 ± 0.009	0.812 ± 0.006
16.5	6218 ± 13	6280 ± 75	13.5	36.9	0.772 ± 0.010	0.771 ± 0.008
14.7	7468 ± 18	7760 ± 85	18.5	47.9	0.720 ± 0.011	0.723 ± 0.011
13.1	8955 ± 30	9629 ± 164	24.6	62.8	0.659 ± 0.013	0.662 ± 0.015
11.4	10537 ± 31	11196 ± 313	32.3	77.8	0.605 ± 0.009	0.588 ± 0.021
9.9	12325 ± 98	12849 ± 75	44.3	97.7	0.543 ± 0.014	0.522 ± 0.027
8.5	14388 ± 143	14825 ± 100	56.1	122.2	0.478 ± 0.014	0.443 ± 0.038
7.3	16414 ± 197	16750 ± 200	71.3	152.7	0.418 ± 0.014	0.376 ± 0.048

[a]Uncertainties are taken from Tables 9 and 14.

[b]Uncertainties are one standard deviation of the mean from the least-square fitting of data.

[c]Average of values from Table 13 unperturbed by air bubbles.

[d]Assumed equal to the average value from the ratio of spectral densities.

[e]The change in neutron lifetime for a change in solution height from 29.5 cm to a solution height of 7.3 cm was a factor of 2.1.

subcritical reactivity and break frequency at a solution height of 29.5 cm, is 187.9 $\pm$ 1.9 s^{-1}. The prompt neutron decay constant at delayed criticality is 1180 + 12 s^{-1}, resulting in a prompt neutron lifetime of 5.2 μs, which is in fair agreement with the calculated neutron lifetime of 5.7 μs at delayed criticality.

The ratio of break frequency at delayed criticality to break frequency for other solution heights was used to obtain the reactivity and the subcritical neutron multiplication factor using Eq. (2) with corrections for changes in the neutron lifetime and effective delayed neutron fraction. These corrections, which varied up to as much as 71% with solution height, are given in Table 14 along with the neutron multiplication factors obtained from the break frequency noise analysis (BFNA) method. The neutron multiplication factors obtained by the two independent measurements are plotted in Fig. 15. These k_{eff} values agree within ~0.005% with those values obtained from the ratios of spectral densities down to solution heights of ~13 cm or k_{eff} = 0.657. For lower solution heights the k_{eff} values from the BFNA method, which involve large corrections for changes of prompt neutron lifetime (as large as a factor of 2.1) and delayed neutron fractions, are higher than those from the ratios of spectral densities. In previous experiments the validity of the BFNA method was usually limited to k_{eff} values down to ~0.8.

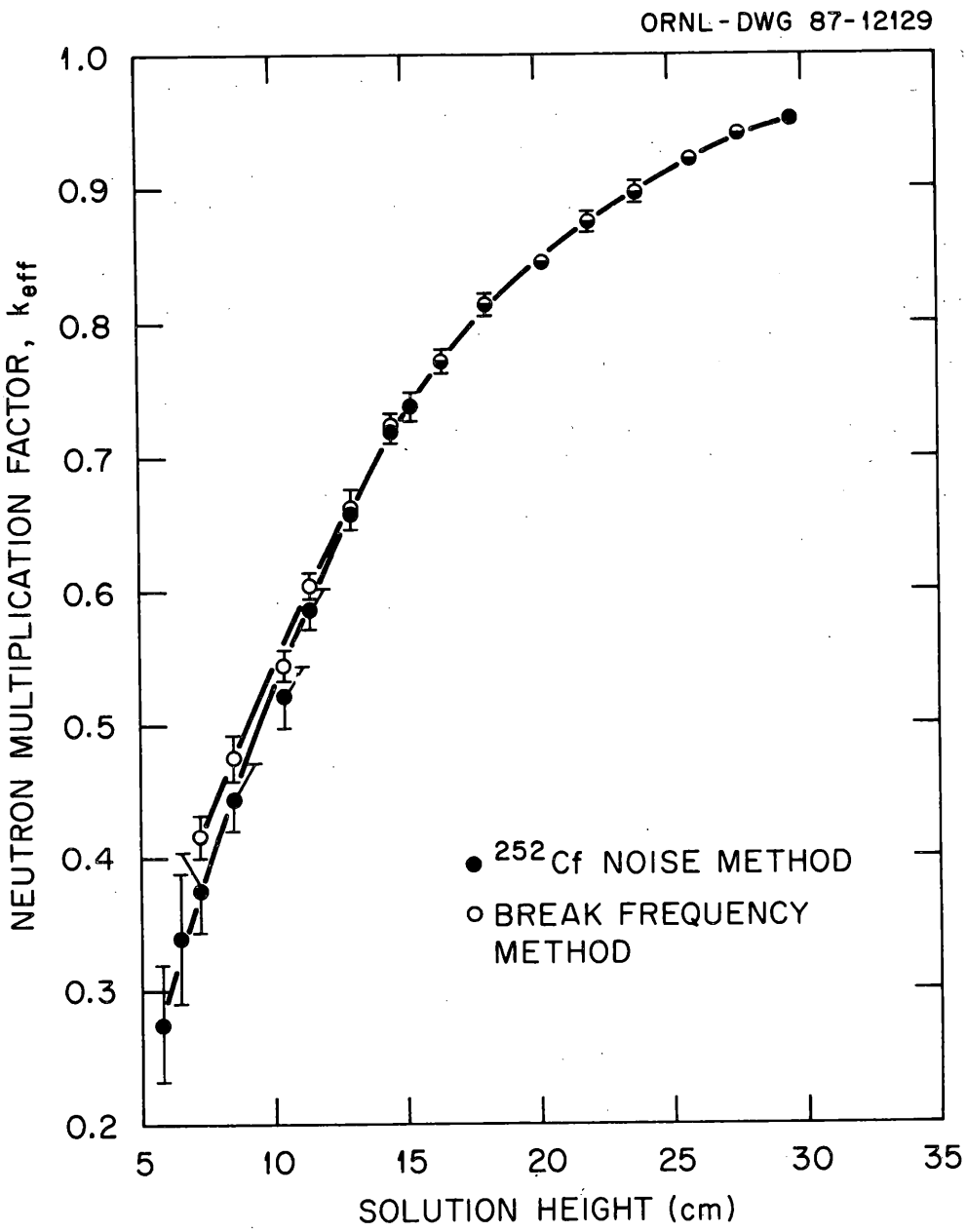

Fig. 15. Comparison of neutron multiplication factors from BFNA with those from ratios of spectral densities.

9. CONCLUSIONS AND RECOMMENDATIONS

The results and conclusions of these experiments are as follows: (1) the capability to measure the subcriticality for a multiplying system to k_{eff} as low as 0.3 was demonstrated; (2) experimental k_{eff} values were obtained from the ratio of spectral densities in times as short as 6 s of data accumulation and a small fraction of a second analysis time as a solution tank was drained from 29.5 to 6.5 cm height in ~60 s with corresponding changes in k_{eff} from 0.95 to 0.30; (3) the measured k_{eff} values obtained did not depend on the speed at which the solution height was changed or whether the tank was filling or draining; (4) the results of the dynamic measurements agreed with the static measurements; (5) as in previous experiments, the ratios of spectral densities at low frequency were used successfully to obtain the k_{eff} values using point kinetics interpretation of the data; (6) the neutron multiplication factors from independent measurements using the BFNA method agree with the values of k_{eff} from the measured ratios of spectral densities down to k_{eff} values of 0.65; (7) this method's effectiveness for systems where k_{eff} is changing, as demonstrated, probably exceeds the dynamic requirements in most nuclear fuel plant processing applications; and (8) the calculated k_{eff} values using KENO code and Hansen-Roach cross sections agree with the experimental values for all solution heights.

Before the dynamic capability of the method can be considered fully explored, additional experiments are required for a variety of dynamic situations. These experiments should include changes in fissile volume for several cylinders with different height-to-diameter ratios, changes in fissile volume for a cylinder with a variety of fuel solution concentrations, changes in fuel solution concentration for a fixed volume cylinder, dissolution of fuel, and situations in which the fuel solution in a tank is perturbed by physical agitation such as introduction of air to the bottom of the tank. These experiments should first be performed with uranyl nitrate solution to understand the physics before a more limited set of experiments is done with plutonium-uranium solutions. Dynamic experiments should also be performed with slab geometry and interacting tanks.

Since the low-frequency values of the ratio of spectral densities are sufficient to obtain the k_{eff} value, a measurement system that rapidly obtains these ratios (at low frequency) can and should be developed for in-plant applications.

REFERENCES

1. J. T. Mihalczo, V. K. Paré, G. L. Ragan, M. V. Mathis, and G. C. Tillett, "Determination of Reactivity from Power Spectral Density Measurements with ^{252}Cf," Nucl. Sci. Eng. 60, 29 (1978).

2. J. T. Mihalczo, W. T. King, and E. D. Blakeman, "^{252}Cf-Source-Driven Neutron Noise Analysis Method," Workshop on Subcriticality Reactivity Measurements, CONF-8508105, Albuquerque, New Mexico, August 1985.

3. Memorandum of Agreement between the U.S. Department of Energy and the Power Reactor and Nuclear Fuel Development Corporation, Japan, in the area of Criticality Data Development, signed August 12, 1983.

4. W. T. King, J. T. Mihalczo, and E. D. Blakeman, "Preliminary Investigation of the ^{252}CF-Source-Driven Noise Analysis Method of Subcriticality Measurements in LWR Fuel Storage and Initial Loading Applications," Trans. Am. Nucl. Soc. 47, 238 (1984).

5. J. T. Mihalczo and W. T. King, "^{252}Cf-Source-Driven Neutron Noise Method for Measuring Subcriticality of Submerged HFIR Fuel Elements," Trans. Am. Nucl. Soc. 43, 408 (1982).

6. J. T. Mihalczo, W. T. King, and E. D. Blakeman, "^{252}Cf-Source-Driven Neutron Noise Analysis Measurements for Coupled Uranium Metal Cylinders," Trans. Am. Nucl. Soc. 49, 241 (1985)

7. J. T. Mihalczo, E. D. Blakeman, and W. T. King, "Subcriticality Measurements For Two Coupled Uranyl Nitrate Solution Tanks using ^{252}Cf-Source-Driven Neutron Noise Analysis Methods," Trans. Am. Nucl. Soc. 52, 640 (1986).

8. W. T. King, J. T. Mihalczo, and E. D. Blakeman, "Decoupling of Uranium Metal with Borated Plaster Using ^{252}Cf Noise Analysis Methods," Trans. Am. Nucl. Soc. 50, 307 (1985).

9. W. T. King and J. T. Mihalczo, "Power Spectral Density Measurements with ^{252}Cf for a Light-Water-Moderated Research Reactor," Trans. Am. Nucl. Soc. 33, 796 (1979).

10. J. T. Mihalczo, W. T. King, E. B. Johnson, and E. D. Blakeman, "Subcriticality Measurements for a Fuel Solution Tank with Changing Fuel Concentration Using ^{252}Cf-Source-Driven Neutron Noise Analysis," Trans. Am. Nucl. Soc. 45, 37 (1983).

11. J. T. Mihalczo, E. D. Blakeman, W. T. King, and R. C. Kryter, "Performance Evaluation of Measurement System for the Cf-Source-Driven Neutron Noise Analysis Determination of Subcriticality," ORNL/TM-10145 (1988).

12. M. V. Mathis, J. T. Mihalczo, and V. K. Paré, "Reactivity Surveillance Instrumentation for Measurements with the FFTF Engineering Mock-Up Core," ORNL/TM-4511, Oak Ridge National Laboratory (1976).

13. J. T. Mihalczo, R. C. Kryter, W. T. King, and E. D. Blakeman, "Cf-Source-Driven Neutron Noise Measurements of Subcriticality for A 4.95 wt % ^{235}U-Enriched Uranyl Fluoride Solution Cylinder," Ann. Nucl. Energy 13(7), 351-362 (1986).

14. C. W. Ricker, D. N. Fry, E. R. Mann, and S. H. Hanauer, "Investigation of Negative Reactivity Measurement by Neutron Fluctuation Analysis," Proc. Symp. Noise Analysis in Nuclear Systems, University of Florida, Gainesville (1963).

APPENDIX A

THEORY OF THE MEASUREMENT METHOD

APPENDIX A. THEORY OF THE MEASUREMENT METHOD

The ^{252}Cf-source-driven neutron noise analysis method for the determination of subcritical reactivities requires the measurement in the frequency domain of four statistical quantities. These quantities are G_{12}, the cross-power spectral density (CPSD) between the Cf source (designated by subscript 1) and a detector (designated by subscript 2) of particles from the fission chain multiplication process; G_{13}, the CPSD between the Cf source and another detector (designated by subscript 3) of particles from fission; G_{23}, the CPSD between both detectors; and G_{11}, the auto-power spectral density (APSD) of the Cf source (Eq. A.1). The pair of detectors (2 and 3) are assumed to detect particles emitted by induced fission chains initiated by (1) neutrons from the spontaneous fission of ^{252}Cf, (2) neutrons from inherent sources, and (3) delayed neutrons, but not particles directly from the spontaneous fission of ^{252}Cf. In experiments this is practical to achieve because detectors can be located far from each other, far from the ^{252}Cf source, and external to the system. In this case the probabilities of detecting particles directly from the ^{252}Cf source and of detecting particles in each detector from the same inherent, induced, or Cf fission are very small. If this is not possible, a white noise source (constant amplitude at all frequencies) term must be added to the spectral densities, G_{22}, G_{12}, G_{13}, and G_{23} [Eqs. A.2-A.4 (G_{13} is given by the expression of Eq. (A.3) with subscript 2 replaced by subscript 3 and G_{33} by replacing subscript 2 of Eq. (A.2) with subscript 3)]. The absence of this white noise source from particles directly from ^{252}Cf fission can be verified experimentally by examination of the CPSD at high frequency $\omega \gg f_b$ to assure that the white noise source term is zero. Since the detectors are usually far from each other adjacent to the outer surface of the system, the probability of detecting a particle in each detector from the same fission is very small. Under these conditions the point kinetics expressions for these spectral densities for detectors 2 and 3 located external to the system of fissile material, as well as the APSD of a detector (Eq. A.2), have been derived previously and are as follows:[1]

$$G_{11}(\omega) = 2\left|h_1(\omega)\right|^2 \left\{\frac{31}{2} F_c \overline{q_\alpha^2} + F_c \overline{q_c^2}\right\} , \tag{A.1}$$

$$G_{22}(\omega) = \left|h_2(\omega)\right|^2 \left\{2W_2 F \overline{q_2^2} + \frac{W_2^2(\bar{q}_2)^2}{\bar{\nu}^2}\left|H_s(\omega)\right|^2 G_s\right\} , \tag{A.2}$$

$$G_{12}(\omega) = 2h_1^*(\omega)h_2(\omega)\bar{q}_c \frac{W_2\bar{q}_2}{\bar{\nu}} H_s(\omega) \frac{\bar{\nu}_c F_c I_c}{I} , \text{ and} \tag{A.3}$$

$$G_{23}(\omega) = h_2^*(\omega)h_3(\omega)\,\frac{W_2\bar{q}_2}{\bar{\nu}}\,\frac{W_3\bar{q}_3}{\bar{\nu}}\,\left|H_s(\omega)\right|^2 G_s \quad , \tag{A.4}$$

where * designates complex conjugation, and

$h_1(\omega)$, $h_2(\omega)$, $h_3(\omega)$ = response of the electronic components of detection systems 1, 2, and 3, respectively, at frequency ω;

$\bar{q}_c$, $\bar{q}_\alpha$ = average charge produced in detector 1 per ^{252}Cf spontaneous fission, and average charge produced per α-decay respectively;

$\overline{q_2}$, $\overline{q_3}$ = average charge produced per interaction in detectors 2 and 3 respectively;

W_2, W_3 = detection efficiency of detection systems 2 and 3, expressed as counts per reactor fission;

W_1 = efficiency for detecting ^{252}Cf fission (assumed ≈ 1)

G_s = APSD of the reactor noise-equivalent source.

For frequencies much larger than delayed neutron decay constants

$$G_s = 2(\bar{\nu})^2\,XFR\left\{1 + \frac{V}{XR} + \frac{F_i I_i^2\,\overline{\nu_i^2}}{FI^2\,XR(\bar{\nu})^2} + \frac{F_c I_c^2\,\overline{\nu_c^2}}{FI^2\,XR(\bar{\nu})^2}\right\} \quad , \tag{A.5}$$

where

$X = \overline{\nu(\nu-1)}/(\bar{\nu})^2$;

R = factor that corrects point kinetics for global spatial effects; $R = \overline{I^2}/(I)^2$

I, I_c, I_i = average importance of a neutron from reactor fission, ^{252}Cf fission, and inherent source fission respectively;

F, F_c, F_i = reactor fission rate, ^{252}Cf fission rate, and inherent source fission rate respectively;

$\bar{\nu}$, $\bar{\nu}_c$, $\bar{\nu}_i$ = average number of prompt neutrons per reactor fission, per ^{252}Cf fission, and per inherent source fission respectively;

$$G_s = 2(\bar{\nu})^2 \, X'FR \quad ; \tag{A.6}$$

X' = modified neutron dispersion number defined by Eqs. (A.5) and (A.6);

$$V = \frac{(2\beta - \rho)}{(1 - \beta)\bar{\nu}} \quad ;$$

β = effective total delayed neutron fraction;

ρ = reactivity = $\frac{(k - 1)}{k}$;

k = neutron multiplication factor;

$H_s(\omega)$ = response of the reactor production rate to the source at frequency ω; and

$$H_s(\omega) = \frac{1}{j\omega\Lambda + (\beta - \rho)} \, , \; (\omega \gg \lambda_i \text{ for all } i) \text{ for fundamental mode;}$$

$j = \sqrt{-1}$;

Λ = neutron generation time;

λ_i = delayed group i precursor decay constant.

The noise equivalent source, Eq. (A.5), was obtained using the Schottky formalism as applied by Cohn.[2] The third and fourth terms in Eq. (A.5) can become significant at low neutron multiplication factors where the denominator of each term (i.e., FI^2), proportional to the fission rate in the system, becomes comparable to the value of $F_i I_i^2$ or $F_c I_c^2$, the inherent and ^{252}Cf source fission rates respectively. If the ^{252}Cf source intensity is larger than the inherent source in the fissile material (such as ^{240}Pu), the third term will be small compared to the fourth term. If the third term of Eq. (A.5) becomes significant, a factor R_i, similar to R but for inherent source neutrons, should multiply the numerator of this term. The validity of the noise equivalent source based on the Schottky method as applied by Cohn has been demonstrated by these experiments. These experiments have shown that the use of $\overline{\nu_c^2}$ in the fourth term on the right side of Eq (A.5) results in k_{eff} values that agree with calculations and independent measurements (see Appendix M and Sect. 8).

The expression for $G_{13}(\omega)$ is similar to Eq. (A.3). Using these spectral densities, the ratio of spectral densities $G_{12}^* G_{13}/G_{11}G_{23}$ is formed

(* denotes complex conjugation). For an ionization chamber and its associated electronics detecting all of the fissions of ^{252}Cf, and each fission contributing the same to the total signal while rejecting the pulses produced by α decay, then

$$G_{11} = 2 \left| h_1(\omega) \right|^2 F_c \quad ,$$

$$\frac{G_{12}^* G_{13}}{G_{11} G_{23}} = F_4 = \frac{\bar{\nu}_c}{\bar{\nu}} \frac{I_c}{I} \frac{1}{R\,X} \frac{(1-k)}{k} \tag{A.7}$$

where $X' \approx X$.

With other inherent neutron sources (i),

$$F_4 = \left\{ \begin{matrix} \text{Right side} \\ \text{Eq. (A.7)} \end{matrix} \right\} S_R$$

where

$$S_R = \frac{\text{Multiplication of all neutrons}}{\text{Multiplication of Cf neutrons}} \frac{1}{A} = \frac{Y}{A} \tag{A.8}$$

or

$$S = \frac{F_c I_c \bar{\nu}_c + F_i I_i \bar{\nu}_i}{F_c I_c \bar{\nu}_c A} \quad . \tag{A.9}$$

The factor Y accounts for the effect of fissions induced by neutrons from the inherent source contributing to G_{23} but not to G_{12} or G_{13}. If not all of the ^{252}Cf fissions are counted in the detection system electronics, then the fraction of Cf fissions counted, A, must be introduced in the denominator of S_R to account for the undetected fissions of Cf producing neutrons which induce fissions in the system that contribute to G_{23} but not to G_{12} and G_{13}.

When a multiplying system is far subcritical, the power spectral density of the noise equivalent source, G_S, must be modified to include X', a modified form of the neutron dispersion number given by Eqs. (A.5) and (A.6). Then, $(1 - k)/k$ is of the form

$$\frac{1-k}{k} = \frac{C_1 \; G_{12}^* G_{13} / G_{11} G_{23}}{1 - C_2 \; G_{12}^* G_{13} / G_{11} G_{23}} \quad , \tag{A.10}$$

instead of

$$\frac{1 - k}{k} = C \frac{G_{12}^{*} \, G_{13}}{G_{11} \, G_{23}} \quad , \tag{A.11}$$

where C, C_1, and C_2 are constants involving parameters which are defined by Eqs. (A.1 - A.11), some of which depend on solution height.

If spatial modal effects are significant, the ratio of spectral densities can be multiplied by a calculated spatial modal correction factor M_c, which is the ratio of $G_{12}^{*}G_{13}/G_{11}G_{23}$, obtained from fundamental mode only to that obtained with all modes present. This factor can be calculated according to the methods of Verdu Martin et al.[3] and Verdu Martin[4] for unreflected cylindrical geometries. An alternate approach, which has been demonstrated,[5,6] is to fit the data to sums of modes and obtain the fundamental mode ratio directly from the experimental data.

APPENDIX A REFERENCES

1. J. T. Mihalczo, W. T. King, E. D. Blakeman, "^{252}Cf-Source-Driven Neutron Noise Analysis Method," Workshop on Subcriticality Reactivity Measurements, CONF-8508105, Albuquerque, New Mexico, August 1985.

2. C. F. Cohn, "A Simplified Theory of Pile Noise," Nucl. Sci. Eng. 7, 472 (1960).

3. G. Verdu Martin, J. L. Munoz-Cobos, J. T. Mihalczo, and W. T. King, "Spatial Effect Corrections to Subcriticality Measurements by the ^{252}Cf-Source-Driven Neutron Noise Analysis Method," Trans. Am. Nucl. Soc. 42, 452 (1984).

4. G. Verdu Martin, "Teoria General del Transporte Estocastico de Neutrones y su Aplicacion a la Medida de Reactividad en Conjuntos Subcriticos," Tesis, Universidad Politecnica de Valencia (April 1984).

5. C. March-Leuba, "Interpretation of Subcriticality Measurement with Strong Spatial Effects," Thesis, The University of Tennessee, Knoxville (1987).

6. C. March-Leuba and J. March-Leuba, "Interpretation of Subcriticality Measurements with Strong Spatial Effects," Trans. Am. Nucl. Soc. 54, 348 (1987).

APPENDIX B

ADDITIONAL DATA FROM STATIC MEASUREMENTS

APPENDIX B. ADDITIONAL DATA FROM STATIC MEASUREMENTS

This appendix presents some additional data from the static measurements. The ratios of spectral densities for the various solution heights in the static measurements as a function of frequency with a central source, as well as some APSDs and CPSDs, are plotted in Figs. B.1-B.14. In some of the plots, the upper limit of the frequency range for the ratio is limited to eliminate extremely high points at very high frequency (resulting from statistically low values of G_{23}); the inclusion of these data was not practical if the graphs were to meaningfully display the data at low frequency. These statistically low values of G_{23} result from the fact that the amplitude of G_{23} falls off faster with frequency than that of G_{12} or G_{13} and the frequency range of the measurement usually was chosen to measure G_{12} or G_{13} to as high a frequency as possible. This effect can be seen in the CPSDs of Fig. B.3. All APSDs and CPSDs are given in arbitrary units.

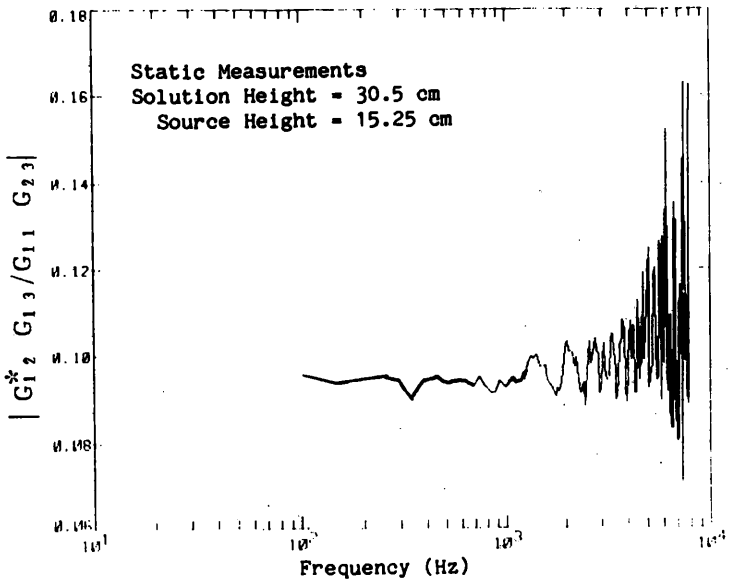

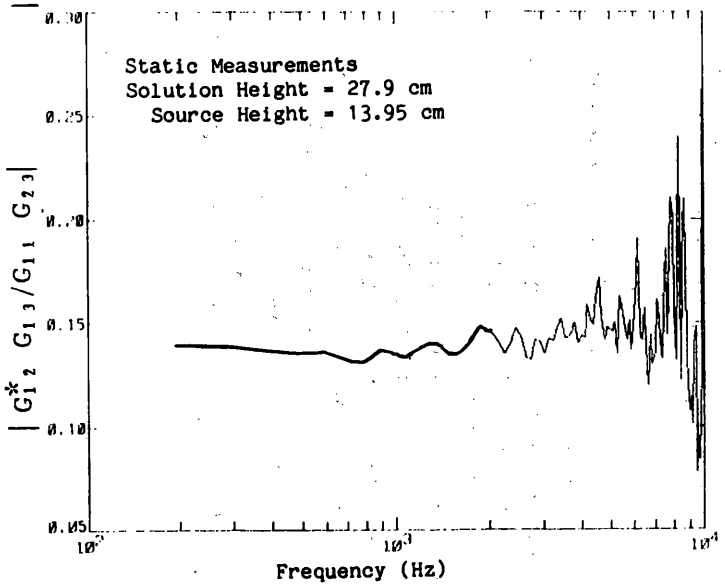

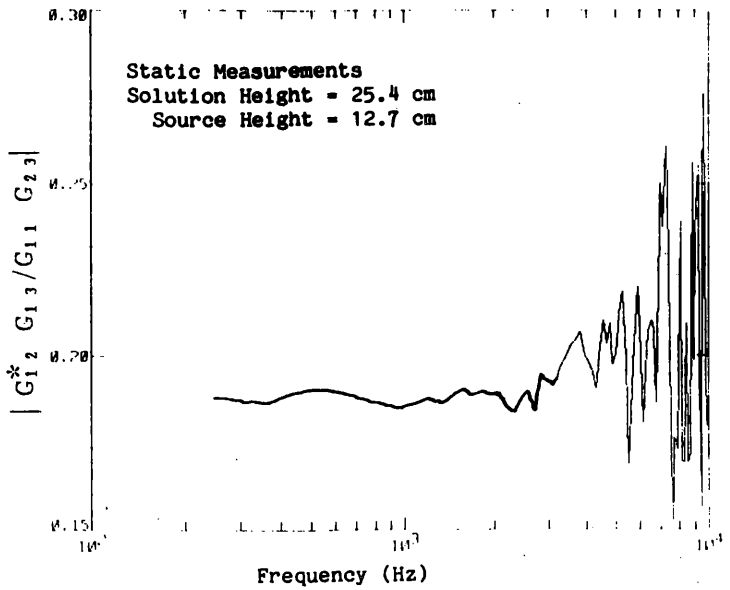

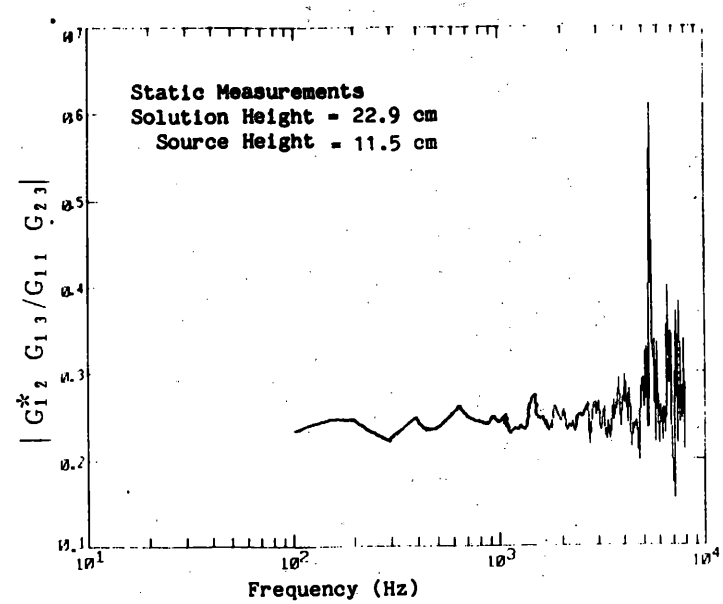

Fig. B.1. Ratios of spectral densities as a function of frequency for various solution heights with the source in the center of the solution.

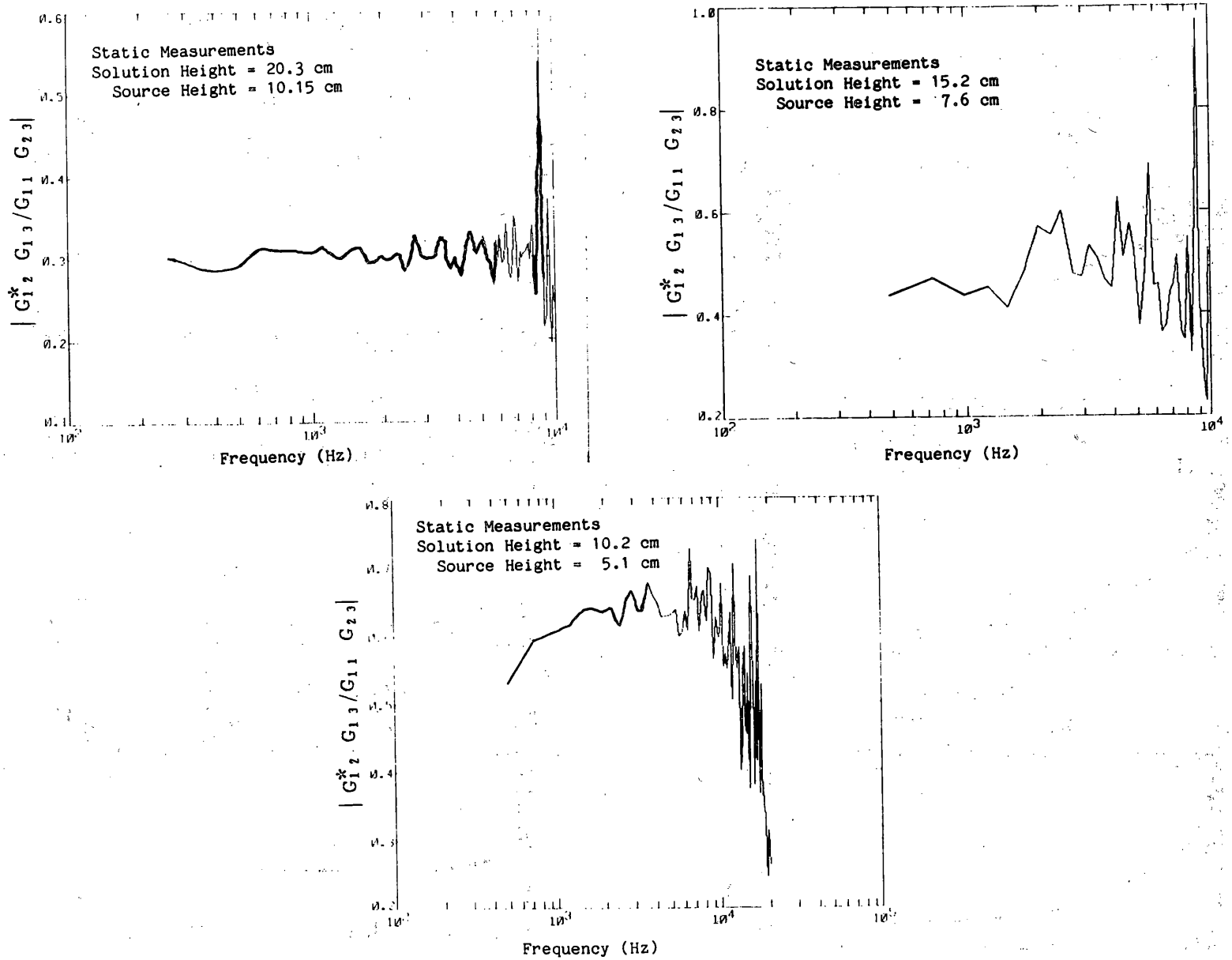

Fig. B.1. (continued)

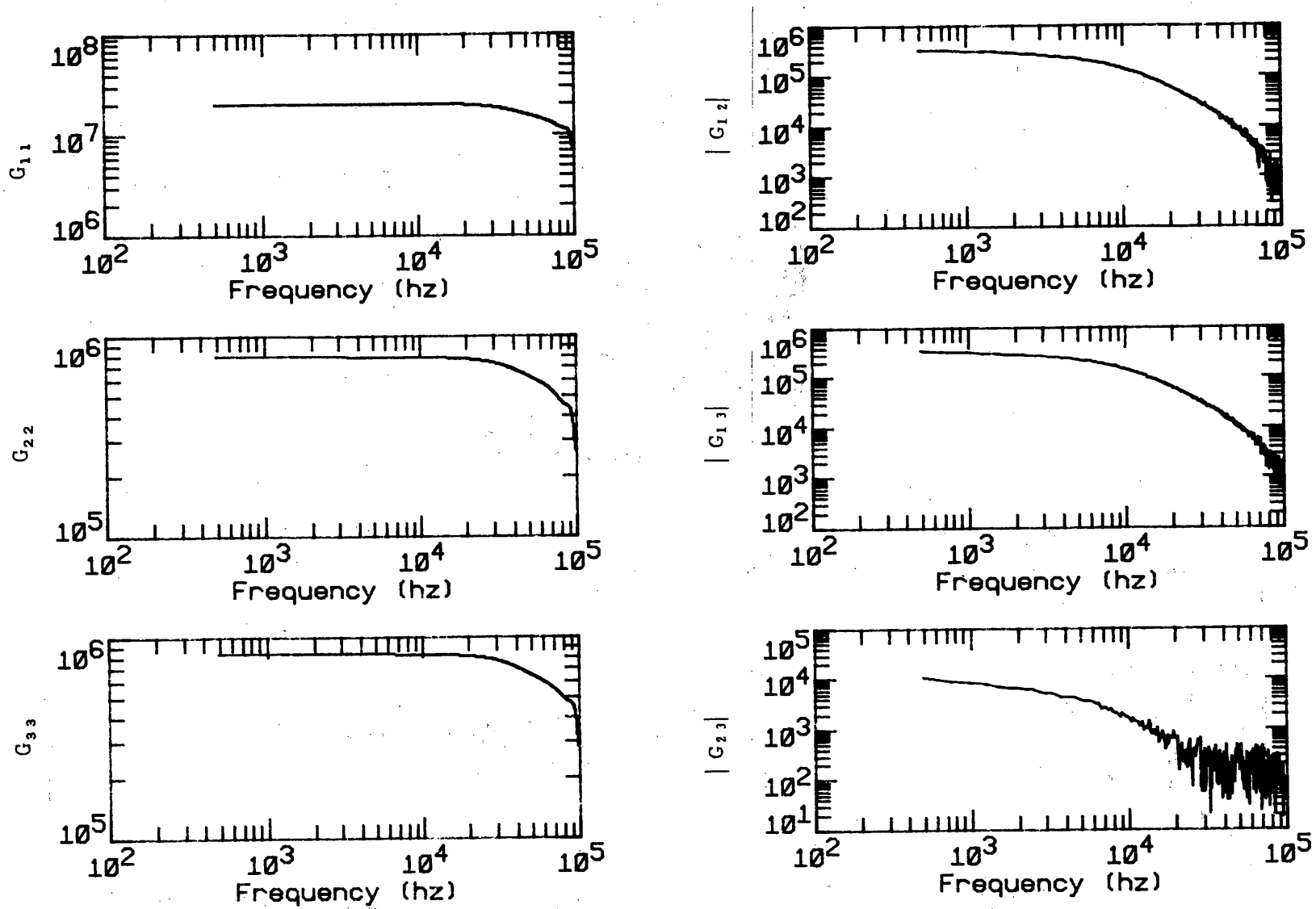

Fig. B.2. APSDs and CPSDs as a function of frequency for a solution height of 10.2 cm with the source in the center of the solution.

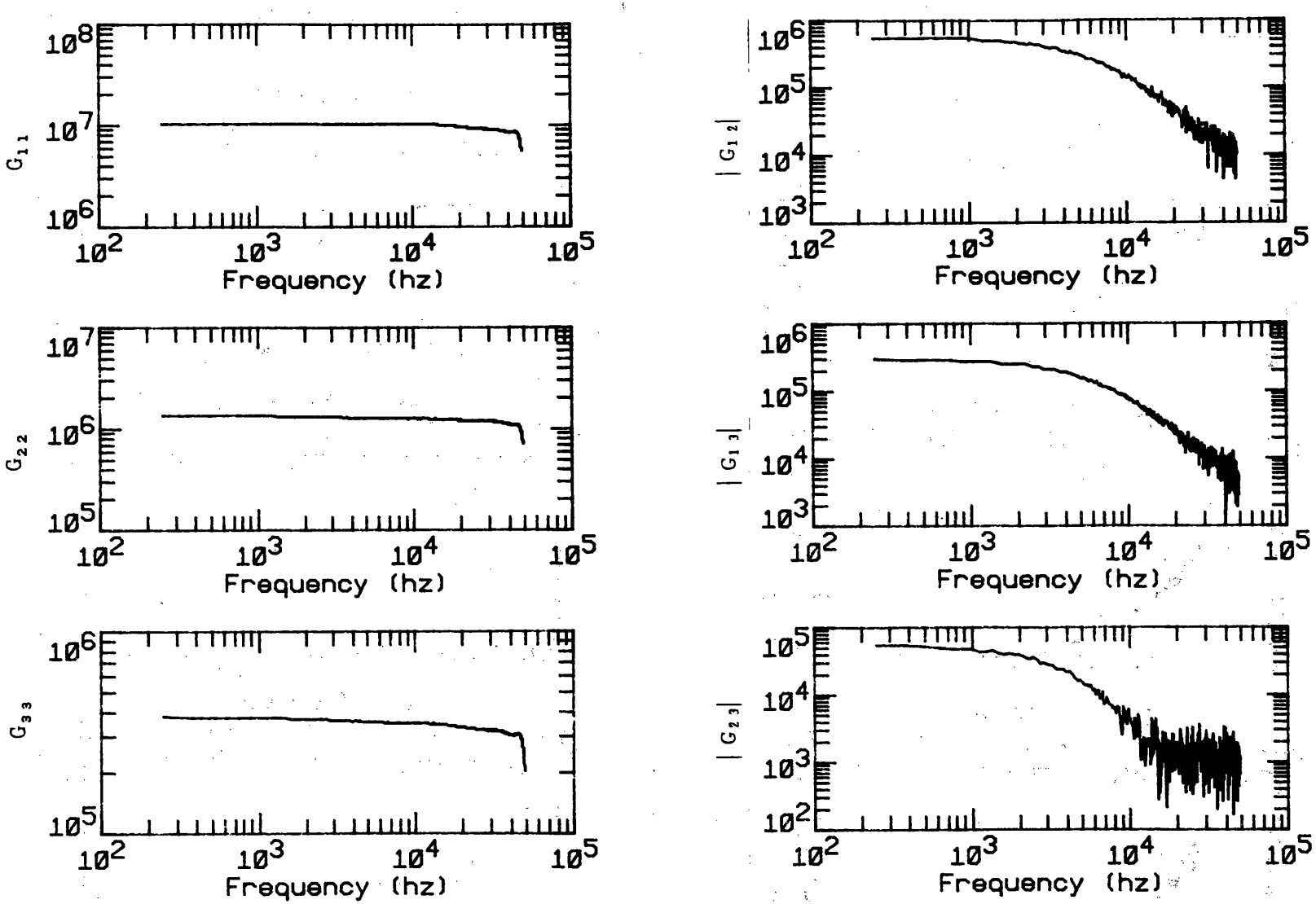

Fig. B.3. APSDs and CPSDs as a function of frequency for a solution height of 20.4 cm with the source in the center of the solution.

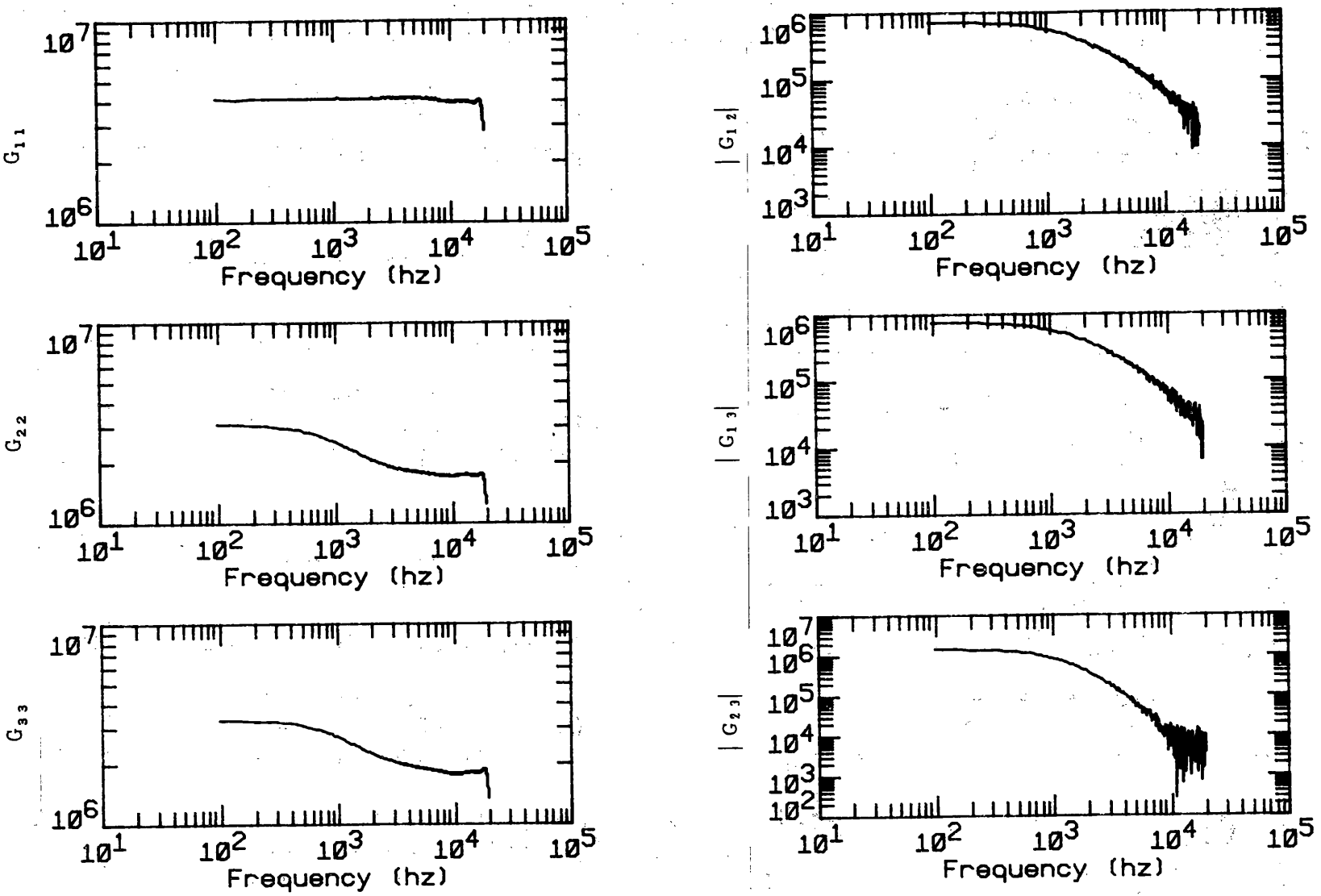

Fig. B.4. APSDs and CPSDs as a function of frequency for a solution height of 30.5 cm with the source in the center of the solution.

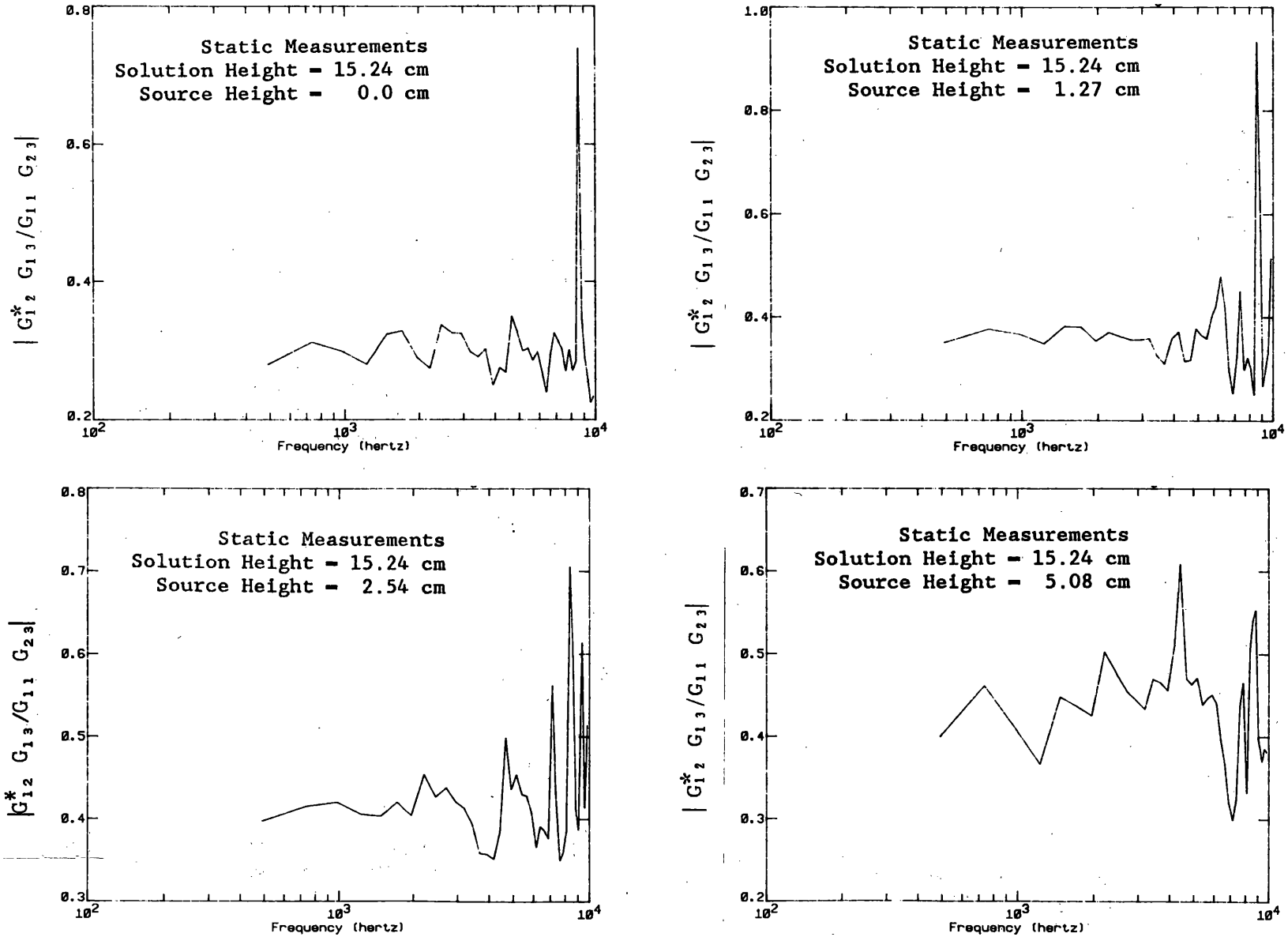

Fig. B.5. Ratios of spectral densities as a function of frequency for a solution height of 15.2 cm and various source heights.

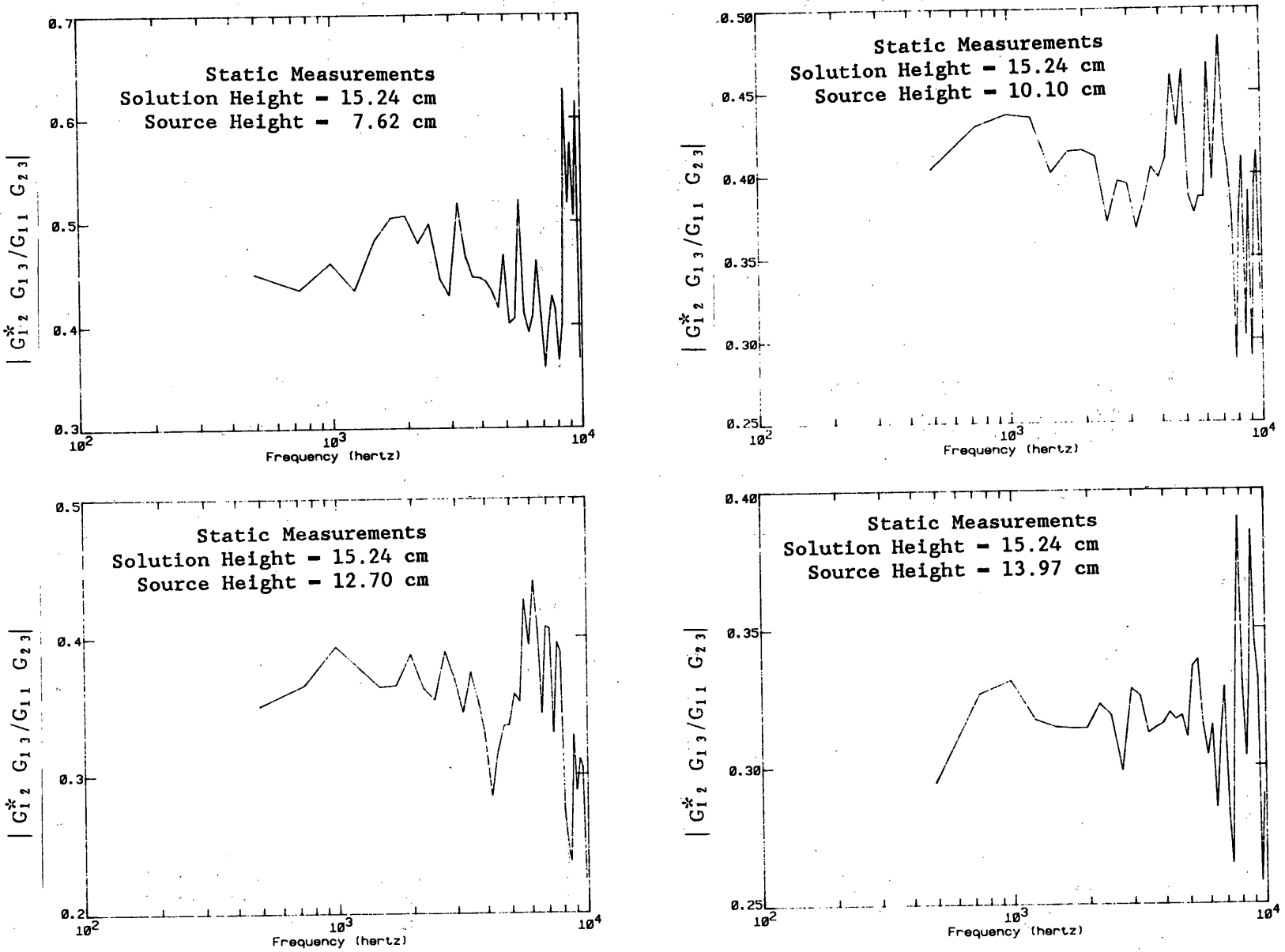

Fig. B.5. (continued)

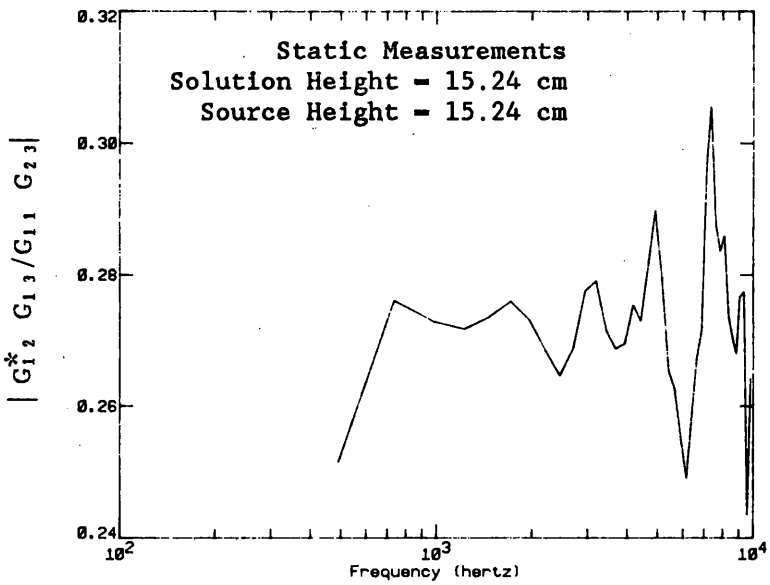

Fig. B.5. (continued)

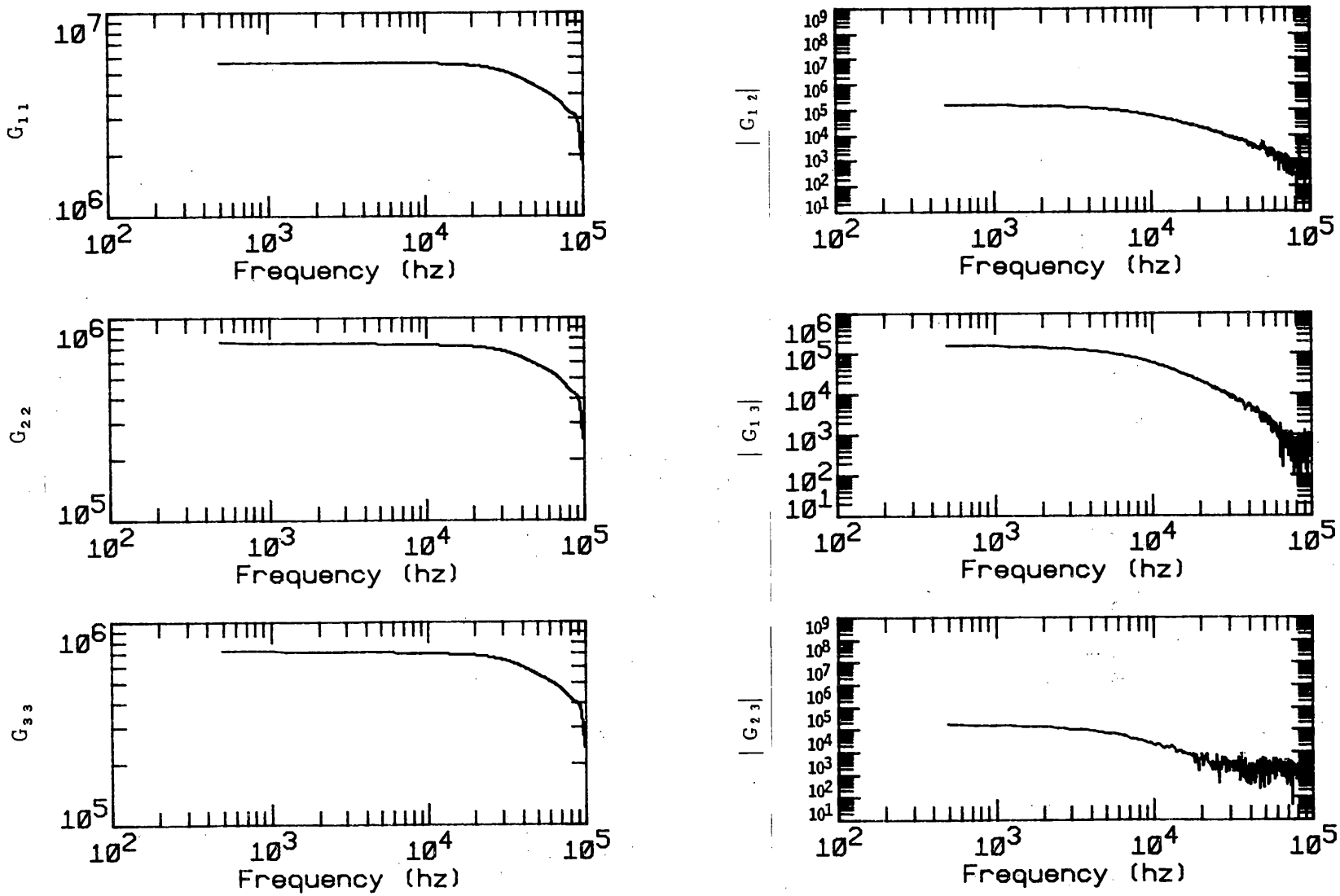

Fig. B.6. APSDs and CPSDs as a function of frequency for a solution height of 15.2 cm and a source height of 0.0 cm.

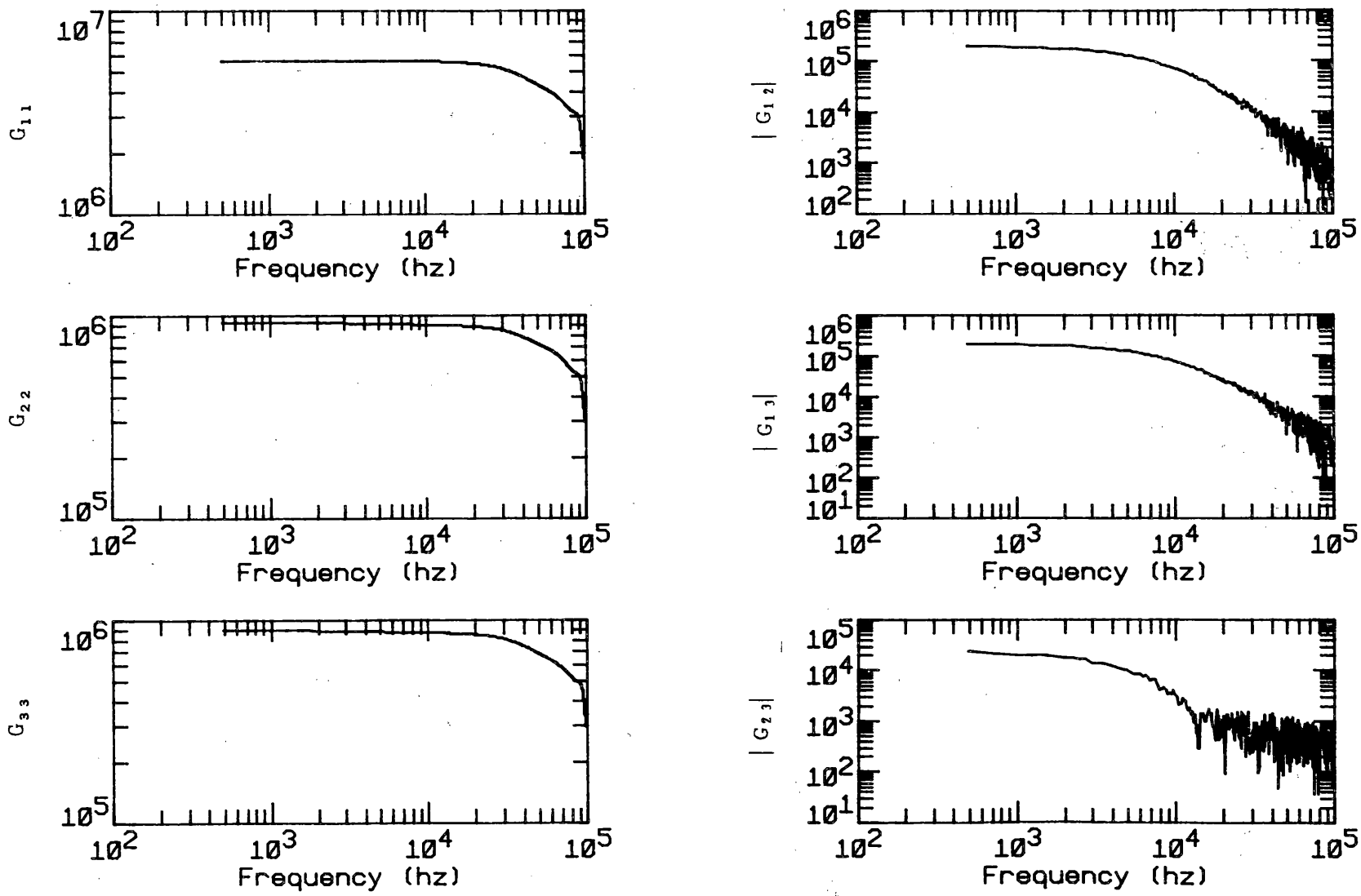

Fig. B.7. APSDs and CPSDs as a function of frequency for a solution height of 15.2 cm and a source height of 1.27 cm.

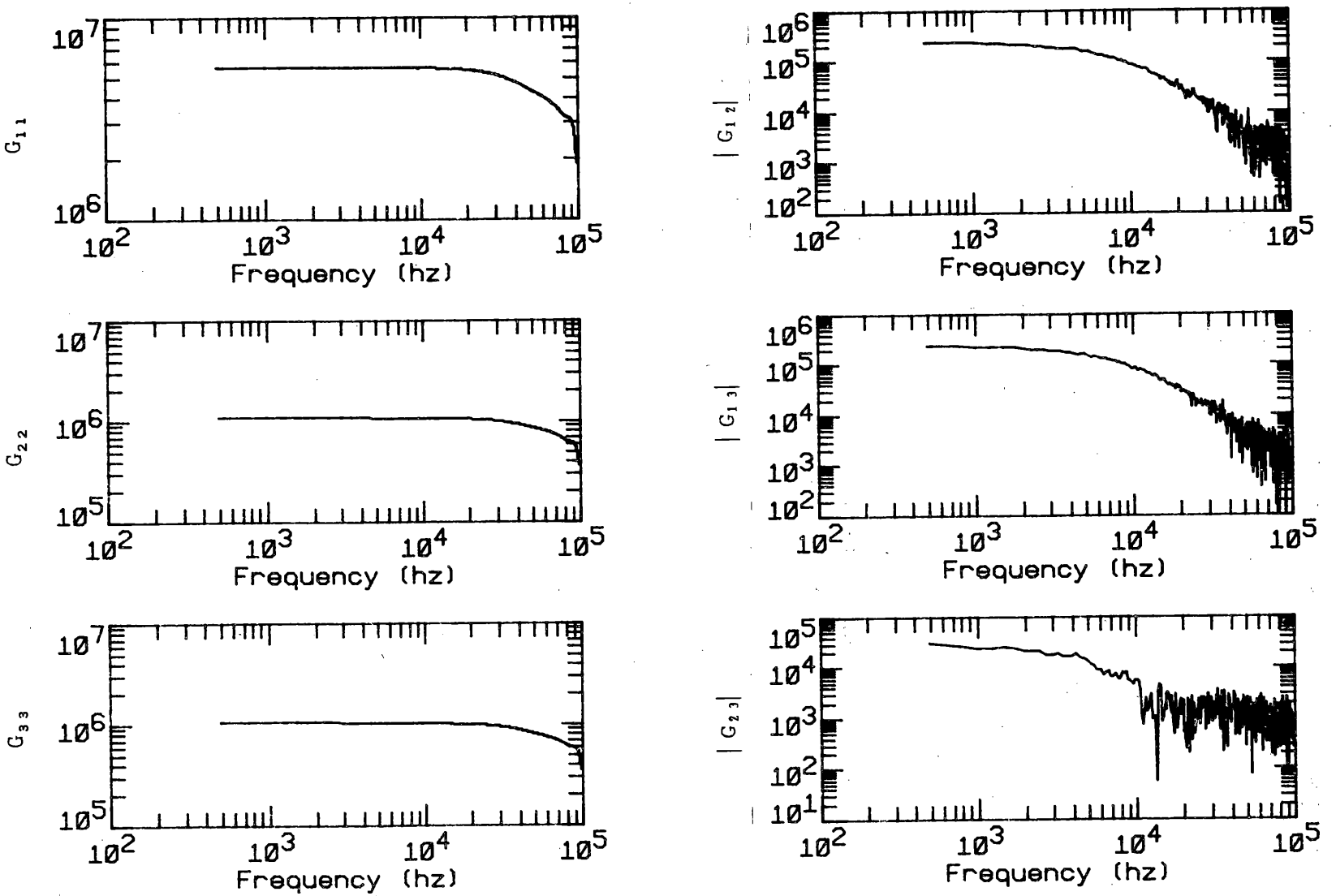

Fig. B.8. APSDs and CPSDs as a function of frequency for a solution height of 15.2 cm and a source height of 2.54 cm.

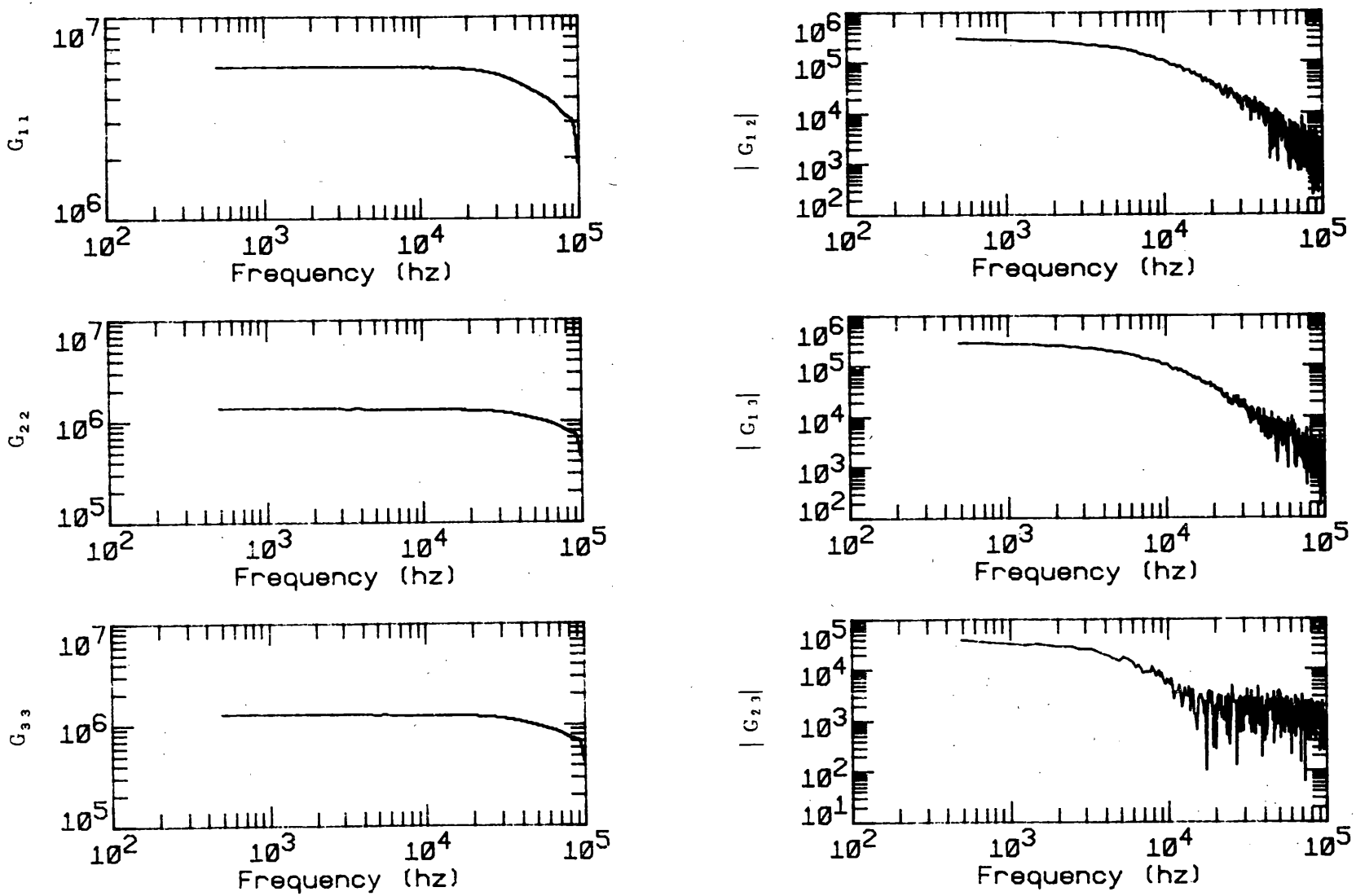

Fig. B.9. APSDs and CPSDs as a function of frequency for a solution height of 15.2 cm and a source height of 5.08 cm.

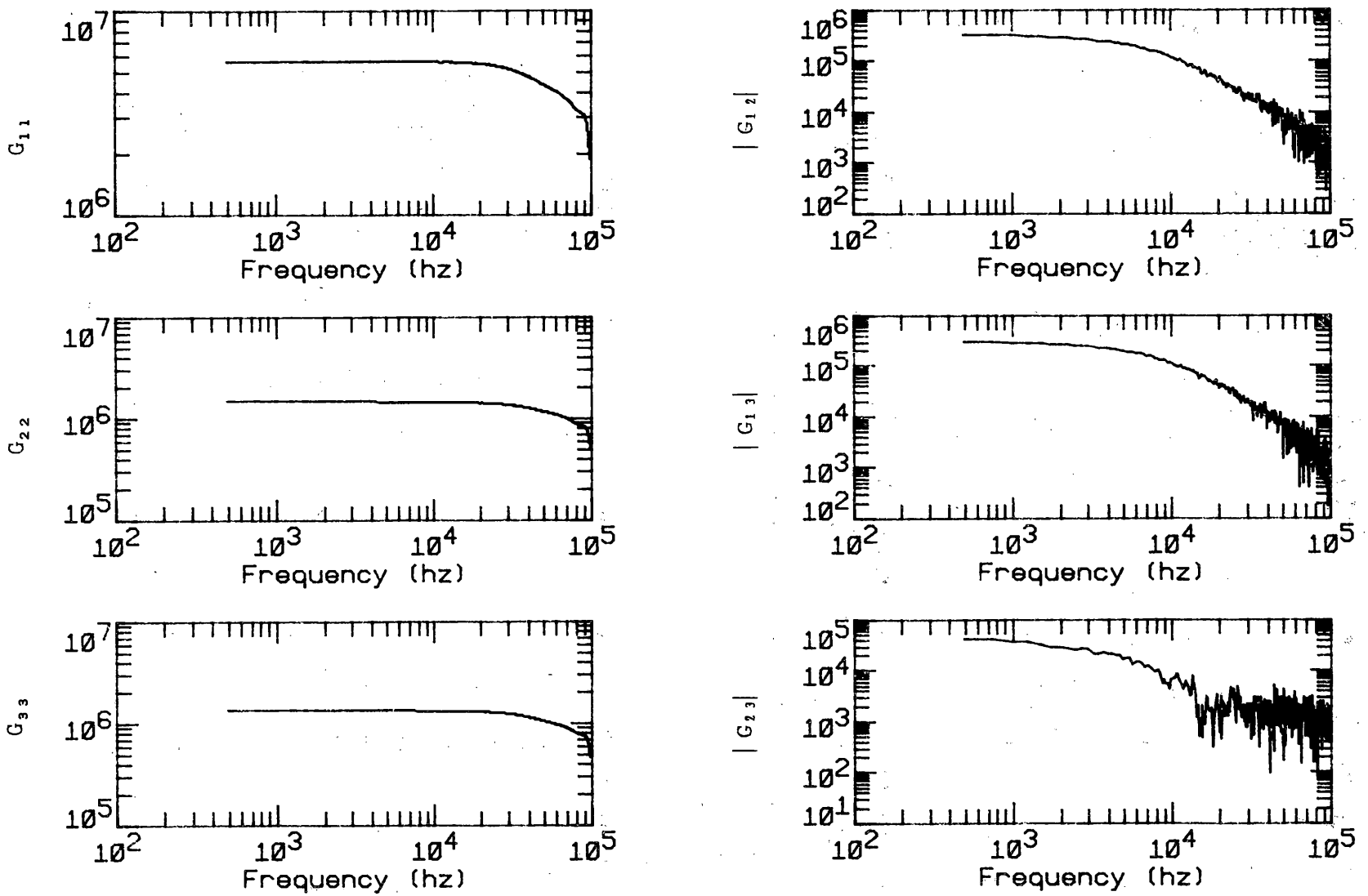

Fig. B.10. APSDs and CPSDs as a function of frequency for a solution height of 15.2 cm and a source height of 7.62 cm.

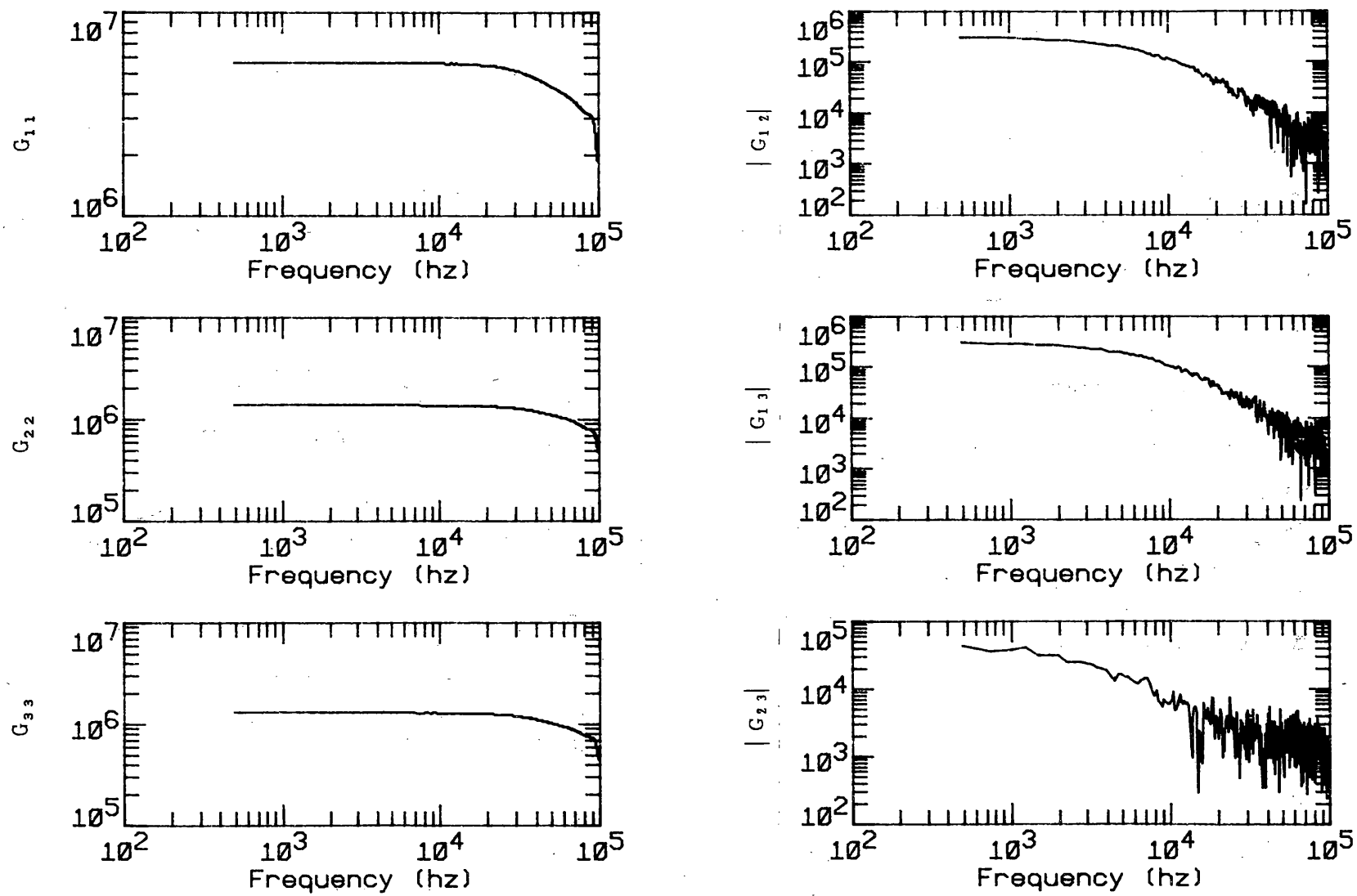

Fig. B.11. APSDs and CPSDs as a function of frequency for a solution height of 15.2 cm and a source height of 10.2 cm.

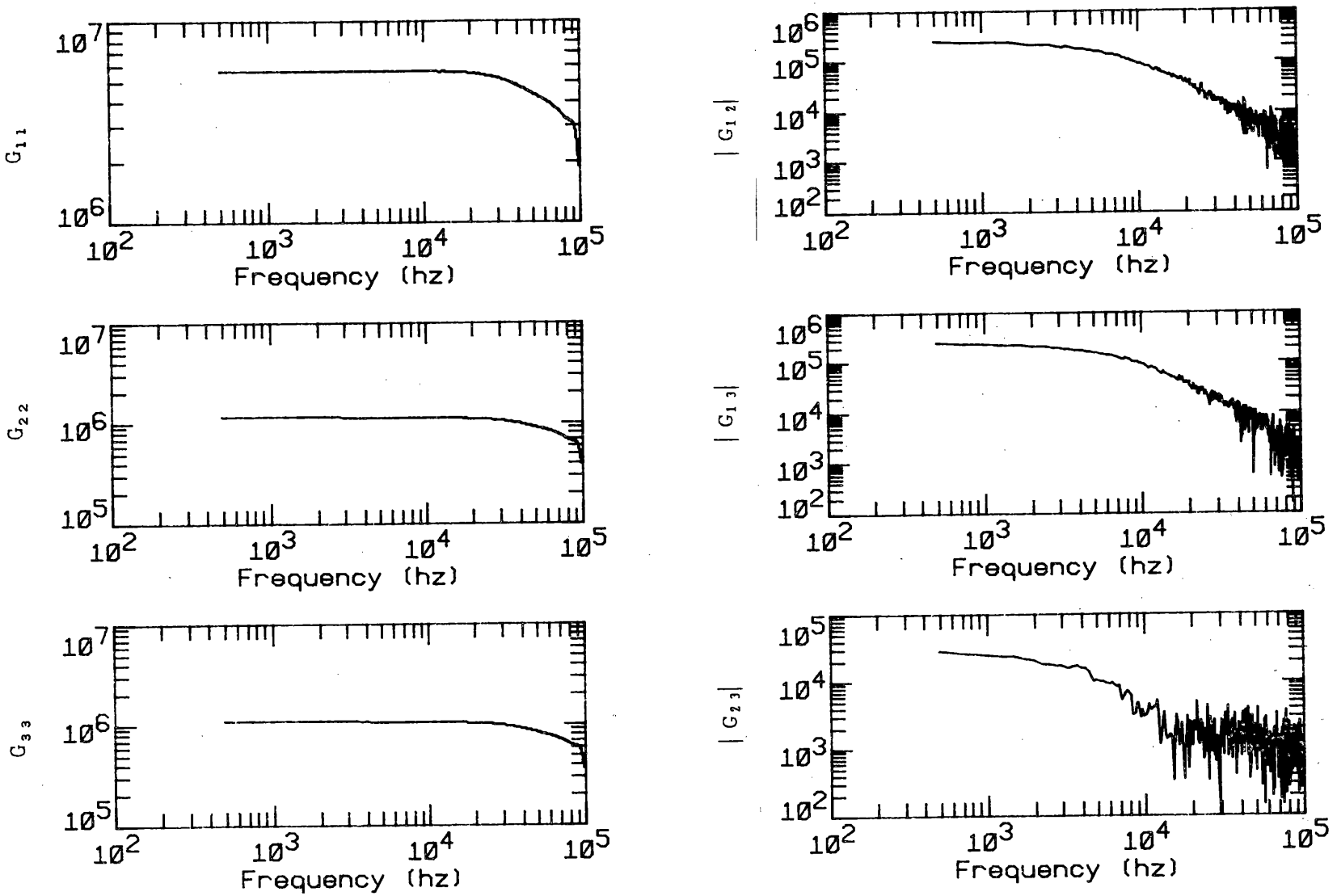

Fig. B.12. APSDs and CPSDs as a function of frequency for a solution height of 15.2 cm and a source of 12.7 cm.

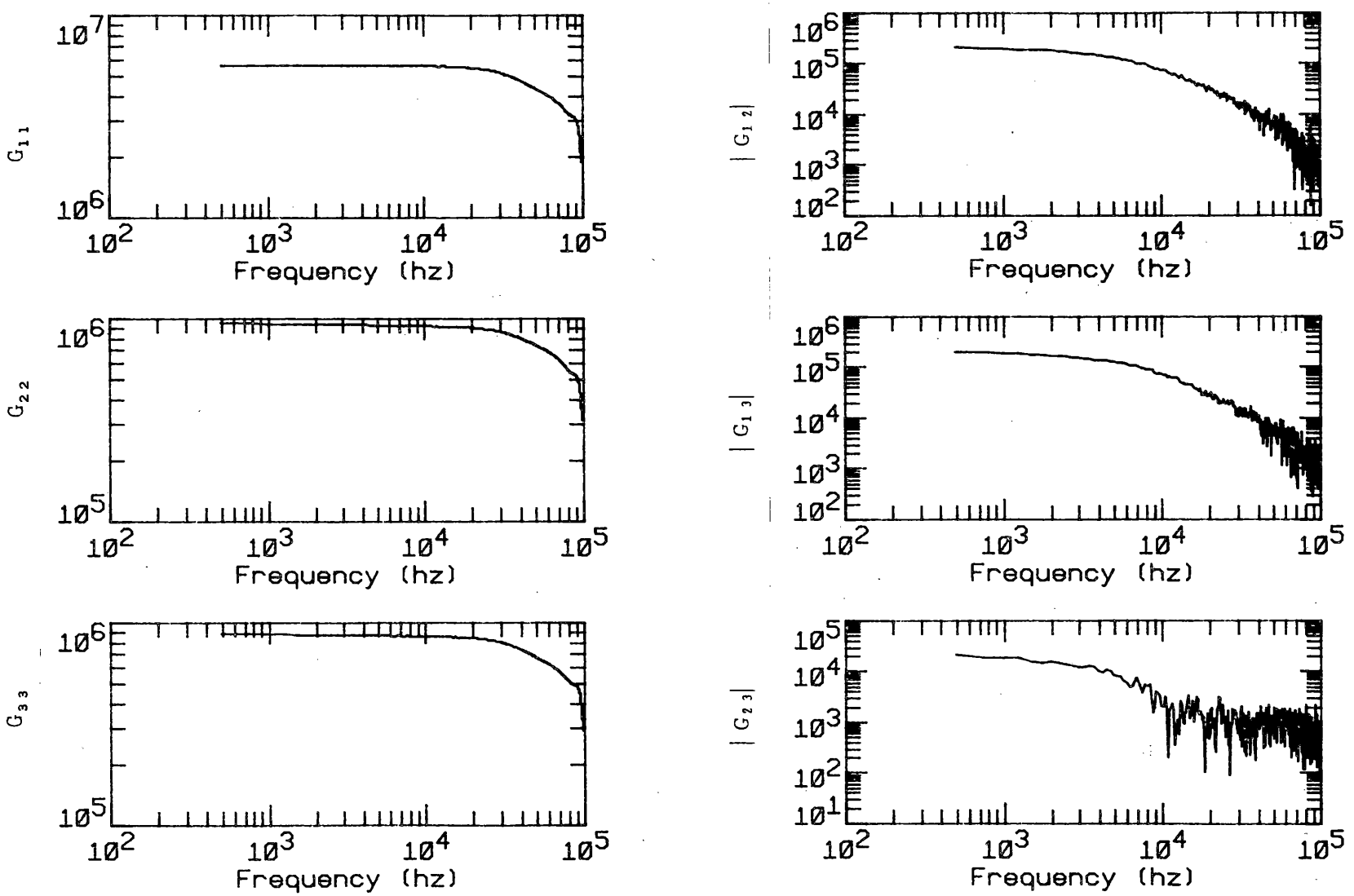

Fig. B.13. APSDs and CPSDs as a function of frequency for a solution height of 15.2 cm and a source height of 13.92 cm.

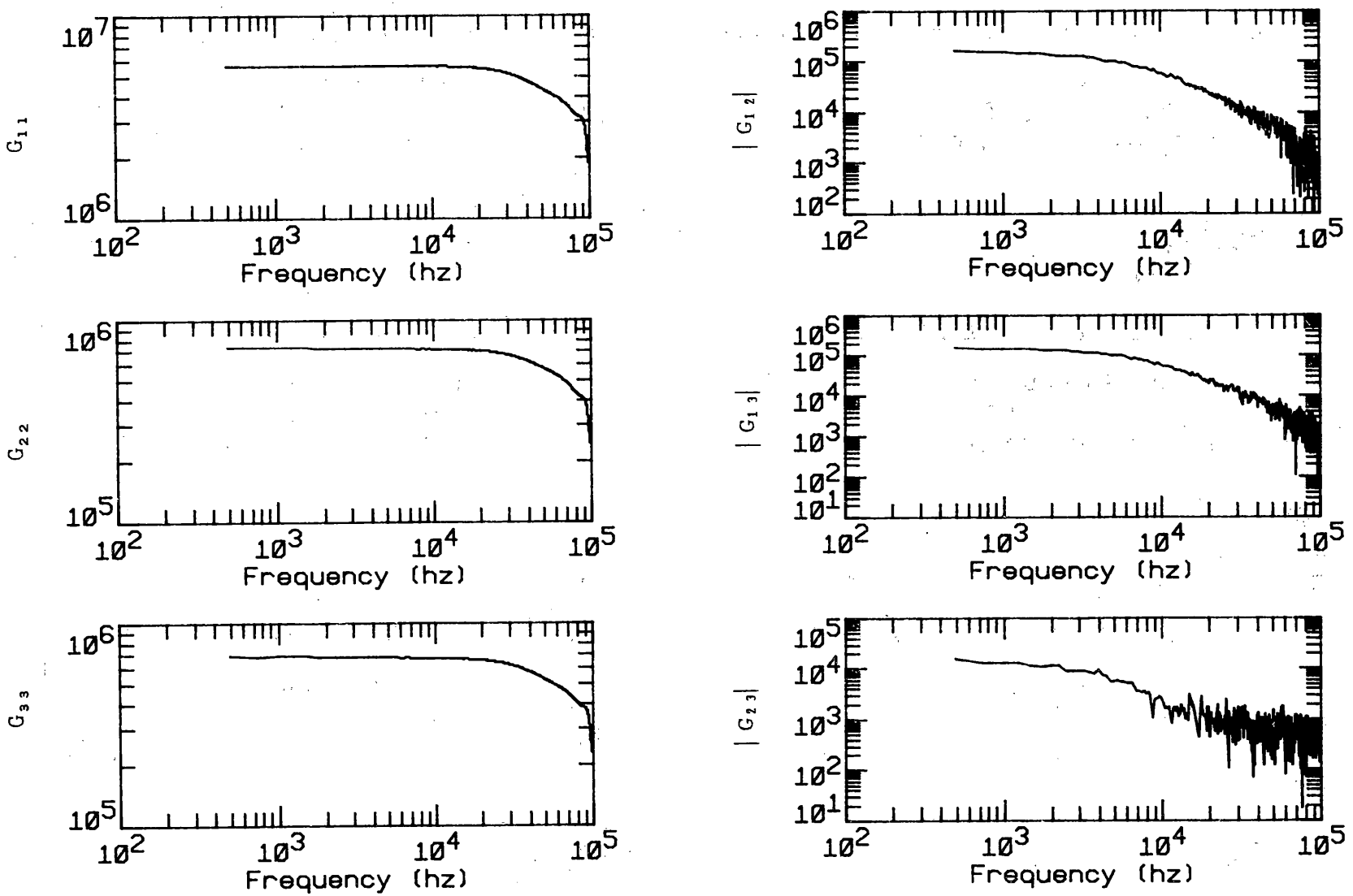

Fig. B.14. APSDs and CPSDs as a function of frequency for a solution height of 15.2 cm and a source height of 15.24 cm.

APPENDIX C

PARAMETERS FOR INTERPRETATION OF THE RATIO OF SPECTRAL DENSITIES TO OBTAIN THE NEUTRON MULTIPLICATION FACTOR

APPENDIX C. PARAMETERS FOR INTERPRETATION OF THE RATIO OF SPECTRAL DENSITIES TO OBTAIN THE NEUTRON MULTIPLICATION FACTOR

Several parameters that appear in Appendix A Eqs. (A.1) through (A.11) and that are used for interpretation of the ratio of spectral densities to obtain the neutron multiplication factor can be independently measured or obtained from measurements of others. The origins of these parameters and their values are described below. Also, the sensitivity of the interpretations to variations in these parameters is presented as a function of k_{eff} value.

The value of $q_\alpha = 0$. This results from the electronics associated with the ^{252}Cf ionization chamber, which discriminates against the contribution to the signal from alpha particle decay in the ionization chamber. The value of q_c is unity because the contributions to the signal from all ^{252}Cf fissions are the same.

Since there is no significant inherent neutron source in the uranyl nitrate solution comparable to the size of the ^{252}Cf source, the third term in Eq. (A.5) is zero, and since more than 99.5% of the ^{252}Cf spontaneous fission produces signals in channel 1 that are counted, $Y = A = S_R = 1$.

The average number of neutrons per uranium fission was obtained by using the fluxes from transport theory calculations and the ENDF/B-IV data[1] to calculate the total number of neutrons per uranium fission. This averaging accounts properly for the dependence of the average number of neutrons per fission on the energy of the neutron inducing the fission. Changing solution height resulted in less than a 0.2% change in the value of the number of neutrons per fission, and the resulting average number of neutrons per uranium fission was 2.426. The value of the average number of prompt neutrons per fission, $\bar{\nu}$, is 2.408 and was used for interpretation at all solution heights.

The number of delayed neutrons per uranium fission was calculated from the delayed neutron yields, the delayed neutron effectiveness factors obtained using the forward and adjoint fluxes from transport theory,[2] and the delayed neutron spectra of Batchelor and McKhyder.[3] The effective delayed neutron fraction calculated in this way is 0.0075.

The value of the Diven factor ($X = \overline{\nu(\nu - 1)}/\bar{\nu}^2$) was obtained from the measurements of prompt neutron multiplicities for uranium. Its value does not depend significantly on the energy of the neutron inducing fission, and varies only from 0.796 to 0.809 when the neutron energy varies from thermal to 2 MeV.[4] The value of X used was 0.80. The value of the number of prompt neutrons per ^{252}Cf fission and its mean square ($\bar{\nu}_c$ and $\overline{\nu_c^2}$) are from the measurements of prompt neutron multiplicities of Spencer, Gwin, and Ingle,[5] $\bar{\nu}_c = 3.773$ and $\overline{\nu_c^2} = 15.818$.

The neutron importance ratios I_c/I used for interpretation of the data were obtained from the KENO[6] code, which calculated the ratios directly. The values of I_c/I are given in Table C.1 and plotted in Fig. C.1 as a function of solution height with the source in the center and at the bottom of the solution. Values of I_c/I, obtained from Monte Carlo calculations, as a function of axial source position for solution heights of 15.2, 20.3 and 25.4 cm are given in Table C.2 and plotted in Fig. C.2. These calculations were done with the source ionization chamber and the Lexan tube included in the geometry of the calculation.

The value of the factor R, which is introduced into the point kinetics equations to account for global spatial effects, was obtained from fluxes obtained from transport theory calculations. The values are tabulated in Table C.1 and plotted in Fig. C.3 for a variety of solution heights with the source at the vertical center of the fuel solution and also on the bottom of the solution. For a fixed solution height the value of R does not depend significantly on the location of the ^{252}Cf source. The largest dependence in the value of R on the source location for a fixed solution height was a change in R of 0.35%; while the values of R varied from 1.063 to 1.149 as the solution height varied from 4 to 30.5 cm, which is a total variation of ~8%.

Table C.1. Parameters I_c/I and R used to interpret the ratio of spectral densities as a function of solution height

Solution height (cm)	Importance ratio, I_c/I[a] for source locations at					Spatial effects factor, R[b] for source locations at	
			Height (cm)				
	Bottom	Center	2.5	5.1	7.6	Bottom	Center
30.5	0.511	1.74	0.904	1.186	1.43	-	1.149
27.9	0.595	1.72	-	-	-	1.149	-
25.4	0.615	1.67	0.980	1.250	1.570	1.145	1.143
20.3	0.698	1.55	1.096	1.330	1.490	1.135	1.135
15.2	0.789	1.43	1.184	1.437	1.432	1.122	1.124
12.7	0.814	-	-	-	-	1.114	-
10.2	0.842	1.28	1.242	1.285	1.044	1.103	1.104
6.5	0.862	-	-	-	-	1.082	-
4.0	0.806	-	-	-	-	1.063	-

[a]Values of I_c/I are from Monte Carlo calculations. Monte Carlo results have a precision of ~3%. Heights are distance above bottom of the tank.

[b]Calculated using transport theory.

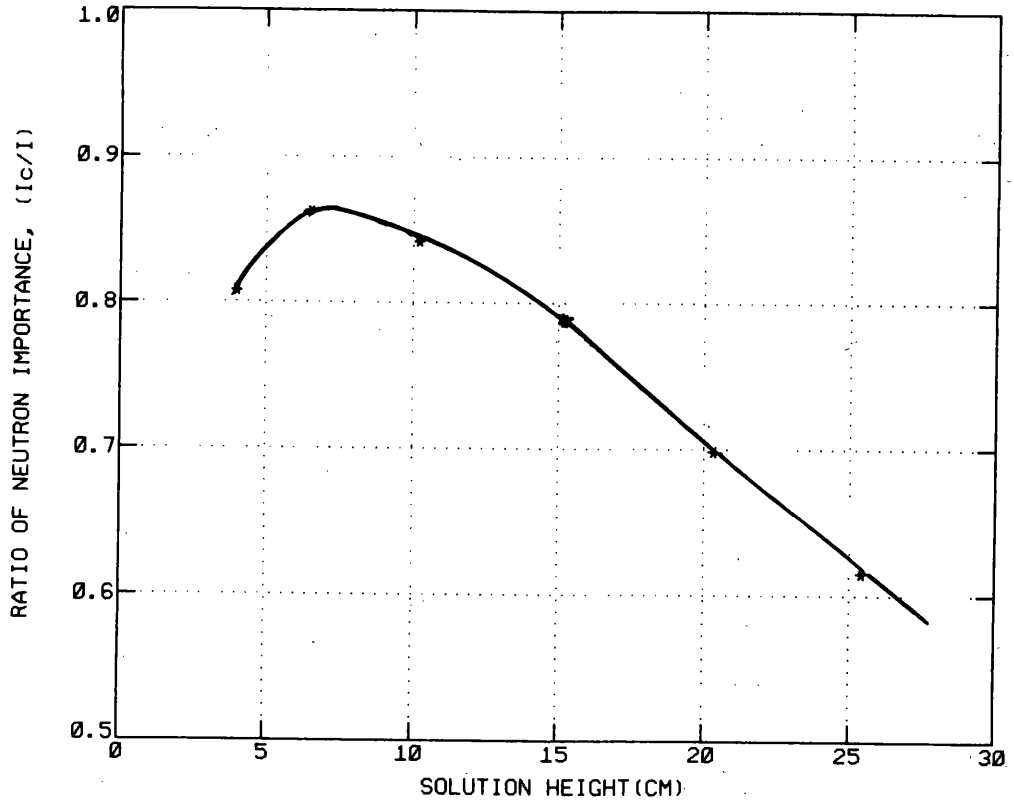

Fig. C.1. Ratio of neutron importance I_c/I as a function of height of uranyl nitrate solution in a 25.1-cm ID cylindrical tank with the source at the bottom of the tank.

The sensitivity of the neutron multiplication factor obtained from the ratio of spectral densities to the various parameters, P_i, used in the equations was determined by calculating the percentage change in k_{eff} for a 10% increase in the various parameters. The sensitivity coefficients, $(\Delta k/k)/(\Delta P_i/P_i)$, along with estimates of the uncertainty in the parameters, are given in Table C.3. At high values of k_{eff} (0.95), a 10% change in any parameter changes the $\Delta k/k$ values by ~0.004 at most. At low k_{eff} values (0.35), a 10% increase in the parameter changes the $\Delta k/k$ values from 0.021 to 0.143. The higher the k_{eff} values the less precisely the parameters have to be known to determine the k_{eff} values to a given precision. Conversely, to obtain the k_{eff} value at very low values, the parameters have to be known more accurately. In practical applications of this method the accuracy requirements of the method are less at lower k_{eff} values.

Table C.2. I_c/I from Monte Carlo calculation as a function of axial source position for solution heights of 15.2, 20.3 and 25.4 cm

Axial position of Cf source[a] (cm)	Importance ratio, I_c/I,[b] for solution height of		
	15.2 cm	20.3 cm	25.4 cm
25.4	-	-	0.375
24.1	-	-	0.555
22.9	-	-	0.770
20.32	-	0.432	1.064
19.1	-	0.641	-
17.8	-	0.832	1.340
16.5	-	-	-
15.2	0.499	1.208	1.519
14.0	0.743	-	-
12.7	0.951	1.430	1.675
10.2	1.280	1.550	1.626
7.6	1.432	1.490	1.566
5.1	1.437	1.330	1.254
2.5	1.184	1.096	0.980
1.3	0.984	0.894	0.836
0	0.789	0.698	0.615

[a]Height above bottom of tank.

[b]All values from Monte Carlo calculations. Precision on the ratios is ~3%.

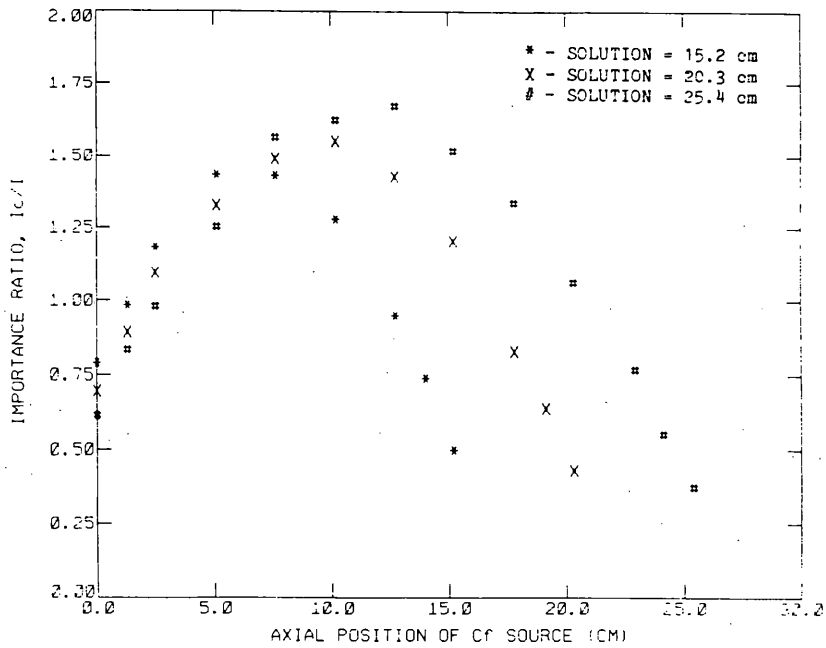

Fig. C.2. Ratio of importance I_c/I as a function of axial location of the source for solution heights of 15.2, 20.3, and 25.4 cm.

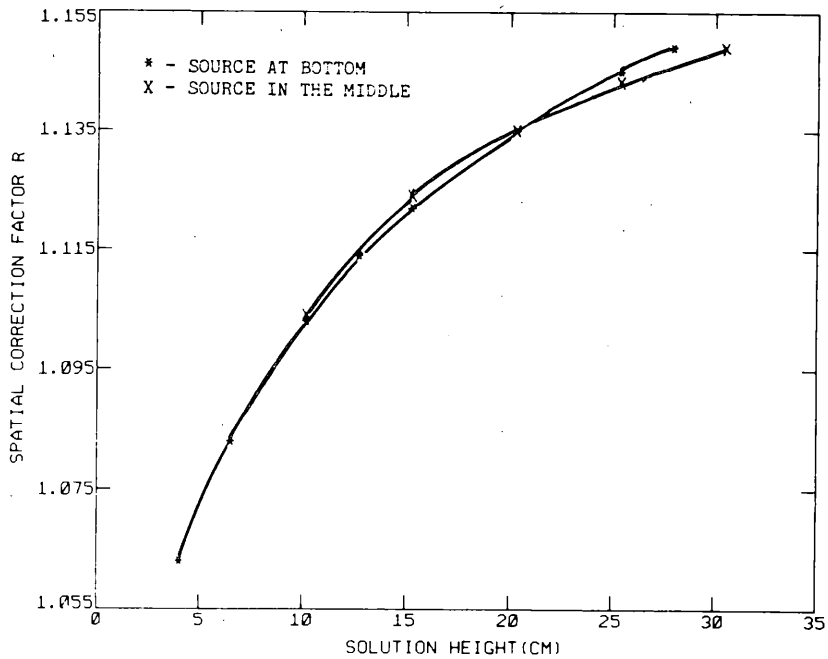

Fig. C.3. Global spatial correction factor R as a function of height of uranyl nitrate solution in a 25.1-cm-ID cylindrical tank.

Table C.3. Sensitivity of k_{eff} to parameters used in interpretation of the experimental data for various k_{eff} values

	Sensitivity coefficient[a] in percent for keff values of					
Parameter, (P[b])	0.95	0.90	0.81	0.72	0.53	0.35
Ratio	-0.42	-1.03	-2.70	-4.97	-14.80	-36.10
I_c/I	0.42	1.00	1.85	3.04	6.27	11.50
R, X, ν	-0.42	-1.00	-1.84	-2.62	-4.56	-6.02
$\bar{\nu}_c$	0.42	1.23	2.83	5.45	16.50	41.00
$\overline{\nu_c^2}$	0	-0.11	-0.62	-1.66	-7.79	-23.50
β_{eff}	<0.01	<0.01	<0.01	<0.01	<0.01	<0.01

[a]Calculated assuming a 10% increase in the parameter P. Values tabulated are the percentage change in $\Delta k/k$ for a 10% change in the parameter P.

[b]The estimates of the actual uncertainties in the parameters are 0.25% for X, 1% for R, 1.7% for β, 0.1% for $\bar{\nu}$, 1% for I_c/I, 0.4% for $\bar{\nu}_c$, and 0.2% for $\overline{\nu_c^2}$.

APPENDIX C REFERENCES

1. G. D. Garber, "ENDF-201, ENDF/B Summary Documentation," Brookhaven National Laboratory Report BNL 17541 (1975).

2. W. A. Rhoades, D. B. Simpson, R. L. Childs, and W. W. Engle, Jr., "The DOT-IV Two-Dimensional Discrete Ordinates Transport Code with Space-Dependent Mesh and Quadrature," ORNL/TM-6529, Oak Ridge National Laboratory, 1979.

3. R. Batchelor and H. R. McKhyder, "The Energy of Delayed Neutrons from Fission," J of Nucl. Energy 3, 7 (1956).

4. M. S. Zucker, N. E. Holden, "Energy Dependence of the Neutron Multiplicity Pν in Fast-Neutron-Induced Fission for ^{235}, ^{238}U, and ^{239}Pu," Trans. Am. Nucl. Soc. 52, 630 (1986).

5. R. R. Spencer, R. Gwin, and R. Ingle, "A Measurement of the Average Number of Prompt Neutrons from Spontaneous Fission of Californium-252, Nucl. Sci. Eng. 80, 603 (1982).

6. L. M. Petrie and N. F. Cross, "KENO-Va: An Improved Monte Carlo Criticality Program with Supergrouping," NUREG/CR-0200. Sect. F11, ORNL/NUREG/CSD-2, Vol. 2, Oak Ridge National Laboratory, 1985.

APPENDIX D

CALCULATED NEUTRON MULTIPLICATION FACTORS

APPENDIX D. CALCULATED NEUTRON MULTIPLICATION FACTORS

The neutron multiplication factors were calculated using the Monte Carlo method with the KENO code and Hansen-Roach[1,2] and ENDF/B-IV[3] cross sections. The calculations included the source and its Lexan tube and the reflection effect of the scintillation detectors as located in the measurements. The results of these calculations are given in Table D.1. The calculated reflection of the scintillation detectors is a slight increase (~0.005) and is approximately equal to the statistical error in the calculations. The k_{eff} values using the ENDF/B-IV data were consistently higher than those from Hansen-Roach cross sections by an average of 2% in k_{eff}. The calculated k_{eff} values with the Hansen-Roach cross sections are in better agreement with the experimental values.

Table D.1. Neutron multiplication factors from Monte Carlo calculations with Hansen-Roach cross sections

Solution height (cm)	Calculated neutron multiplication factors[a]			
	Hansen-Roach cross sections			ENDF/B-IV 27 group.
	Source and scintillators[b]	Source only[c]	No source, no scintillators[d]	No source, no scintillators[d]
30.48	0.949	0.950	0.963	0.982
27.9	0.939	0.916	-	-
25.4	0.894	0.896	0.902	0.938
24.0	0.897	-	-	-
22.9	0.867	0.870	-	-
22.0	0.862	-	-	-
20.4	0.844	0.831	0.841	0.868
15.2	0.721	0.721	0.741	0.763
10.2	0.553	0.547	0.544	0.574
5.08	-	0.241	0.249	0.256

[a]Statistical error is ~0.005. All calculations included the bottom, sides, and top of the tank. Where the source was included in the calculation, the 2.54-cm-OD Lexan tube was included in the calculation. As a result, with the source located at any height of solution the Lexan tube displaced solution on the axis of the cylinder above the source position.

[b]Source located at the bottom of the tank and the scintillators as in Fig. 6 were included in the calculation.

[c]Source at the center of solution height on the axis of the tank was included in the calculation.

APPENDIX D REFERENCES

1. G. E. Hansen and W. H. Roach, "Six and Sixteen-Group Cross Sections for Fast and Intermediate Critical Assemblies," Los Alamos Scientific Laboratory Report LAMS-2543, 1961.

2. L. M. Petrie and N. F. Cross, "KENO-IV: An Improved Monte Carlo Criticality Program," ORNL-4983, Oak Ridge National Laboratory, 1975.

3. G. D. Garber, "ENDF-201, ENDF/B Summary Documentation", Brookhaven National Laboratory Report BNL 17541, 1975.

APPENDIX E

REACTIVITY EFFECT OF THE DETECTORS

APPENDIX E. REACTIVITY EFFECT OF THE DETECTORS

The reactivity effect of the scintillation detectors as positioned in the dynamic measurements was estimated from experiments, and the results are given in Table E.1. The reactivity effect of the scintillators was obtained experimentally from changes in the neutron count rate and from measured ratios of spectral densities obtained from ^{3}He proportional counters as the scintillators were added. Measurements were also performed with the scintillators upright in contact with the surface of the tank (in this case, one 15.2 x 15.2 x 10.7 cm scintillator in each pair was above the other and in contact with the experimental vessel). This location of detectors is similar to that of Fig. 6 (p.10) but with each adjacent pair of detectors rotated 90°. These results are given in Table E.1.

The change in neutron count rates in external ^{3}He proportional counters before and after the scintillators were in place was measured when the scintillators were added to a system with a central source and a solution height of 25.4 cm. The average increase in the neutron count rates was 24%. Since the k_{eff} value for this solution height is 0.91, then from this change in the count rate, the increase in k_{eff} resulting from the addition of the scintillators is estimated to be 0.018 with the detectors upright and in contact with the experimental vessel. This evaluation assumes that the detection efficiency of the ^{3}He proportional counters used for this measurement is not changed by the addition of the scintillators. The reactivity effect of the scintillators upright and in contact with the experimental vessel can also be obtained from the change in the ratio of spectral densities when the scintillators are added to a system with a solution height of 25.4 cm. This change in ratios was 17% and indicates that the change in k_{eff} is 0.015.

The low-reflection effect of these scintillators, which contain considerable plastic, is due to the location of the ^{6}Li glass adjacent to the experimental vessel with the plastic scintillator part of the detector separated from the experimental vessel by the ^{6}Li glass. Thermal neutrons leaking from the experimental vessel are absorbed by the ^{6}Li glass. Most of the fast neutrons leaking from the experimental vessel pass through the ^{6}Li glass and are slowed down in the plastic. The slow neutrons that are reflected back toward the experimental vessel are absorbed in the ^{6}Li. These estimates are for the scintillation detectors upright and in contact with the experimental vessel.

In the dynamic noise analysis measurements, the ^{6}Li-glass-plastic scintillators were 2.54 cm from the experimental vessel and were located as shown in Fig. 6, with their centers 8 cm above the bottom of the tank. For this configuration with solution heights lower than 15 cm, the thermal neutrons reflected back to the solution were absorbed by the ^{6}Li. However, for solutions with heights greater than the height of the detectors, thermal neutrons reflected back toward the vessel and above

Table E.1. Summary of reactivity effects of the ^{6}Li-glass-plastic scintillators from several measurements

Detector-source-system configuration	Without scintillators	With scintillators	Δk[a]
Detectors upright against experimental vessel with solution height of 25.4 cm with source height of 12.7 cm	Count rate = 4644 cps	Count rate = 5785 cps	0.018
Detectors upright against experimental vessel with solution height of 25.4 cm with source height of 12.7 cm	Ratio[b] = 0.197	Ratio = 0.164	0.015
Detectors as shown in Fig. 6., 2.5 cm back from the experimental vessel for a solution height of 25.4 cm and source height of 7.62 cm	Ratio = 0.178	Ratio = 0.148	0.015
Detectors as shown in Fig. 6., 2.5 cm back from the experimental vessel for a solution height of 25.4 cm and source height of 5.1 cm	Ratio = 0.158	Ratio = 0.134	0.014
Detectors as shown in Fig. 6., 2.5 cm back from the experimental vessel for a solution height of 20.3 cm and source height of 0 cm	Ratio = 0.162	Ratio = 0.142	0.013

[a]All estimates based on k_{eff} of 0.91 for a solution height of 25.4 cm.

[b]Ratio designates the ratio of spectral densities.

the ^{6}Li glass of the front face of the detectors could reenter the solution and produce fissions. In this case, the change in k_{eff} due to the location of the scintillators, obtained by comparing how the ratios of spectral densities measured with ^{3}He detectors changed when the scintillators were located as shown in Fig. 6, was 0.014, which was an average of three measurements (0.015, 0.014, and 0.013).

The reactivity effect of the ^{3}He proportional counters was negligible since they are thin-walled aluminum, filled with ^{3}He gas.

APPENDIX F

ADDITIONAL DYNAMIC EXPERIMENTS

APPENDIX F. ADDITIONAL DYNAMIC EXPERIMENTS

Dynamic measurements were also performed with the Cf source at axial positions other than on the bottom of the tank, namely 2.5, 5.1, and 7.6 cm from the bottom of the tank and on the axis of the cylinder. Experiments were performed while the vessel was filled and drained, and the results are presented in Tables F.1 through F.4. The k_{eff} values given in the tables assumed a point kinetics interpretation of the data. For low solution heights, the source locations for these experiments produce modal effects in the measurements, and modal corrections must be included to obtain the proper k_{eff} values. These modal effect corrections have not been included in this interpretation of the data. Thus, the differences in k_{eff} values obtained from those given previously in this report are estimates of the magnitude of modal effects on the ratio of spectral densities and k_{eff} values. As in the measurements with the source at the bottom of the solution, the results do not depend on whether the vessel was filled or drained. The ratios of spectral densities are also plotted as a function of frequency in Figs. F.1 through F.3. The squares of the coherences, γ^2_{12} and γ^2_{23}, at low frequency are plotted in Fig. F.4. The values of γ^2_{12} at low frequency are generally larger with the source closer to the center while those of γ^2_{23} do not depend significantly on source position.

Table F.1. Ratios of spectral densities at low frequency and neutron multiplication factors for dynamic measurements while filling the experimental vessel with the source 2.5 cm from the bottom of the vessel

Time[a] (h:m:s)	Solution height[b] (cm)	Ratio of spectral densities[c]	k_{eff} from ratio of spectral densities[d]
17:01:36	10.92	0.489 ± 0.002	0.606 ± 0.003
17:03:18	12.17	0.446 ± 0.002	0.659 ± 0.002
17:05:00	13.58	0.404 ± 0.001	0.704 ± 0.002
17:06:42	14.93	0.360 ± 0.001	0.747 ± 0.001
17:08:24	16.33	0.320 ± 0.001	0.782 ± 0.001
17:10:06	17.75	0.280 ± 0.001	0.814 ± 0.001
17:11:48	19.19	0.243 ± 0.001	0.841 ± 0.001
17:13:30	20.63	0.207 ± 0.001	0.866 ± 0.001
17:15:12	22.02	0.179 ± 0.001	0.884 ± 0.001
17:16:53	23.55	0.152 ± 0.001	0.900 ± 0.001
17:18:35	25.01	0.123 ± 0.001	0.918 ± 0.001
17:20:17	26.48	0.100 ± 0.001	0.933 ± 0.001
17:21:59	27.93	0.080 ± 0.001	0.946 ± 0.001
17:23:40	28.78	0.070 ± 0.001	0.952 ± 0.001
17:25:21	28.78	0.068 ± 0.001	0.953 ± 0.001

[a]End of a measurement time interval of ~102 s over which the data were averaged and the interpreted results displayed on a computer terminal. This time does not correspond to the average height during the measurement interval, but to the height at the end of the interval. The time which corresponds to the average height can be obtained by averaging the time listed with the time at the end of the previous interval. The number of points per data block was 1024, and the number of data blocks averaged in ~102 s was 20,000 with a sampling rate of ~200 kHz.

[b]Average height of solution during the time interval of the measurement, which ends at the time given in Col. 1.

[c]Average value during the time interval of the measurement. The statistical uncertainty given here is one standard deviation of the mean. The ratio of spectral densities was averaged up to a frequency of 10 kHz for heights <20 cm, 6 kHz for heights between 20 and 25 cm, and 2 kHz for height of >25 cm.

[d]These values are not corrected for modal effects. Estimates of the correction can be obtained by comparing these values with those for the source at the bottom of the tank. The uncertainty in k_{eff} is from the statistical uncertainty in the ratio of spectral densities only.

Table F.2. Ratios of spectral densities at low frequency and neutron multiplication factors for dynamic measurements while draining the experimental vessel at a rate of ~12 cm/min with the source 2.5 cm from the bottom of the vessel

Time[a] (h:m:s)	Solution height[b] (cm)	Ratio of spectral densities[c]	k_{eff} from ratio of spectral densities[d]
17:27:26	28.78	0.072 ± 0.001	0.950 ± 0.001
17:27:32	28.78	0.063 ± 0.002	0.957 ± 0.002
17:27:38	28.78	0.063 ± 0.002	0.957 ± 0.002
17:27:44	28.78	0.063 ± 0.003	0.957 ± 0.002
17:27:50	28.78	0.068 ± 0.001	0.954 ± 0.001
17:27:57	28.78	0.068 ± 0.001	0.953 ± 0.001
17:28:05	28.78	0.067 ± 0.003	0.954 ± 0.002
17:28:08	28.78	0.066 ± 0.006	0.955 ± 0.005
17:28:14	28.04	0.077 ± 0.000	0.948 ± 0.001
17:28:21	26.85	0.097 ± 0.005	0.934 ± 0.003
17:28:27	25.54	0.115 ± 0.001	0.923 ± 0.001
17:28:33	24.24	0.136 ± 0.003	0.911 ± 0.002
17:28:40	22.76	0.167 ± 0.003	0.892 ± 0.002
17:28:46	21.49	0.185 ± 0.003	0.881 ± 0.002
17:28:52	20.43	0.208 ± 0.003	0.866 ± 0.002
17:28:59	19.19	0.240 ± 0.003	0.844 ± 0.003
17:29:05	17.96	0.257 ± 0.005	0.833 ± 0.004
17:29:12	16.55	0.310 ± 0.004	0.791 ± 0.003
17:29:18	14.55	0.344 ± 0.004	0.765 ± 0.004
17:29:24	12.95	0.388 ± 0.002	0.724 ± 0.002
17:29:30	12.17	0.410 ± 0.006	0.701 ± 0.006
17:29:37	11.20	0.455 ± 0.007	0.650 ± 0.009
17:29:43	10.44	0.462 ± 0.009	0.643 ± 0.011
17:29:49	10.20	0.515 ± 0.010	0.569 ± 0.015
17:29:56	10.12	0.506 ± 0.010	0.582 ± 0.016
17:30:03	10.12	0.510 ± 0.011	0.578 ± 0.017
17:30:10	10.14	0.519 ± 0.007	0.563 ± 0.010
17:30:17	10.14	0.548 ± 0.012	0.517 ± 0.021
17:30:21	10.15	0.513 ± 0.017	0.572 ± 0.026
17:30:27	10.16	0.495 ± 0.008	0.599 ± 0.012

Table F.2 (continued)

Time[a] (h:m:s)	Solution height[b] (cm)	Ratio of spectral densities[c]	k_{eff} from ratio of spectral densities[d]
17:30:34	10.16	0.521 ± 0.008	0.561 ± 0.012
17:30:41	10.15	0.517 ± 0.015	0.567 ± 0.023
17:30:48	10.14	0.494 ± 0.009	0.600 ± 0.014
17:30:55	10.14	0.523 ± 0.007	0.558 ± 0.012

[a]End of a measurement time interval of ~6.4 s over which the data were averaged and the interpreted results displayed on a computer terminal. This time does not correspond to the average height during the measurement interval, but to the height at the end of the interval. The time which corresponds to the average height can be obtained by averaging the time listed with the time at the end of the previous interval. The number of points per data block was 256, and the number of data blocks averaged in ~6.4 s was 5000 with a sampling rate of ~200 kHz.

[b]Average height of solution during the time interval of the measurement, which ends at the time given in Col. 1.

[c]Average value during the time interval of the measurement. The statistical uncertainty given here is one standard deviation of the mean. The ratio of spectral densities was averaged up to a frequency of 10 kHz for heights <21 cm, 6 kHz for heights of 22 to 25 cm, and 2.5 kHz for heights of >25 cm.

[d]These values are not corrected for modal effects. Estimates of this correction can be obtained by comparing these values with those for the source at the bottom of the tank. The uncertainty in k_{eff} is from the statistical uncertainty in the ratio of spectral densities only.

Table F.3. Ratios of spectral densities at low frequency and neutron multiplication factors for dynamic measurements while draining the experimental vessel at a rate of ~16 cm/min with the source 5.1 cm from bottom of the vessel

Time[a] (h:m:s)	Solution height[b] (cm)	Ratio of spectral densities[c]	k_{eff} from ratio of spectral densities[d]
11:00:53	29.21	0.077 ± 0.003	0.962 ± 0.0018
11:00:59	29.21	0.082 ± 0.004	0.959 ± 0.0019
11:01:05	29.21	0.078 ± 0.000	0.962 ± 0.0003
11:01:11	29.21	0.076 ± 0.003	0.963 ± 0.0017
11:01:17	29.21	0.083 ± 0.001	0.959 ± 0.0006
11:01:23	29.21	0.072 ± 0.001	0.965 ± 0.0004
11:01:29	29.21	0.085 ± 0.004	0.958 ± 0.0021
11:01:35	29.21	0.077 ± 0.002	0.962 ± 0.0012
11:01:42	29.17	0.086 ± 0.002	0.958 ± 0.0012
11:01:49	28.80	0.078 ± 0.001	0.962 ± 0.0004
11:01:56	27.75	0.089 ± 0.002	0.957 ± 0.0008
11:02:02	26.03	0.115 ± 0.006	0.944 ± 0.0035
11:02:08	24.42	0.158 ± 0.002	0.921 ± 0.0014
11:02:14	22.83	0.189 ± 0.003	0.904 ± 0.0018
11:02:20	20.93	0.229 ± 0.005	0.882 ± 0.0033
11:02:27	18.73	0.291 ± 0.004	0.843 ± 0.0027
11:02:34	16.57	0.325 ± 0.005	0.823 ± 0.0042
11:02:40	15.06	0.410 ± 0.008	0.753 ± 0.0079
11:02:46	13.26	0.422 ± 0.005	0.736 ± 0.0046
11:02:52	11.23	0.504 ± 0.012	0.632 ± 0.0162
11:02:58	10.10	0.509 ± 0.011	0.617 ± 0.0149
11:03:04	9.80	0.541 ± 0.009	0.570 ± 0.0139
11:03:10	9.77	0.517 ± 0.020	0.605 ± 0.0299
11:03:16	9.75	0.534 ± 0.010	0.580 ± 0.0148
11:03:22	9.77	0.542 ± 0.007	0.568 ± 0.0110
11:03:28	9.75	0.518 ± 0.019	0.603 ± 0.0281
11:03:35	9.77	0.499 ± 0.011	0.630 ± 0.0145

Table F.3 (continued)

Time[a] (h:m:s)	Solution height[b] (cm)	Ratio of spectral densities[c]	k_{eff} from ratio of spectral densities[d]
11:03:41	9.78	0.531 ± 0.008	0.584 ± 0.0120
11:03:47	9.78	0.541 ± 0.009	0.569 ± 0.0136
11:03:52	9.78	0.529 ± 0.009	0.587 ± 0.0133
11:04:08	9.78	0.537 ± 0.013	0.576 ± 0.0206
11:04:14	9.78	0.553 ± 0.007	0.551 ± 0.0118
11:04:21	9.78	0.538 ± 0.011	0.574 ± 0.0168

[a]End of a measurement time interval of ~6.4 s over which the data were averaged and the interpreted results displayed on a computer terminal. This times does not correspond to the average height during the measurement interval, but to the height at the end of the interval. The time which corresponds to the average height can be obtained by averaging the time listed with the time at the end of the previous interval. The number of points per data block was 256, and the number of data blocks averaged in ~6.4 s was 5000 with a sampling rate of ~200 kHz.

[b]Average height of solution during the time interval of the measurement, which ends at the time given in Col. 1.

[c]Average value during the time interval of the measurement. The statistical uncertainty given here is one standard deviation of the mean. The ratio of spectral densities was averaged up to a frequency of 10 kHz for heights <20 cm, 6 kHz for heights of 20 to 25 cm, and 2.5 kHz for heights of >25 cm.

[d]These values are not corrected for modal effects. Estimates of this correction can be obtained by comparing these values with those for the source at the bottom of the tank. The uncertainty in k_{eff} is from the statistical uncertainty in the ratio of spectral densities only.

Table F.4. Ratios of spectral densities at low frequency and neutron multiplication factors for dynamic measurements while draining the experimental vessel at a rate of 23 cm/min with the source 7.6 cm from the bottom of the vessel

Time[a] (h:m:s)	Solution height[b] (cm)	Ratio of spectral densities[c]	k_{eff} from ratio of spectral densities[d]
11:36:40	29.24	0.092 ± 0.002	0.959 ± 0.001
11:36:50	29.24	0.087 ± 0.002	0.960 ± 0.001
11:37:00	29.24	0.091 ± 0.002	0.958 ± 0.001
11:37:10	29.24	0.091 ± 0.002	0.958 ± 0.001
11:37:20	28.41	0.104 ± 0.002	0.952 ± 0.001
11:37:30	26.29	0.153 ± 0.003	0.931 ± 0.002
11:37:40	23.38	0.216 ± 0.003	0.898 ± 0.002
11:37:50	19.90	0.291 ± 0.003	0.844 ± 0.002
11:38:00	16.80	0.368 ± 0.004	0.779 ± 0.003
11:38:10	14.07	0.421 ± 0.005	0.728 ± 0.005
11:38:20	11.68	0.480 ± 0.008	0.663 ± 0.010
11:38:30	10.47	0.510 ± 0.012	0.624 ± 0.017
11:38:40	10.14	0.465 ± 0.008	0.682 ± 0.010
11:38:50	10.14	0.481 ± 0.008	0.662 ± 0.010
11:39:00	10.14	0.517 ± 0.010	0.615 ± 0.014
11:39:10	10.14	0.495 ± 0.008	0.645 ± 0.010
11:39:20	10.14	0.487 ± 0.009	0.654 ± 0.012
11:39:30	10.14	0.540 ± 0.011	0.581 ± 0.017
11:39:39	10.14	0.507 ± 0.009	0.628 ± 0.013

[a]End of a measurement time interval of ~10 s over which the data were averaged and the interpreted results displayed on a computer terminal. This time does not correspond to the average height during the measurement interval, but to the height at the end of the interval. The time which corresponds to the average height can be obtained by averaging the time listed with the time at the end of the previous interval. The number of points per data block was 256, and the number of data blocks averaged in ~10 s was 1000 with a sampling rate of ~50 kHz.

[b]Average height of solution during the time interval of the measurements, which ends at the time given in Col. 1.

[c]Average value during the time interval of the measurement. The statistical uncertainty given here is one standard deviation of the mean. The ratio of spectral densities was averaged up to a frequency of 5 kHz.

[d]These values are not corrected for modal effects. Estimates of this correction can be obtained by comparing these values with those for the source at the bottom of the tank. The uncertainty in k_{eff} is from the statistical uncertainty in the ratio of spectral densities only.

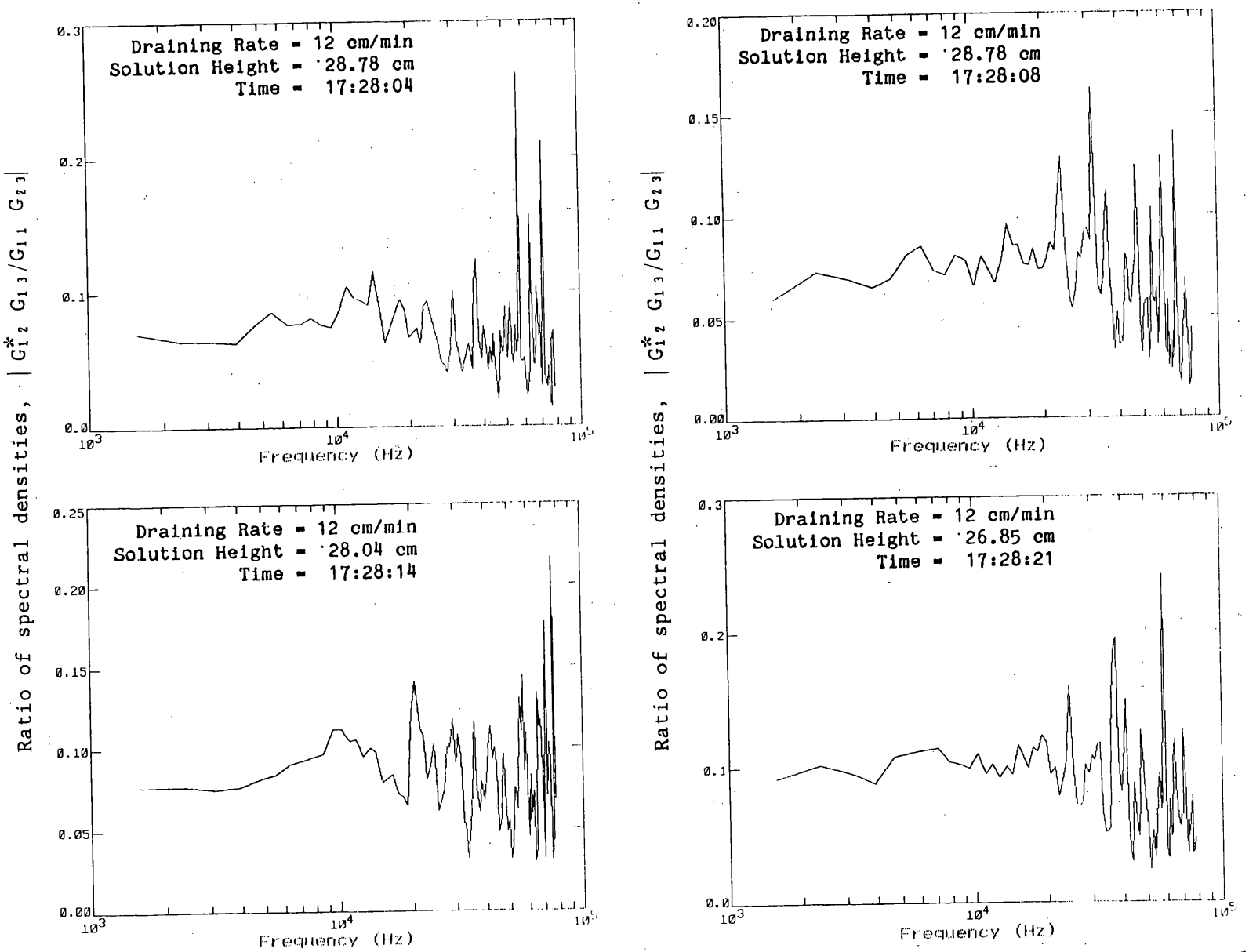

Fig. F.1. Ratios of spectral densities as a function of frequency as the experimental vessel was draining at a rate of ~12 cm/min with the source 2.5 cm from the bottom of the tank.

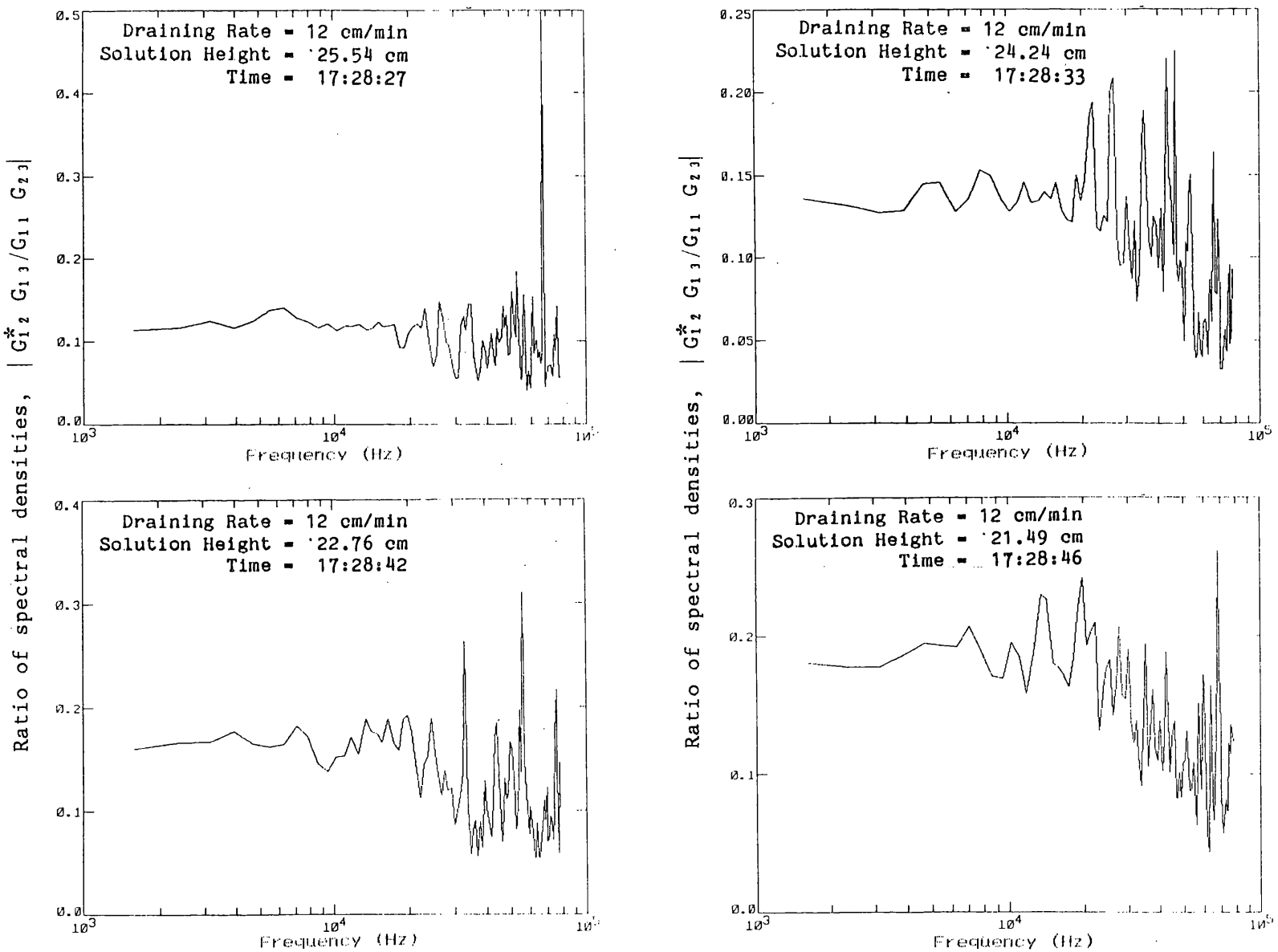

Fig. F.1. (continued)

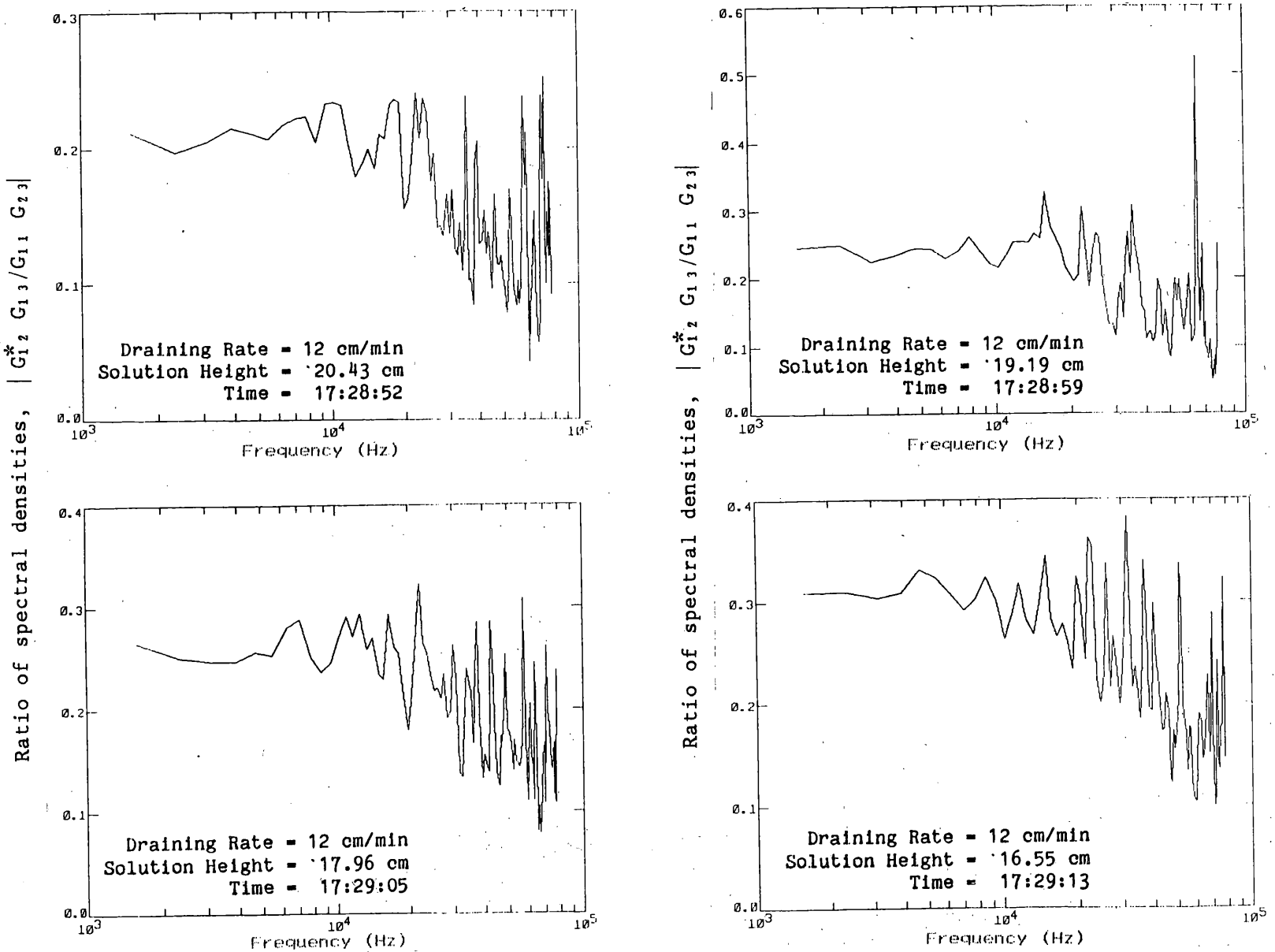

Fig. F.1. (continued)

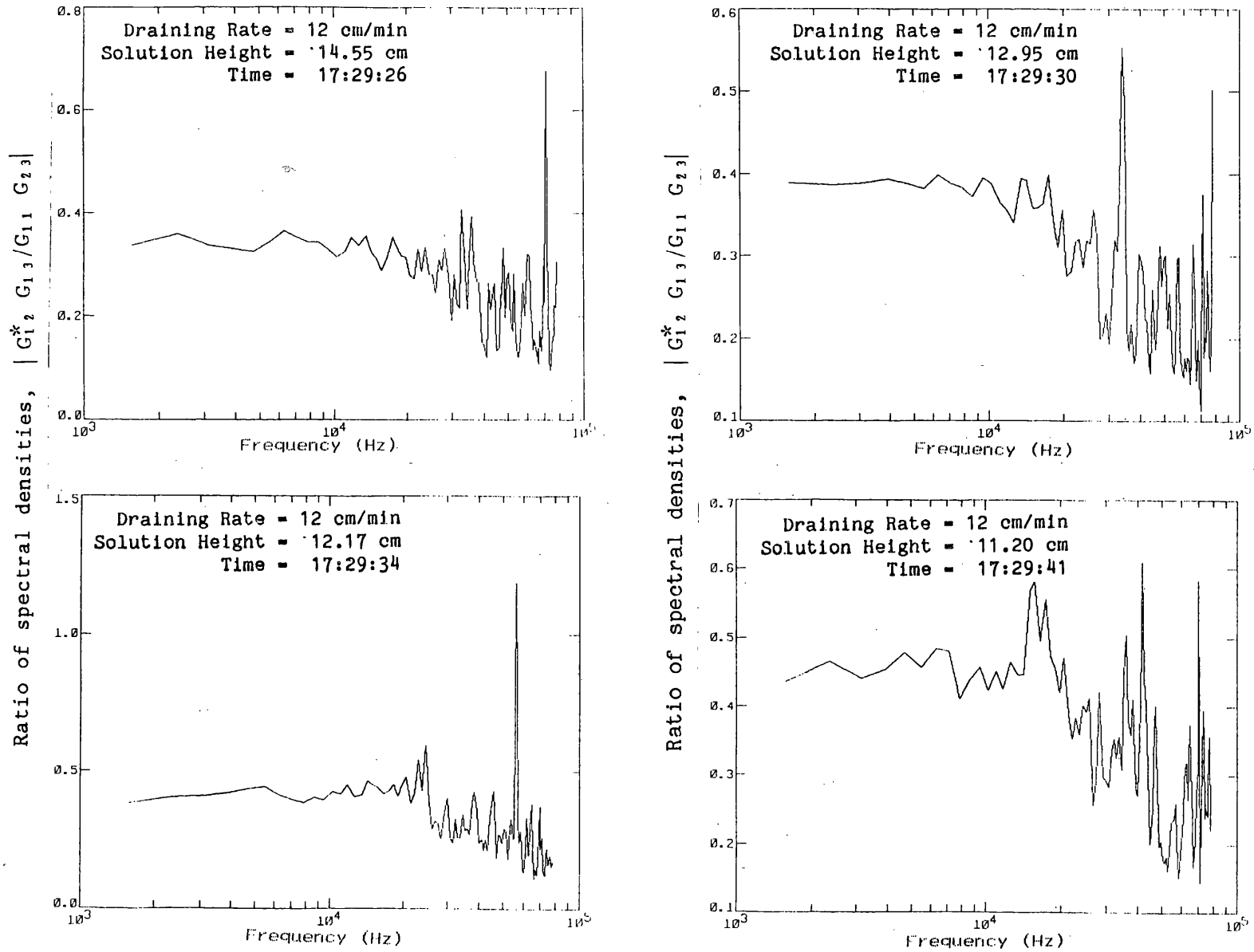

Fig. F.1. (continued)

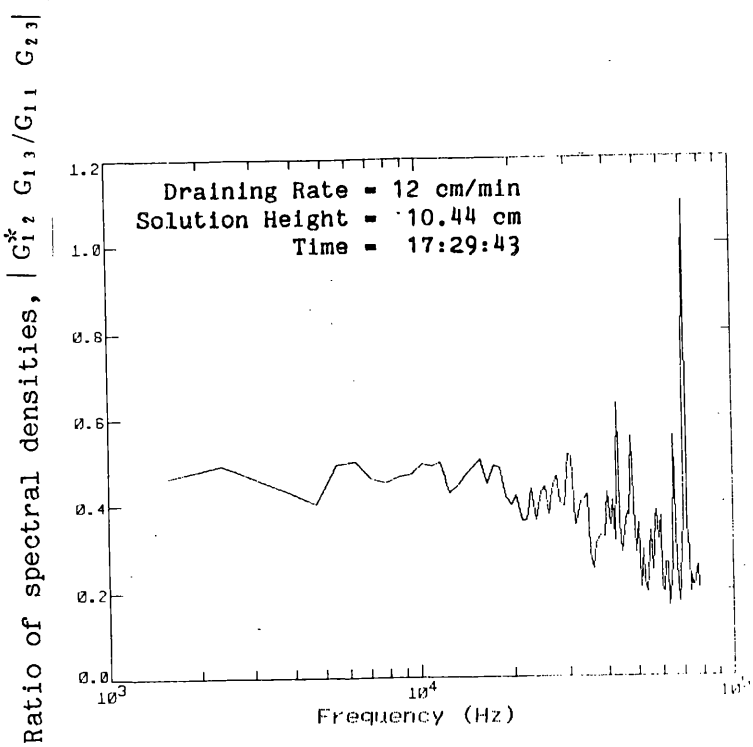

Fig. F.1. (continued)

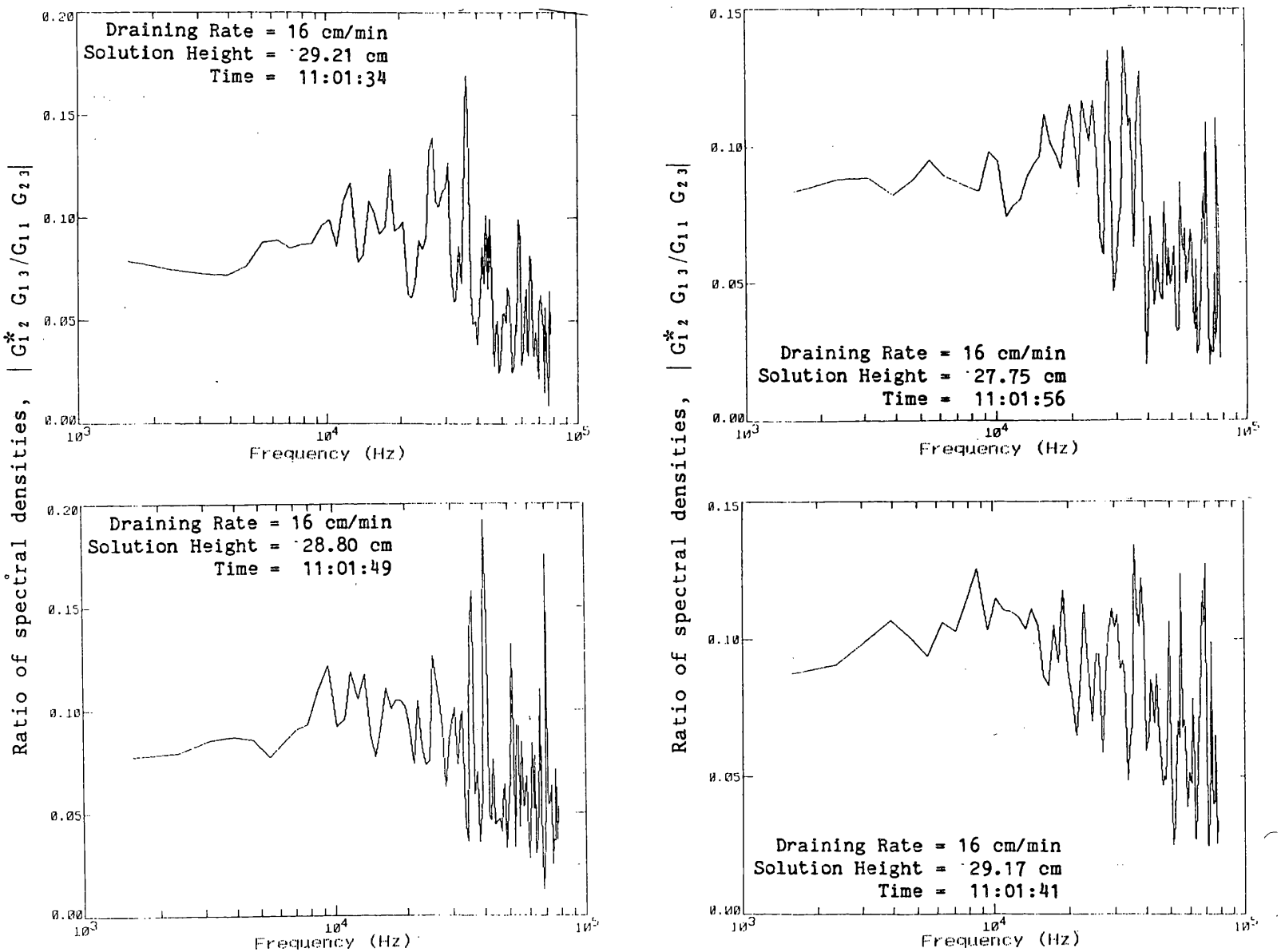

Fig. F.2. Ratios of spectral densities as a function of frequency as the experimental vessel was draining at a rate of ~16 cm/min with the source 5.1 cm from the bottom of the tank.

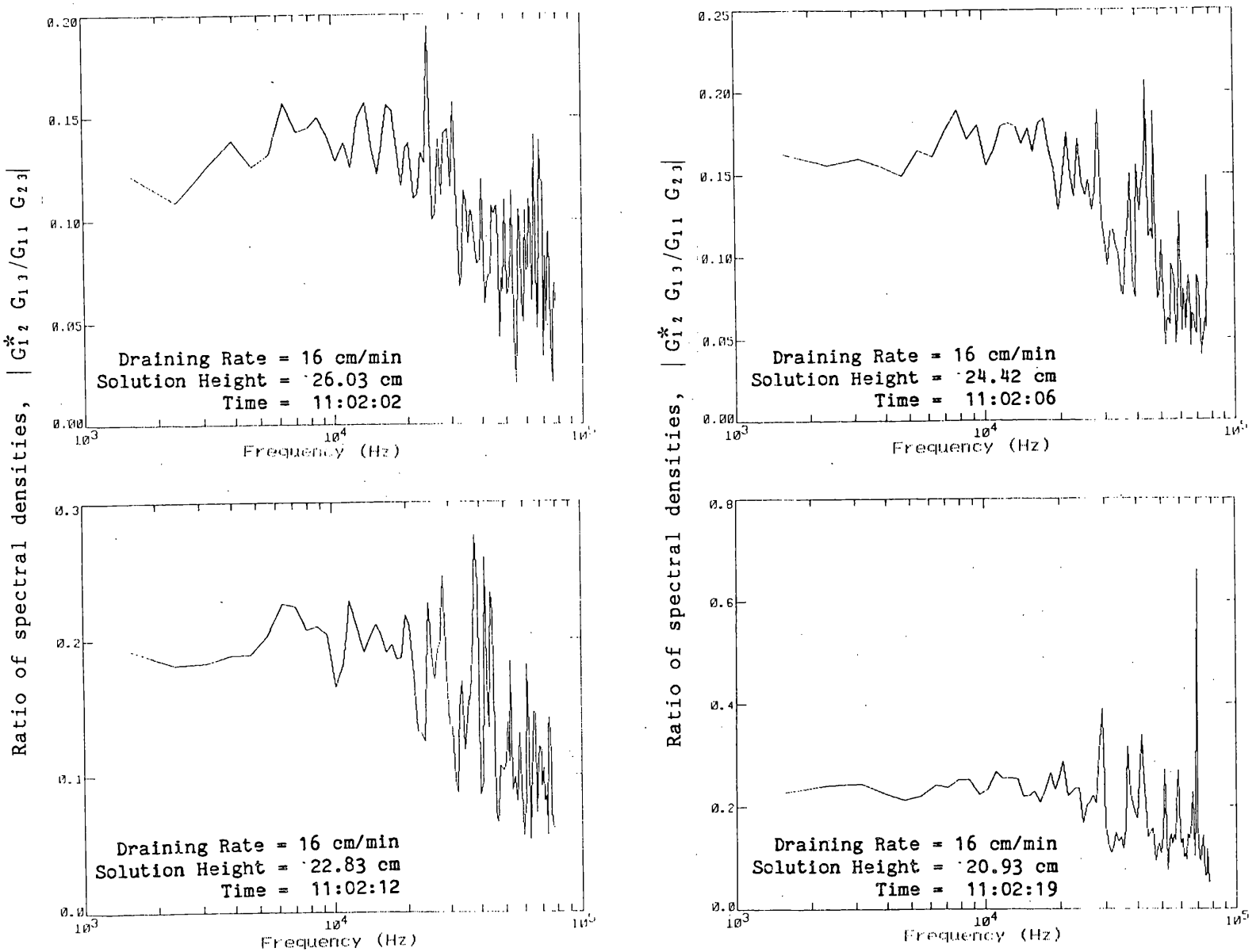

Fig. F.2. (continued)

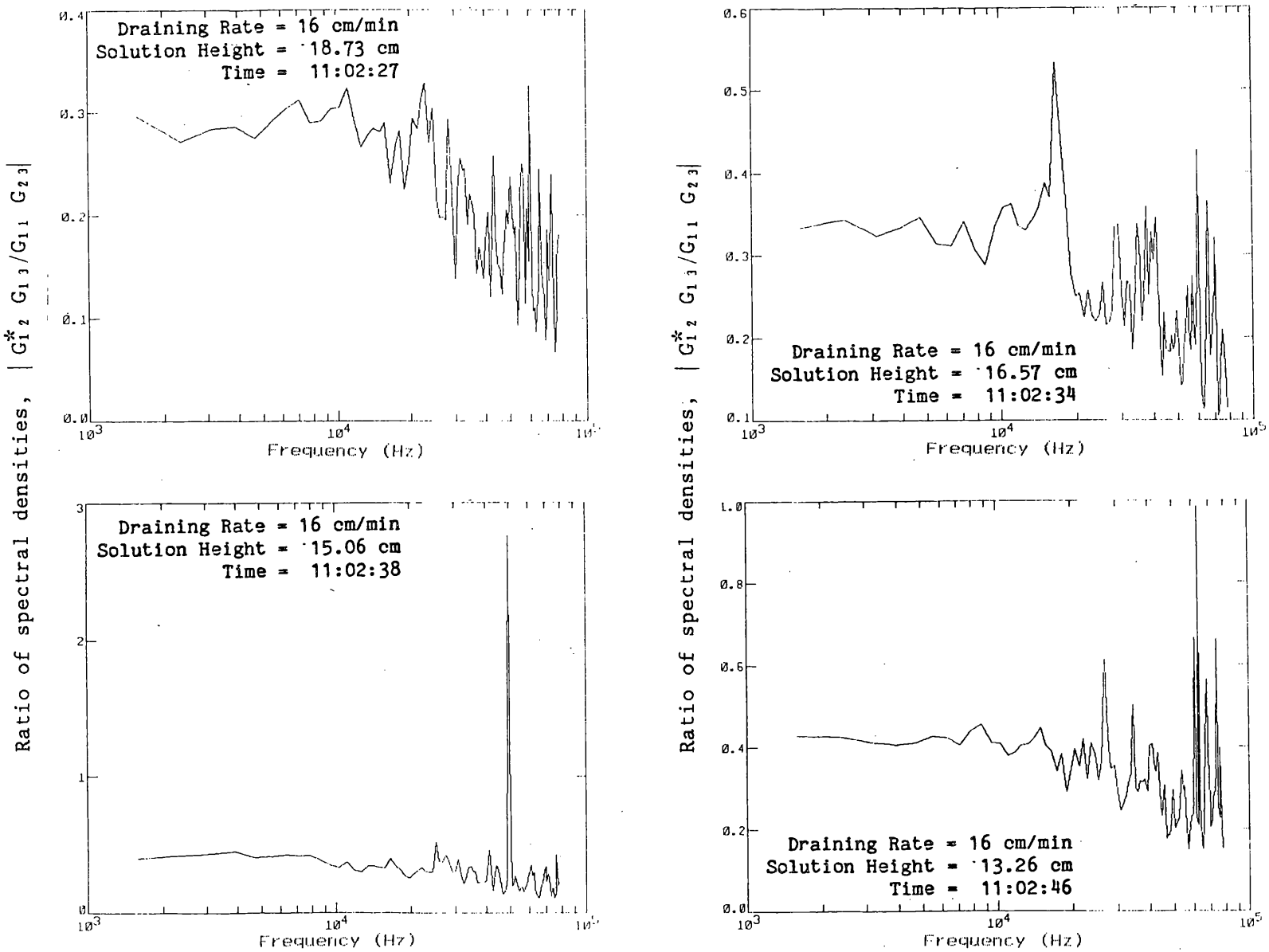

Fig. F.2. (continued)

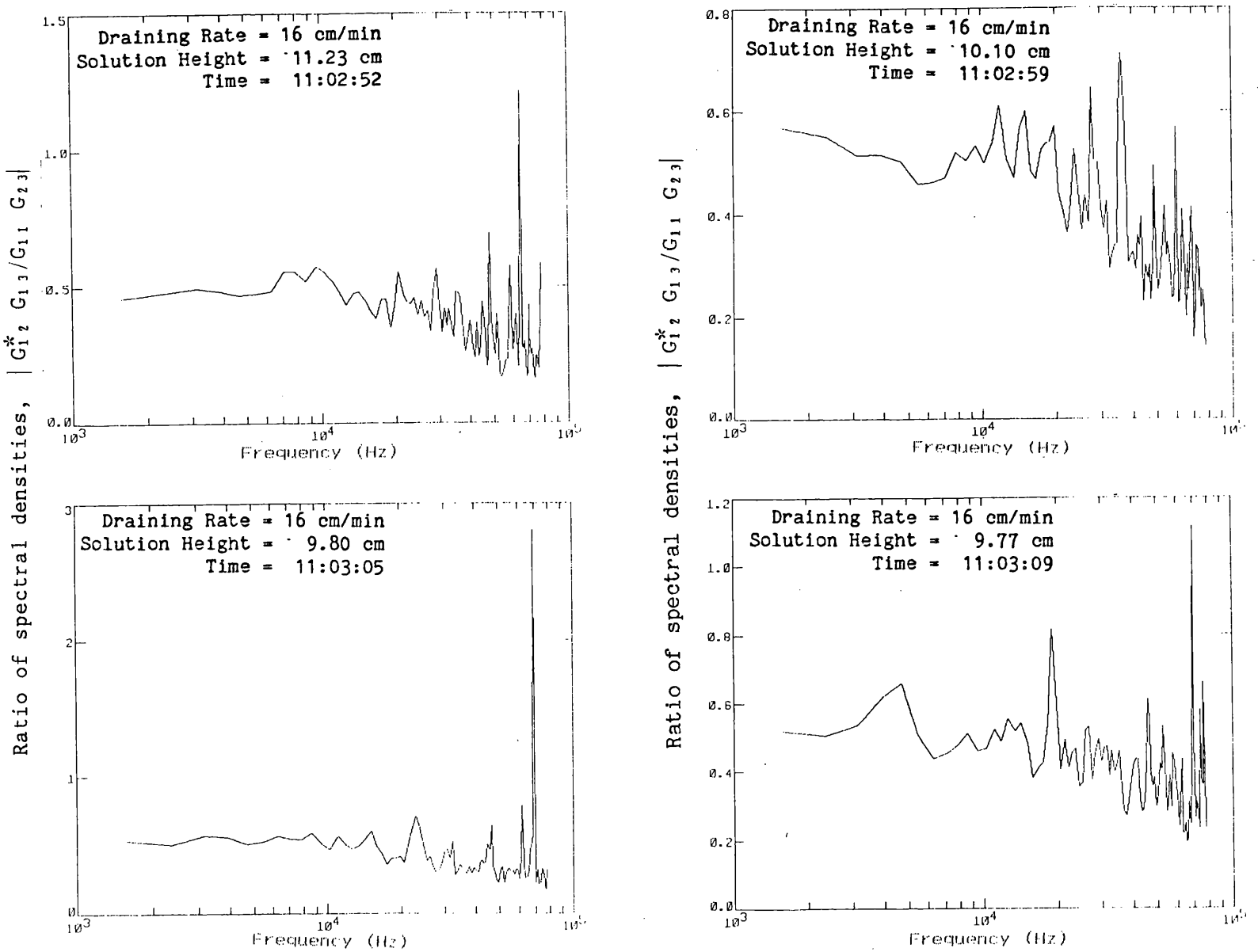

Fig. F.2. (continued)

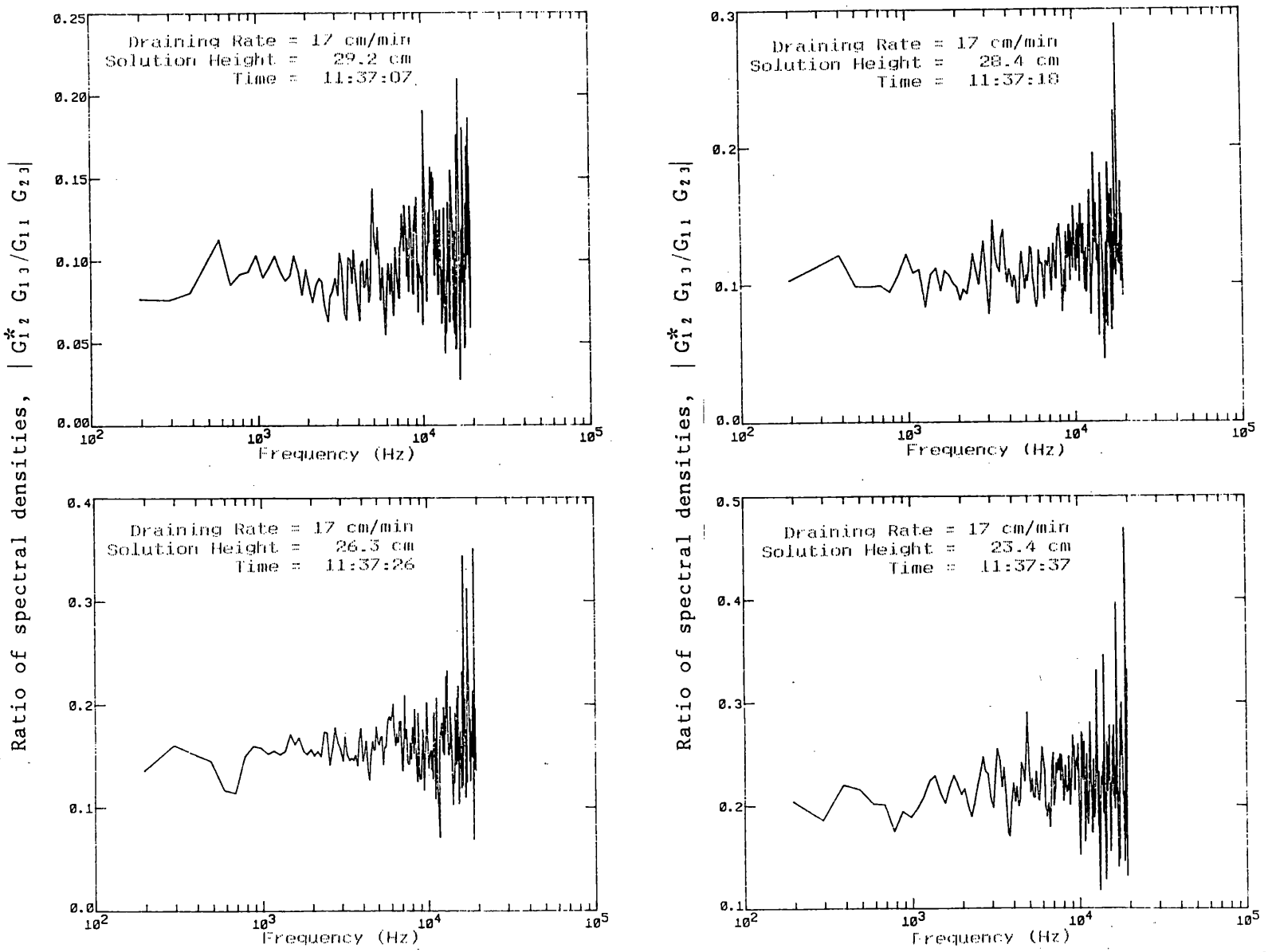

Fig. F.3. Ratios of spectral densities as a function of frequency as the experimental vessel was draining at a rate of ~17 cm/min with the source 7.6 cm from the bottom of the tank.

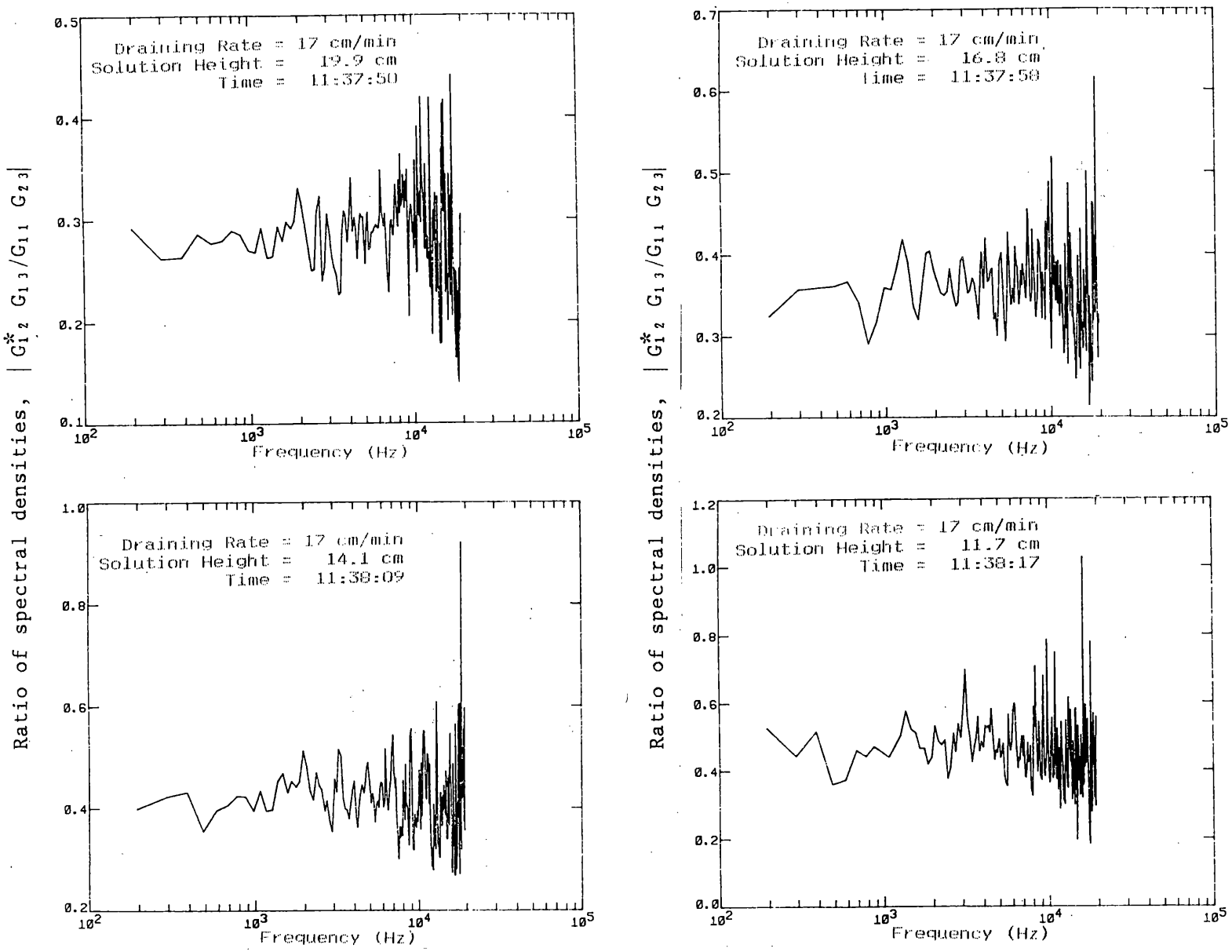

Fig. F.3. (continued)

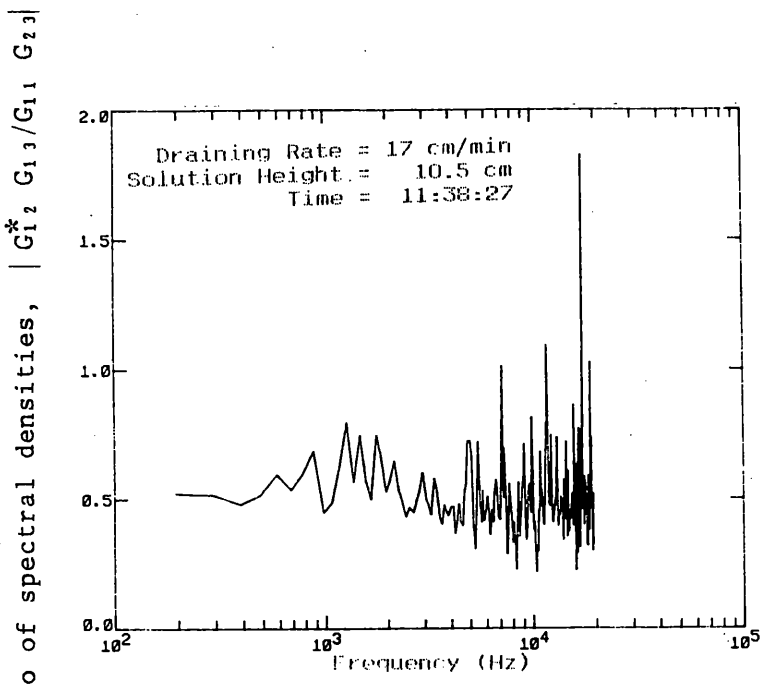

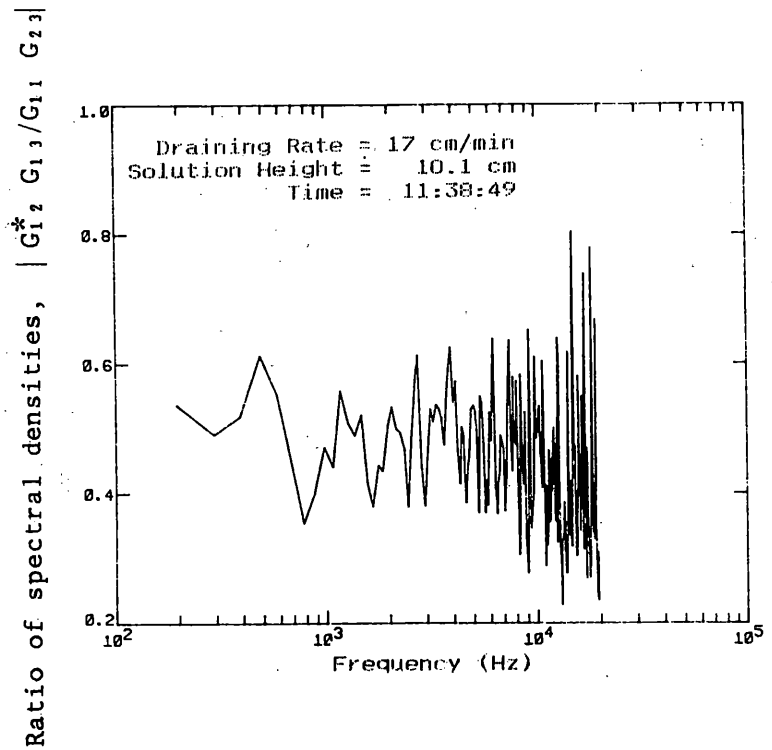

Fig. F.3. (continued)

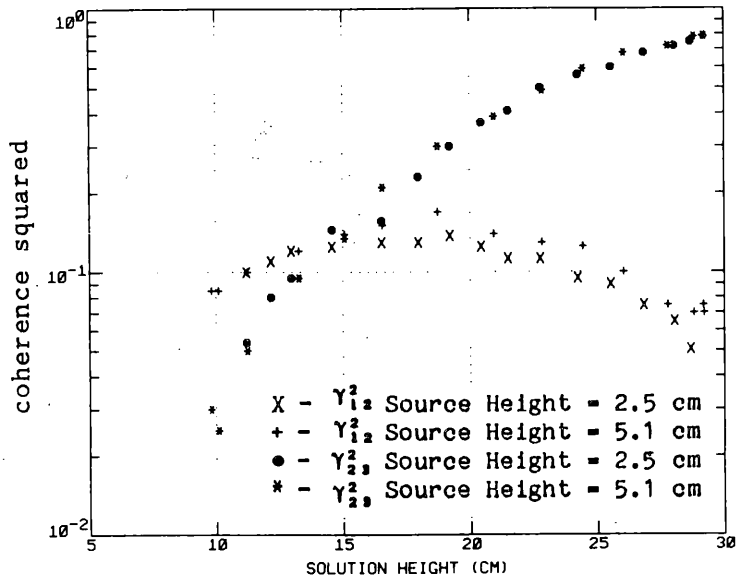

Fig. F.4. Coherence squared at low frequency as a function of solution height with the source 2.5 and 5.1 cm from the bottom of the tank.

APPENDIX G

ADDITIONAL DATA FROM DYNAMIC MEASUREMENTS WITH THE EXPERIMENTAL VESSEL FILLING AT A RATE OF 1 CM/MIN

APPENDIX G. ADDITIONAL DATA FROM DYNAMIC MEASUREMENTS WITH THE EXPERIMENTAL VESSEL FILLING AT A RATE OF 1 CM/MIN

This appendix presents some additional data from dynamic measurements with the experimental vessel filling at a rate of 1 cm/min. The ratios of spectral densities as a function of frequencies for various heights in this filling as well as some APSDs and CPSDs are plotted in Figs. G.1 through G.16. Table G.1 lists the interpretation of the dynamic measurement performed on-line during this filling of the vessel. The values in this table are different from those in Table 9 (Sect. 7.1), since the parameters used in the interpretation were slightly different and average ratios of spectral densities up to 5 kHz were used for all solution heights in the on-line interpretation.

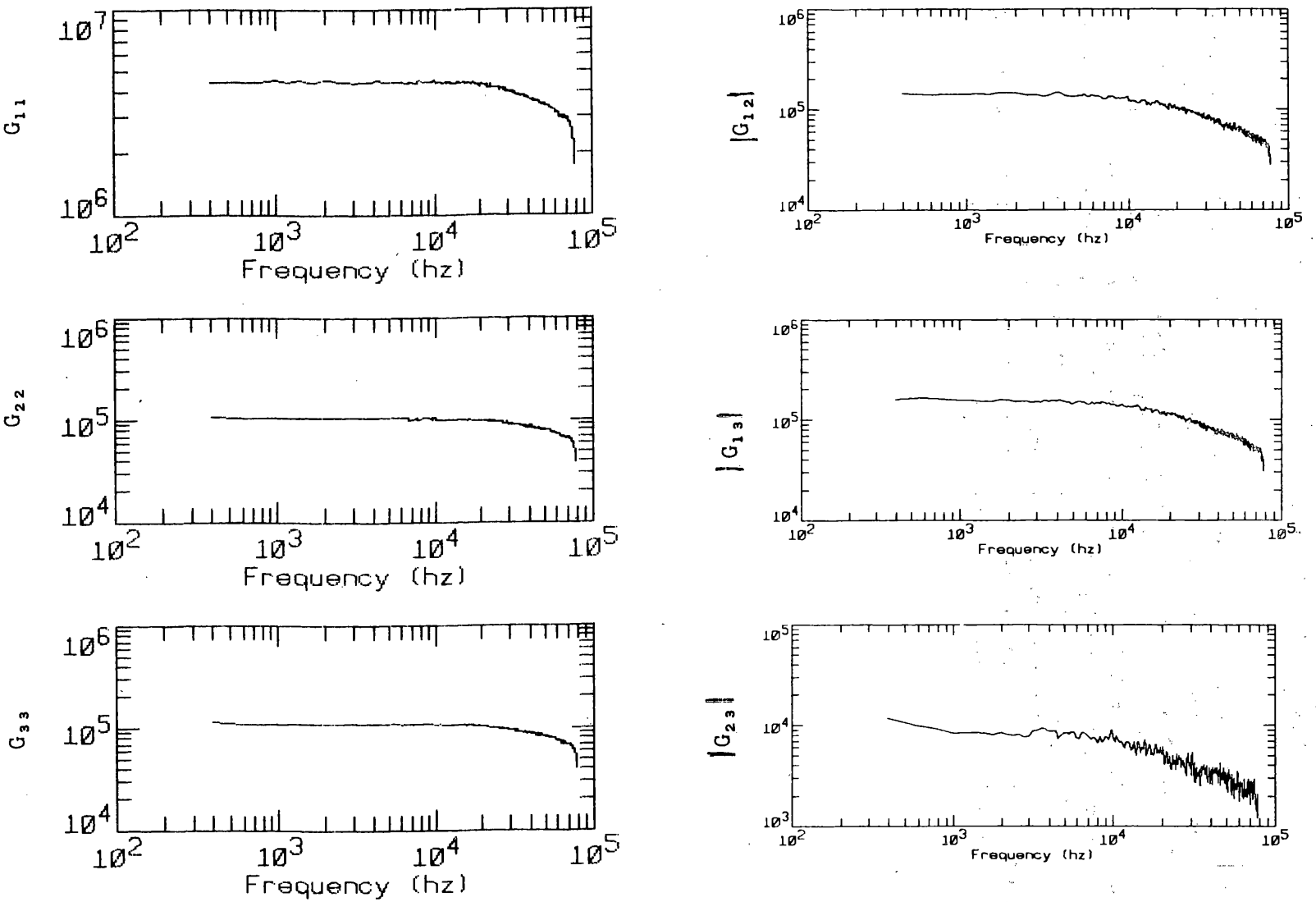

Fig. G.1. APSDs and CPSDs as a function of frequency for a dynamic measurement with a filling rate of 1 cm/min, average solution height of 6.46 cm, and a Cf source located on the bottom of the tank.

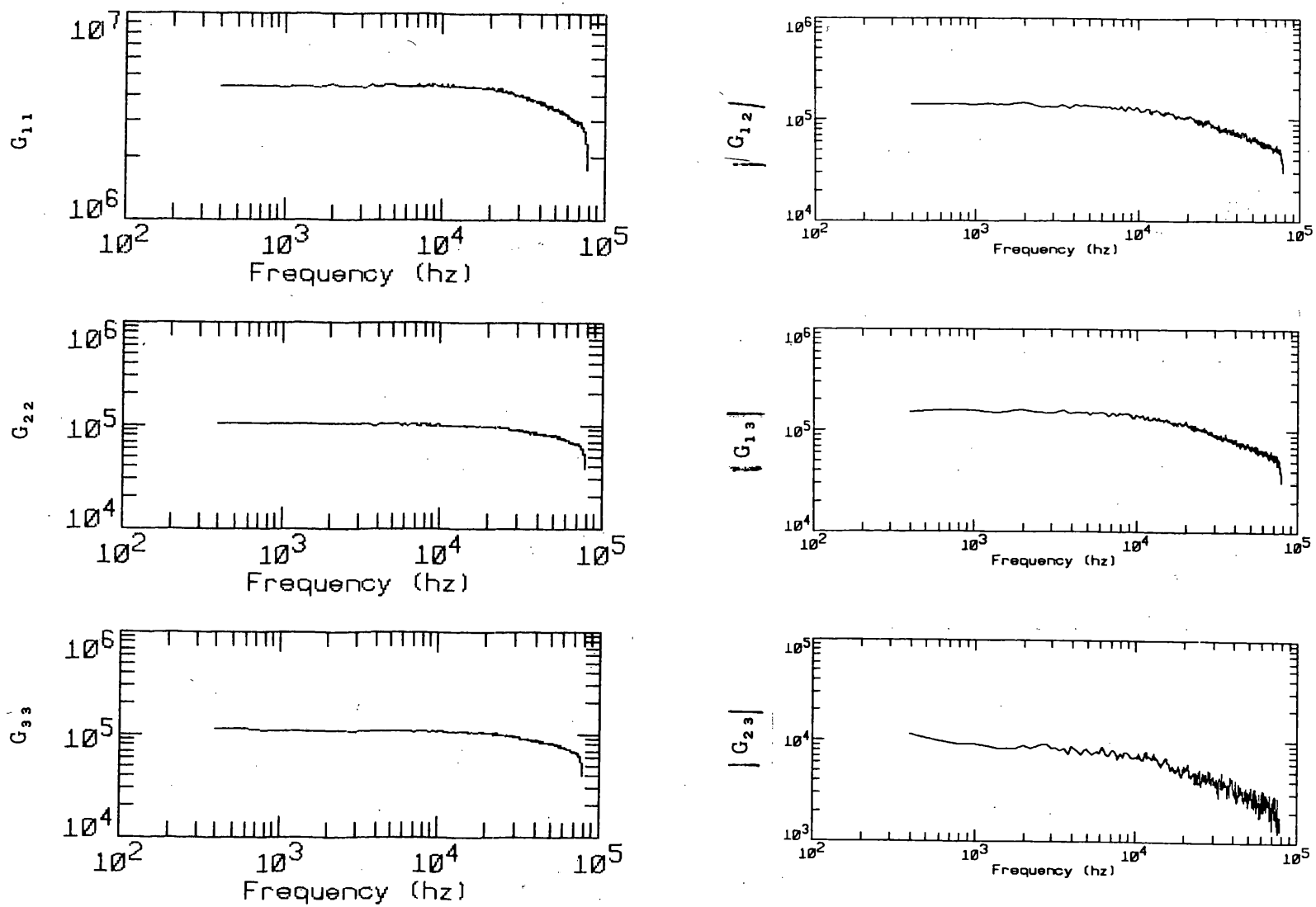

Fig. G.2. APSDs and CPSDs as a function of frequency for a dynamic measurement with a filling rate of 1 cm/min, average solution height of 6.61 cm, and a Cf source located on the bottom of the tank.

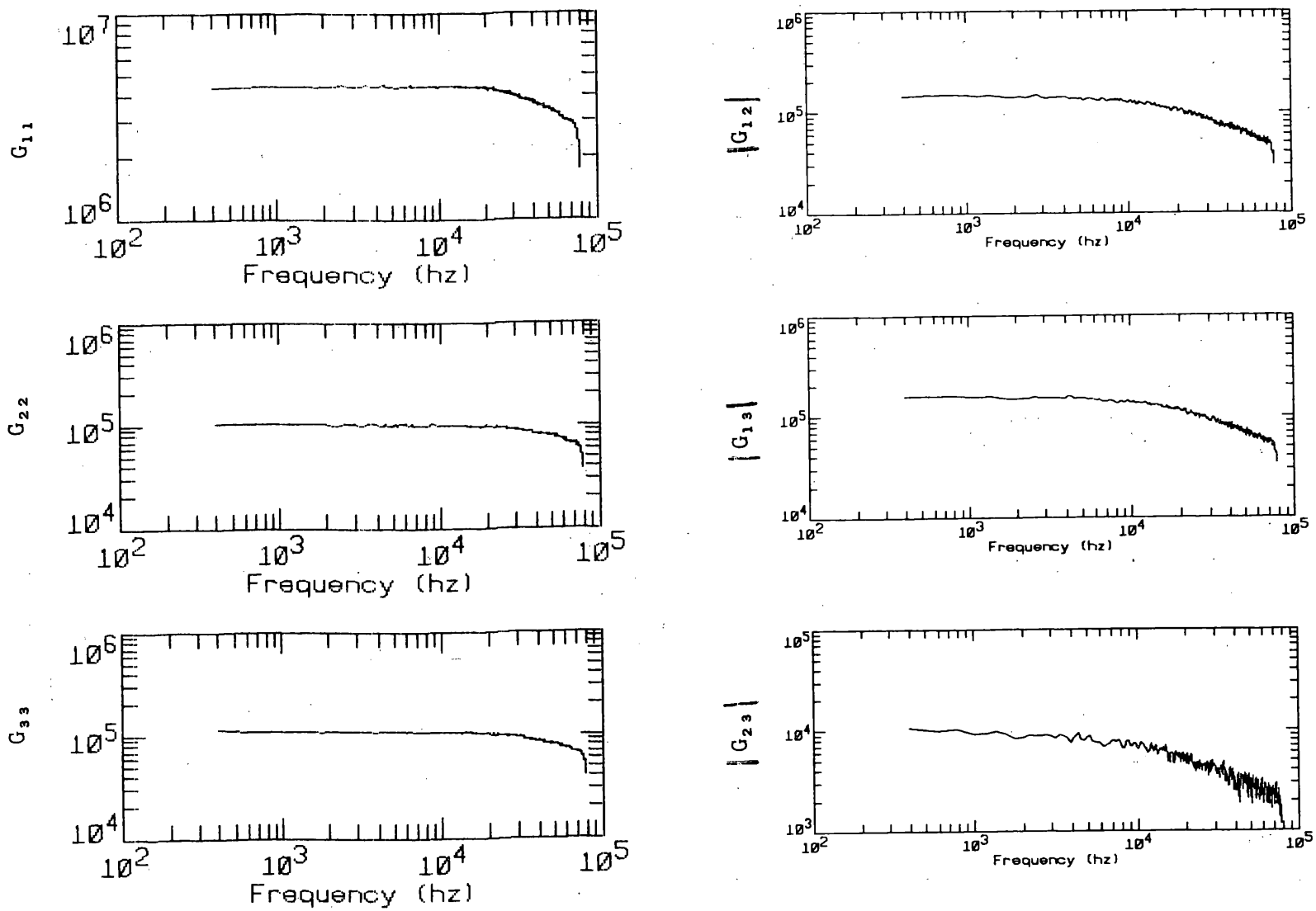

Fig. G.3. APSDs and CPSDs as a function of frequency for a dynamic measurement with a filling rate of 1 cm/min, average solution height of 7.36 cm, and a Cf source located on the bottom of the tank.

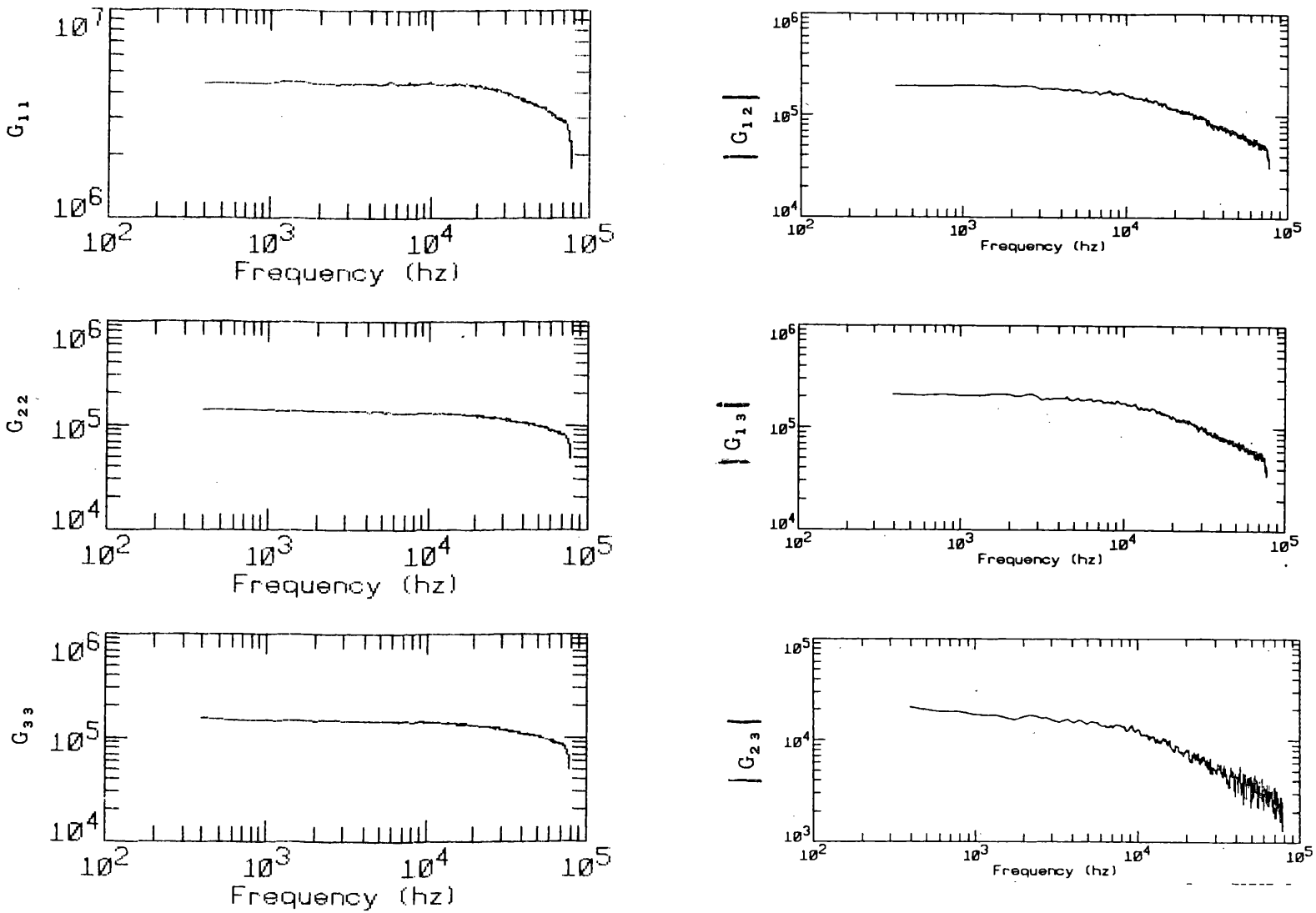

Fig. G.4. APSDs and CPSDs as a function of frequency for a dynamic measurement with a filling rate of 1 cm/min, average solution height of 8.50 cm, and a Cf source located on the bottom of the tank.

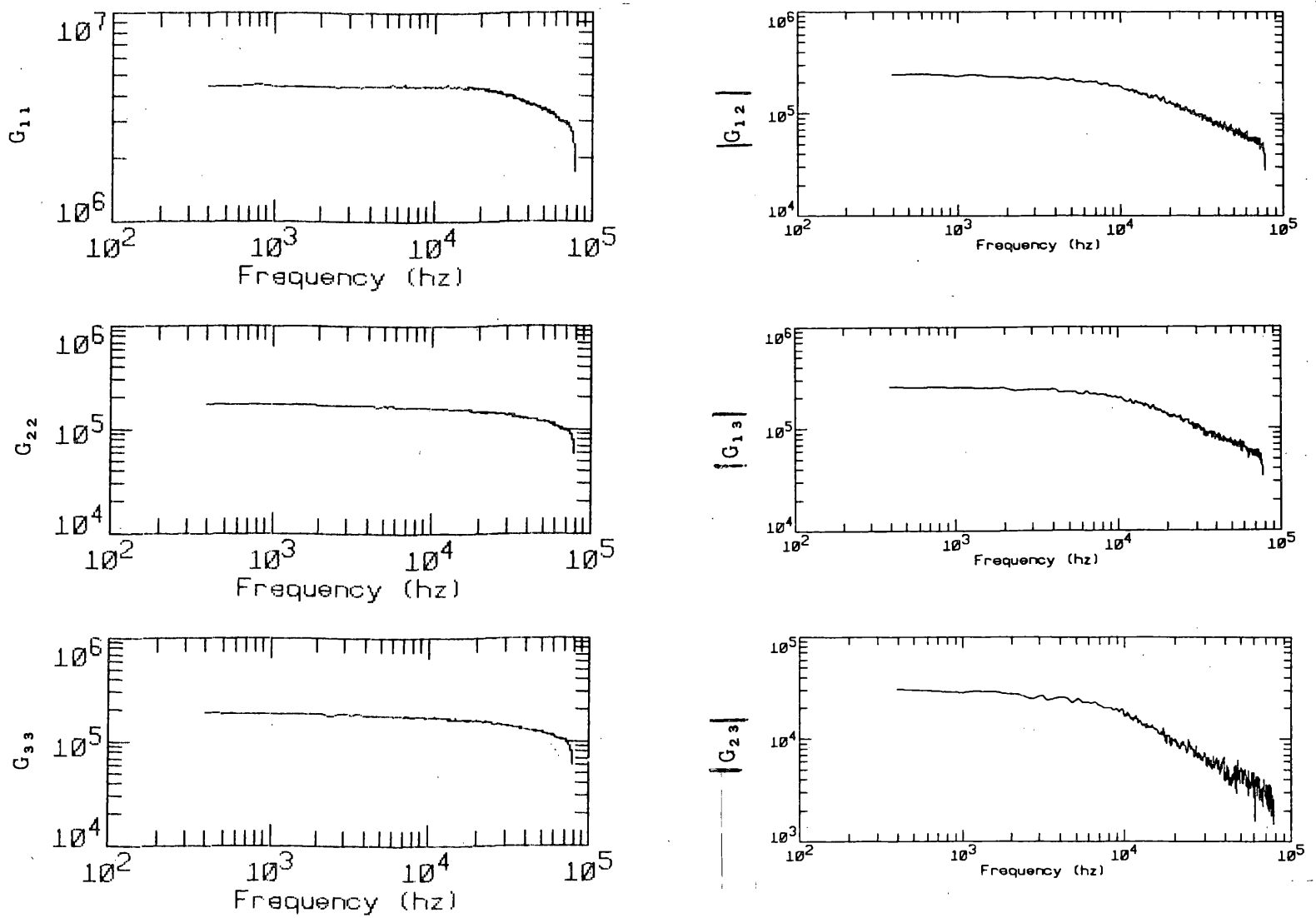

Fig. G.5. APSDs and CPSDs as a function of frequency for a dynamic measurement with a filling rate of 1 cm/min, average solution height of 9.88 cm, and a Cf source located on the bottom of the tank.

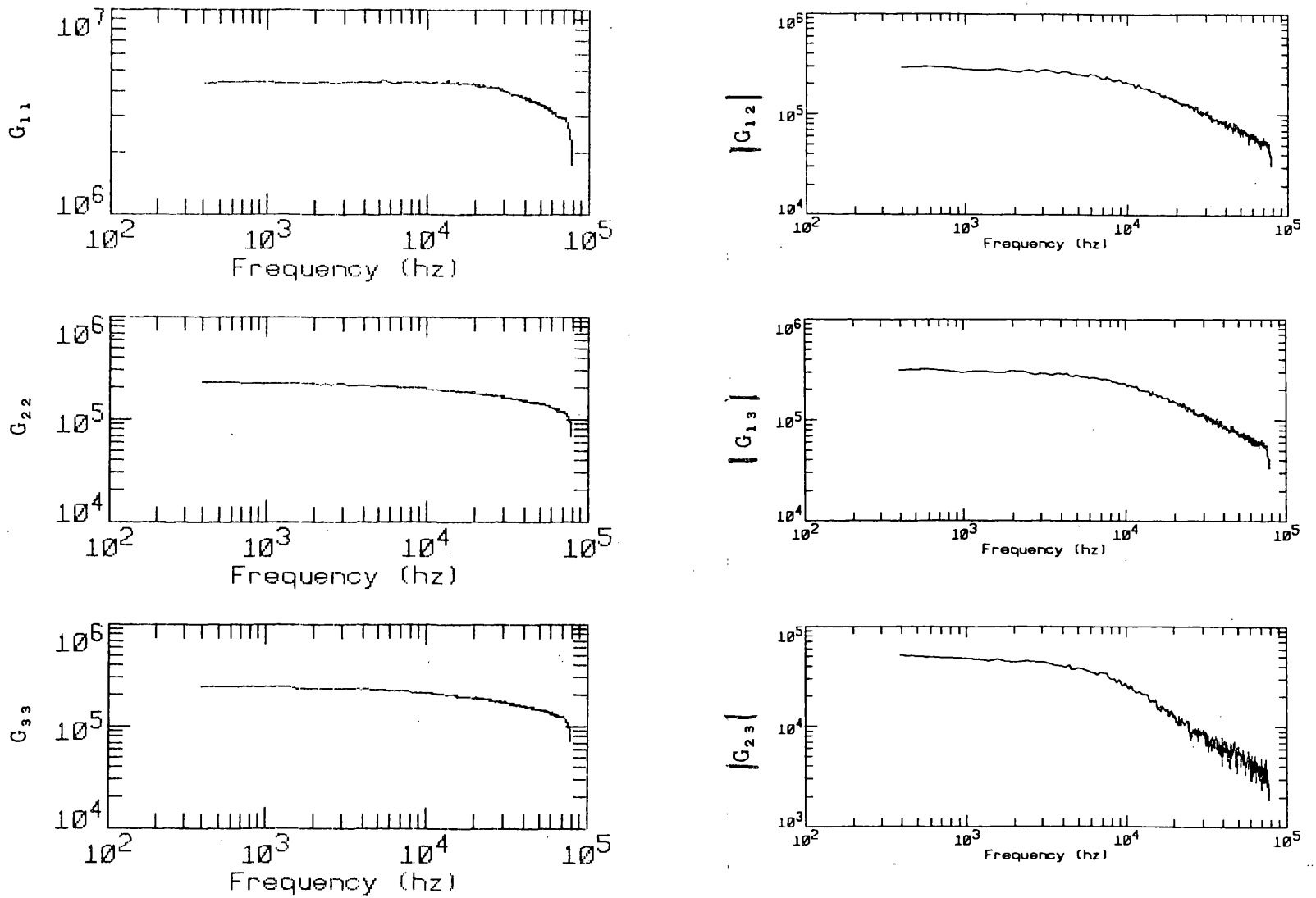

Fig. G.6. APSDs and CPSDs as a function of frequency for a dynamic measurement with a filling rate of 1 cm/min, average solution height of 11.44 cm, and a Cf source located on the bottom of the tank.

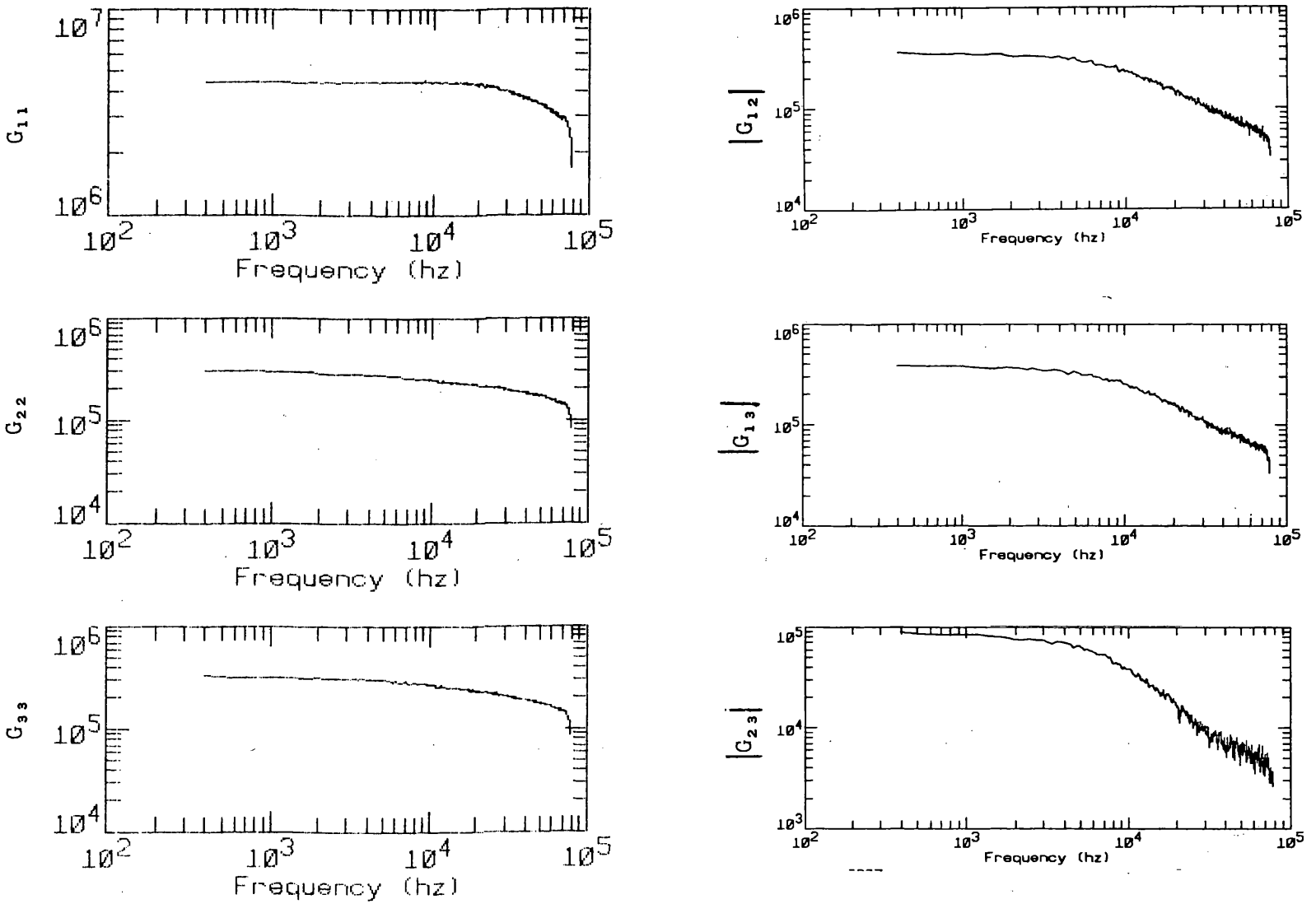

Fig. G.7. APSDs and CPSDs as a function of frequency for a dynamic measurement with a filling rate of 1 cm/min, average solution height of 13.08 cm, and a Cf source located on the bottom of the tank.

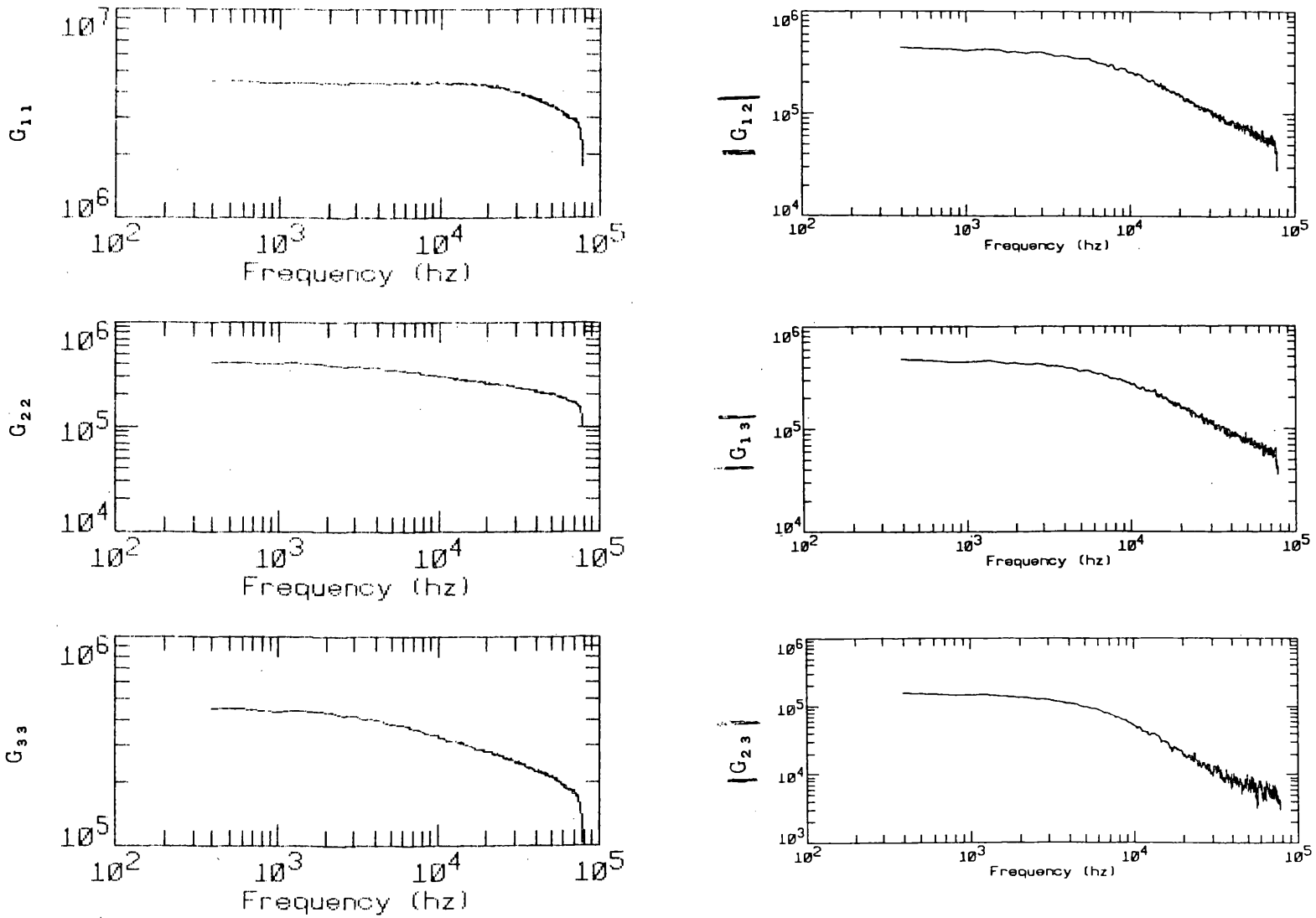

Fig. G.8. APSDs and CPSDs as a function of frequency for a dynamic measurement with a filling rate of 1 cm/min, average solution height of 14.75 cm, and a Cf source located on the bottom of the tank.

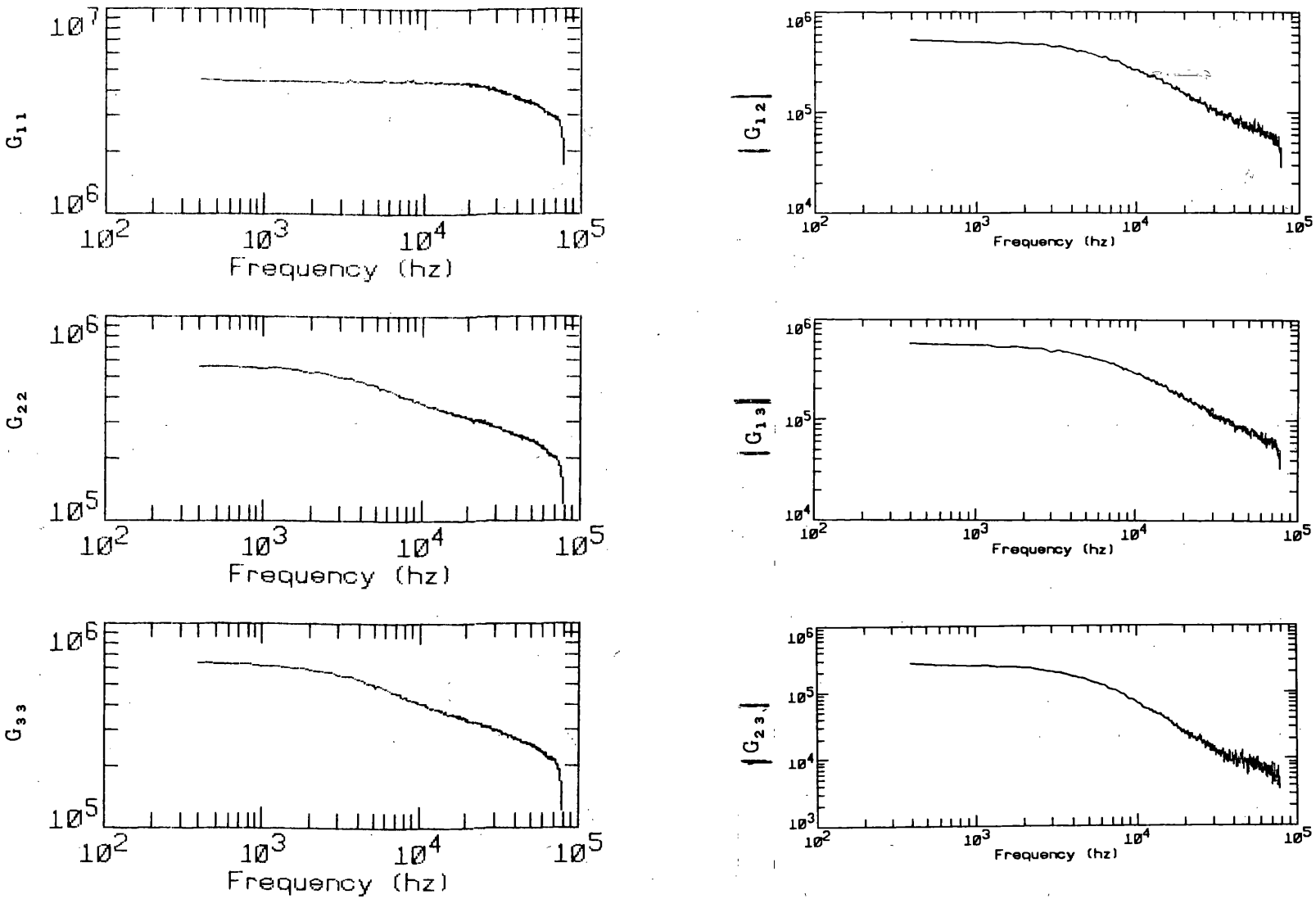

Fig. G.9. APSDs and CPSDs as a function of frequency for a dynamic measurement with a filling rate of 1 cm/min, average solution height of 16.54 cm, and a Cf source located on the bottom of the tank.

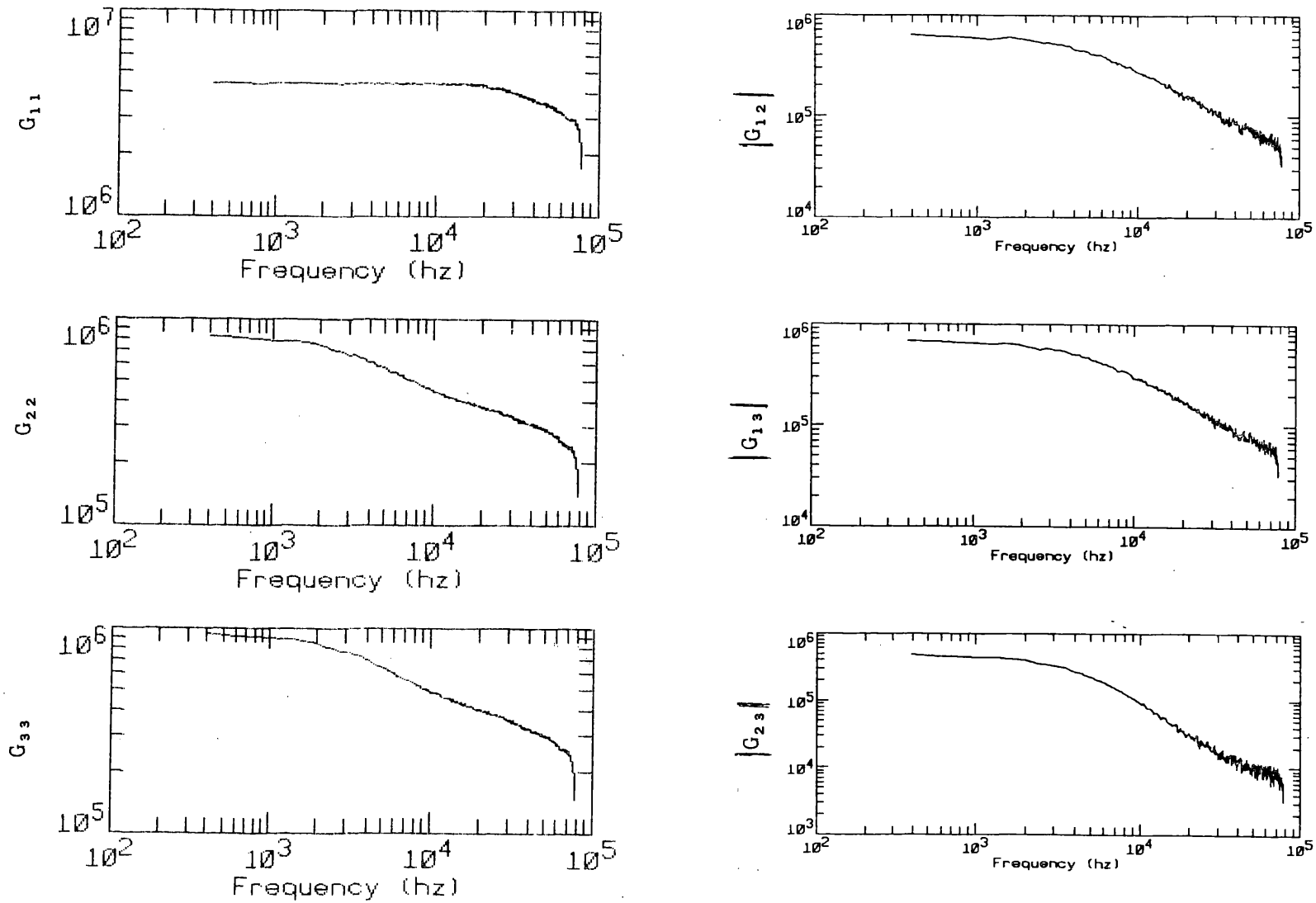

Fig. G.10. APSDs and CPSDs as a function of frequency for a dynamic measurement with a filling rate of 1 cm/min, average solution height of 18.36 cm, and a Cf source located on the bottom of the tank.

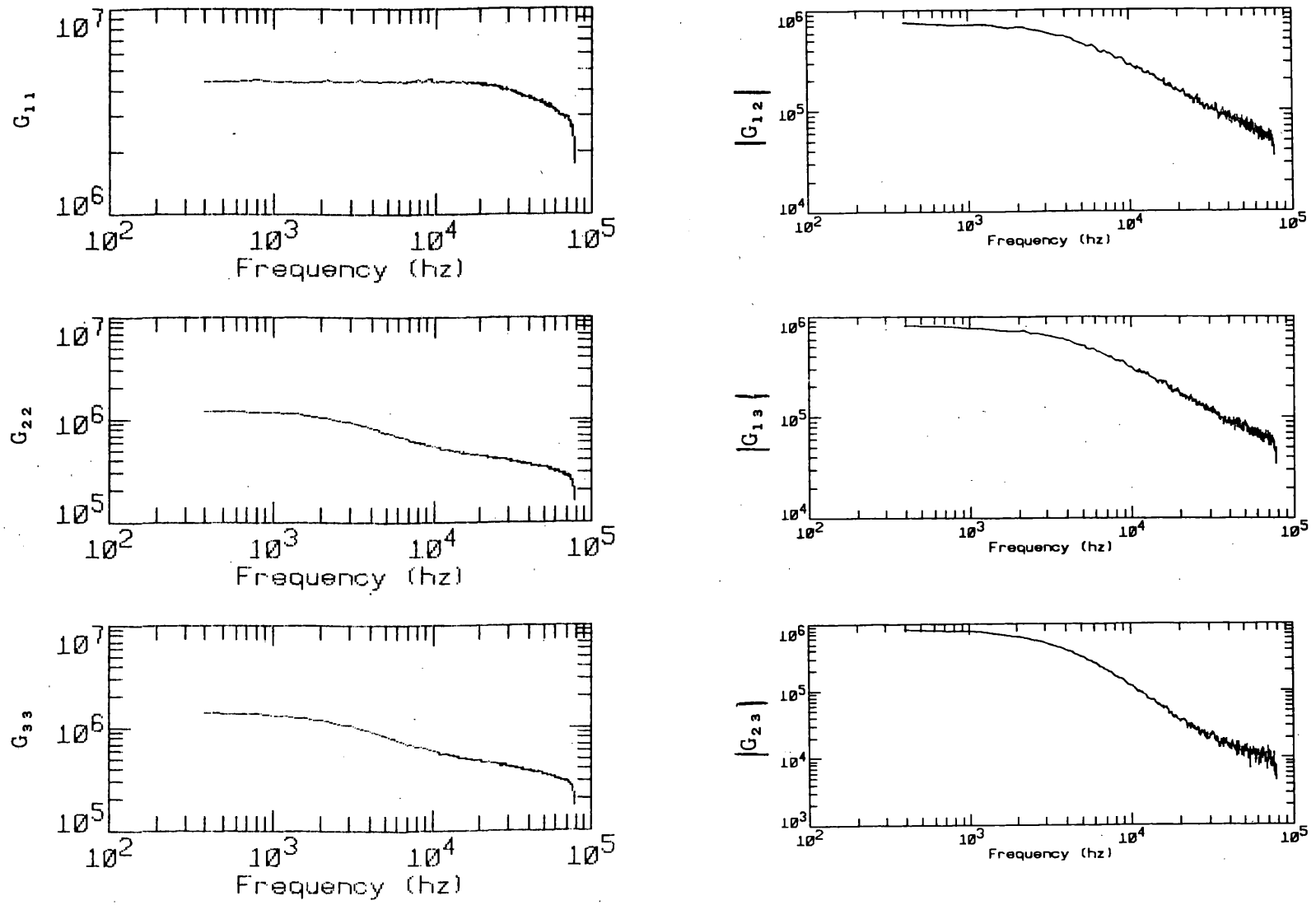

Fig. G.11. APSDs and CPSDs as a function of frequency for a dynamic measurement with a filling rate of 1 cm/min, average solution height of 20.17 cm, and a Cf source located on the bottom of the tank.

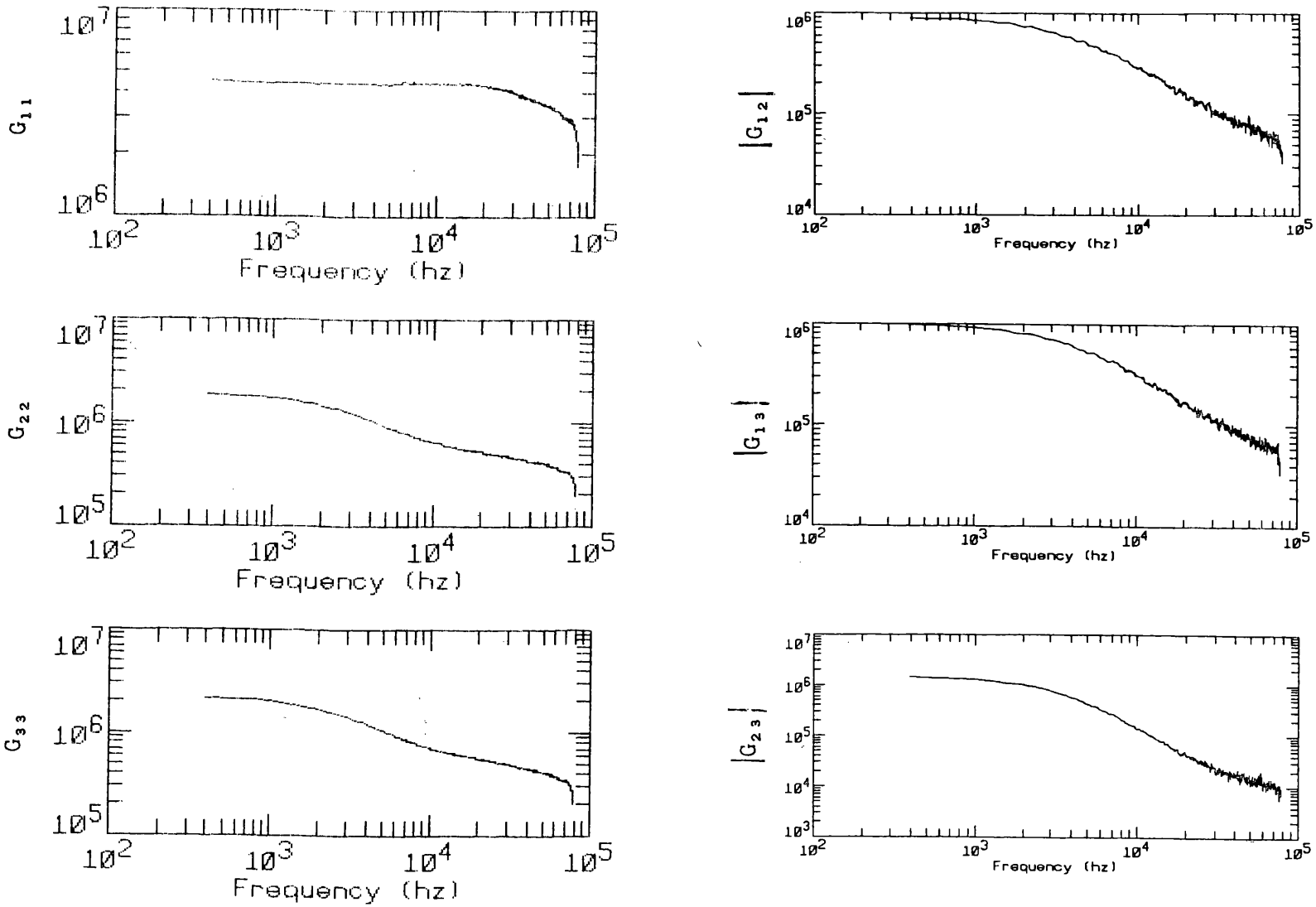

Fig. G.12. APSDs and CPSDs as a function of frequency for a dynamic measurement with a filling rate of 1 cm/min, average solution height of 22.01 cm, and a Cf source located on the bottom of the tank.

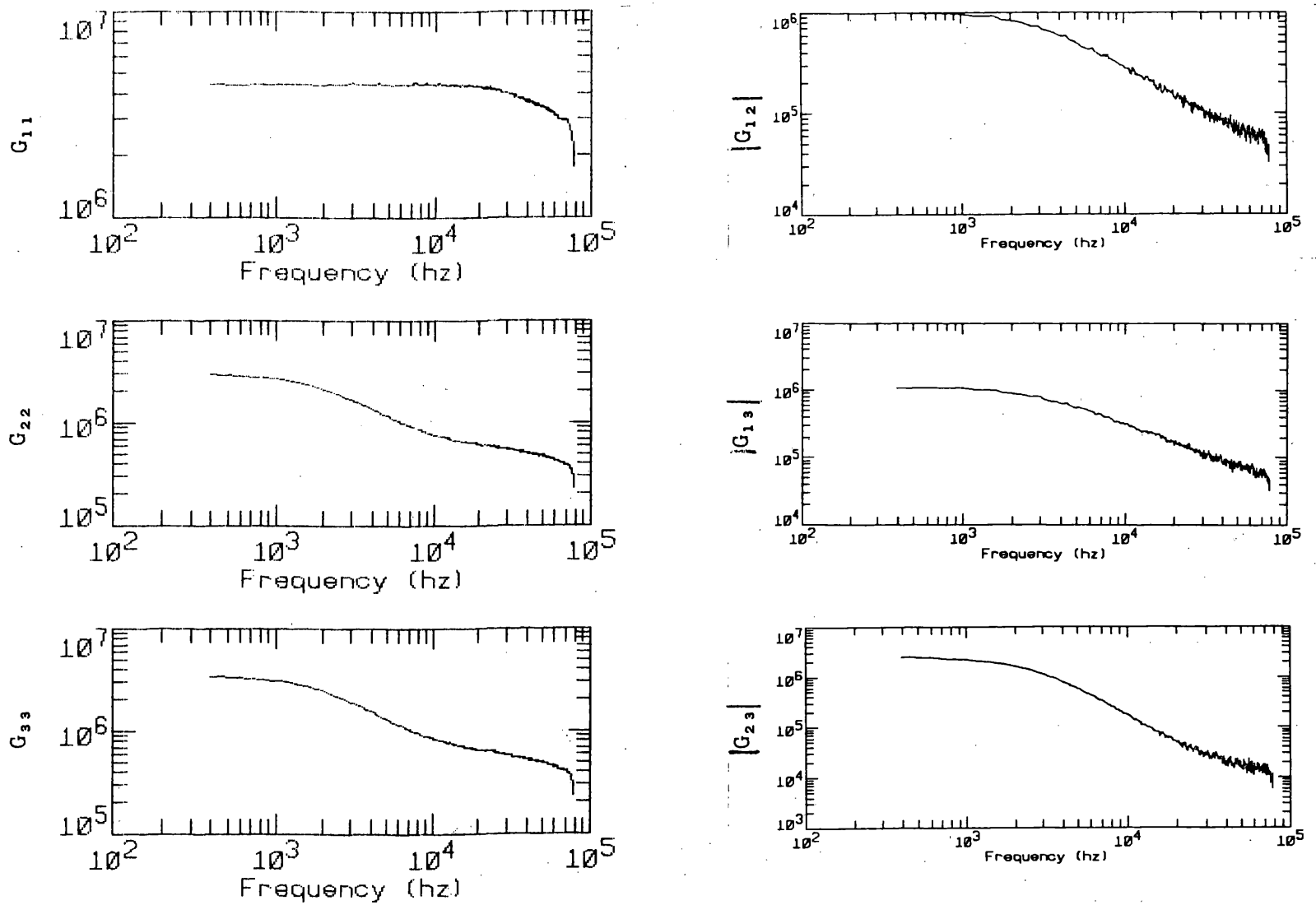

Fig. G.13. APSDs and CPSDs as a function of frequency for a dynamic measurement with a filling rate of 1 cm/min, average solution height of 23.84 cm, and a Cf source located on the bottom of the tank.

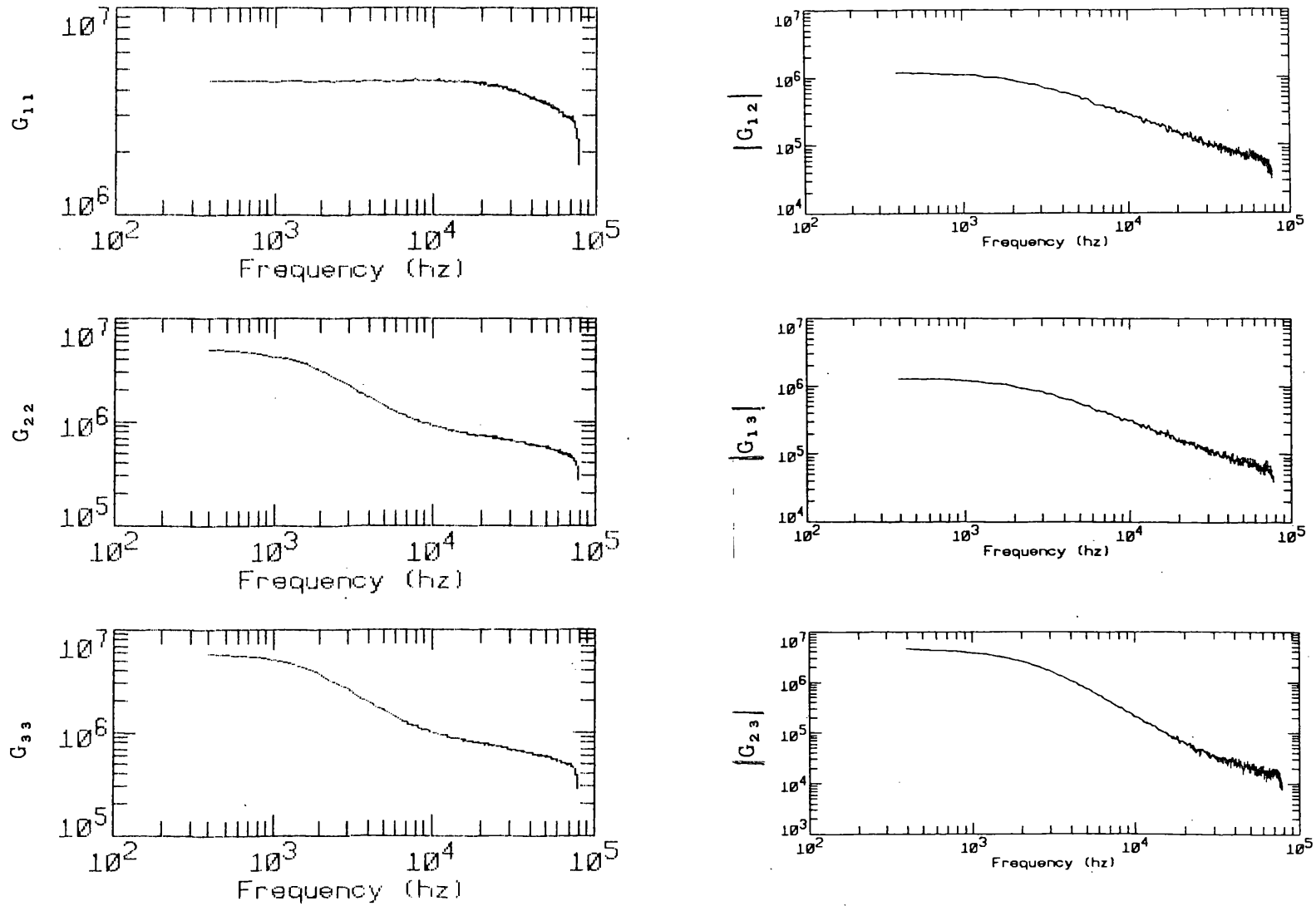

Fig. G.14. APSDs and CPSDs as a function of frequency for a dynamic measurement with a filling rate of 1 cm/min, average solution height of 25.70 cm, and a Cf source located on the bottom of the tank.

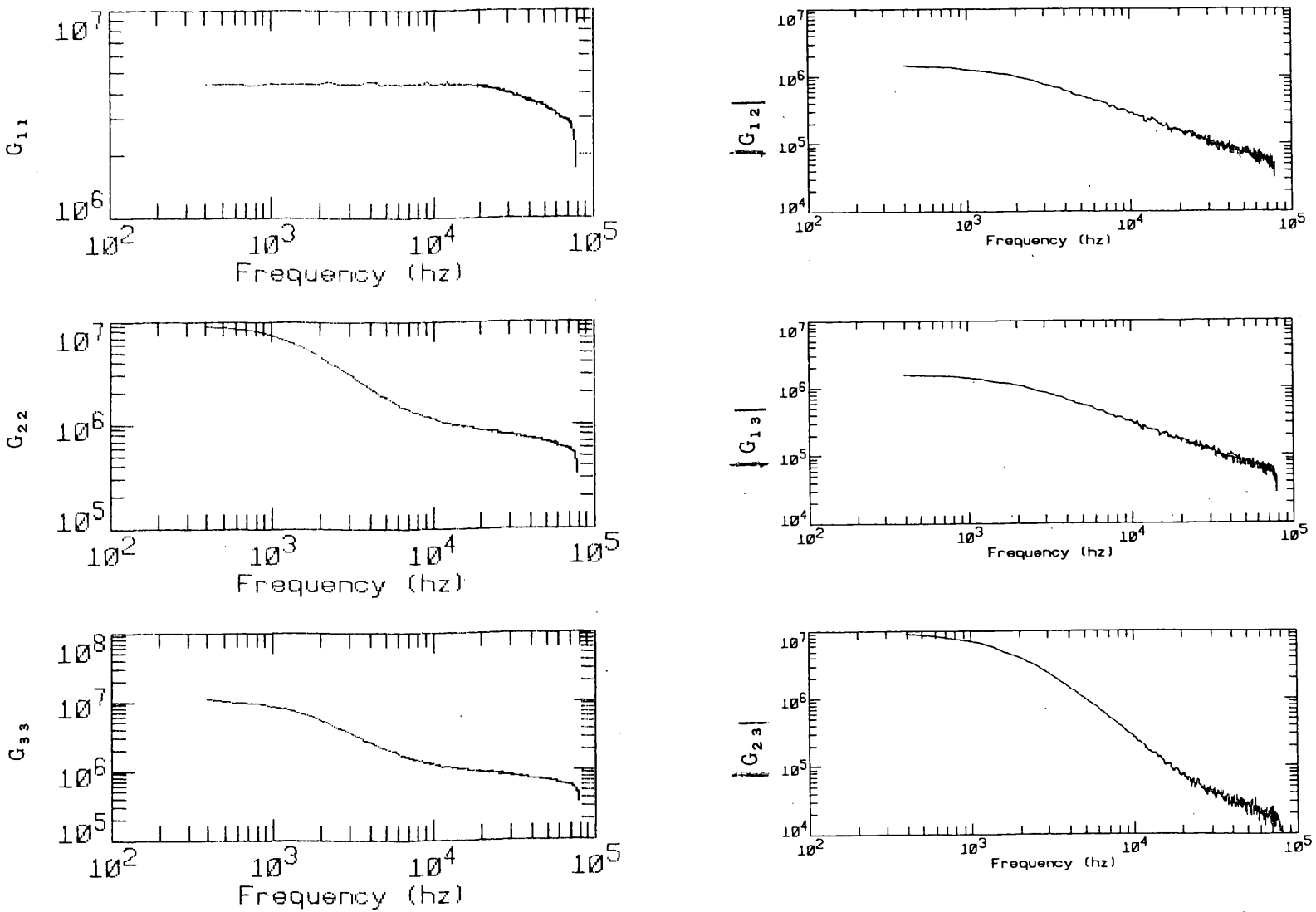

Fig. G.15. APSDs and CPSDs as a function of frequency for a dynamic measurement with a filling rate of 1 cm/min, average solution height of 27.59 cm, and a Cf source located on the bottom of the tank.

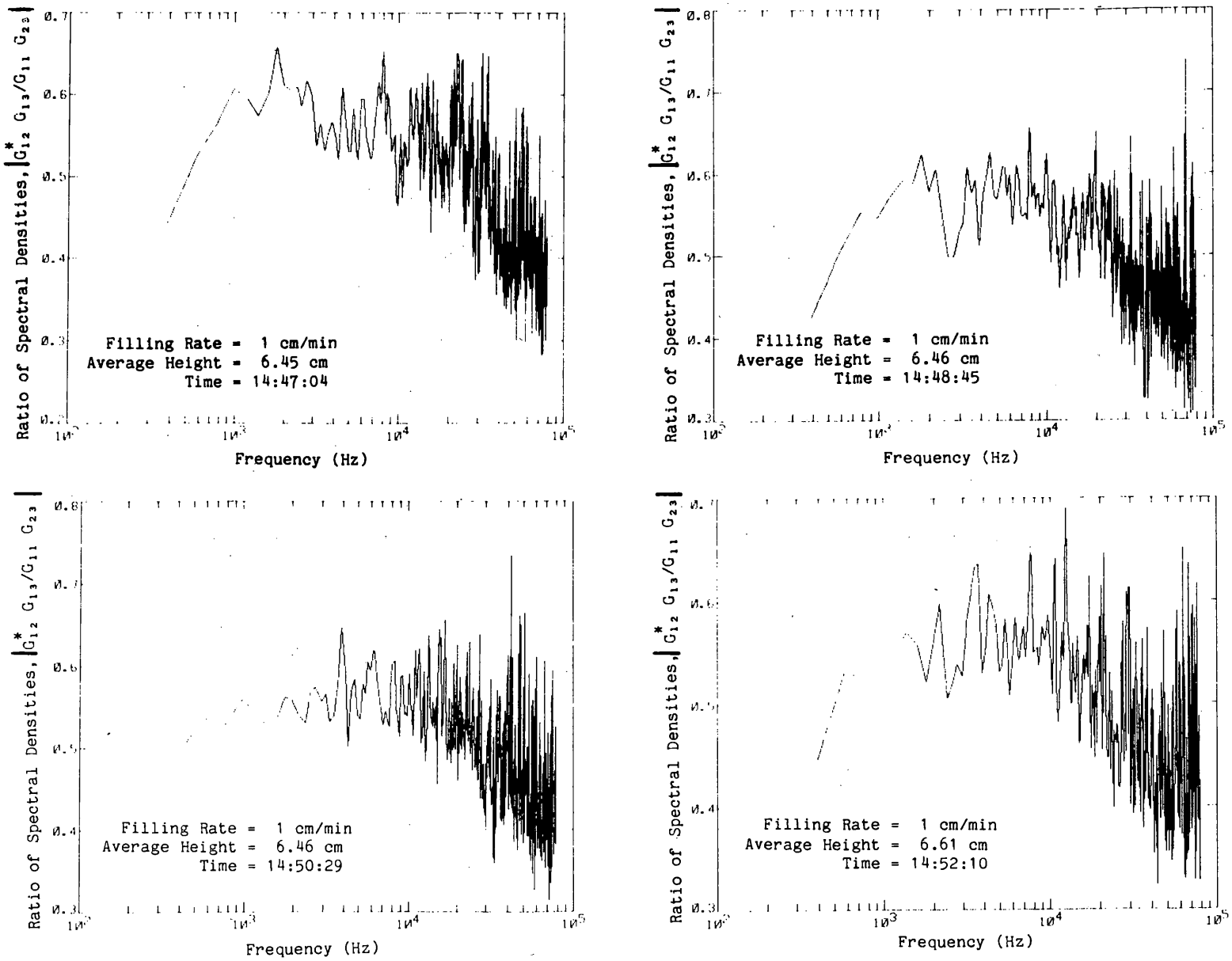

Fig. G.16. Ratios of spectral densities as a function of frequency as the experimental vessel was filling at a rate of 1 cm/min.

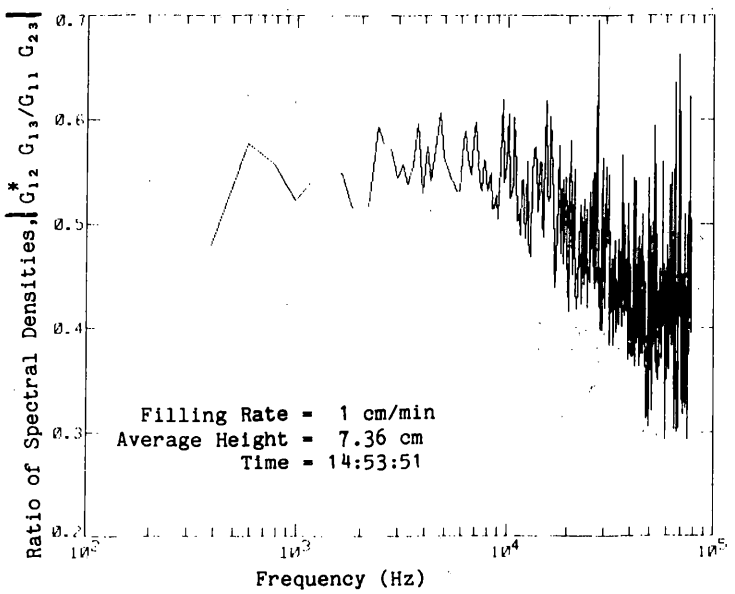

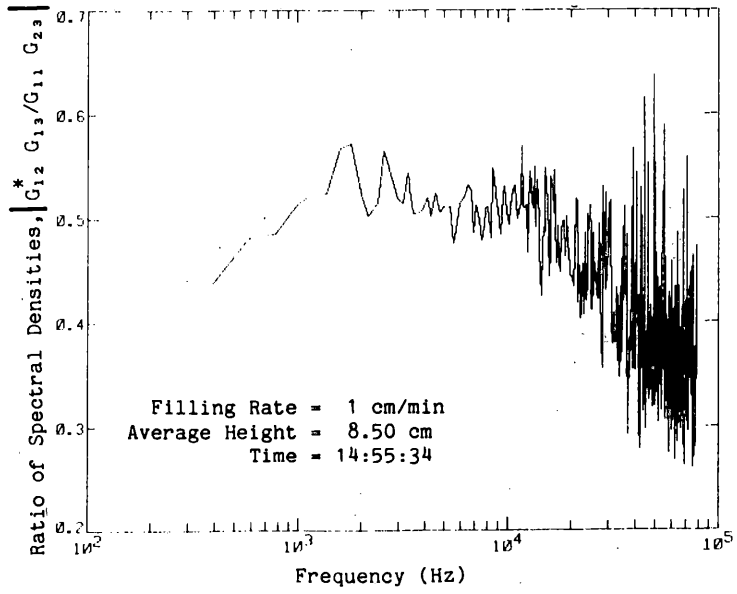

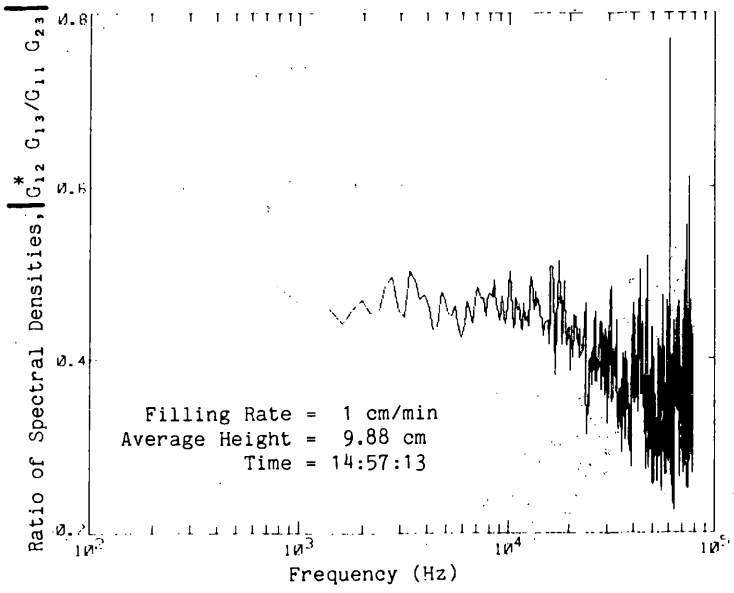

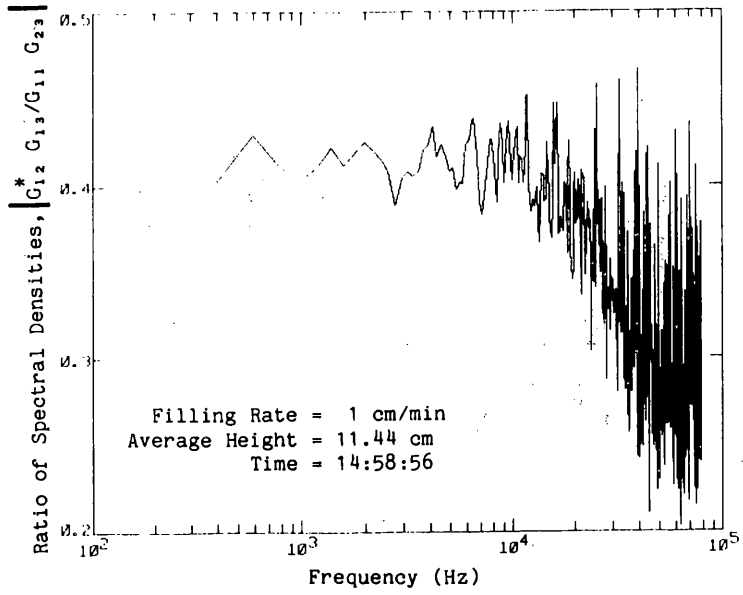

Fig. G.16 (continued)

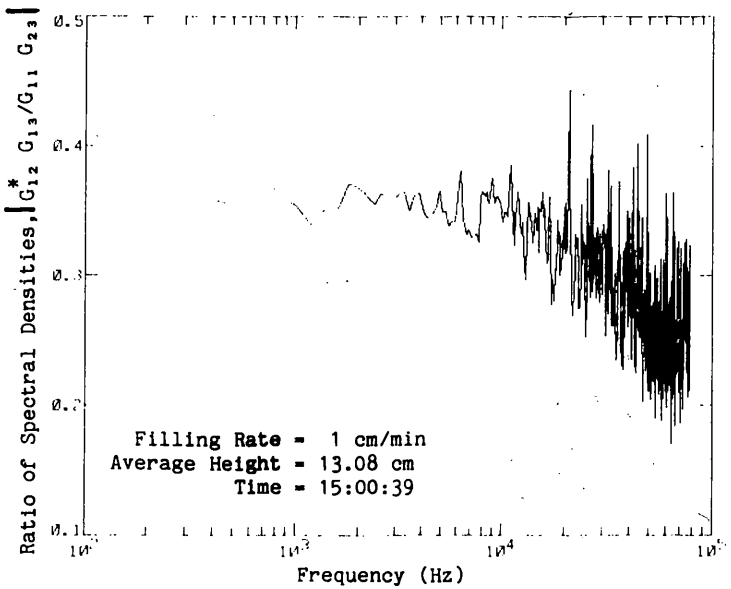

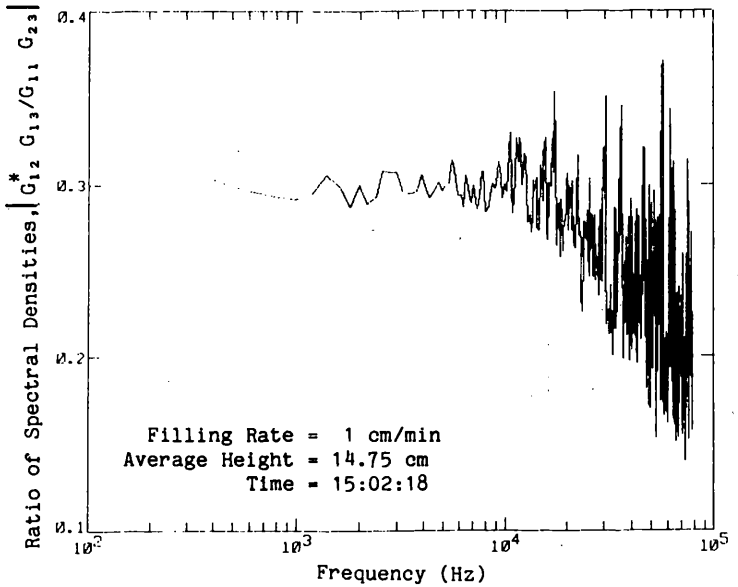

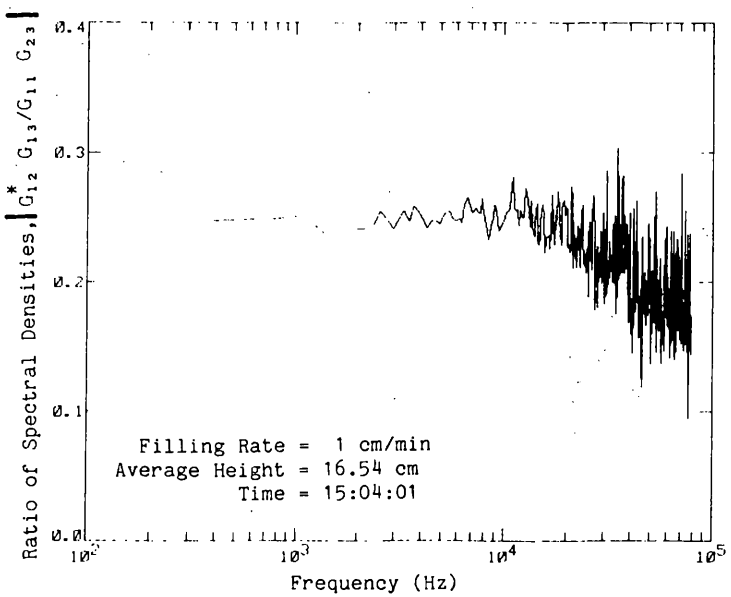

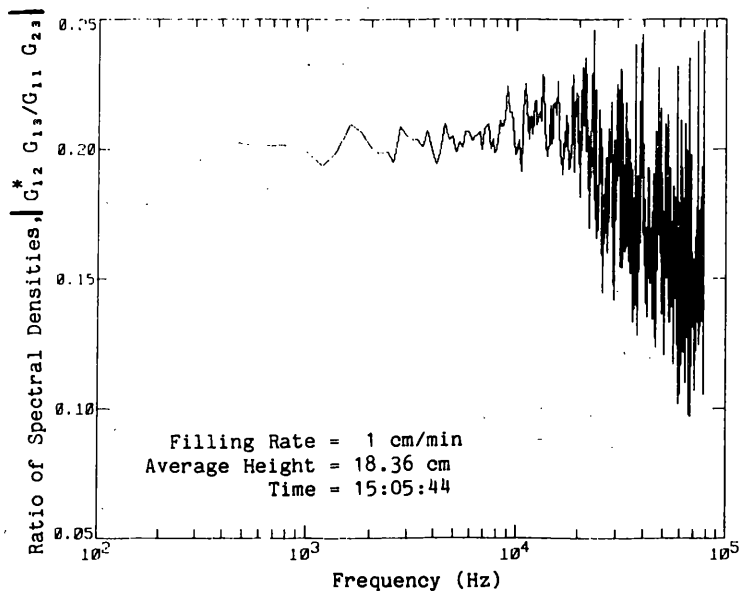

Fig. G.16 (continued)

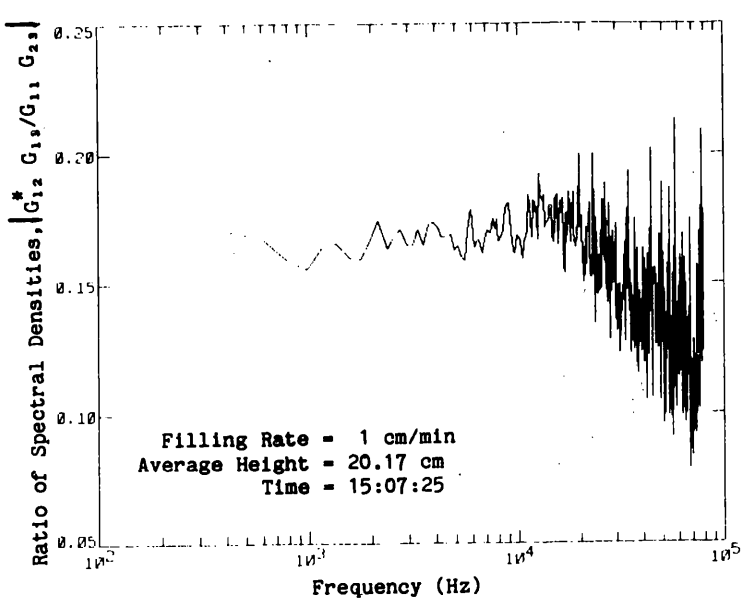

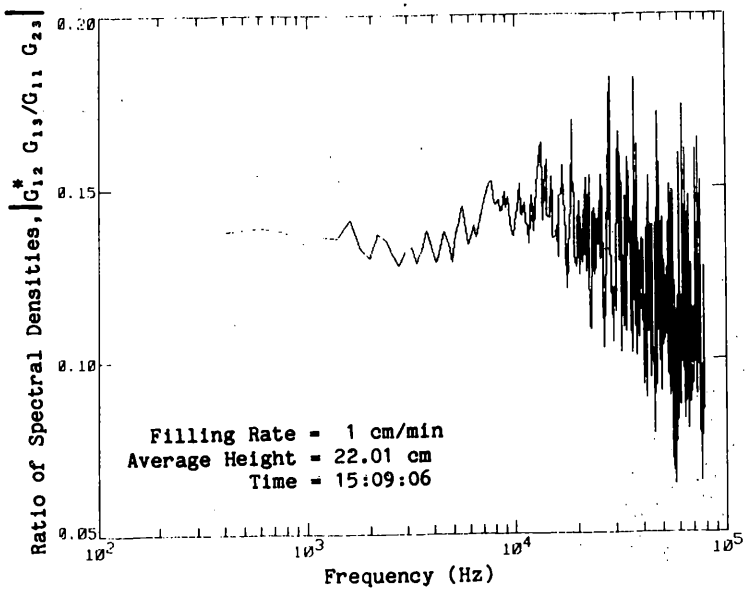

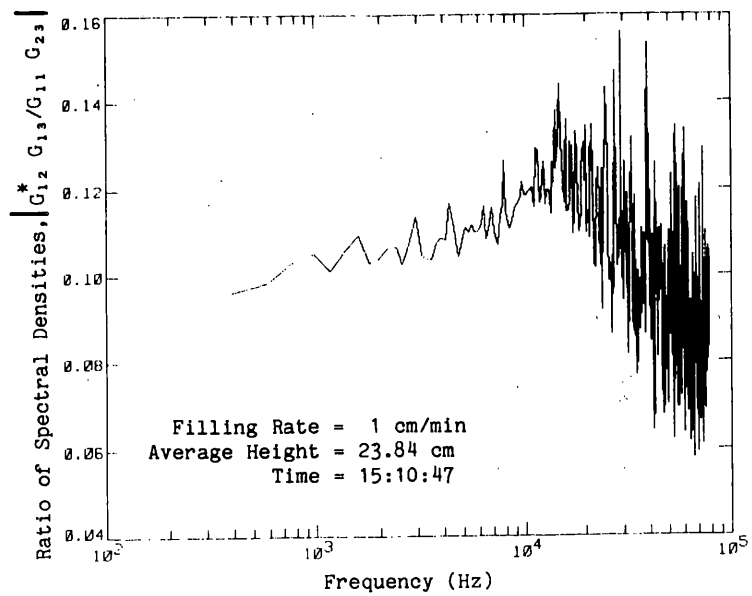

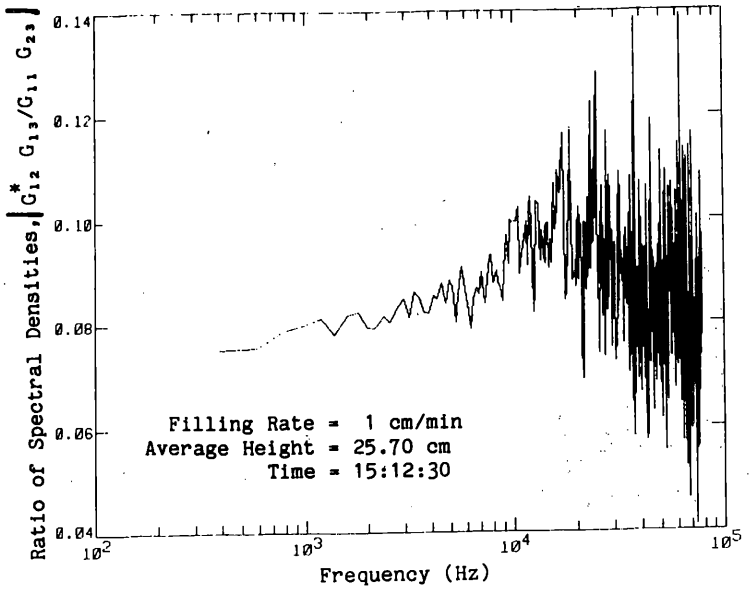

Fig. G.16 (continued)

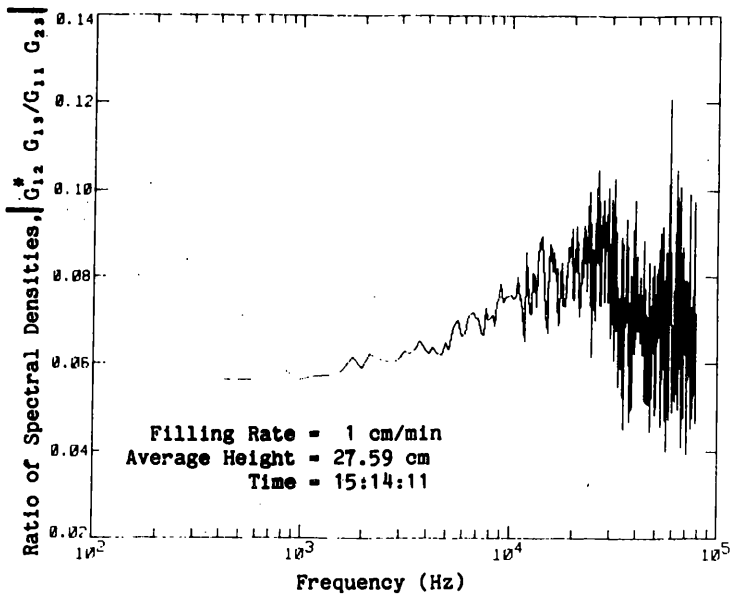

Fig. G.16 (continued)

Table G.1. On-line ratios of spectral densities at low frequency and neutron multiplication factors for dynamic measurements while filling the experimental vessel at a rate of 1 cm/min

Time[a] (h:m:s)	Solution height[b] (cm)	Ratio of spectral densities[c]	k_{eff} from ratio of spectral densities[d]
14:47:04	6.45	0.572 ± 0.009	0.300 ± 0.020
14:48:46	6.46	0.560 ± 0.010	0.325 ± 0.020
14:50:29	6.46	0.553 ± 0.006	0.339 ± 0.013
14:52:12	6.61	0.558 ± 0.009	0.326 ± 0.018
14:53:53	7.36	0.552 ± 0.006	0.345 ± 0.013
14:55:34	8.50	0.517 ± 0.006	0.417 ± 0.011
14:57:16	9.88	0.462 ± 0.002	0.511 ± 0.006
14:58:58	11.44	0.414 ± 0.002	0.586 ± 0.003
15:00:39	13.08	0.357 ± 0.002	0.657 ± 0.002
15:02:20	14.75	0.298 ± 0.001	0.723 ± 0.001
15:04:02	16.54	0.247 ± 0.001	0.774 ± 0.001
15:05:44	18.36	0.202 ± 0.001	0.815 ± 0.001
15:07:25	20.17	0.167 ± 0.001	0.845 ± 0.001
15:09:06	22.01	0.134 ± 0.001	0.872 ± 0.001
15:10:47	23.84	0.106 ± 0.001	0.896 ± 0.001
15:12:29	25.70	0.082 ± 0.001	0.917 ± 0.001
15:14:11	27.59	0.061 ± 0.001	0.935 ± 0.001

[a]End of a measurement time interval of ~102 s over which the data were averaged and the interpreted results displayed on a terminal. This time does not correspond to the average height during the measurement interval, but to the height at the end of the interval. The time that corresponds to the average height can be obtained by averaging the time listed with the time at the end of the previous interval.

[b]Average height of solution during the time interval of the measurement, which ends at the time given in Col. 1.

[c]Average value during the time interval of the measurement. The statistical uncertainty given here is one standard deviation of the mean. The ratio of spectral densities was averaged up to a frequency of 5 kHz. The number of points per data block was 1024, and 20,000 data blocks were averaged in ~102 s with a sampling rate of ~200 kHz.

[d]The uncertainty in k_{eff} is from the statistical uncertainty in the ratio of spectral densities only.

APPENDIX H

ADDITIONAL DATA FROM DYNAMIC MEASUREMENTS WITH THE EXPERIMENTAL VESSEL DRAINING AT A RATE OF 3 CM/MIN

APPENDIX H. ADDITIONAL DATA FROM DYNAMIC MEASUREMENTS WITH THE EXPERIMENTAL VESSEL DRAINING AT A RATE OF 3 CM/MIN

This appendix presents additional data from dynamic measurements with the experimental vessel draining at a rate of 3 cm/min. Typical ratios of spectral densities as a function of frequencies for various heights in this draining are plotted in Fig. H.1. Table H.1 lists the interpretation of the dynamic measurement that was performed on-line during this draining of the vessel. The values in this table are different from those in Table 10 (Sect. 7.2) since the parameters used in the interpretation were slightly different and average ratios of spectral densities up to 5 kHz were used for all solution heights in the on-line interpretation.

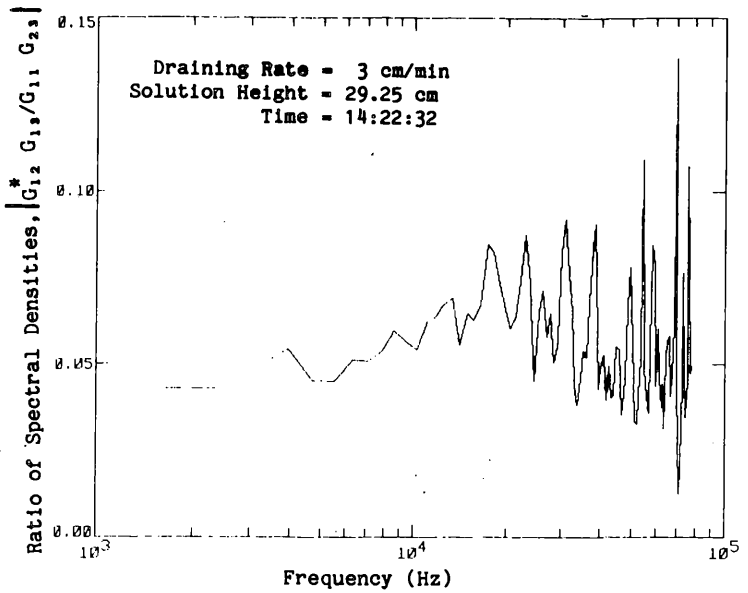

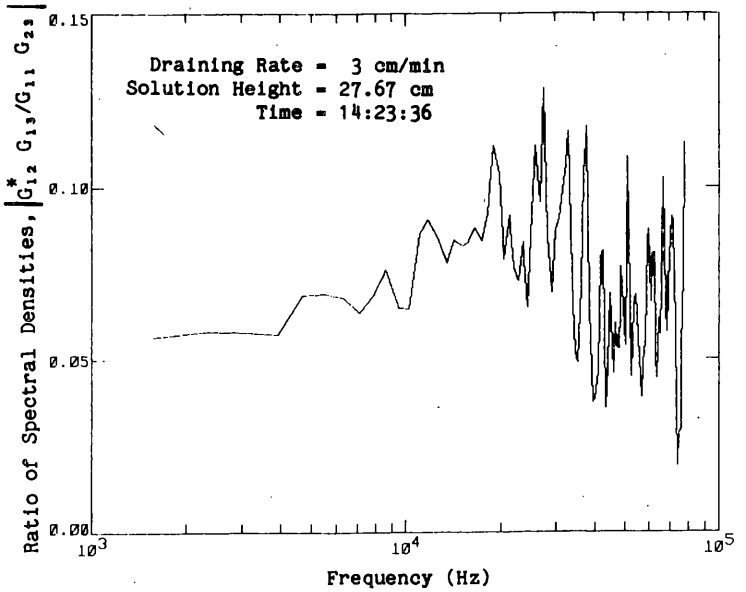

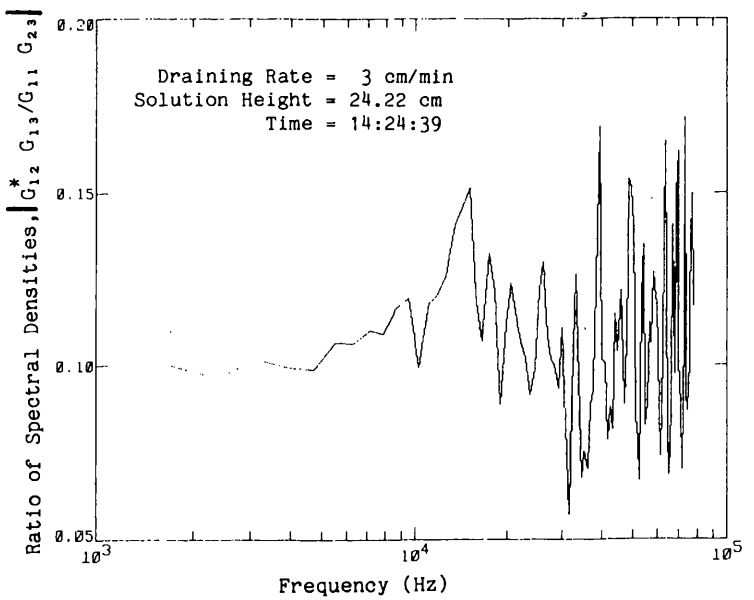

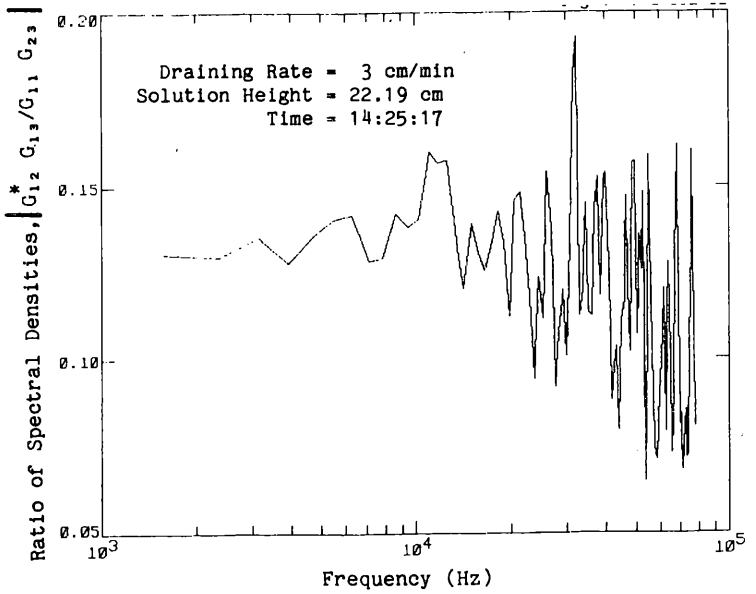

Fig. H.1. Ratios of spectral densities as a function of frequency for a draining rate of 3 cm/min at various solution heights.

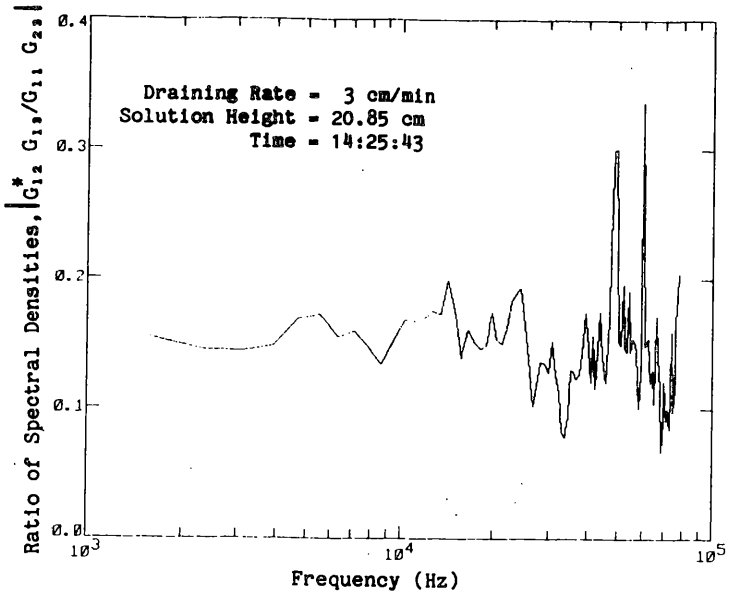

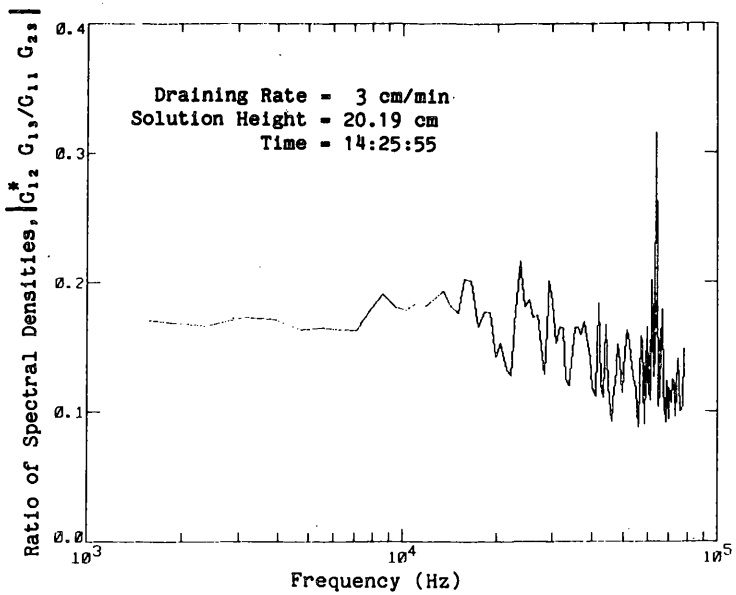

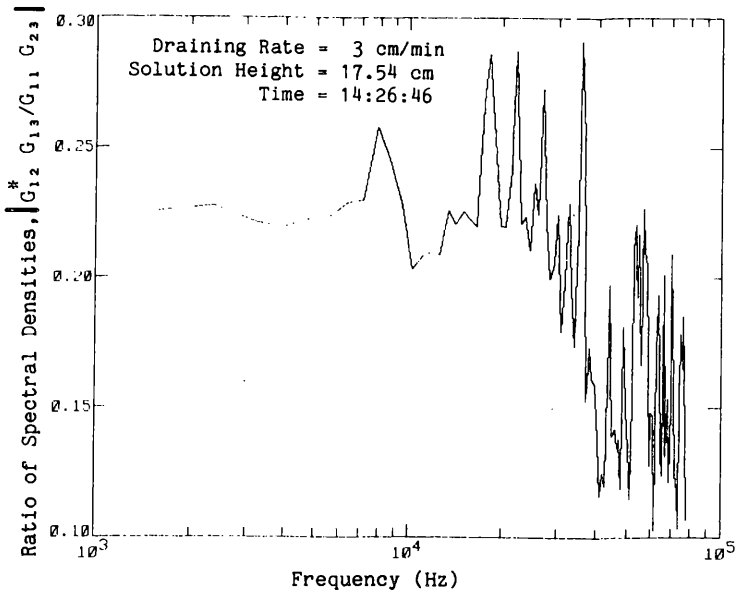

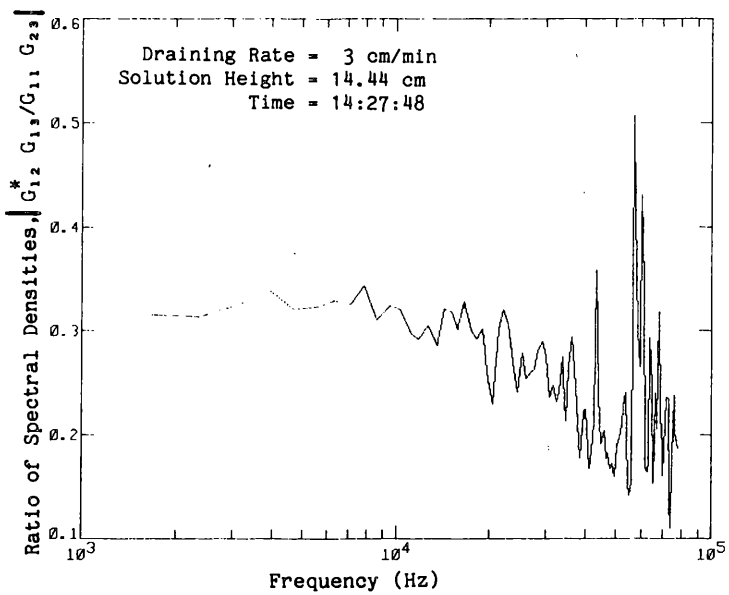

Fig. H.1 (continued)

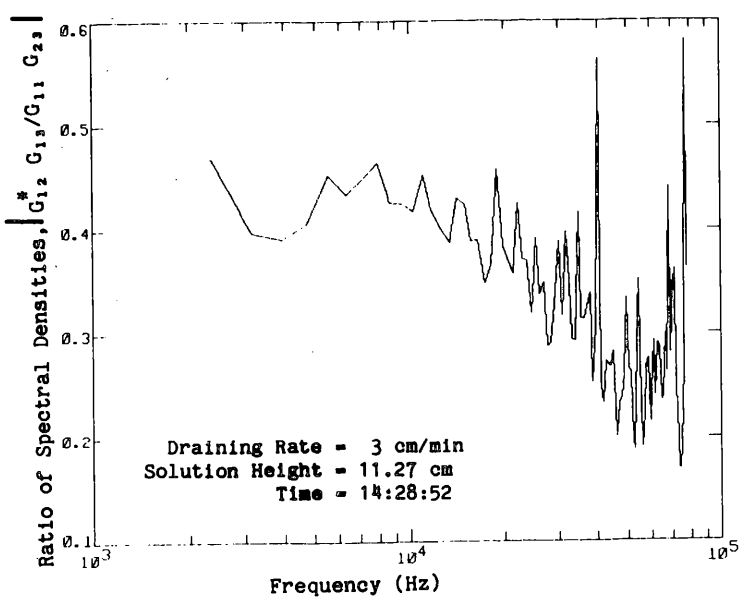

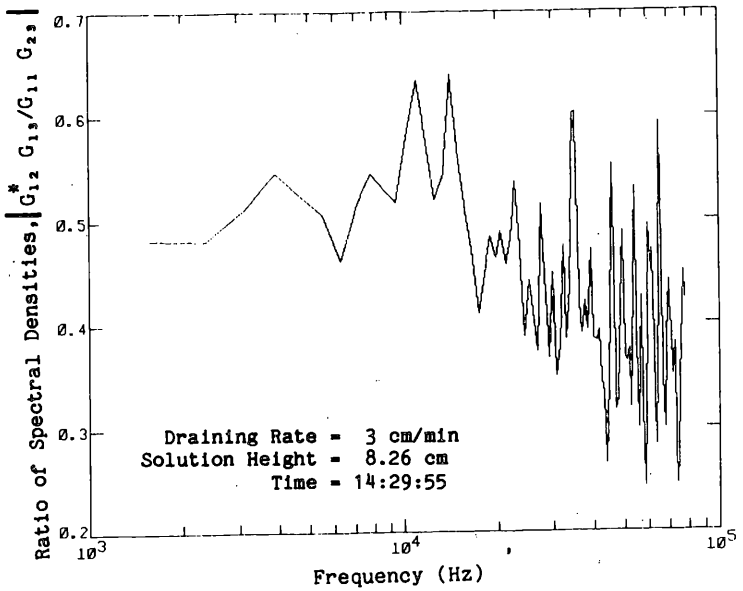

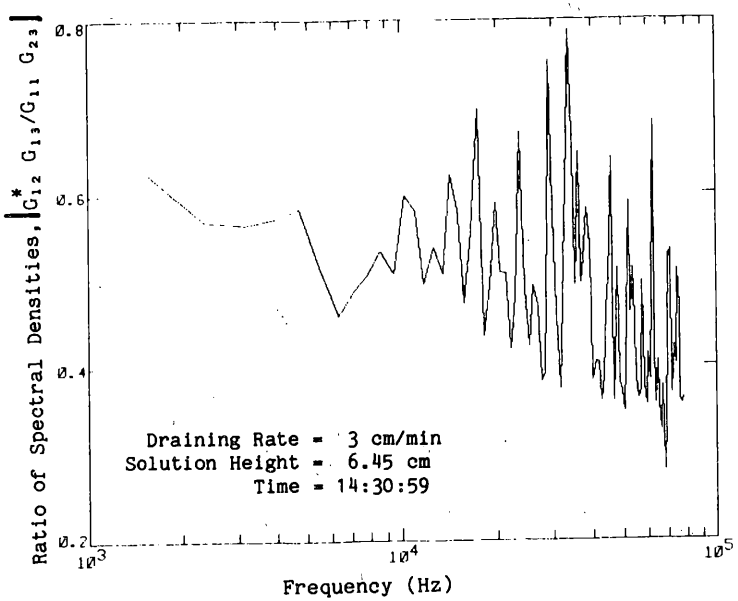

Fig. H.1 (continued)

Table H.1. On-line ratios of spectral densities at low frequency and neutron multiplication factors for dynamic measurements while draining the experimental vessel at a rate of ~3 cm/min

Time[a] (h:m:s)	Solution height[b] (cm)	Ratio of spectral densities[c]	k_{eff} from ratio of spectral densities[d]
14:22:32	29.25	0.047 ± 0.002	0.947 ± 0.003
14:22:44	29.26	0.044 ± 0.001	0.951 ± 0.002
14:22:57	29.25	0.045 ± 0.001	0.949 ± 0.001
14:23:10	28.96	0.050 ± 0.002	0.945 ± 0.002
14:23:22	28.36	0.058 ± 0.002	0.936 ± 0.002
14:23:35	27.67	0.060 ± 0.002	0.936 ± 0.003
14:23:48	27.00	0.073 ± 0.003	0.923 ± 0.003
14:24:01	26.34	0.075 ± 0.000	0.923 ± 0.001
14:24:13	25.62	0.081 ± 0.001	0.918 ± 0.002
14:24:26	24.88	0.091 ± 0.002	0.910 ± 0.002
14:24:39	24.22	0.099 ± 0.001	0.902 ± 0.001
14:24:52	23.57	0.109 ± 0.002	0.895 ± 0.002
14:25:05	22.86	0.124 ± 0.005	0.881 ± 0.005
14:25:17	22.19	0.132 ± 0.002	0.874 ± 0.002
14:25:29	21.54	0.148 ± 0.003	0.859 ± 0.003
14:25:42	20.85	0.152 ± 0.005	0.858 ± 0.005
14:25:55	20.19	0.169 ± 0.002	0.843 ± 0.002
14:26:07	19.56	0.185 ± 0.005	0.828 ± 0.005
14:26:20	18.87	0.193 ± 0.003	0.822 ± 0.003
14:26:34	18.19	0.212 ± 0.003	0.805 ± 0.003
14:26:46	17.54	0.233 ± 0.001	0.796 ± 0.002
14:26:58	16.92	0.253 ± 0.004	0.766 ± 0.005
14:27:11	16.28	0.266 ± 0.003	0.754 ± 0.003
14:27:23	15.66	0.290 ± 0.002	0.730 ± 0.003
14:27:36	15.05	0.298 ± 0.004	0.724 ± 0.005
14:27:49	14.44	0.323 ± 0.004	0.696 ± 0.006
14:28:02	13.78	0.344 ± 0.008	0.671 ± 0.010
14:28:15	13.12	0.359 ± 0.007	0.655 ± 0.010
14:28:28	12.48	0.392 ± 0.011	0.613 ± 0.016
14:28:40	11.85	0.397 ± 0.006	0.609 ± 0.008

Table H.1 (continued)

Time[a] (h:m:s)	Solution height[b] (cm)	Ratio of spectral densities[c]	k_{eff} from ratio of spectral densities[d]
14:28:52	11.27	0.421 ± 0.015	0.577 ± 0.022
14:29:06	10.63	0.444 ± 0.014	0.545 ± 0.021
14:29:18	9.99	0.445 ± 0.006	0.544 ± 0.009
14:29:30	9.32	0.476 ± 0.006	0.493 ± 0.010
14:29:43	8.75	0.480 ± 0.016	0.483 ± 0.028
14:29:55	8.26	0.509 ± 0.013	0.431 ± 0.023
14:30:08	7.63	0.554 ± 0.011	0.341 ± 0.024
14:30:21	7.05	0.599 ± 0.009	0.242 ± 0.022
14:30:34	6.63	0.574 ± 0.027	0.296 ± 0.061
14:30:47	6.46	0.526 ± 0.031	0.393 ± 0.062
14:30:59	6.45	0.583 ± 0.011	0.275 ± 0.024
14:31:11	6.45	0.550 ± 0.022	0.344 ± 0.046
14:31:24	6.45	0.568 ± 0.020	0.307 ± 0.045
14:31:37	6.46	0.549 ± 0.027	0.347 ± 0.056

[a]End of a measurement time interval of ~12.8 s over which the data were averaged and the interpreted results displayed on a computer terminal as the solution was drained. This time does not correspond to the average height during the measurement interval, but rather to the height at the end of the interval. The time which corresponds to the average height can be obtained by averaging the time listed with the time at the end of the previous interval.

[b]Average height of solution during the time interval of the measurement, which ends at the time given in Col. 1.

[c]Average value during the time interval of the measurement. The statistical uncertainty given here is one standard deviation of the mean. The ratio of spectral densities was averaged up to a frequency of 5 kHz. The number of points per data block was 256, and 10,000 data blocks were averaged in ~12.8 s at a sampling rate of 200 kHz.

[d]The uncertainty in k_{eff} is from the statistical uncertainty in the ratio of spectral densities only.

APPENDIX I

ADDITIONAL DATA FROM DYNAMIC MEASUREMENTS WITH THE EXPERIMENTAL VESSEL DRAINING AT A RATE OF 5 CM/MIN

APPENDIX I. ADDITIONAL DATA FROM DYNAMIC MEASUREMENTS WITH THE EXPERIMENTAL VESSEL DRAINING AT A RATE OF 5 CM/MIN

This appendix presents additional data from dynamic measurements with the experimental vessel draining at a rate of 5 cm/min. Typical ratios of spectral densities as a function of frequencies for various heights in this draining are plotted in Fig. I.1. Table I.1 lists the interpretation of the dynamic measurement that was performed on-line during this draining of the vessel. The values in this table are different from those in Table 11 (Sect. 7.2) since the parameters used in the interpretation were slightly different, and average ratios of spectral densities up to 5 kHz were used for all solution heights in the on-line interpretation.

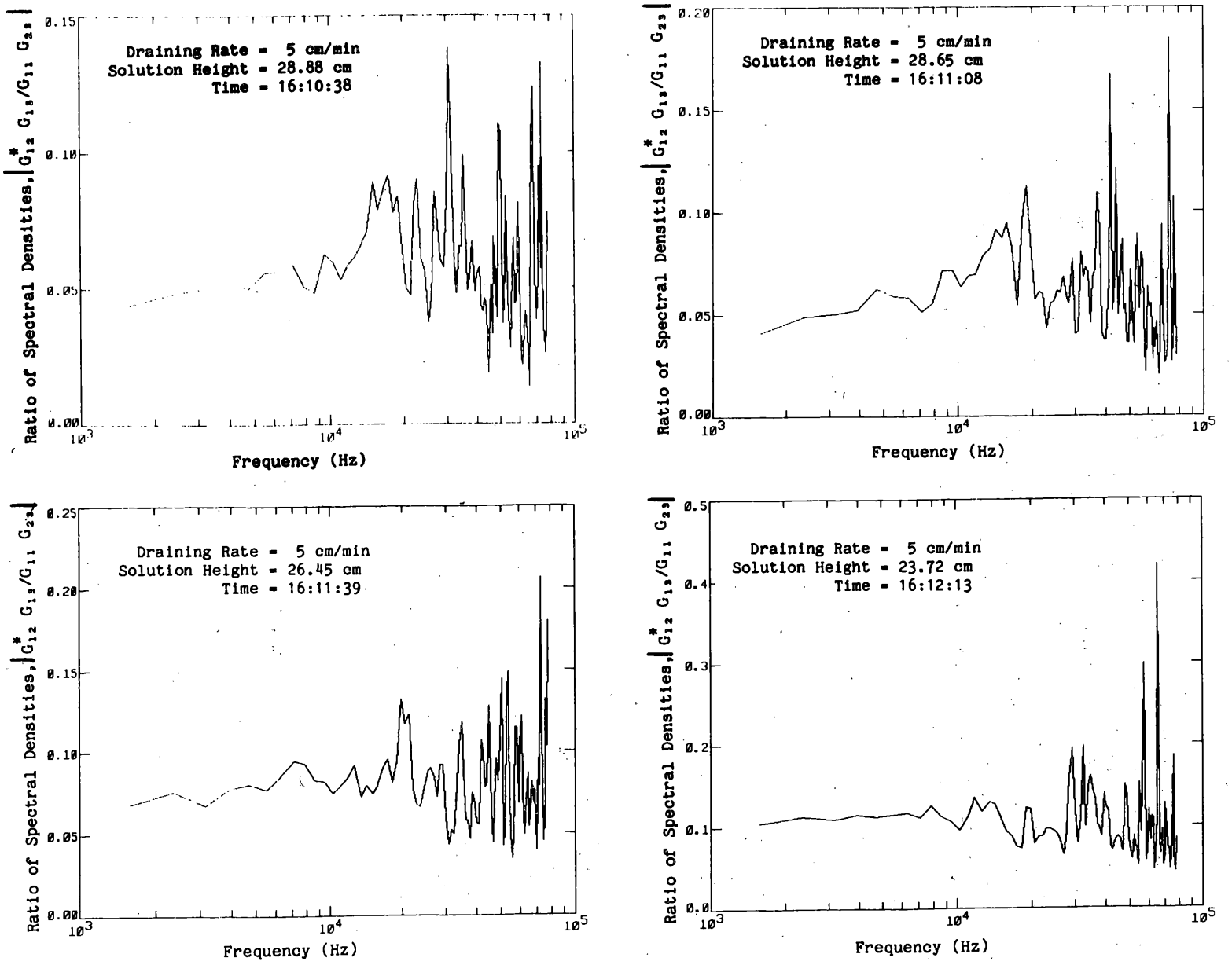

Fig. I.1. Ratios of spectral densities as a function of frequency for a draining rate of 5 cm/min at various solution heights.

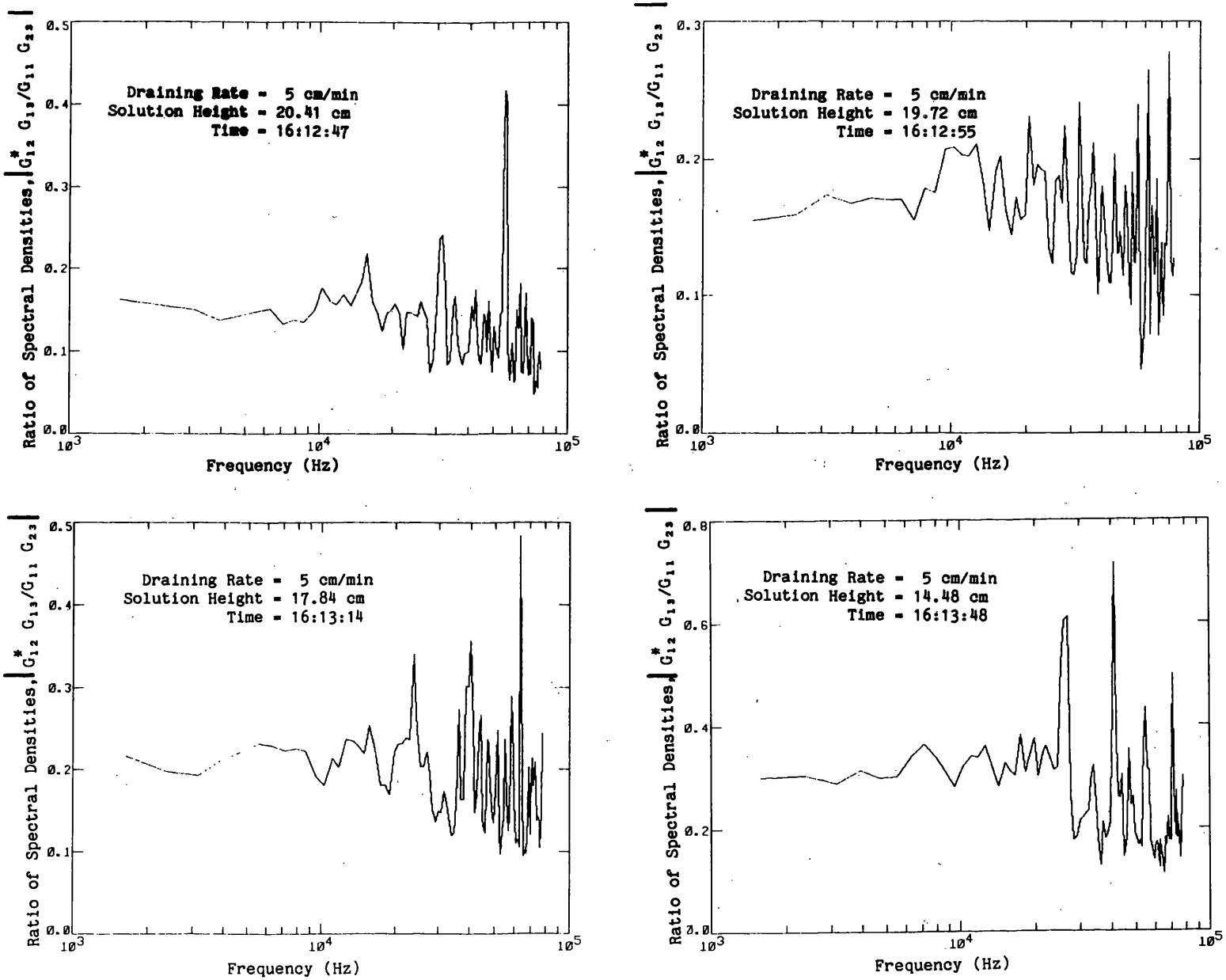

Fig. I.1 (continued)

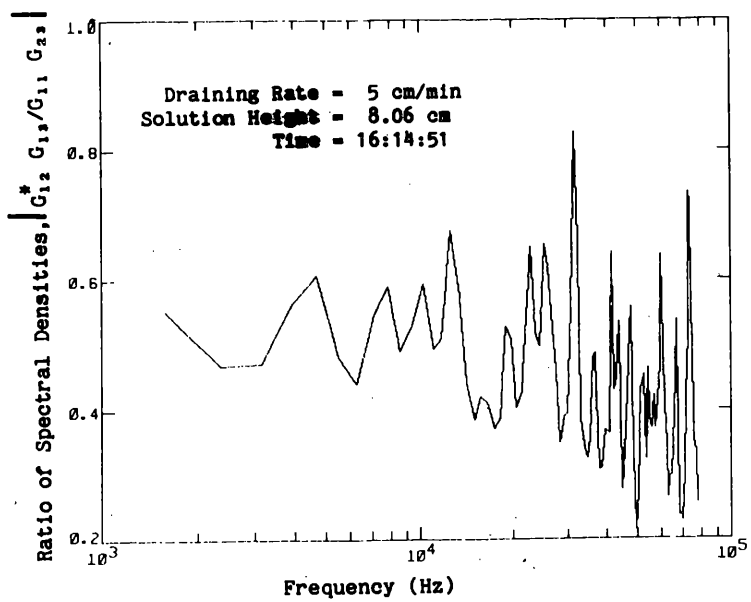

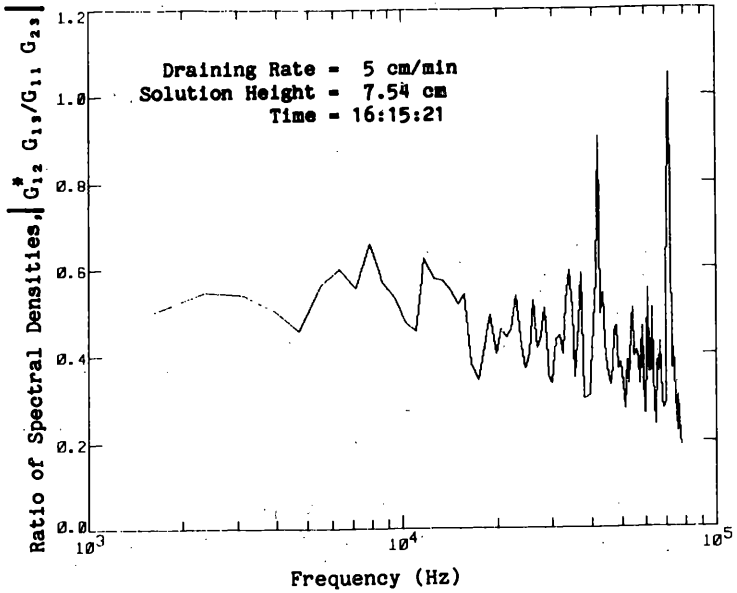

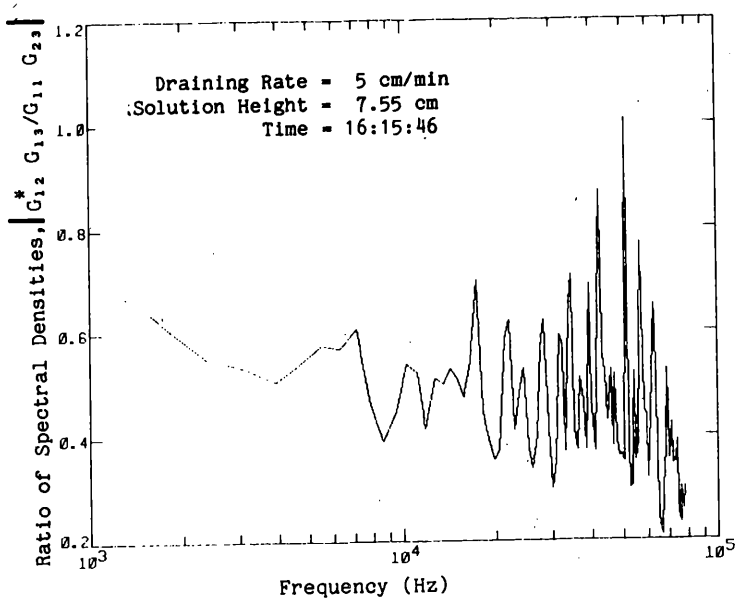

Fig. I.1 (continued)

Table I.1. On-line ratios of spectral densities at low frequency and neutron multiplication factors for dynamic measurements while draining the experimental vessel at a rate of 5 cm/min

Time[a] (h:m:s)	Solution height[b] (cm)	Ratio of spectral densities[c]	k_{eff} from ratio of spectral densities[d]
16:10:36	28.88	0.049 ± 0.002	0.945 ± 0.002
16:10:42	28.88	0.051 ± 0.002	0.944 ± 0.002
16:10:49	28.88	0.047 ± 0.001	0.948 ± 0.001
16:10:55	28.88	0.047 ± 0.002	0.948 ± 0.002
16:11:01	28.87	0.049 ± 0.002	0.945 ± 0.002
16:11:08	28.65	0.051 ± 0.003	0.944 ± 0.004
16:11:14	28.23	0.055 ± 0.003	0.940 ± 0.004
16:11:20	27.80	0.063 ± 0.004	0.933 ± 0.004
16:11:27	27.36	0.064 ± 0.001	0.932 ± 0.001
16:11:33	26.91	0.067 ± 0.003	0.930 ± 0.003
16:11:39	26.45	0.074 ± 0.003	0.924 ± 0.003
16:11:46	25.96	0.082 ± 0.004	0.916 ± 0.004
16:11:52	25.46	0.091 ± 0.004	0.908 ± 0.005
16:11:58	24.94	0.089 ± 0.002	0.911 ± 0.002
16:12:05	24.40	0.096 ± 0.002	0.906 ± 0.003
16:12:11	23.72	0.111 ± 0.002	0.892 ± 0.002
16:12:17	23.11	0.115 ± 0.001	0.889 ± 0.001
16:12:23	22.62	0.123 ± 0.002	0.883 ± 0.002
16:12:29	21.95	0.122 ± 0.006	0.885 ± 0.006
16:12:35	21.08	0.147 ± 0.003	0.862 ± 0.003
16:12:42	20.41	0.149 ± 0.005	0.862 ± 0.005
16:12:49	20.12	0.163 ± 0.005	0.849 ± 0.005
16:12:55	19.72	0.165 ± 0.004	0.848 ± 0.004
16:13:02	19.14	0.187 ± 0.002	0.827 ± 0.002
16:13:08	18.50	0.216 ± 0.004	0.799 ± 0.004
16:13:14	17.84	0.209 ± 0.006	0.810 ± 0.006
16:13:21	17.20	0.221 ± 0.006	0.800 ± 0.006
16:13:27	16.55	0.254 ± 0.004	0.767 ± 0.004
16:13:33	15.91	0.265 ± 0.005	0.757 ± 0.006
16:13:40	15.25	0.286 ± 0.004	0.737 ± 0.005

Table I.1 (continued)

Time[a] (h:m:s)	Solution height[b] (cm)	Ratio of spectral densities[c]	k_{eff} from ratio of spectral densities[d]
16:13:46	14.48	0.302 ± 0.004	0.721 ± 0.005
16:13:52	13.83	0.334 ± 0.003	0.684 ± 0.004
16:14:59	12.97	0.346 ± 0.007	0.673 ± 0.009
16:14:05	12.13	0.378 ± 0.007	0.634 ± 0.010
16:14:11	11.82	0.421 ± 0.008	0.574 ± 0.012
16:14:18	11.38	0.429 ± 0.004	0.564 ± 0.006
16:14:24	10.74	0.427 ± 0.007	0.570 ± 0.010
16:14:30	10.13	0.447 ± 0.011	0.543 ± 0.018
16:14:37	9.51	0.523 ± 0.014	0.411 ± 0.027
16:14:44	8.78	0.465 ± 0.017	0.508 ± 0.029
16:14:50	8.06	0.532 ± 0.027	0.386 ± 0.055
16:14:57	7.67	0.509 ± 0.012	0.429 ± 0.023
16:15:04	7.56	0.559 ± 0.016	0.330 ± 0.034
16:15:10	7.54	0.542 ± 0.009	0.365 ± 0.018
16:15:16	7.56	0.493 ± 0.030	0.457 ± 0.055
16:15:22	7.54	0.510 ± 0.016	0.426 ± 0.030
16:15:29	7.52	0.597 ± 0.027	0.249 ± 0.065
16:15:36	7.53	0.480 ± 0.014	0.479 ± 0.024
16:15:42	7.54	0.550 ± 0.027	0.349 ± 0.056

[a]End of a measurement time interval of ~6.4 s over which the data were averaged and the interpreted results displayed on a computer terminal. This time does not correspond to the average height during the measurement interval, but rather to the height at the end of the interval. The time which corresponds to the average height can be obtained by averaging the time listed with the time at the end of the previous interval.

[b]Average height of solution during the time interval of the measurement, which ends at the time given in Col. 1.

[c]Average value during the time interval of the measurement. The statistical uncertainty given here is one standard deviation of the mean. The ratio of spectral densities was averaged up to a frequency of 5 kHz. The number of points per data block was 256, and 5000 data blocks were averaged in ~6.4 s with a sampling rate of ~200 kHz.

[d]The uncertainty in k_{eff} is from the statistical uncertainty in the ratio of spectral densities only.

APPENDIX J

ADDITIONAL DATA FROM DYNAMIC MEASUREMENTS WITH THE EXPERIMENTAL VESSEL DRAINING AT A RATE OF 23 CM/MIN

APPENDIX J. ADDITIONAL DATA FROM DYNAMIC MEASUREMENTS WITH THE EXPERIMENTAL VESSEL DRAINING AT A RATE OF 23 CM/MIN

This appendix presents some additional data from dynamic measurements with the experimental vessel draining at a rate of 23 cm/min. Typical ratios of spectral densities as a function of frequencies for various heights in this draining are plotted in Fig. J.1. Table J.1 lists the interpretation of the dynamic measurement that was performed on-line during this draining of the vessel. The values in this table are different from those in Table 12 (Sect. 7.2) since the parameters used in the interpretation were slightly different and average ratios of spectral densities up to 5 kHz were used for all solution heights in the on-line interpretation.

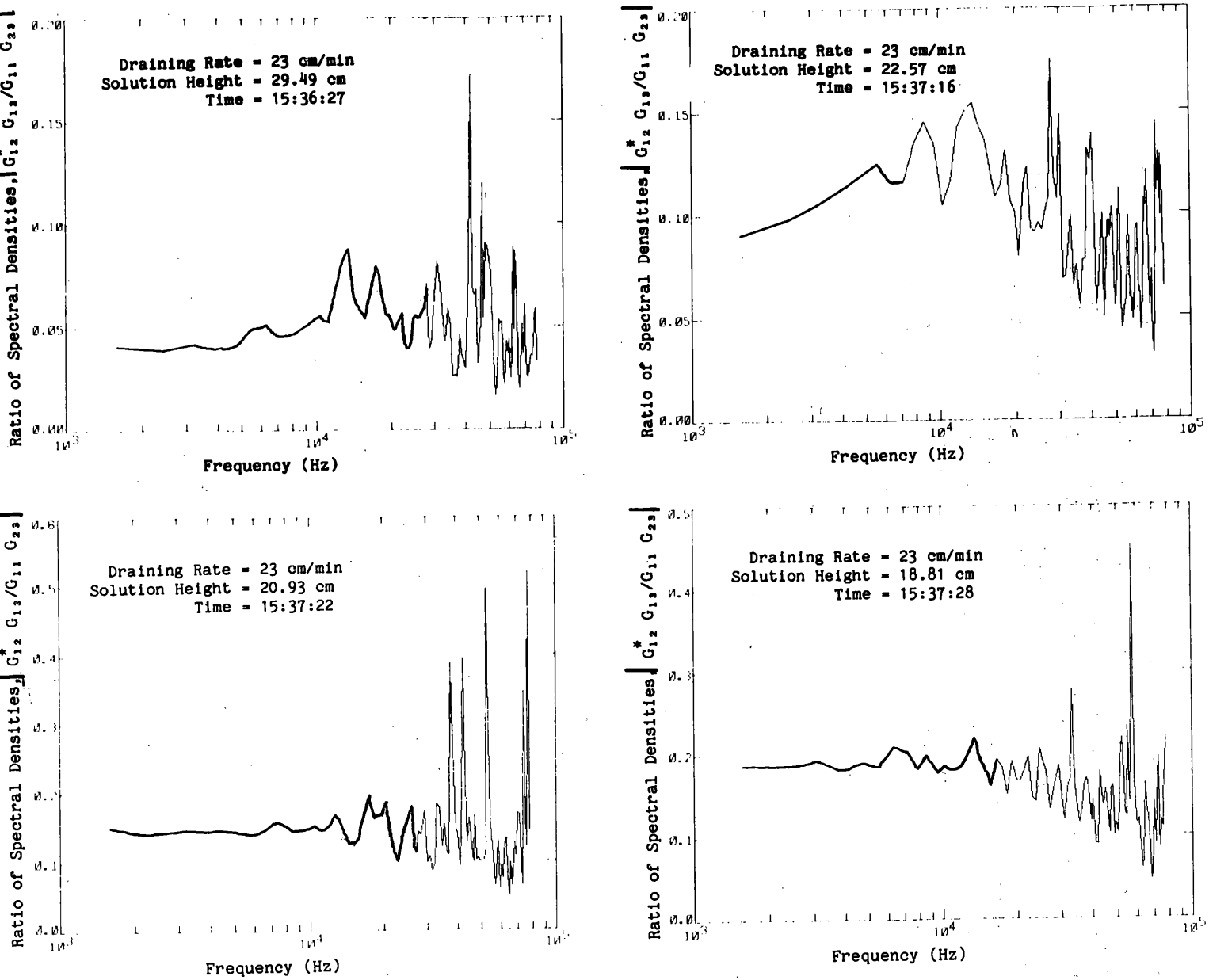

Fig. J.1. Ratios of spectral densities as a function of frequency for a draining rate of 23 cm/min at various solution heights.

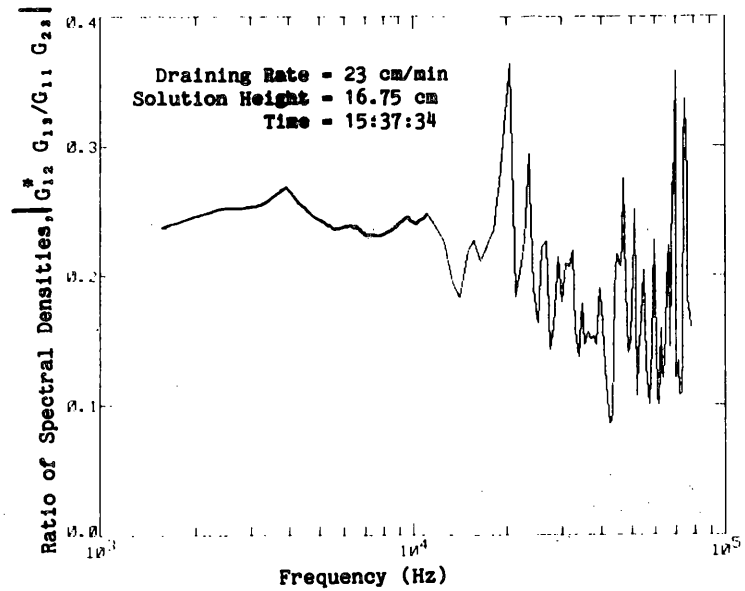

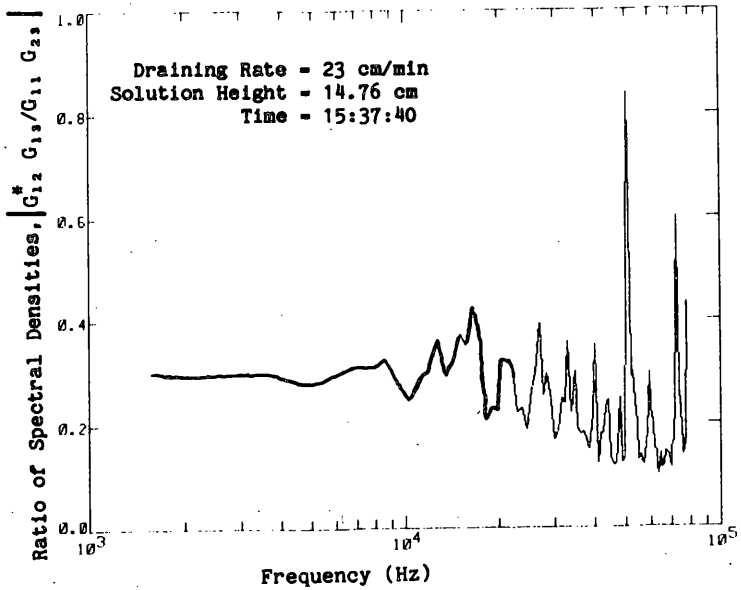

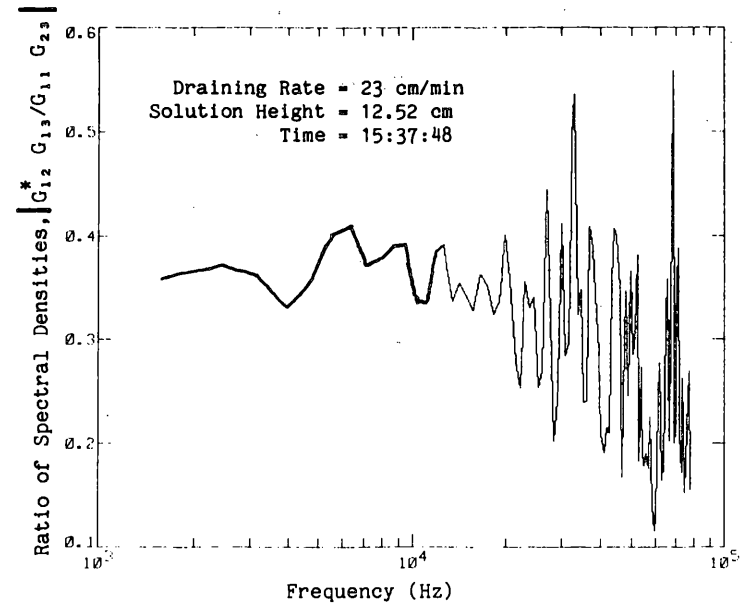

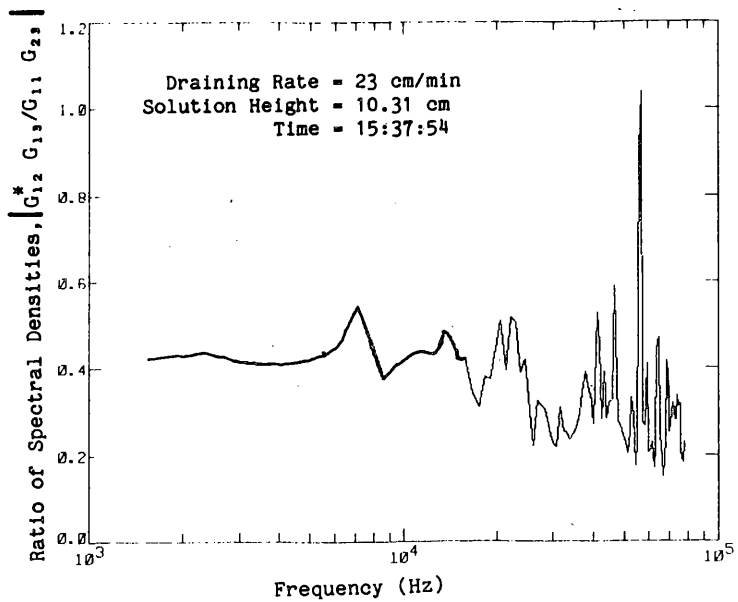

Fig. J.1 (continued)

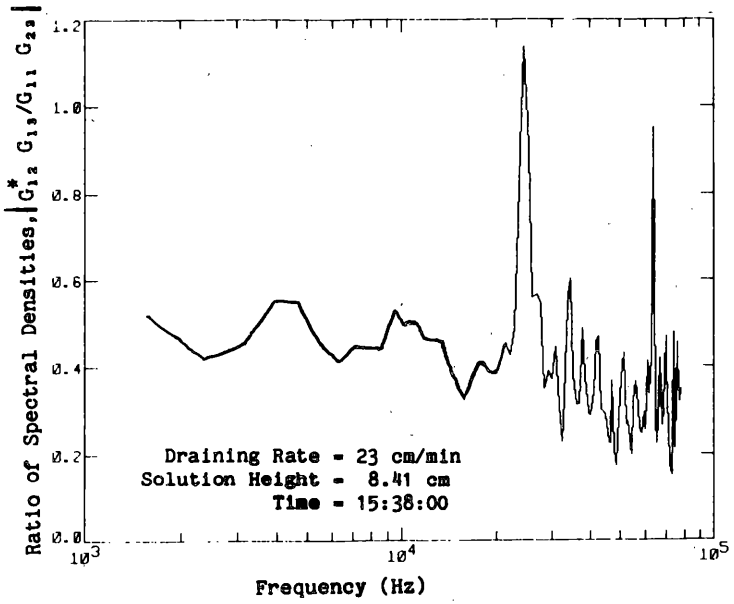

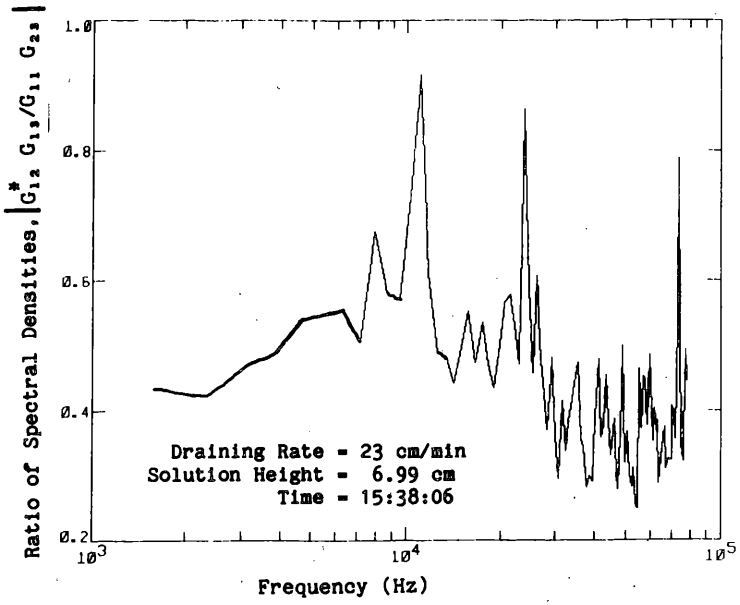

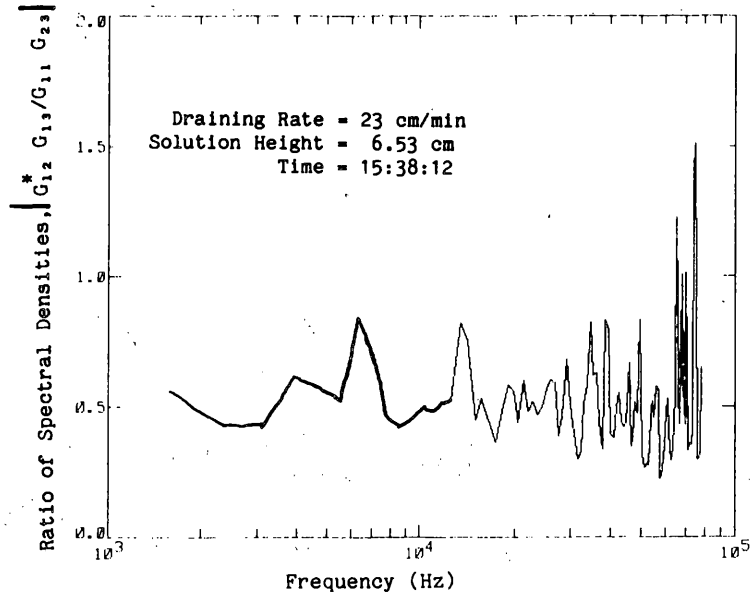

Fig. J.1 (continued)

Table J.1. Ratios of spectral densities at low frequency and neutron multiplication factors for dynamic measurements while draining the experimental vessel at a rate of 23 cm/min

Time[a] (h:m:s)	Solution height[b] (cm)	Ratio of spectral densities[c]	k_{eff} from ratio of spectral densities[d]
16:50:60	28.91	0.049 ± 0.001	0.945 ± 0.001
16:51:07	28.91	0.045 ± 0.002	0.950 ± 0.003
16:51:14	28.91	0.047 ± 0.003	0.948 ± 0.004
16:51:20	28.88	0.048 ± 0.002	0.947 ± 0.002
16:51:26	27.96	0.049 ± 0.001	0.947 ± 0.002
16:51:33	25.97	0.079 ± 0.002	0.920 ± 0.002
16:51:39	23.77	0.103 ± 0.003	0.900 ± 0.003
16:51:45	21.59	0.138 ± 0.003	0.870 ± 0.003
16:51:51	19.42	0.171 ± 0.003	0.843 ± 0.003
16:51:58	17.30	0.221 ± 0.005	0.800 ± 0.005
16:52:04	15.22	0.288 ± 0.003	0.734 ± 0.004
16:52:10	13.49	0.353 ± 0.006	0.661 ± 0.007
16:52:16	11.81	0.423 ± 0.004	0.571 ± 0.006
16:52:23	9.49	0.446 ± 0.009	0.541 ± 0.015
16:52:30	6.93	0.502 ± 0.029	0.439 ± 0.055
16:52:36	5.69	0.629 ± 0.031	0.162 ± 0.083
16:52:42	5.68	0.502 ± 0.005	0.433 ± 0.008
16:52:48	5.71	0.607 ± 0.036	0.215 ± 0.090
16:52:55	5.73	0.675 ± 0.078	0.037 ± 0.259
16:53:01	5.72	0.622 ± 0.055	0.178 ± 0.147
16:53:07	5.72	0.601 ± 0.022	0.230 ± 0.054
16:53:14	5.72	0.586 ± 0.021	0.263 ± 0.049
16:53:20	5.72	0.559 ± 0.046	0.323 ± 0.101
16:53:26	5.70	0.537 ± 0.023	0.368 ± 0.047
16:53:33	5.32	0.536 ± 0.043	0.367 ± 0.090

Table J.1 (continued)

Time[a] (h:m:s)	Solution height[b] (cm)	Ratio of spectral densities[c]	k_{eff} from ratio of spectral densities[d]
16:53:39	5.70	0.547 ± 0.029	0.345 ± 0.062
16:53:45	5.70	0.514 ± 0.027	0.411 ± 0.053
16:53:52	5.70	0.595 ± 0.035	0.243 ± 0.085
16:53:58	5.73	0.577 ± 0.039	0.283 ± 0.091

[a]End of a measurement time interval of ~6.4 s over which the data were averaged and the interpreted results displayed on a computer terminal. This time does not correspond to the average height during the measurement interval, but rather to the height at the end of the interval. The time which corresponds to the average height can be obtained by averaging the time listed with the time at the end of the previous interval.

[b]Average height of solution during the time interval of the measurement, which ends at the time given in Col. 1.

[c]Average value during the time interval of the measurement. The statistical uncertainty given here is one standard deviation of the mean. The ratio of spectral densities was averaged up to a frequency of 5 kHz. The number of points per data block was 256, and 5000 data blocks were averaged in ~6.4 s with a sampling rate of ~200 kHz.

[d]The uncertainty in k_{eff} is from the statistical uncertainty in the ratio of spectral densities only.

APPENDIX K

ADDITIONAL DATA FROM DYNAMIC MEASUREMENTS WITH SOLUTION PERTURBED BY BUBBLES

APPENDIX K. ADDITIONAL DATA FROM DYNAMIC MEASUREMENTS WITH SOLUTION PERTURBED BY BUBBLES

This appendix presents some additional data from dynamic measurements with the solution perturbed by bubbles. The ratios of spectral densities as a function of frequencies with and without bubbles as well as some APSDs and CPSDs are plotted in Figs. K.1 through K.5.

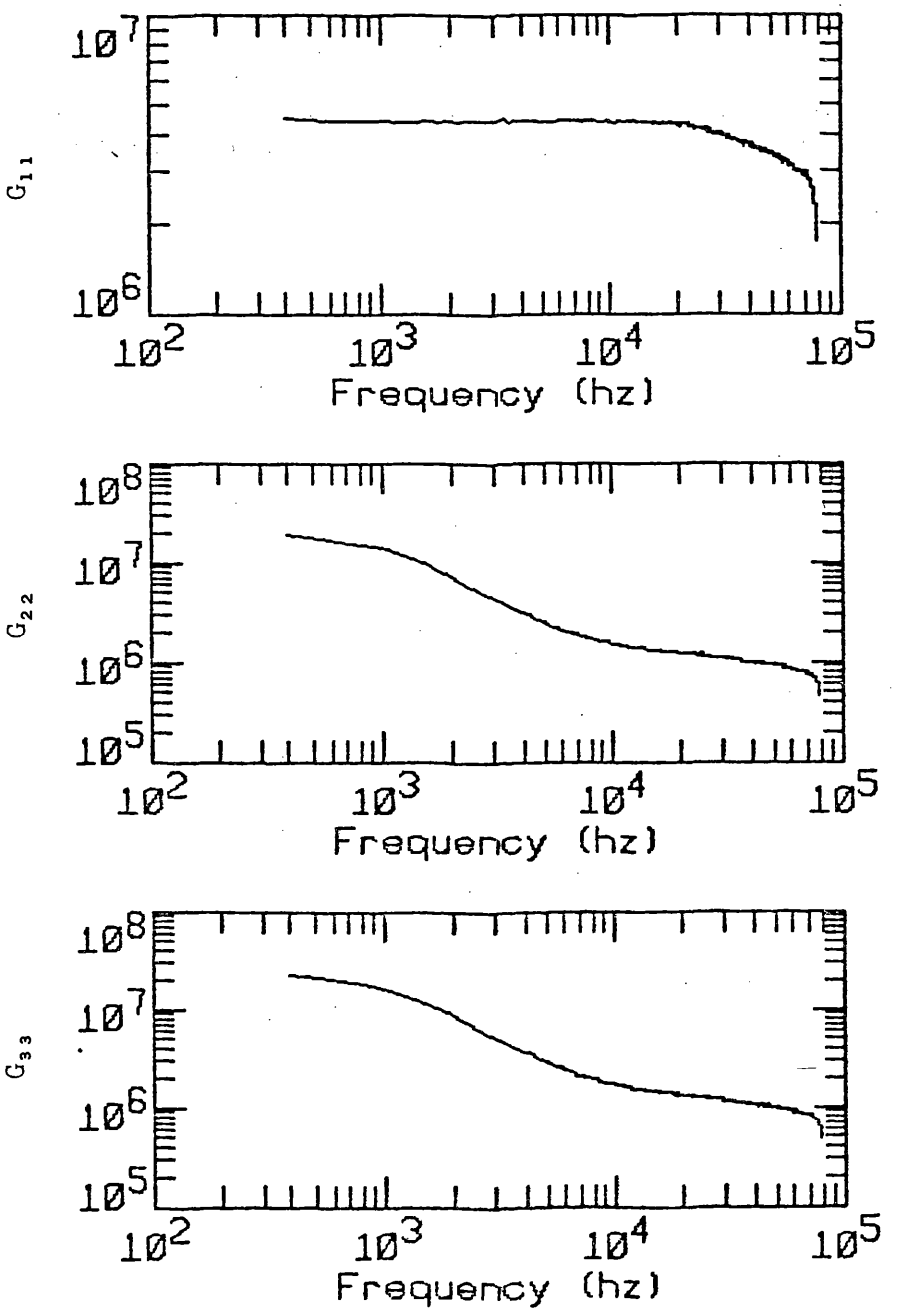

Fig. K.1. APSDs as a function of frequency for the solution unperturbed by bubbles (solution height = 29.5 cm).

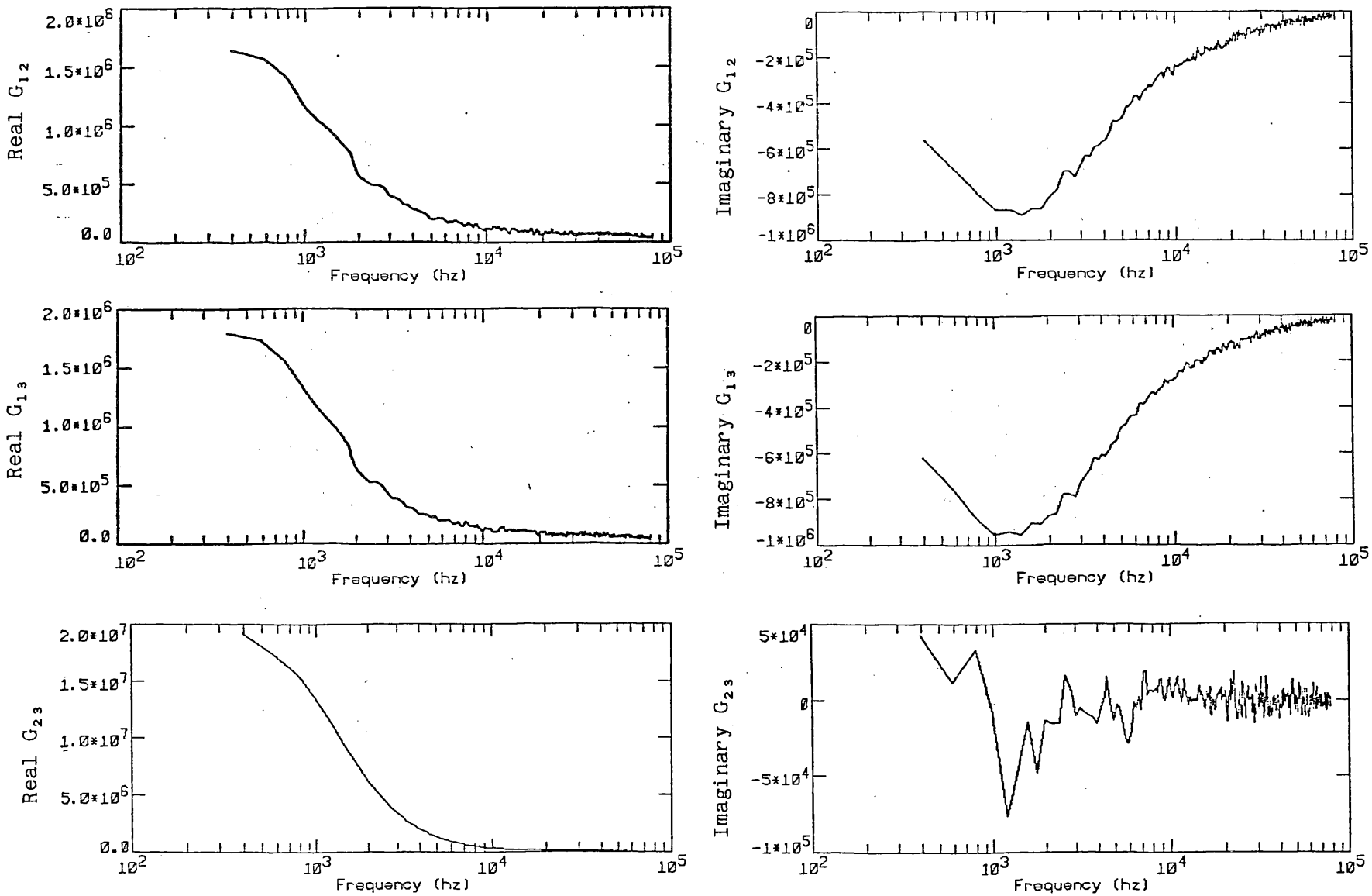

Fig. K.2. Real and imaginary parts of the CPSDs as a function of frequency for the solution unperturbed by bubbles (solution height = 29.5 cm).

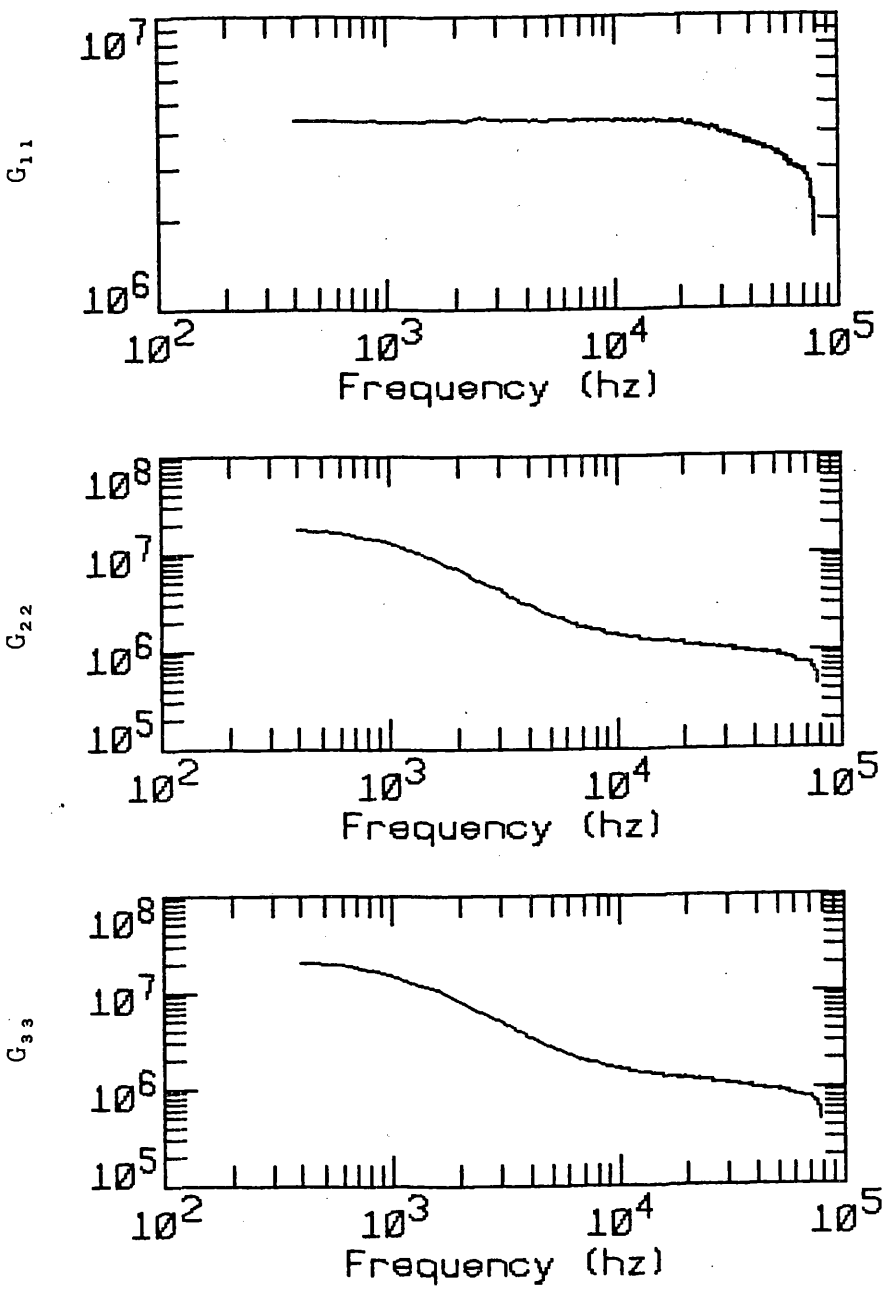

Fig. K.3. APSDs as a function of frequency for the solution perturbed by bubbles (solution height = 29.5 cm).

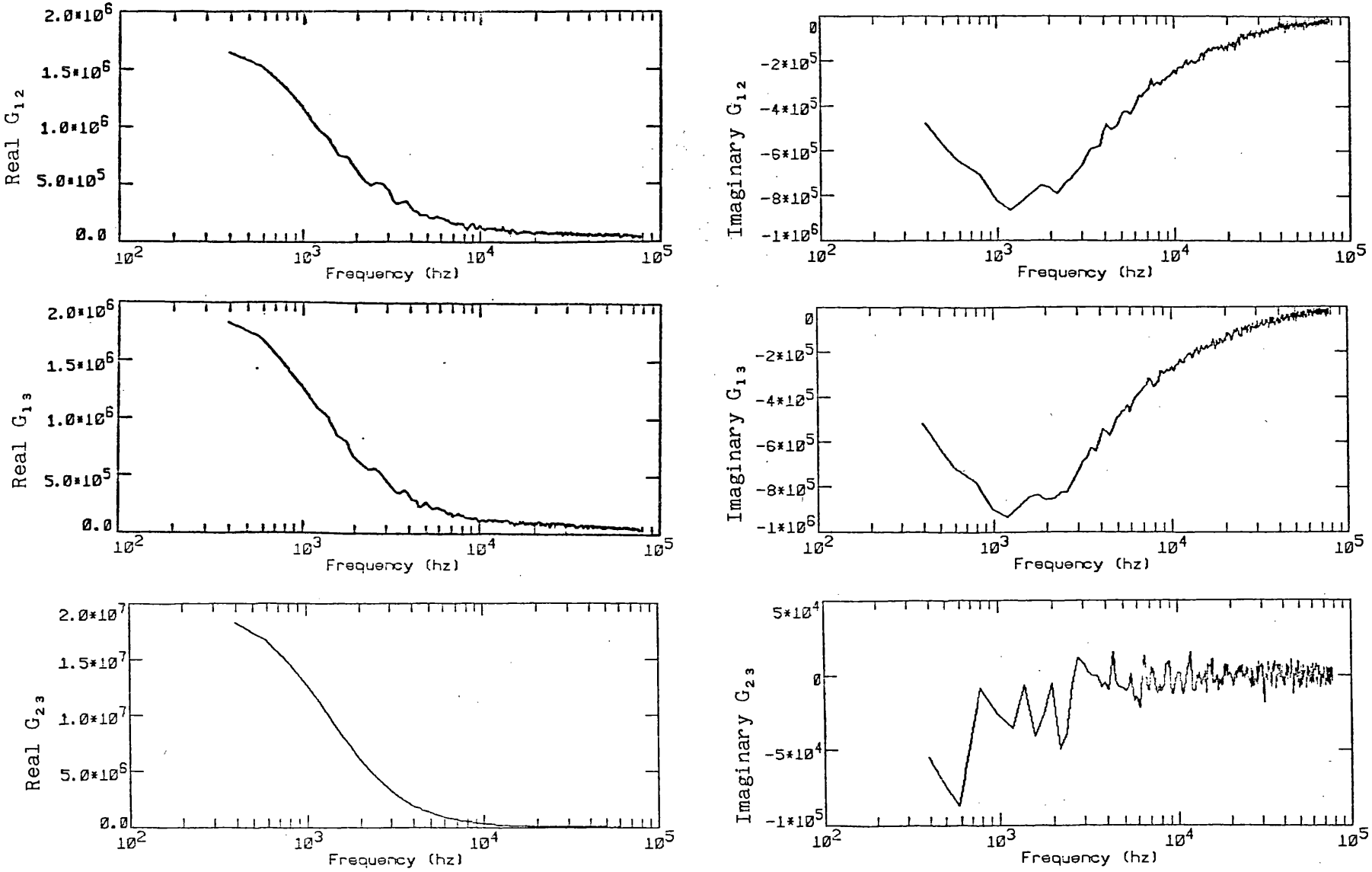

Fig. K.4. CPSDs as a function of frequency for the solution perturbed by bubbles (solution height = 29.5 cm).

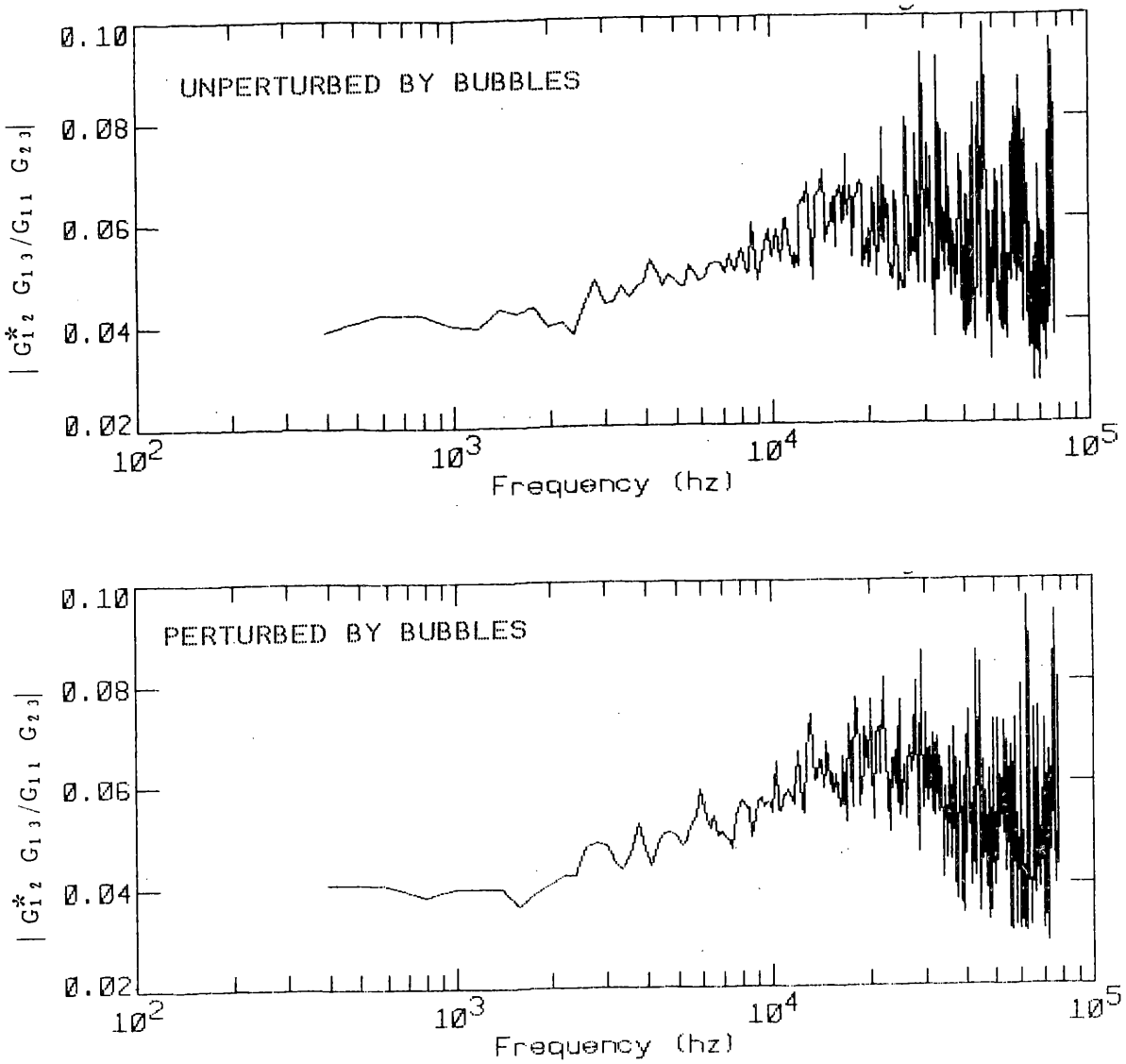

Fig. K.5. Ratios of spectral densities as a function of frequency for a solution height of 29.5 cm.

APPENDIX L

TYPICAL LEAST-SQUARES FITTING OF APSDs AND CPSDs

APPENDIX L. TYPICAL LEAST-SQUARES FITTING OF APSDs AND CPSDs

After correction for the frequency response of the detection systems, the APSDs and CPSDs were fitted using nonlinear least-squares techniques. All APSDs and real and imaginary parts of the CPSDs were fitted simultaneously to find the two break frequencies for the fits to a model consisting of two modes, $H(\omega) = [a_0/(\alpha_0 + j\omega) + a_1/(\alpha_1 + j\omega)]$. For the one-mode fits the functional form fitted was $H(\omega) = a_0/(\alpha_0 + j\omega)$. Typical results of the fitting are shown in Figs. L.1 through L.6 for a solution height of 29.5 cm and for solution heights of 20.2 cm and 13.1 cm while the experimental vessel was being filled at a rate of 1 cm/min.

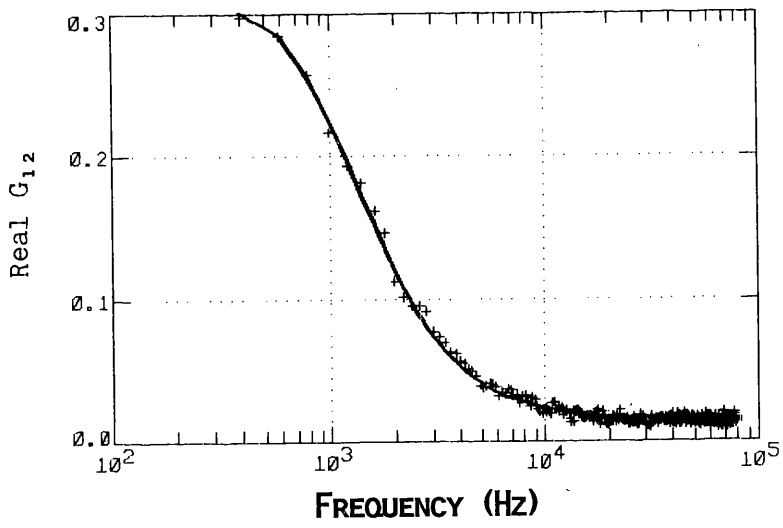

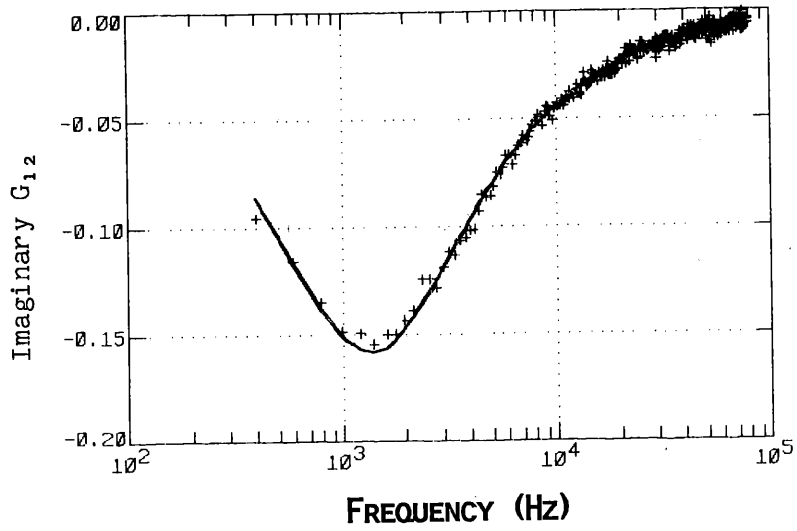

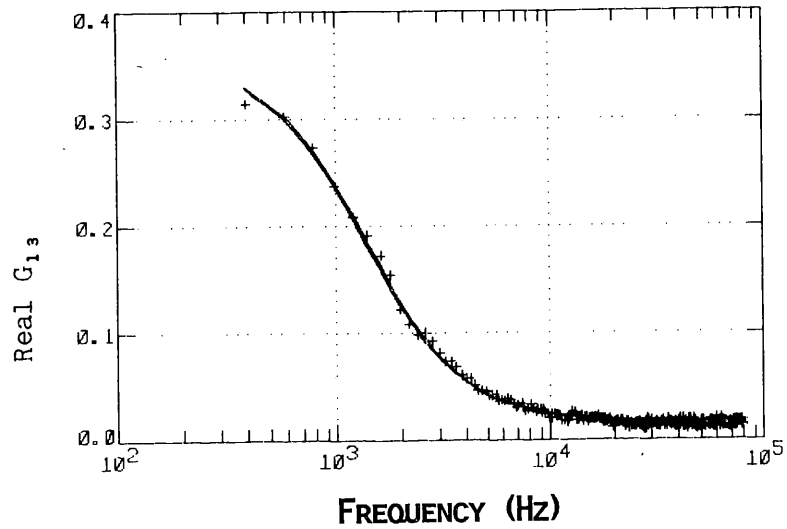

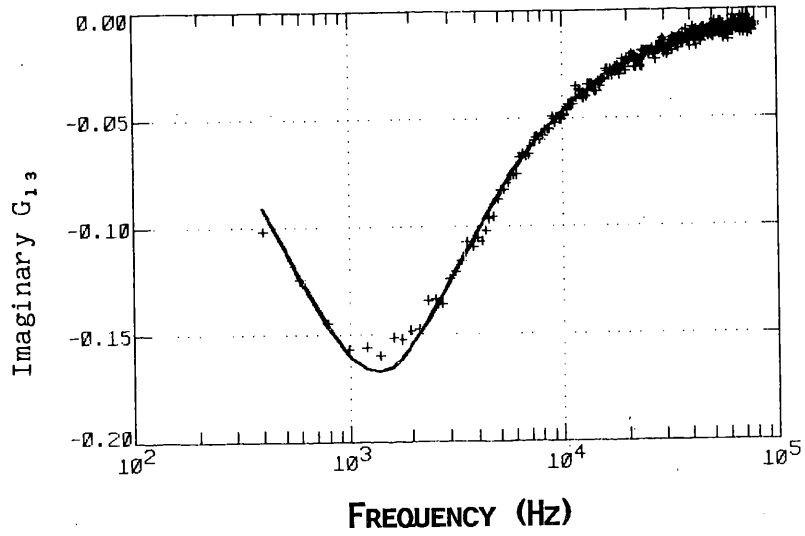

Fig. L.1. CPSDs, G_{12} and G_{13}, as a function of frequency for a solution height of 29.5 cm with the source on the bottom of the tank and the scintillators located as in Fig. 6. (Lines are fitted functions.)

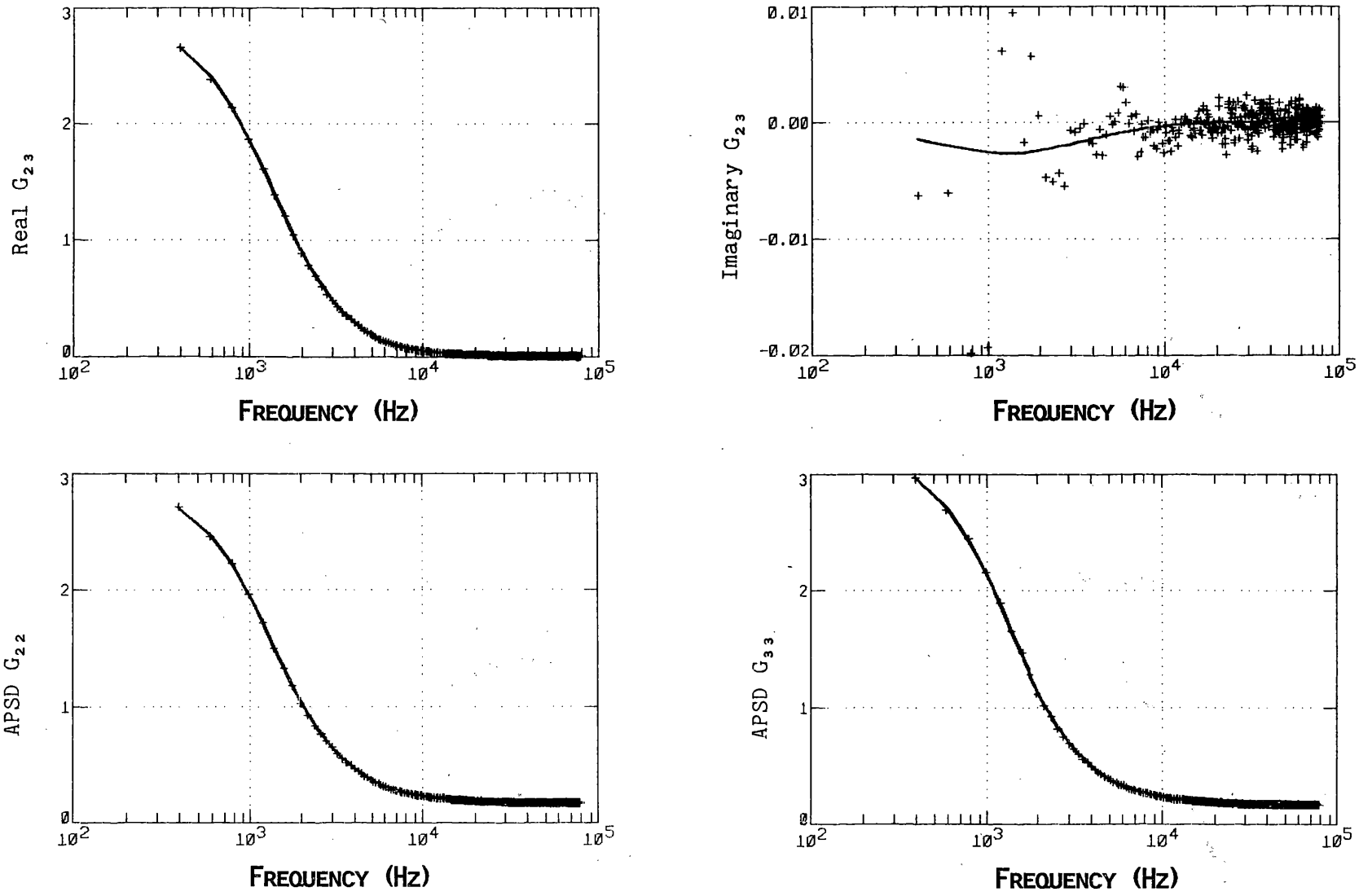

Fig. L.2. CPSD, G_{23}, and APSDs, G_{22} and G_{33}, as a function of frequency for a solution height of 29.5 cm with the source on the bottom of the tank and the scintillators located as in Fig. 6. (Lines are fitted functions.)

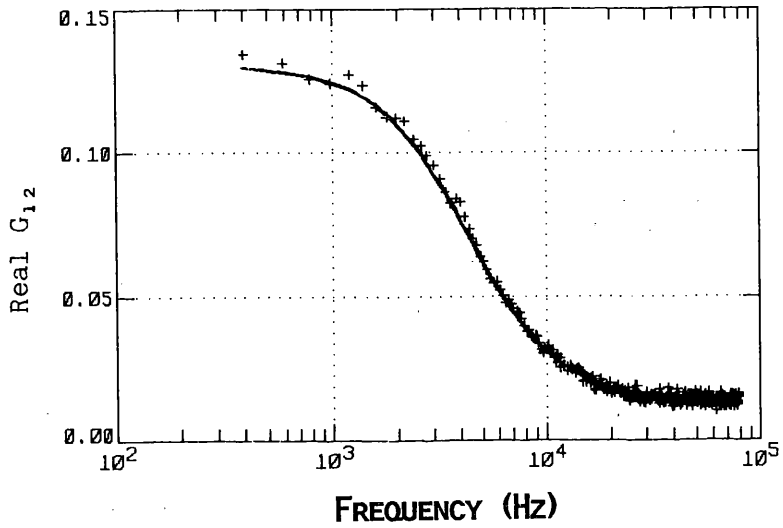

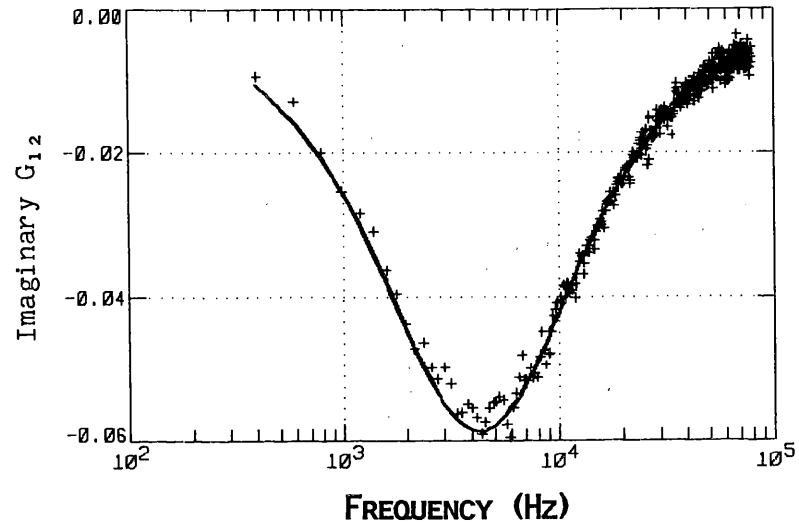

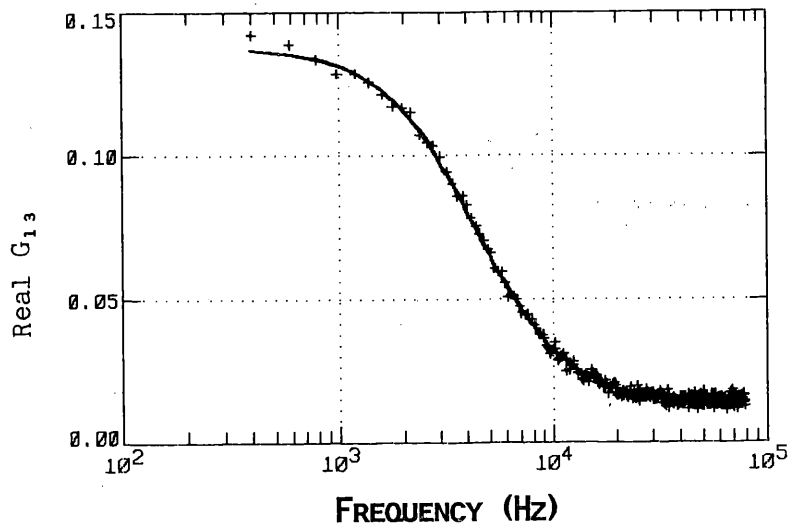

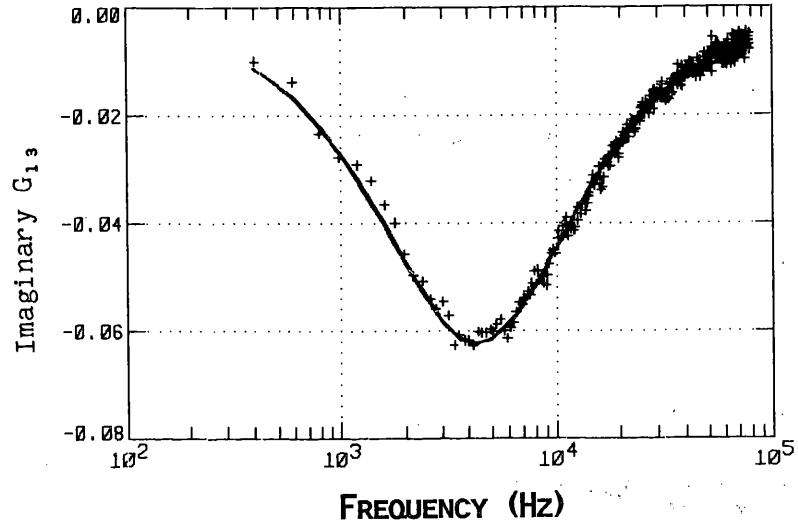

Fig. L.3. CPSDs, G_{12} and G_{13}, as a function of frequency for a solution height of 20.2 cm with the source on the bottom of the tank and the scintillators located as in Fig. 6. (Lines are fitted functions.)

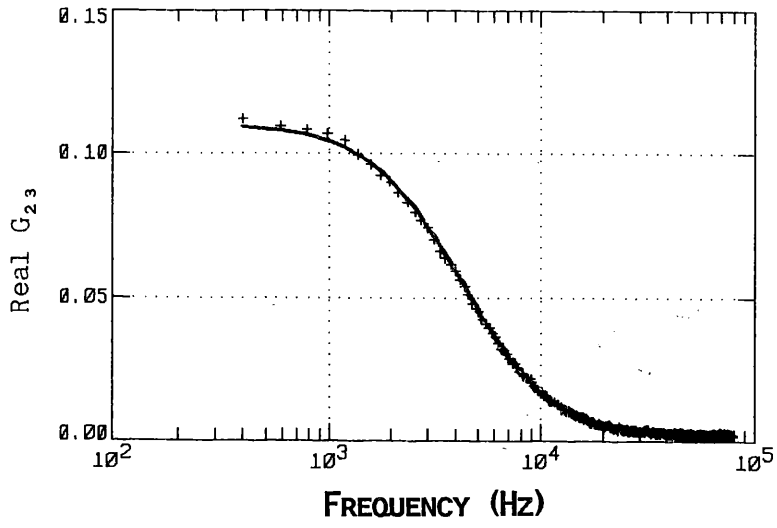

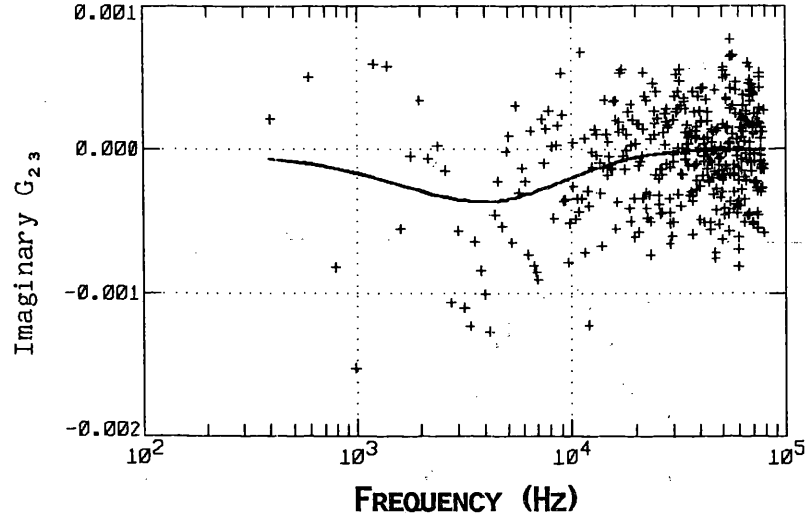

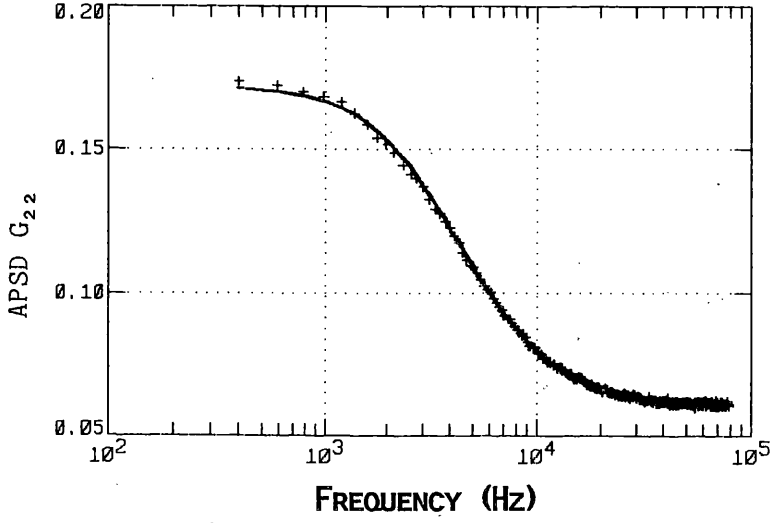

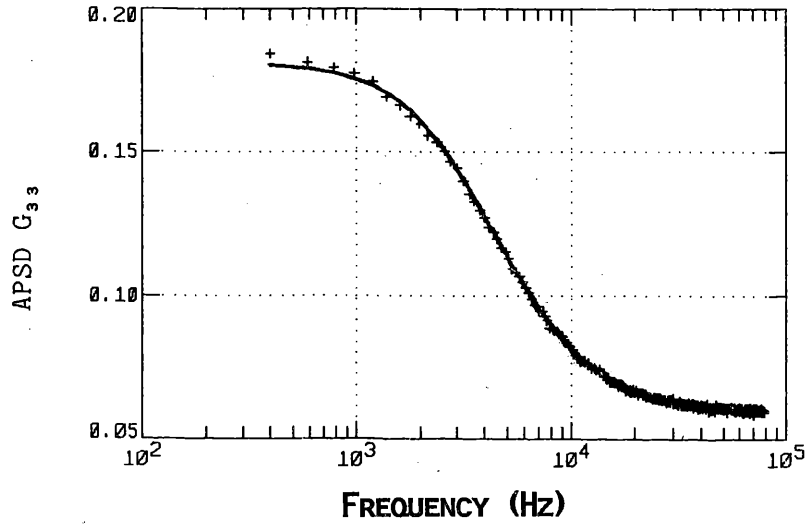

Fig. L.4. CPSD, G_{23}, and APSDs, G_{22} and G_{33}, as a function of frequency for a solution height of 20.2 cm with the source on the bottom of the tank and the scintillators located as in Fig. 6. (Lines are fitted functions.)

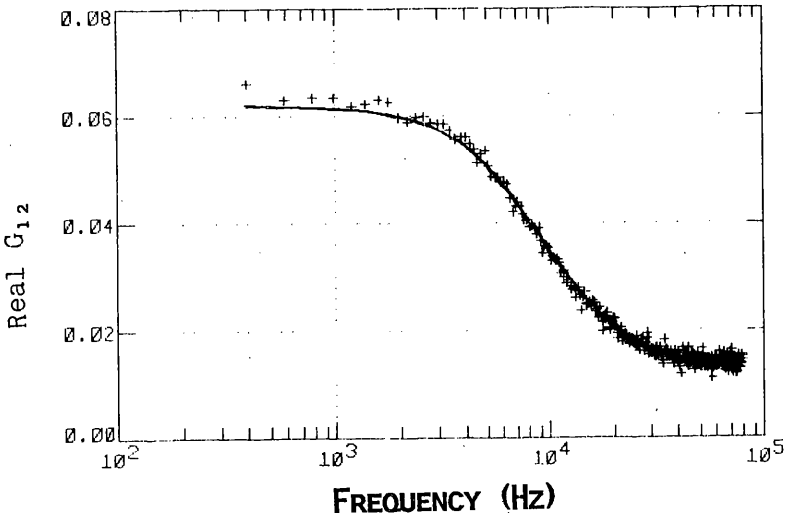

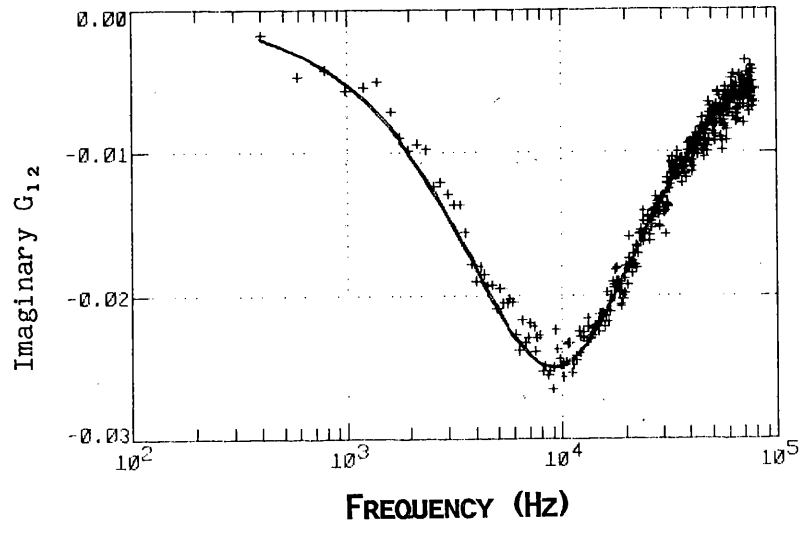

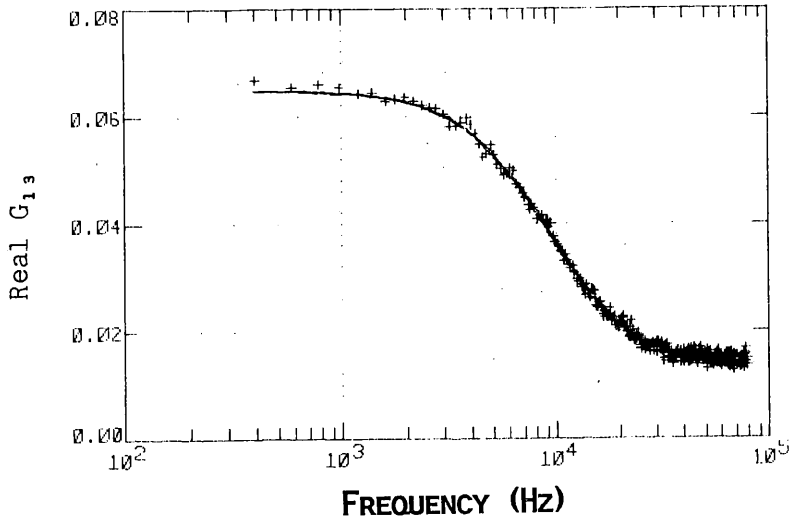

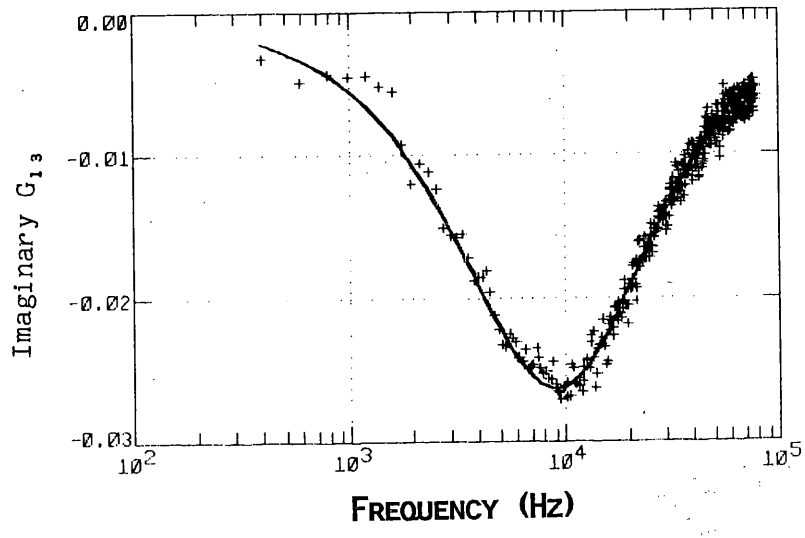

Fig. L.5. CPSDs, G_{12} and G_{13}, as a function of frequency for a solution height of 13.1 cm with the source on the bottom of the tank and the scintillators located as in Fig. 6. (Lines are fitted functions.)

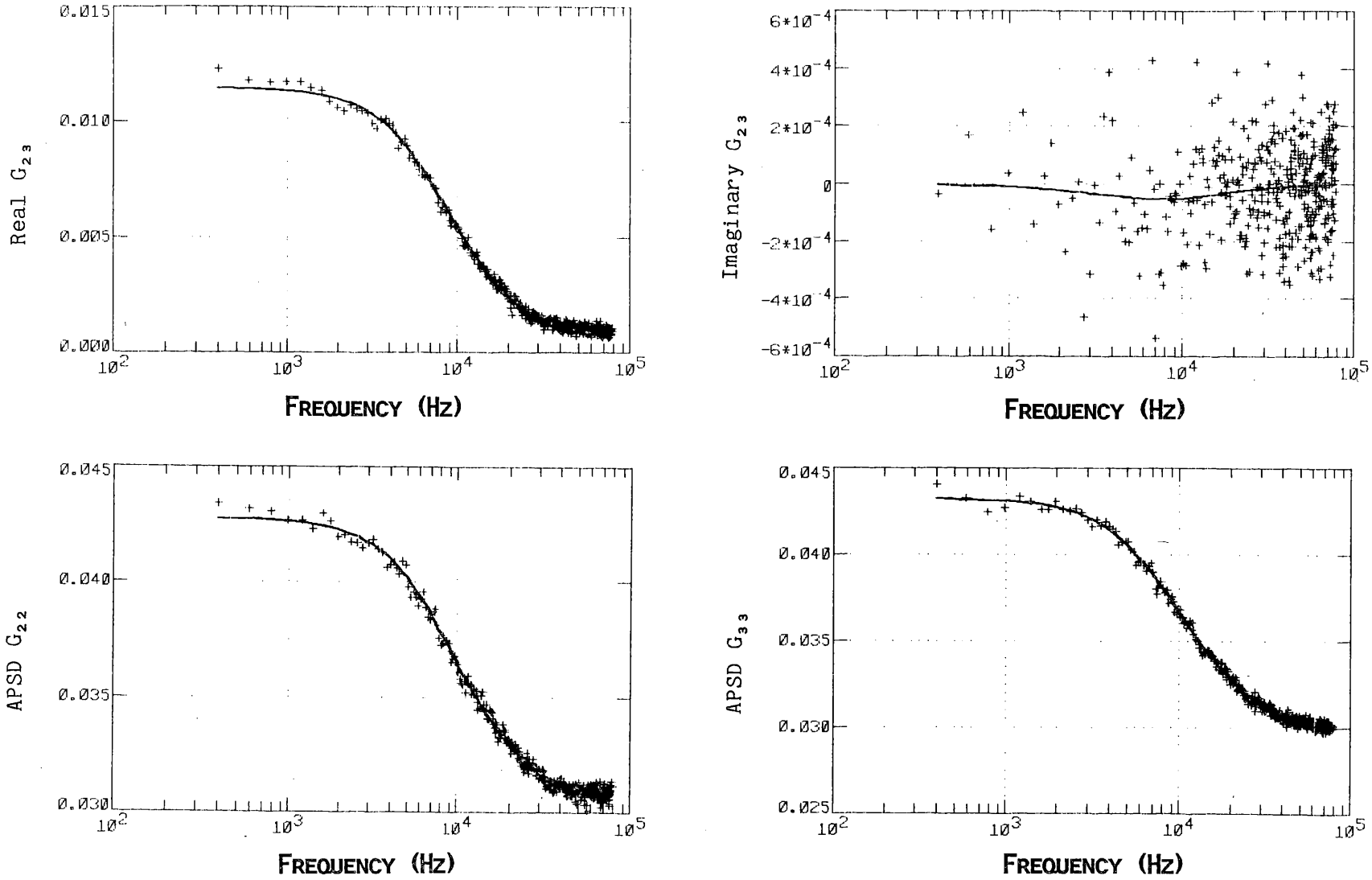

Fig. L.6. CPSD, G_{23}, and APSDs, G_{22} and G_{33}, as a function of frequency for a solution height of 13.1 cm with the source on the bottom of the tank and the scintillators located as in Fig. 6. (Lines are fitted functions.)

APPENDIX M

OTHER NOISE EQUIVALENT SOURCE FORMULATIONS

APPENDIX M. OTHER NOISE EQUIVALENT SOURCE FORMULATIONS

Various theories of the noise equivalent source term for spontaneously fissioning isotopes such as ^{252}Cf and ^{240}Pu have been formulated. The approach we have used results in the quantity $\overline{\nu_c^2}$ in Eq. (A.5) of Appendix A. Other theories, such as that of Verdu Martin et al.,[1] result in the expression

$$G_S = 2(\bar{\nu})^2 \, XFR \left\{ 1 + \frac{V}{XR} + \frac{F_i I_i^2}{FI^2} \frac{\overline{\nu_i(\nu_i - 1)}}{(\bar{\nu})^2} + \frac{F_c I_c^2}{FI^2} \frac{\overline{\nu_c(\nu_c - 1)}}{(\bar{\nu})^2} \right\} . \quad (1)$$

The difference between Eq. (A.5) of Appendix A and the above is significant only at low neutron multiplication factors. For this experiment the use of $\overline{\nu_c(\nu_c - 1)}$ instead of $\overline{\nu_c^2}$ results in higher neutron multiplication factors which do not agree as well those with values obtained from independent break-frequency noise analysis measurements or with calculated neutron multiplication factors. A comparison of both interpretations and calculations is given in Fig. M.1. Above k_{eff} of 0.8 the difference is not significant. As k_{eff} decreases, the use of the term $\overline{\nu_c(\nu_c - 1)}$ yields significantly higher k_{eff} values. For a solution height of 6.5 cm, a k_{eff} of 0.49 is obtained as compared to a value of 0.35 obtained by using $\overline{\nu_c^2}$ and a calculated value of 0.33.

The k_{eff} values obtained from BFNA are also shown in Fig. M.1. The use of an alternative noise equivalent source (to that given in Appendix A) with point kinetics to interpret the ratio of spectral densities results in values of k_{eff} that do not agree with the independent BFNA measurements (Sect. 8). For example, for a solution height of 13.08 cm, the k_{eff} value from the BFNA measurements, 0.659 ± 0.013, agrees with that from the ratio of spectral density measurements, 0.662 ± 0.015, while that for interpretation of the ratio of spectral densities using the alternative noise equivalent source is 0.705 ± 0.015, which does not agree with the BFNA measurements.

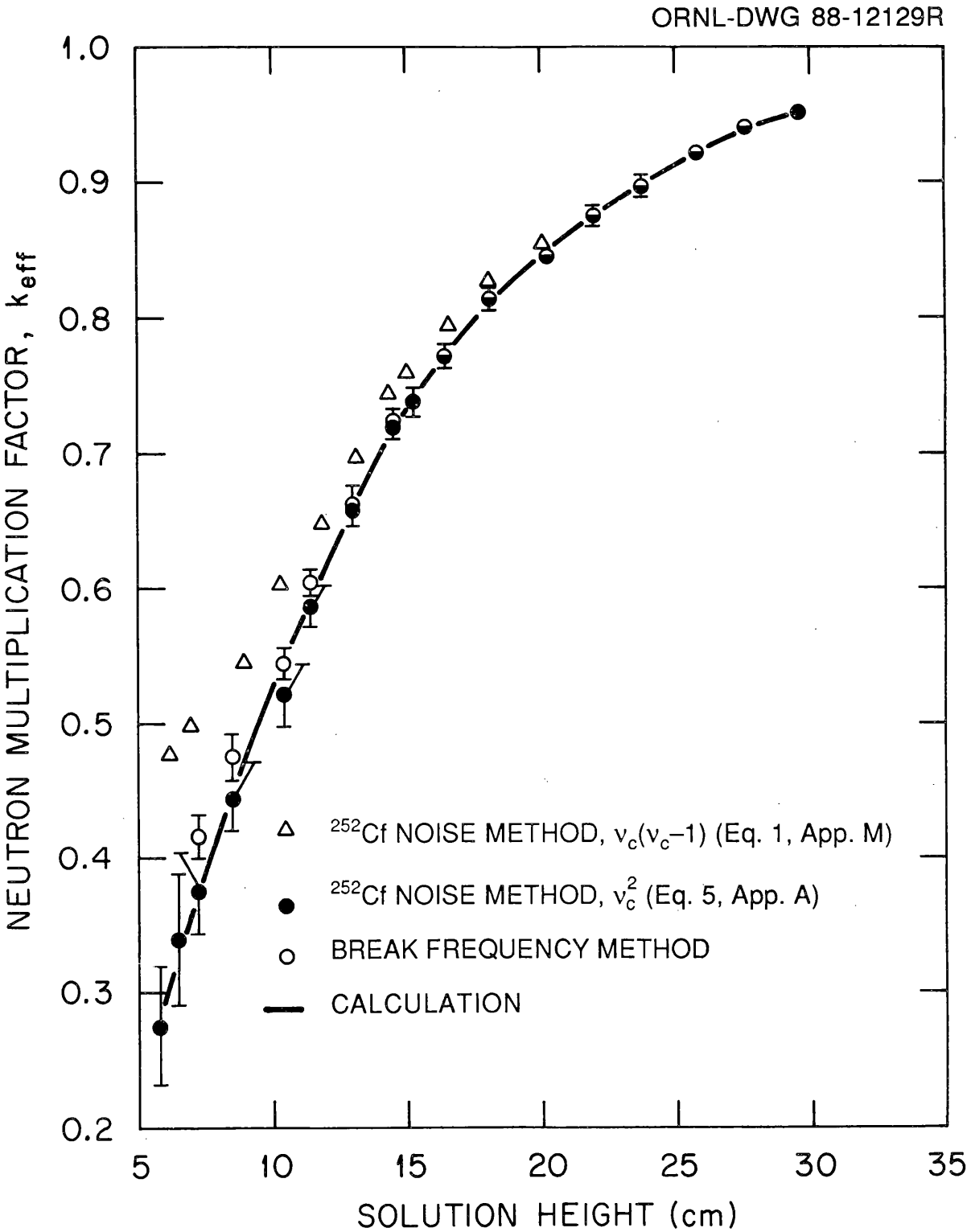

Fig. M.1. Comparison of neutron multiplication factors obtained from the ratios of spectral densities using various noise equivalent source terms for spontaneous fission with independent BFNA measurements and with calculated values.

APPENDIX M REFERENCE

1. G. Verdu Martin, "Teoria General del Transporte Estocastico de Neutrones y su Aplicacion a la Medida de Reactividad en Conjuntos Subcriticos," Tesis, Universidad Politecnica de Valencia (April 1984).

ORNL/TM-10122
Dist. Category S-526
(Applied)

INTERNAL DISTRIBUTION

1-2. E. D. Blakeman
3. H. R. Brashear
4-6. W. D. Burch
7. G. H. Burger
8. B. G. Eads
9. M. J. Feldman
10. D. N. Fry
11. J. M. Googin
12. W. S. Groenier
13-17. M. J. Haire
18. W. R. Hamel
19. C. M. Hopper
20. E. B. Johnson
21-22. R. C. Kryter
23. D. W. McDonald
24. S. A. Meacham
25. W. T. Mee
26-35. J. T. Mihalczo
36. C. A. Mossman
37. D. R. Miller
38. L. C. Oakes
39. A. M. Perry
40. L. M. Petrie
41. R. T. Primm, III
42. G. E. Ragan
43-44. C. W. Ricker
45-46. G. R. Smolen
47-51. J. G. Stradley
52. R. G. Taylor
53. J. T. Thomas
54. R. E. Uhrig
55. R. M. Westfall
56. G. E. Whitesides
57. R. S. Wiltshire
58. J. B. Ball (Advisor)
59. P. F. McCrea (Advisor)
60. Fuel Recycle Division Publications
61. Central Research Library
62-64. I&C Division Publications
65-66. Laboratory Records
67. Laboratory Records, ORNL-RC
68. ORNL Patent Section

EXTERNAL DISTRIBUTION

69. F. M. Alcorn, Lynchburg Research Center, P.O. Box 239, Lynchburg, VA 24505.
70. D. E. Bailey, Director, Fuels and Reprocessing Division, NE-551, U.S. Department of Energy, Washington, DC 20545.
71. W. W. Ballard, Battelle Pacific Northwest Laboratory, P.O. Box 999, Richland, WA 99352.
72. F. P. Baranowski, 1110 Dapple Grey Court, Great Falls, VA 22066.
73. S. R. Bierman, Battelle Pacific Northwest Laboratory, P.O. Box 999, Richland, WA 99352.
74. E. D. Clayton, Battelle Pacific Northwest Laboratory, P.O. Box 999, Richland, WA 99352.
75. C. J. Emert, Bettis Atomic Power Laboratory, 2AP 34N, P.O. Box 79, West Mifflin, PA 15122-0079.
76. F. Feiner, Knolls Atomic Power Laboratory, Schenectady, NY 12301.

77. N. Frances, Knolls Atomic Power Laboratory, Schenectady, NY 12301.
78. E. M. Gelbard, Argonne National Laboratory, Argonne, IL 60439.
79. H. Kouts, Brookhaven National Laboratory, Upton, NY 11793.
80. R. Little, Princeton Plasma Physics Laboratory, James Forrestal Campus, P.O. Box 451, Princeton, NJ 08544.
81. R. C. Lloyd, Battelle Pacific Northwest Laboratory, P.O. Box 999, Richland, WA 99352.
82. L. Lois, U.S. Nuclear Regulatory Commission, Core Performance Branch/NRR, Washington, D.C. 20555.
83. J. L. McElroy, Pacific Northwest Laboratories, P.O. Box 999, Richland, WA 99352.
84. J. W. Morfitt, Idaho Falls Laboratory, P.O. Box 1625, Idaho Falls, ID 83415.
85. M. J. Ohanian, Associate Dean for Research, College of Engineering, 300 Weil Hall, University of Florida, Gainesville, FL 32611.
86. H. F. Raab, Code 008A, Naval Reactors, Department of Energy, Washington, D.C. 20585.
87. M. J. Rohr, Program Manager, Consolidated Fuel Reprocessing Program, Energy Programs Division, Energy Technology Branch, Department of Energy-Oak Ridge Operations, Oak Ridge, TN 37831.
88. T. Sanders, Sandia National Laboratory, Albuquerque, NM 87120
89. L. N. Terry (CML record copy) Battelle Pacific Northwest Laboratory, P.O. Box 999, Richland, WA 99352.
90. Francis V. Thome, Sandia National Laboratory, Albuquerque, NM 87120.
91. H. H. Van Tuyl, Battelle Pacific Northwest Laboratory, P.O. Box 999, Richland, WA 99352.
92. Office of Assistant Manager for Energy Research and Development, Department of Energy, Oak Ridge Operations, Oak Ridge, TN 37831.

93-119. Given distribution under Category S-526, Consolidated Fuel Reprocessing Program--Criticality Data Development.